

THE ROLES OF TUNGSTEN AND MOLYBDENUM IN THE GROWTH AND
METABOLISM OF *PYROBACULUM AEROPHILUM*

by

LUCY ELLEN FEINGOLD

(Under the Direction of MICHAEL W. W. ADAMS)

ABSTRACT

The fundamental issue addressed by this research is how and why do organisms choose to use Mo or W at the catalytic sites of key enzymes. The model organism is the hyperthermophilic archaeon *Pyrobaculum aerophilum*, and the model system is respiratory nitrate reduction. Nitrate reductase (NR) catalyzes a high potential reaction ($E_o' = + 420$ mV), and in organisms such as *Escherichia coli* the physiological electron donor is formate via formate dehydrogenase (FDH) ($E_o' = - 430$ mV) in the formate-nitrate respiratory chain. Both of these enzymes are molybdoenzymes in *E. coli*, yet W is the preferred element in enzymes in hyperthermophiles. However, FDH has also been purified as a naturally-occurring tungstoenzyme from various thermophilic bacteria, but NR had not been previously purified from a thermophilic organism, let alone one growing at 100 °C.

Growth of *P. aerophilum* at 98 °C in the presence of nitrate requires tungstate and is inhibited by the presence of molybdate in higher or equimolar concentrations. However, both oxyanions support growth at low (78 °C) temperature. Elemental analyses showed that both oxyanions were taken up by the organism under both of these growth conditions. The results are the first to show a temperature-dependent difference in W and Mo requirements.

Purification of NR from *P. aerophilum* revealed two forms of the enzyme, NR (NR1 and NR2) and two forms of a NR-FDH complex (NR1-FDH1 and NR2-FDH2). The purified NR enzymes and the NR/FDH enzyme complexes of *P. aerophilum* all exhibited maximal activity at 90 °C. NR1 is a Mo-containing enzyme with a specific activity of 534 U/mg and resembles other respiratory NRs found in mesophilic microorganisms not only in metal content, but also in subunit composition. NR2 is the first example of a W-containing NR and has a specific activity of 223 U/mg. The NR1/FDH1 complex contained 0.6 g-atoms Mo and 0.3 g-atoms W per mol of complex with specific activities of 712 and 33 U/mg for NR and FDH, respectively. The NR2/FDH2 complex contained 0.6 mol W and 0.2 g-atoms Mo per mol of complex, with specific activities of 373 and 3 U/mg for NR and FDH, respectively.

INDEX WORDS: *Pyrobaculum aerophilum*, archaea, hyperthermophile, nitrate reductase, formate dehydrogenase, molybdenum, tungsten.

THE ROLES OF TUNGSTEN AND MOLYBDENUM IN THE GROWTH AND
METABOLISM OF *PYROBACULUM AEROPHILUM*

by

LUCY ELLEN FEINGOLD

B.S., University of Florida, 1983

M.S., University of Delaware, 1988

A Dissertation Submitted to the Graduate Faculty of The University of Georgia in Partial
Fulfillment of the Requirements for the Degree

DOCTOR OF PHILOSOPHY

ATHENS, GEORGIA

2006

© 2006

Lucy Ellen Feingold

All Rights Reserved

THE ROLES OF TUNGSTEN AND MOLYBDENUM IN THE GROWTH AND
METABOLISM OF *PYROBACULUM AEROPHILUM*

by

LUCY ELLEN FEINGOLD

Major Professor: Michael W.W. Adams

Committee: Robert A. Scott
Michael K. Johnson
Debra Mohnen
Robert Maier

Electronic Version Approved:

Maureen Grasso
Dean of the Graduate School
The University of Georgia
August 2006

DEDICATION

I would like to dedicate this dissertation to the memory of my Dad, Robert J. Feingold, who introduced me to the ocean, shared my love for science, and has influenced my life more than anyone has.

ACKNOWLEDGEMENTS

First and foremost, I would like to thank Dr. Michael W.W. Adams for his support, guidance, and for sharing his knowledge with me throughout my graduate studies. I also owe a great deal of thanks to my current committee members, Dr. Mike Johnson, Dr. Bob Scott, Dr. Deb Mohnen and Dr. Rob Maier, and my past committee members, Dr. Dan DerVartanian and Dr. James Travis. All of them had an enormous role in helping me to complete my research and my dissertation, above and beyond that of most committees. A special thank you goes to Dick Cammack for recording the EPR spectra, and for many interesting and delightful conversations. I would also like to thank Dr. David Puett for help on many occasions and in many situations. Thanks also to Dr. Mary Ann Moran and Dr. Harry Dailey for use of their microscopes during the extremely long period of time in which I was conducting growth studies.

To members of the Adams Lab, past and present, thank you for the many helpful discussions, laughs and fun in and out of the lab. In particular, I would like to thank Dr. Marc Verhagen, Dr. Angeli Menon, Dr. Gerti Schut, Dr. Frank Jenney, and Farris Poole. I must also thank Dr. Neil Bhowmick, Dr. Amy Medlock and Dr. Mike Weinberg for help in many arenas related to research, but more than anything for their friendship. I am blessed to have many friends in Athens that have made my life full and fun. I thank all of you!

Last but never least; I would like to thank my family, Mom, Louis, Susan, Bobby, Julie, Natalie, Lynn and Henry. I simply don't know what I would do without all of you, and I am thankful for you and your continued love and support everyday. Finally, thanks to Noah, who always makes me smile and laugh, and gives unconditionally, as only the best dog ever, could.

TABLE OF CONTENTS

	Page
ACKNOWLEDGEMENTS	v
LIST OF TABLES	vii
LIST OF FIGURES	ix
CHAPTER	
1 INTRODUCTION	1
2 UPTAKE AND INCORPORATION OF MOLYBDATE AND TUNGSTATE DURING GROWTH OF <i>PYROBACULUM AEROPHILUM</i>	66
3 PURIFICATION AND CHARACTERIZATION OF THE RESPIRATORY NITRATE REDUCTASE FROM THE HYPERTHERMOPHILIC ARCHAEON <i>PYROBACULUM AEROPHILUM</i>	100
4 PURIFICATION AND CHARACTERIZATION OF THE NITRATE-INDUCIBLE FORMATE DEHYDROGENASE COMPLEX FROM THE HYPERTHERMOPHILIC ARCHAEON <i>PYROBACULUM AEROPHILUM</i>	169
5 COMPARISON OF MOLYBDENUM- AND TUNGSTEN-CONTAINING ENZYMES, COFACTOR BIOSYNTHESIS, AND METAL TRANSPORT IN <i>ESCHERICHIA COLI</i> , <i>PYROBACULUM AEROPHILUM</i> , AND <i>PYROCOCCUS</i> <i>FURIOSUS</i>	204
6 SUMMARY AND CONCLUSIONS	241

LIST OF TABLES

	Page
Table 1.1: Genera and Metabolic properties of Hyperthermophilic Microorganisms.....	4
Table 1.2: Characteristics of Prokaryotic Nitrate Reductase	16
Table 1.3: Molybdenum Enzyme Families.....	25
Table 1.4: Tungsten Enzyme Families.....	28
Table 2.1: Intercellular Concentrations of W and Mo in <i>P. aerophilum</i> growth media and cells under variable conditions.....	82
Table 2.2: Specific Activities* of NR, FDH, and GDH at 90 °C in Solubilized Membranes under various growth conditions of <i>P. aerophilum</i>	84
Table 3.1: Solubilization of nitrate reductase from <i>P. aerophilum</i> cells with n-octyl β -glucoside	115
Table 3.2: Purification of nitrate reductase from <i>P. aerophilum</i> membranes.....	118
Table 3.3: Method of and identification of subunits and additional proteins in the purified nitrate reductases in <i>P. aerophilum</i> identified from SDS-PAGE analysis.....	128
Table 4.1: Solubilization of formate dehydrogenase from <i>P. aerophilum</i> cells with n-octyl β - glucoside	178
Table 4.2: Purification of formate dehydrogenase from <i>P. aerophilum</i> membranes.....	182
Table 5.1: Comparison of the genes encoding the respiratory nitrate reductases from <i>Escherichia coli</i> to the homologous genes in <i>Pyrobaculum aerophilum</i> and <i>Pyrococcus furius</i>	211

Table 5.2: Comparison of the genes encoding the formate dehydrogenases from <i>Escherichia coli</i> to the homologous genes in <i>Pyrobaculum aerophilum</i> and <i>Pyrococcus furiosus</i>	214
Table 5.3: Comparison of the genes encoding the aldehyde-oxidizing enzymes in <i>Pyrococcus furiosus</i> to the homologous genes in <i>Pyrobaculum aerophilum</i> and <i>Escherichia coli</i>	220
Table 5.4: Comparison of <i>Escherichia coli</i> molybdopterin biosynthetic genes, molybdenum uptake and molybdenum transport genes to homologs in <i>Pyrobaculum aerophilum</i> and <i>Pyrococcus furiosus</i>	224

:

LIST OF FIGURES

	Page
Figure 1.1: Universal phylogenetic tree depicting the three domains, <i>Archaea</i> , <i>Bacteria</i> and <i>Eukarya</i>	2
Figure 1.2: Electron micrograph of (a) <i>Pyrobaculum aerophilum</i> in exponential growth phase, and (b) in stationary growth phase	11
Figure 1.3: Global biogeochemical nitrogen cycle	12
Figure 1.4: Structural model of the pyranopterin cofactor	22
Figure 1.5: The Crystal structure of the respiratory nitrate reductase Nar from <i>E. coli</i>	37
Figure 1.6: Cofactors forming the electron transfer chain of Nar in <i>E. coli</i>	41
Figure 1.7: The Crystal structure of the nitrate-inducible FDH (Fdh-N) from <i>E. coli</i>	43
Figure 1.8: Cofactors forming the electron transfer chain of Fdh-N in <i>E. coli</i>	46
Figure 1.9: Proposed model of the Fdh-N/Nar respiratory chain in <i>E. coli</i>	47
Figure 2.1: Specific activities of nitrate reductase and formate dehydrogenase in <i>P. aerophilum</i>	77
Figure 2.2: Growth of <i>P. aerophilum</i> cells at 98 °C and 78 °C	79
Figure 2.3: Direct cell counts of <i>P. aerophilum</i> cultures at time of harvest	81
Figure 2.4: Phylogentic tree of all W- and Mo-containing enzymes found in <i>P. aerophilum</i> , as determined by genomic sequence analysis	86
Figure 3.1: Respiratory nitrate reductase operons from <i>P. aerophilum</i> and <i>E. coli</i> (NRA)	105

Figure 3.2: Generalized schematic of the methodology of purification of NR from 50 g of cells	108
Figure 3.3: Purification of NR from 50 g of cells.....	116
Figure 3.4: Nitrate reductase and formate dehydrogenase activity-stained gels	119
Figure 3.5: Kinetic parameters of NR1	122
Figure 3.6: The effect of pH on the nitrate reductase activity of NR1	123
Figure 3.7: Effect of temperature on various forms of nitrate reductase in <i>P. aerophilum</i>	124
Figure 3.8: SDS-PAGE of NR1 from nondenaturing gel band	126
Figure 3.9: SDS-PAGE analysis of the two peaks of nitrate reductase activity from <i>P. aerophilum</i>	127
Figure 3.10: UV-Visible spectra of nitrate reductase	133
Figure 3.11: EPR spectra of whole cells and purified NR1 of <i>P. aerophilum</i>	135
Figure 3.12: EPR spectra of <i>P. aerophilum</i> nitrate reductase.....	136
Figure 3.13: Alignment of sequences of the α , β , γ , and δ subunits of the respiratory NR from <i>Pyrobaculum aerophilum</i> , and <i>Escherichia coli</i> NRA (<i>narGHJI</i>) and NRZ (<i>narZYWV</i>).....	140
Figure 3.14: Alignment of NR and FDH sequences with the structure of DMSO reductase	144
Figure 3.15: Redox potentials of the cofactors in NRA from <i>E. coli</i>	150
Figure 4.1: Respiratory formate dehydrogenase operons from <i>P. aerophilum</i> and <i>E. coli</i>	173
Figure 4.2: Purification of NR and the FDH complex from 50 g of cells	180
Figure 4.3: Formate dehydrogenase and Nitrate reductase activity-stained gels.....	184
Figure 4.4: The effect of pH on the formate dehydrogenase activity of the NR1/FDH1 complex	186

Figure 4.5: Effect of temperature on the formate dehydrogenase complex in <i>P. aerophilum</i>	187
Figure 4.6: SDS-PAGE analysis of the two formate dehydrogenase complexes from <i>P. aerophilum</i>	189
Figure 4.7: Nitrate reductase/Formate dehydrogenase complex from <i>P. aerophilum</i>	190
Figure 4.8: Alignment of sequences of the α , β and γ subunits of the respiratory FDH from <i>Pyrobaculum aerophilum</i> and <i>Escherchia coli</i> FDH-N (<i>fdnGHI</i>) and FDH-O (<i>fdhoGHI</i>)	193
Figure 5.1: Phylogenetic tree of nitrate reductase (NR) and formate dehydrogenase (FDH) subunits.....	217
Figure 5.2: Phylogentic tree of the AOR family of tungstoenzymes.....	221

CHAPTER 1

INTRODUCTION

Molecular phylogeny based on 16S/18S rRNA sequences, divides cellular life into three major lineages, two of which are solely microbial and consist exclusively of prokaryotic cells. These lineages or domains are the *Bacteria*, *Archaea* and *Eukarya* (Fig. 1.1). As early as the 1960s, there was evidence for the two different types of prokaryote, resulting in the most recently recognized lineage, the *Archaea* (112). Such evidence included the discovery of branched chains of ether-linked lipids, found in extreme halophiles and later in *Sulfolobus* and *Thermoplasma*, as well as the lack of peptidoglycan in cell walls of methanogens, and an array of new coenzymes found in various microorganisms. Prior to the 'discovery' of archaea in 1977, however, these differences were merely explained by either theories of convergent evolution or most often as adaptations by the microbes to the extreme environments in which they were found (111). This research focuses on *Pyrobaculum aerophilum*, an archaeon that thrives in an extreme temperature environment that is dependent on molybdenum and tungsten for growth and nitrate respiration.

Archaea and Hyperthermophiles. The domain *Archaea* is comprised of essentially those prokaryotes that thrive in extreme environments. Archaea have been isolated and surveyed from shallow and deep-sea hydrothermal vents, terrestrial hot-springs and solfataric fields, coastal waters, a freshwater lake, temperate and polar seas, and a salt marsh (2, 26, 28, 71, 88, 97). In

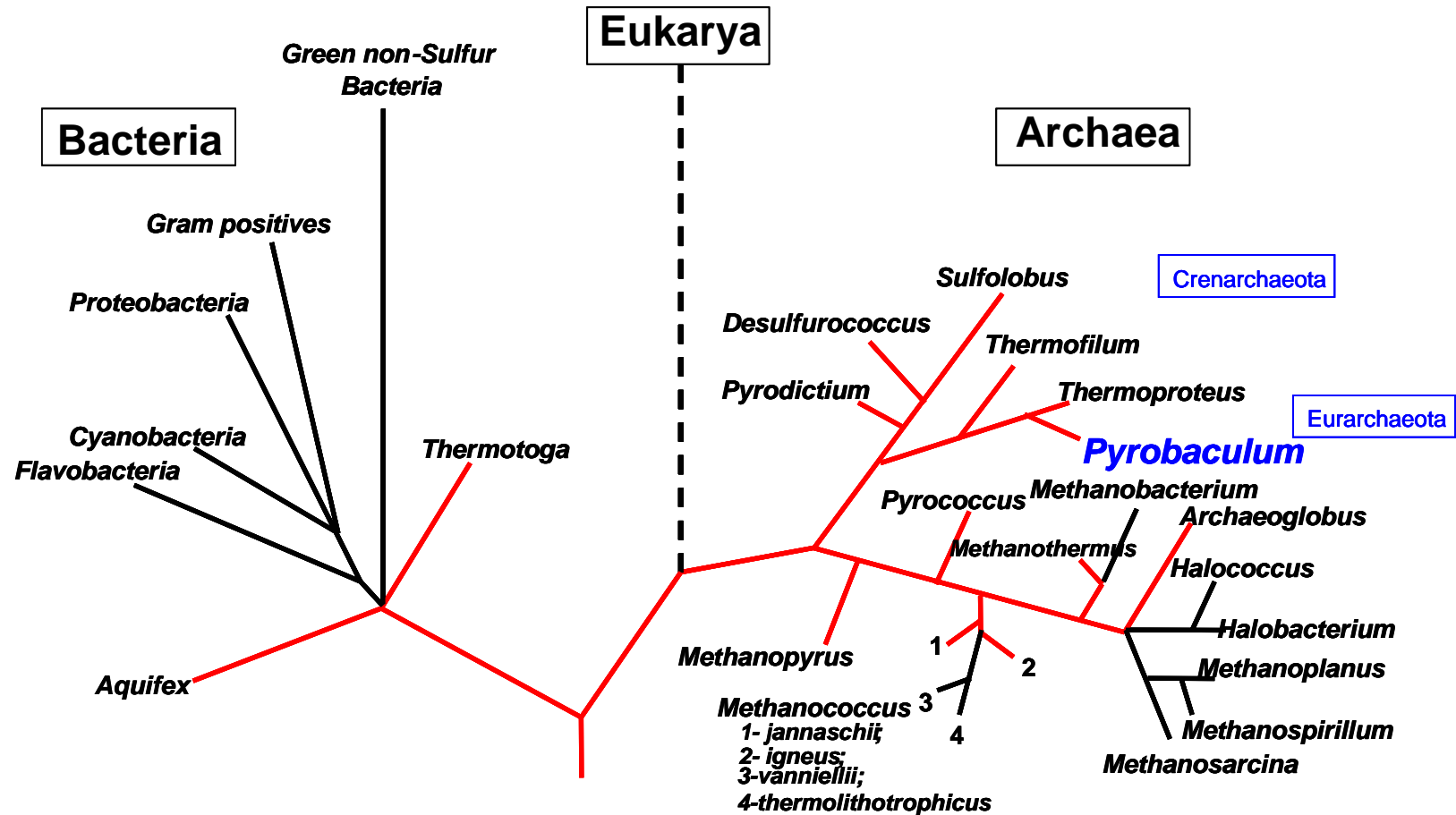


Fig. 1.1. Universal phylogenetic tree depicting the three domains, *Archaea*, *Bacteria* and *Eukarya*. Tree is based upon rRNA sequence comparisons. Root position was determined from the paralogous gene couple, elongation factors EFTu and EFG (50). Hyperthermophilic lineage is depicted by the red lines. Figure was modified from (97, 112).

addition, archaea have been found in agricultural soils, oil wells, coal refuse piles, geothermal power plants and seafloor sediments (14, 99).

Many members of the domain *Archaea* have been isolated from both shallow and deep-sea hydrothermal vents and continental hot springs, and they thrive at temperatures at or above 90 °C. These organisms, termed hyperthermophiles, were discovered in the early 1980s shortly after the discovery of deep-sea hydrothermal vents (100). More than 25 genera of hyperthermophiles are known to date with confirmed maximum growth temperatures up to 113 °C (Table 1.1). The majority of hyperthermophilic organisms are classified within the domain *Archaea*. In fact, only two genera, *Aquifex* and *Thermotoga*, are within the domain *Bacteria* and they exhibit maximum growth temperatures of 95 °C and 90 °C respectively. Hyperthermophiles are well suited for the extreme environments in which they live. These extreme conditions are not limited only to high temperatures, but also include extremes of pH and salinity. Furthermore, due to the presence of reducing gasses and the low solubility of oxygen at high temperatures, the hyperthermal environment is typically anoxic. The mode of metabolism for hyperthermophiles is therefore predominantly anaerobic (Table 1.1). In lieu of oxygen, many of these organisms obtain energy necessary for growth via respiration of elemental sulfur (S°). In addition to reduction of S° , reduction of sulfate has been shown in *Archaeoglobus*, and reduction of thiosulfate in *Pyrolobus*, *Archaeoglobus*, *Pyrobaculum*, and *Ferroglobus* with H_2 as the electron donor and the production of H_2S . To the contrary, however, some species of *Pyrococcus* and *Thermococcus* grow by fermentation of peptides, carbohydrates or amino acids in the absence of S° . Furthermore, in *Aquifex*, *Sulfolobus*, *Acidianus* and *Metallosphaera*, aerobic growth is achieved by the reduction of S° to H_2S . Other means of aerobic respiration have been found in *Aeropyrum pernix*, which is an obligate aerobe, and in *Pyrobaculum*, *Pyrolobus*, and *Aquifex*,

Table 1.1. Genera and Metabolic properties of Hyperthermophilic Microorganisms.[§]

Genus	T _{max} [†]	Metabolism [‡]	Substrates [¶]	Acceptors
'S[°] - dependent' archaea				
<i>Thermofilum</i> (c)*	100 [°]	Hetero	Peptides	S [°] , H ⁺
<i>Staphylothermus</i> (d/m)	98 [°]	Hetero	Peptides	S [°] , H ⁺
<i>Thermodiscus</i> (m)	98 [°]	Hetero	Peptides	S [°] , H ⁺
<i>Desulfurococcus</i> (d/c)	95 [°]	Hetero	Peptides	S [°] , H ⁺
<i>Thermoproteus</i> (c)	92 [°]	Hetero / Auto	Peptides, CBH, H ₂	S [°] , H ⁺
<i>Pyrodictium</i> (d/m)	110 [°]	Hetero / Auto	Peptides, CBH, H ₂	S [°] , H ⁺
<i>Pyrococcus</i> (d/m)	105 [°]	Hetero	Peptides	±S [°] , H ⁺
<i>Thermococcus</i> (d/m)	97 [°]	Hetero	Peptides, CBH	±S [°] , H ⁺
<i>Hyperthermus</i> (m)	110 [°]	Hetero	Peptides, H ₂	±S [°] , H ⁺
<i>Stetteria</i> (m)	103 [°]	Hetero	Peptides+H ₂	S [°] , S ₂ O ₃ ²⁻
<i>Pyrobaculum</i> (d/m)	102 [°]	Hetero / Auto	Peptides, H ₂ , S ₂ O ₃ ²⁻	±S [°] , S ₂ O ₃ ²⁻ , SO ₃ ²⁻
<i>Acidianus</i> (m/c)	96 [°]	Auto	S [°] , H ₂	S [°] , O ₂
<i>Metallosphaera</i> (m/c)	80 [°]	Hetero	S [°] , H ₂ , FeS ₂	S [°] , O ₂
<i>Sulfolobus</i> (c)	87 [°]	Hetero / Auto	S [°] , Peptides, CBH, H ₂ , FeS ₂	S [°] , O ₂
<i>Thermodiscus</i> (m)	98 [°]	Hetero	Peptides, H ₂	S [°]
<i>Desulfurolobus</i> (c)	95 [°]	Auto	S [°] , H ₂	S [°]
<i>Staphylothermus</i> (m)	98 [°]	Hetero	Peptides + S	S [°]
'S[°] - independent' archaea				
<i>Pyrobaculum</i> (d/m/c)	102 [°]	Hetero / Auto	Peptides, H ₂	NO ₃ ⁻ , NO ₂ ⁻ , mO ₂ [†] , O ₂
<i>Sulfobococcus</i> (c)	96 [°]	Hetero	Peptides	-
<i>Aeropyrum</i> (m)	100 [°]	Hetero	Peptides	O ₂
<i>Pyrolobus</i> (d)	113 [°]	Auto	H ₂	S ₂ O ₃ ²⁻ , NO ₃ ⁻ , mO ₂

Sulfate - reducing archaea

<i>Archaeoglobus</i> (d/m)	95°	Hetero / Auto	CBH, H ₂	SO ₄ ²⁻ , S ₂ O ₃ ²⁻
----------------------------	-----	---------------	---------------------	---

Iron - oxidizing archaea

<i>Ferroglobus</i>	95°	Auto	Fe ²⁺ , H ₂ , S ₂ ⁻	NO ₃ ⁻ , S ₂ O ₃ ²⁻
--------------------	-----	------	---	--

Methanogenic archaea

<i>Methanococcus</i> (d/c)	91°	Auto	H ₂	CO ₂
<i>Methanothermus</i> (c)	97°	Auto	H ₂	CO ₂
<i>Methanopyrus</i> (d/m)	110°	Auto	H ₂	CO ₂

Bacteria

<i>Thermotoga</i> (d/m)	90°	Hetero	Peptides, CBH	S°, H ⁺
<i>Aquifex</i> (m)	95°	Auto	S°, H ₂ , S ₂ O ₃ ²⁻	mO ₂ , NO ₃ ⁻

§ Table adapted from (1). Data taken from (1, 15, 83, 91, 97).

† Maximum growth temperature.

‡ Growth by means of heterotrophy or autotrophy.

¶ Growth substrates serving as electron donors are peptides, carbohydrates (CBH), hydrogen (H₂) and elemental sulfur (S°).

* Isolation of species is from deep sea (d), shallow marine (m) environments or continental hot springs (c).

∫ Microaerophilic conditions.

which are facultative microaerophiles, and in *Pyrobaculum* facultative aerobic respirators. The aforementioned microaerophiles also obtain energy via reduction of nitrate to N_2 . Additional modes of metabolism in the hyperthermophilic archaea include the production of methane from H_2 and CO_2 by methanogens, and the oxidation of iron using thiosulfate and nitrate as electron acceptors by *Ferroglobus* (1, 91, 97).

Many of hyperthermophiles known to date are obligate heterotrophs (Table 1.1). Most of these obligate heterotrophs use proteinaceous substrates as their carbon and energy source. In culture, this translates to the use of complex media containing peptides from yeast, meat or bacterial extracts, as well as peptone and tryptone. Some hyperthermophiles, (*Thermoproteus*, *Pyrodictium*, *Pyrococcus*, *Thermococcus* and *Thermotoga*), however, can also utilize carbohydrates. The primary carbon sources are either complex carbohydrates such as starch and glycogen, or disaccharides such as maltose and cellobiose (55, 91). The relatively few autotrophic species known use a variety of electron donors (Table 1.1) such as H_2 , ferrous iron, sulfide and S° .

Geologic evidence suggests that the extreme high temperature and anaerobic conditions that exist in shallow and deep-sea hydrothermal vent ecosystems today are probably much the same as the Earth's environment over 4 billion years ago when life originated. This evidence, coupled with the fact that hyperthermophiles are the deepest and shortest branches of both the archaeal and bacterial domains of the 16S rRNA-based universal phylogenetic tree, led to the suggestion that hyperthermophiles may be still rather primitive and possibly the last common ancestor (25). Of course, many other factors need to be considered, including sources of chemical, light and heat energy and organic compounds that were available on early earth. There have been studies illustrating the activation of amino acids and the formation of peptides under

primordial conditions, which further supports a hyperthermophilic origin of life (45). Of course, the research available addressing the origin of life is immense, considering that it encompasses areas of science from astrophysics to geology to biochemistry to name but a few; and discussion of the topic in detail is far beyond the scope of this dissertation. Suffice it to say, whether a hyperthermophile was the last common ancestor, or a representative of a life form that was just as prolific today as it was in the days of the early earth, there is much to be learned from these organisms' role in global cycles, their biochemistry and their ecology, in addition to their role in evolution.

The archaeal domain consists of two kingdoms, the *Euryarchaeota* and the *Crenarchaeota* (Fig 1.1). The more diverse of the two kingdoms, the *Euryarchaeota*, is comprised of mesophilic, thermophilic and hyperthermophilic microorganisms. The organisms in this kingdom include methanogens, extreme halophiles, and thermophiles (the genus *Thermoplasma* and the *Thermococcus-Pyrococcus* group). Aerobic microorganisms are represented among the extreme halophiles (mesophilic) and the thermoacidophiles (94). Of relevance to this work, dissimilatory nitrate reduction coupled with organic substrates is carried out by some of the extreme halophiles (44, 114).

The *Crenarchaeota*, on the other hand, have been traditionally described as a group consisting solely of thermophilic and hyperthermophilic organisms. Two orders of *Crenarchaeota* have been described, the *Sulfolobales* (98) and the *Thermoproteales* (115). Within *Sulfolobales* growth by aerobic oxidation with hydrogen was first reported in 1992 (48). Most significantly, however, is that within *Thermoproteales*, often referred to as the branch of sulfur-metabolizing hyperthermophiles, neither an aerobic representative nor a nitrate reducer had been found until the isolation of *Pyrobaculum aerophilum* in 1993, the organism upon which

this research is based. Remarkably, S° inhibits the growth of this organism even though it is placed phylogenetically among an order of obligate anaerobic S° -respirers (105). Since 1993 additional organisms have been isolated which demonstrate physiological diversity within this order. Among them are *Pyrolobus fumarii* (15) and *Pyrobaculum calidifontis* (4), which are also capable of utilizing either nitrate or oxygen as electron acceptors and are inhibited by S° , and *Aeropyrum pernix*, which is an obligate aerobe that does not utilize S° (83).

Further physiological diversity amongst the archaea was apparent during recent ecological surveys of temperate and polar seas that resulted in the identification of nonthermophilic crenarchaeotes. Based on rRNA and lipid analyses, these as-yet-uncultivated groups of archaeal plankton are closely related to known cultured *Crenarchaeota* (27). Due to the diverse physiological characteristics emerging within this order, in conjunction with the fact that these two orders have been classified based primarily on biochemical and physiological characteristics as there are relatively few 16S rRNA sequences available, a review of this classification was recently undertaken based on 16S r-DNA (20). These analyses demonstrated that the order *Sulfolobales* was monophylogenetic (33). Analyses of the order *Thermoproteales*, based on known families (*Thermoproteaceae*, to which *P. aerophilum* belongs, and *Desulfurococcaceae*) and genera tentatively placed within the order (*Pyrodictium*, *Thermodiscus* and *Staphylothermus*) as well as new isolates, however, rendered quite different results. Based on three different algorithms yielding the same topology, a new order temporarily named *Igneococcales*, was established (20). Within this new order, two families originated. They are *Pyrodictiaceae*, which includes the genera *Pyrodictium*, *Hyperthermus*, and *Pyrolobus*, and the *Sulfurococcaceae*, which includes the genera *Desulfurococcus*, *Thermosphaera*, *Staphylothermus*, *Aeropyrum*, *Thermodiscus*, and *Igneococcus*. With the advent of newly-found isolates and as-

yet-uncultivated *Crenarchaeota*, the identification of many new families or orders within the kingdom of *Archaea* seems inevitable. Although more are undoubtedly to come, *P. aerophilum* was the first organism to be classified within this group of S° -dependent hyperthermophiles as the exception rather than the rule.

The genus *Pyrobaculum*. The species within the genus *Pyrobaculum* are able to use oxygen, nitrate, nitrite, S° , thiosulfate and sulfite as terminal electron acceptors, making them the most versatile of the hyperthermophiles (Table 1.1). The genus now comprises six species. The first isolated in 1987 were *P. organotrophum* and *P. islandicum*, which are obligate anaerobic S° -respirers (46). Conversely, *P. aerophilum*, isolated in 1993, is classified as a true denitrifier and reduces nitrate to N_2 through respiratory dissimilatory nitrate reduction. It is similar to bacterial nitrate reducers in that it is also a facultative anaerobe. However, unlike bacterial counterparts, aerobic growth occurs only in the presence of 0.3 – 3.0% (w/v) oxygen, and optimally between 0.6 to 1.0%, classifying this organism as a microaerophile (105). The isolation of *P. arsenaticum* in 2000, which is a strict anaerobe able to use arsenate, thiosulfate or S° as electron acceptors (47), was followed in 2001 by the isolation of *P. oguniense*, a facultative aerobe, with the ability to grow aerobically as well as under microaerobic conditions (84). Like *P. aerophilum*, growth under aerobic conditions is inhibited by S° . However, under anaerobic conditions, *P. oguniense* utilizes S° and thiosulfate as electron acceptors (84). The most recently isolated species (2002) within this genus is *P. calidifontis*, and the first to be isolated from a terrestrial hot spring (4). *P. calidifontis* is inhibited by S° under anaerobic conditions and utilizes nitrate as a terminal electron acceptor, like *P. aerophilum*. Unlike *P. aerophilum*, however, *P. calidifontis* is classified as a facultative aerobe, as oppose to a microaerobe, and is able to grow in only low

NaCl concentrations with optimum growth in the absence of NaCl (4). The present body of work focuses on anaerobic respiration, in particular nitrate reduction, in *P. aerophilum*.

During both anaerobic and aerobic growth, *P. aerophilum* is able to utilize complex organic mixtures such as yeast extract, tryptone and peptone, organic acids (propionate and acetate) and inorganics (molecular hydrogen and thiosulfate) as substrates (105). Both nitrate and nitrite serve as electron acceptors during anaerobic growth.

P. aerophilum was isolated in strongly-gassed marine water holes in the tidal zones off of the coast of Ischia, Italy (105). This rod-shaped hyperthermophilic archaeon has a width of approximately 0.6 μm and is 3 to 8 μm in length. It is motile with monopolar flagellation (Fig. 1.2a). Growth temperatures for *P. aerophilum* range from 75 °C to 104 °C, with optimal growth occurring at 100 °C. Growth is maintained over a pH range of 5.8 to 9.0, and optimally at pH 7.0. Cells aggregate and often form raft-shapes during log phase growth (105). Remarkably, during stationary and late log phase or during stress, such as pH above 8.0 or high nitrite concentrations, spherical bodies begin to form at the end of the rods, referred to as ‘golf clubs’ (Fig. 1.2b). Similar patterns have been seen in other species of *Pyrobaculum* and in *Thermoproteus* and *Thermofilum*. Unlike *Thermoproteus* and *Thermophilum* however, continued growth under these conditions can result in completely coccoid cells in *P. aerophilum*.

Nitrogen Cycle and Nitrate Reduction. Nitrate reduction plays a major role as one of the biological processes that sustain the global biogeochemical nitrogen (N) cycle. In simple terms, the global biogeochemical N cycle is the transfer of N species [N(V) to N(-III)] in and out of the atmosphere and between terrestrial and aquatic environments (Fig. 1.3). Nitrogen, a basic element for life as a component of proteins and nucleic acids, is made available through key

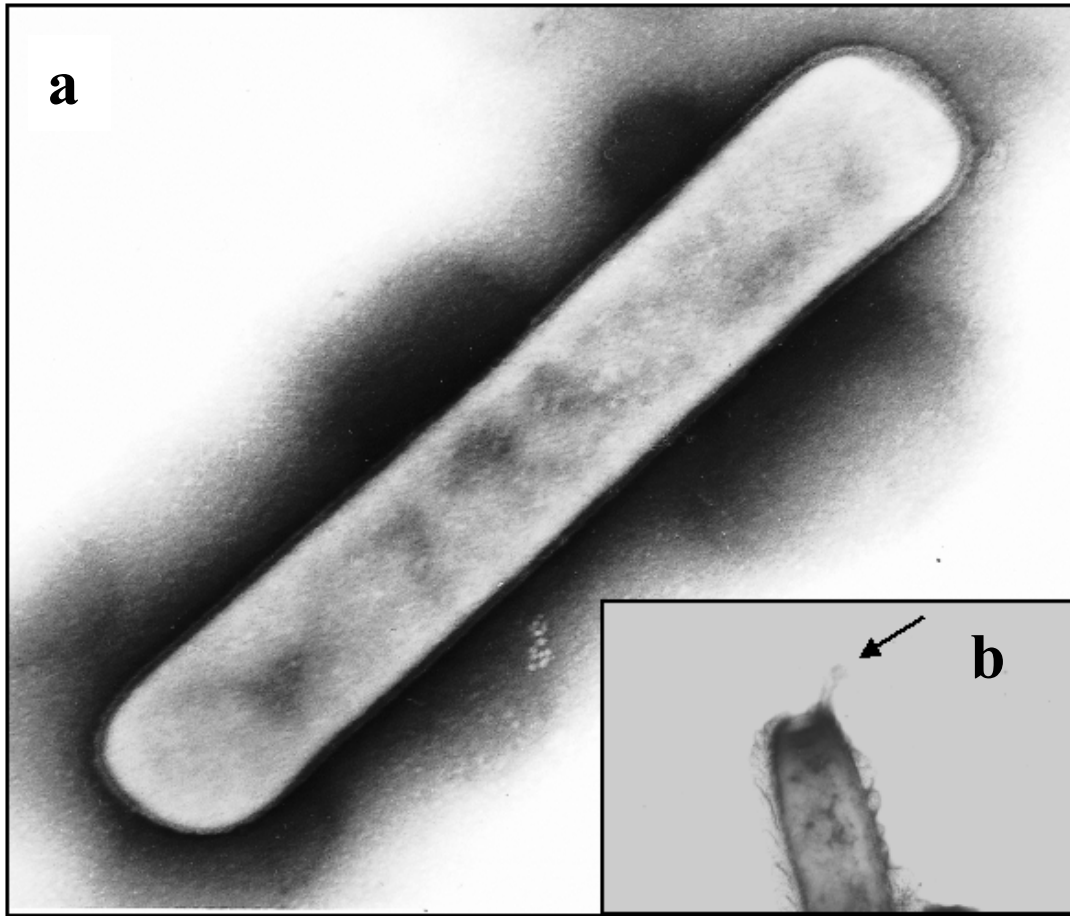


Fig. 1.2. Electron micrograph of (a) *Pyrobaculum aerophilum* in exponential growth phase, and (b) in stationary growth phase. The arrow indicates the spherical bodies that are beginning to form at the end of the rod. These spherical bodies are referred to as 'golf clubs'. Continued growth in stationary phase or under stress conditions will result in the spherical bodies forming completely coccoid cells. Photographs were taken at the Electron Microscopy Laboratory of the University of Georgia by the author, of cells grown and utilized in the current research.

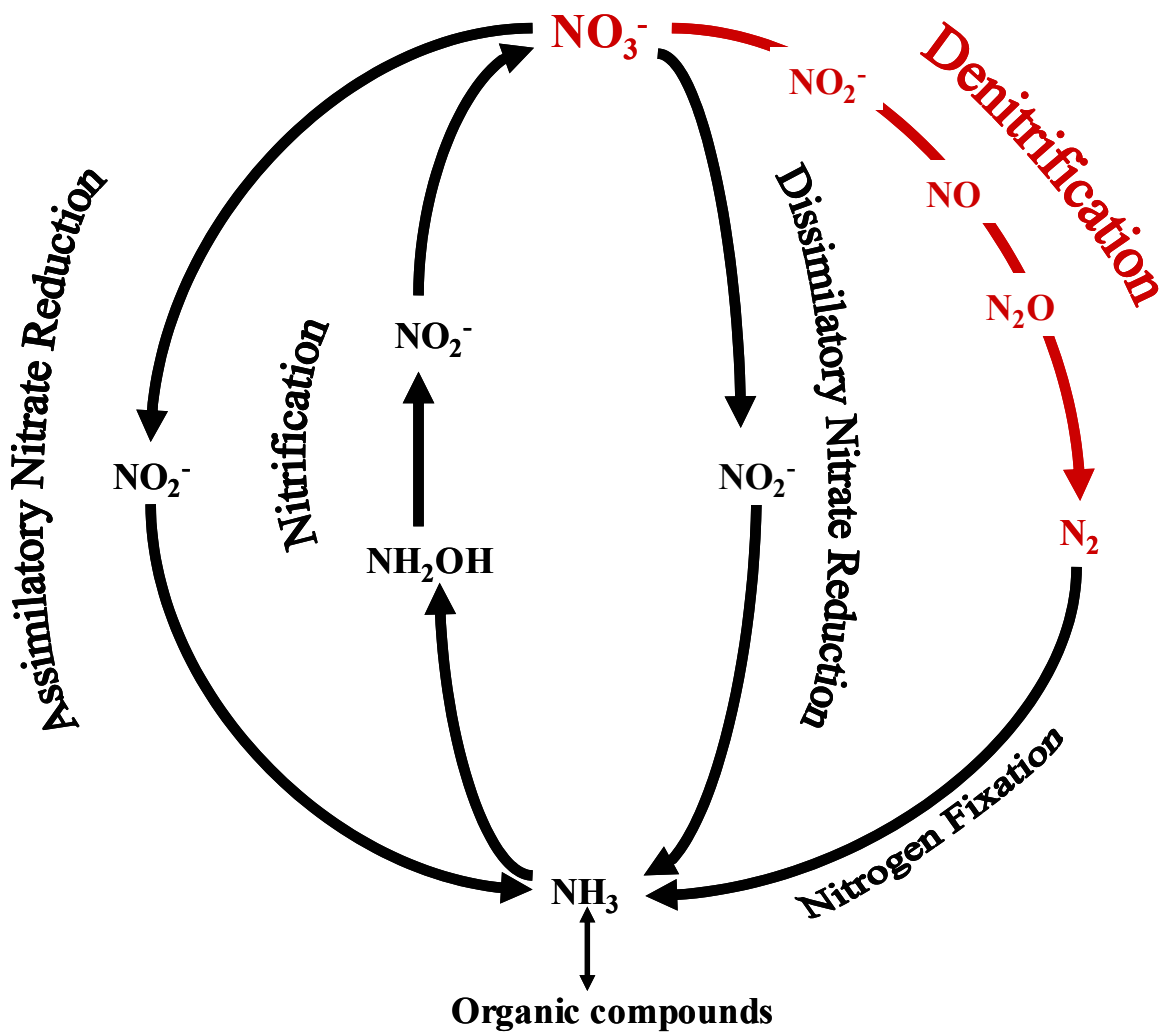


Fig. 1.3. Global biogeochemical nitrogen cycle. Denitrification, the pathway that is the focus of this study, is depicted in red. Figure was adapted from (59).

redox reactions in this cycle that is carried out almost entirely by microorganisms. Transfer of dinitrogen (N_2) from the atmosphere occurs via N_2 fixation ($N_2 \rightarrow 2NH_3$). Fixed nitrogen sources are removed from terrestrial and aquatic habitats via nitrification ($NH_3 \rightarrow NO_2^- \rightarrow NO_3^-$) and denitrification ($2NO_3^- \rightarrow 2NO_2^- \rightarrow 2NO \rightarrow N_2O \rightarrow N_2$). In denitrification, the overall scheme of the reduction of nitrate via nitrite, nitric oxide and nitrous oxide to dinitrogen occurs through respiration. The four terminal oxidases involved in each reaction of these pathways, nitrate reductase (NR), nitrite reductase, nitric oxide reductase and nitrous oxide reductase, are coupled to energy-conserving electron transport.

There are two types of nitrate reduction. One involves N assimilation ($NO_3^- \rightarrow NO_2^- \rightarrow NH_3$), in which nitrate is utilized as a nitrogen source for growth, and the other involves N dissimilation ($NO_3^- \rightarrow NO_2^-$ or $NO_3^- \rightarrow NO_2^- \rightarrow NH_3$). In dissimilation, nitrate is used for redox balancing (nitrite is excreted by the cell or first reduced to ammonia and then is excreted by the cell), or is used as a terminal electron acceptor in respiration as in the case of *P. aerophilum*. When an organism reduces NO_3^- to N_2O or N_2 and this reduction is used as a source of energy and coupled to an increase in growth yield, it can be termed a respiratory denitrifier (62). Denitrification is widespread in bacteria as an anaerobic process of energy conservation, and is found among some archaea, as previously discussed. Traditionally, nitrate respiration is inhibited by the presence of oxygen, but recently facultative anaerobes, such as *Thiosphaera pantotropha* (10), *Escherichia coli* E4 (18), *Paracoccus denitrificans* and *Pseudomonas aeruginosa* (24) have been found to reduce nitrate even in the presence of oxygen. Furthermore, some eukaryotes, in particular fungi and yeast, have been identified as denitrifiers. Interestingly, a low concentration of oxygen (microaerophilic conditions) is needed for intact mitochondria, the site of denitrification in these organisms (104). Studies on the fungus *Fusarium oxysporum*

have shown that solubilization of the mitochondrial membrane renders NR inactive to physiological electron donors, although activity was maintained with artificial electron donors such as methyl viologen, thus indicating that the NR activity is associated with the membrane. Most importantly, formate was found to support the NR mitochondrial activity. This led to the first eukaryotic example of the association of formate dehydrogenase providing electrons to NR in the respiratory chain (104). The coupling of the dissimilatory enzymes formate dehydrogenase and nitrate reductase is common in prokaryotic denitrification. The formate-nitrate reductase respiratory pathway is exclusively membrane-associated and involves quinones as intermediate electron carriers. This enzyme complex catalyzes the oxidation of formate to carbon dioxide coupled with the transfer of reducing equivalents to nitrate in an energy-conserving pathway.

Both formate dehydrogenase and nitrate reductase are the focus of this study. In addition to their coupled role in nitrate respiration, both of these enzymes typically contain the metal molybdoenum. An overview of the enzymes as well as the role of molybdenum, and the related metal tungsten, follows.

Nitrate Reductases. The enzyme responsible for nitrate reduction is nitrate reductase (NR). NR catalyzes a two-electron transfer in the reduction of nitrate to nitrite (Eq. 1).



Six types of nitrate reductases have been identified. The eukaryotic assimilatory nitrate reductase, a cytosolic enzyme which uses pyridine nucleotides as electron donors (65), the

eukaryotic dissimilatory NR previously discussed (104) and four types which are found in bacteria. They are the cytoplasmic assimilatory NR (referred to as Nas), the periplasmic dissimilatory NR (Nap), the membrane-bound respiratory NR (Nar, encoded by *narGHJI* and referred to as NRA) and found in *E. coli* and *Salmonella typhimurium*, a second membrane-bound respiratory NR (encoded by *narZYWV*, referred to as NRZ) (16, 65, 96) (Table 1.2).

NRA is a well-characterized enzyme from bacterial sources and is composed of three primary subunits. The catalytic α subunit, (NarG, 140 kDa), contains a *bis*-molybdopterine guanine dinucleotide (Mo-*bis*MGD) cofactor and a [4Fe-4S] cluster (53). The β subunit (NarH, 60 kDa) contains a [3Fe-4S] and three [4Fe-4S] centers, which function in electron transfer. The membrane-bound γ subunit (NarI, 30 kDa) binds the $\alpha\beta$ complex to the membrane and transfers electrons to it via two heme *b* groups. A fourth subunit, the δ subunit (NarJ, 26 kDa), has not been associated with any purified NR and is assumed to function in either the stabilization or in the assembly of the $\alpha\beta$ complex prior to interaction with the γ subunit (16, 23, 49, 53, 73).

NRZ has many similarities to NRA. Both enzymes have the same subunit composition, with similar molecular masses, and contain the same cofactors. In *E. coli* cells lacking NRA, NRZ catalyzes the same reaction with the same physiological substrates as electron donors. When both enzymes are present, it has been proposed that NRZ assists *E. coli* in the transition from an aerobic to an anaerobic metabolism. Interestingly, NRZ is constitutively expressed, while NRA is produced only during anaerobiosis and the presence of nitrate (16, 49). New contradictory evidence, however, indicates the expression of NRZ is highly dependent on growth phase and is stress-induced (22). These findings illustrate that even in the best studied nitrate reductases, roles that were considered redundant or speculative are in-fact distinctive, and the possibility of additional roles in the cell cannot be ruled out.

Table 1.2. Characteristics of Prokaryotic Nitrate Reductases.^a

Characteristic	Assimilatory		Dissimilatory	
	NO ₃ ⁻ Assimilation		NO ₃ ⁻ Respiration	NO ₃ ⁻ Reduction
Nitrate reductase type	Nas		Nar	Nap
Localization	Cytoplasm		Membrane	Periplasm
Structural genes	<i>nasCA</i> / <i>narB</i> ^b		<i>narGHI/narZYV</i> ^c	<i>napAB</i>
Cofactors	Molybdopterin Fe-S cluster <i>cyt c</i> ^d FAD ^e		Molybdopterin Fe-S clusters <i>cyt b</i> ^d	Molybdopterin Fe-S clusters <i>cyt c</i>
Anaerobiosis	No effect		Induction	Constitutive
Nitrate transport	Yes		Yes	No
Effect of ammonia	Repression		No effect	No effect
Function	Biosynthesis of N compounds		PMF ^f (respiration and denitrification)	Dissipation of reducing power and denitrification
Energy conservation (ATP)	No		Yes	Yes

^a Data from (16, 65).

^b Represents the gene designation for NADH-nitrate reductase in *Klebsiella oxytoca* and ferredoxin-nitrate reductase in cyanobacteria, respectively.

^c Found in *Escherichia coli* and *Salmonella typhimurium*.

^d *cyt c* / *cyt b*, cytochrome *c* and cytochrome *b*.

^e FAD is found only in the NADH-dependent nitrate reductases.

^f PMF, Proton motive force.

Although all NRs are assumed to contain molybdenum (Mo) in their active site, there are exceptions. To date, the exceptions include the two NRs from *Pseudomonas isachenkovii*, one periplasmic and one membrane-bound, and the membrane-bound NRs from *Geobacter metallireducens* and *Thioalkalivibrio nitratirereducens*. The periplasmic NR from *P. isachenkovii* contains vanadium (V) rather than Mo in its active site, and the membrane-bound NR contains neither a metal nor a molybdopterin structure (7). The membrane-bound NR from *T. nitratirereducens* also contains V rather than Mo, but unlike the periplasmic NR from *P. isachenkovii*, it also contains a heme-*c* group and exhibits nitrite reductase activity (8). The NR from *G. metallireducens* also contains no metal in its active site (63). This membrane-bound NR, however, is also atypical in that it is insensitive to tungsten (as might be expected since it lacks Mo), exhibits nitrite reductase activity, and contains a *c*-type cytochrome.

The first crystal structure of a NR was that of the periplasmic NR (NAP) from *D. desulfuricans*, and it was determined to a resolution of 1.9 Å (29). NAP has a molecular mass of 80 kDa and is the simplest of all nitrate reductases in that it contains no hemes or flavins and is a monomeric protein. It does contain a Mo-*bis*MGD and one [4Fe-4S] cluster per mole of protein contained within a single polypeptide chain. Additional structures of NR have now been reported and include the NarGH heterodimer of the integral membrane respiratory NR (53), the structure of NarGHI (12), NarGHI in complex with a quinol binding inhibitor (11). In addition, the structure of the nitrate-inducible formate dehydrogenase (Fdh-N) (54) from *E. coli* has been reported. These have provided molecular details of the formate-nitrate respiration chain in *E. coli*. Details of these structures and a model of this respiration pathway are discussed in detail at the end of this chapter.

Formate Dehydrogenases. Like nitrate, formate can play two roles inside a cell, that of a nutrient as well as a component of redox reactions for energy conservation. Specifically, formate can serve as a carbon source via the reduction of CO₂, or as an electron donor via the production of CO₂. The versatile metabolic role of formate by its interconversion with CO₂ is catalyzed by the enzyme formate dehydrogenase (FDH) (Eq2). A variety of FDHs have been found in both eukaryotes and prokaryotes, and in aerobic and anaerobic organisms. They are a heterogeneous group of enzymes. In aerobic organisms, FDH is primarily dependent on NAD as an electron carrier, but in anaerobes, FDHs typically contain a complex group of redox centers and are extremely sensitive to oxygen.



Studies in the 1950s through the early 1970s clarified the role of FDH in metabolism and gave indications of the metal content of the enzyme, but all of these studies were determined on partially purified fractions. It was not until 1975 (32) that the molecular characteristics of a FDH were defined, when a highly purified enzyme was obtained from *E. coli*. The *E. coli* cells were grown anaerobically in the presence of nitrate. Due to similarity in charge and size, FDH and NR co-purified in the initial steps of the purification. The purified FDH contained three subunits in the ratio of $\alpha_4\beta_4\gamma_2$, with a total molecular weight of 608 kDa ($\alpha=110$ kDa, $\beta=32$ kDa and $\gamma=20$ kDa). The enzyme also contained Mo, heme, non-heme iron, and Se. Formate is produced in anaerobically growing *E. coli* cells from the CoA-dependent cleavage of pyruvate by the pyruvate formate-lyase enzyme (57). When nitrate is present in these anaerobically growing cells, a formate-nitrate respiratory chain is synthesized (85).

Following from pioneering research conducted in the early 1950s, by Peck and Gest (72), three genetically distinct FDH isozymes have now been identified in *E. coli* (35, 86). Named according to the optimal growth condition for induction, they are FDH-O, which is synthesized in the presence of oxygen or nitrate, FDH-N, which is induced by nitrate and anaerobic conditions, and FDH-H, which is induced during fermentation. All three enzymes contain Mo, Se, and Fe-S centers. The FDH purified in the initial studies in the 1970s was FDH-N (32). Much less is known biochemically about the FDH-O isozyme. It has been reported to be present when cells are grown aerobically, and that it has a selenopolypeptide with a molecular weight of 110 kDa. It has been suggested that its structure is very similar to FDH-N (85).

Role of Molybdenum and Tungsten. Mo and W are both group VI transition metals and are the only members of the second and third transition series with known biological function. While most organisms (bacteria, archaea, fungi, plants and animals, including humans) are dependent on Mo for their existence, only hyperthermophilic archaea are known to require W. These requirements for the two metals stems from their presence in the active sites of metalloenzymes. Mo-containing enzymes have a critical part in the global nitrogen and sulfur cycles, and both molybdo- and tungstoenzymes have roles in the anaerobic portions of the global carbon cycle.

Chemistry and Abundance in the Environment

Mo and W share are very similar chemically. Their atomic radii (1.40 Å) and their ionic radii (0.68Å) are identical, and their electronegativity is similar (1.4 for W and 1.3 for Mo). Furthermore, the coordination chemistries of W and Mo are analogous. Although both elements

can be in oxidation states -II to +VI and are able to form polynucleotide complexes, only oxidation states +IV to +VI are biologically accessible. The redox potential of Mo complexes are always more positive than those of the analogous W complex, since the W complex is significantly more stable at the higher oxidation state than its Mo counterpart. The most stable oxidation state for W is W(VI). Due to the presence of the V valence state, however, Mo and W can catalyze two-electron and one-electron oxidation-reduction reactions in biological systems.

Although the abundance of Mo and W in nature is equal in the earth's crust (15 g/metric ton), Mo is the most abundant transition metal in the oceans. The concentration of Mo in seawater is approximately 11 $\mu\text{g/L}$; which is about two orders of magnitude higher than the concentration of W (0.12 $\mu\text{g/L}$). Most significantly, however, the abundance of W in hyperthermophilic environments such as hot springs (15-300 $\mu\text{g/kg}$) and vent flanges (180-585 mg/kg) is far greater than that of Mo (3-60 $\mu\text{g/kg}$ and 47 mg/kg , respectively) (95). Under aerobic conditions, Mo and W compete for uptake in the cells and in the binding sites within enzymes as they are principally in the forms of molybdate and tungstate (MoO_4^{2-} and WO_4^{2-}). Under anaerobic conditions, however, Mo can be reduced to Mo(V) or (IV) and coordination with sulfur is likely (especially in the marine environment where levels of sulfur are high). The dominant form of Mo under these conditions is MoS_2 , which is insoluble, rendering Mo essentially unavailable to cells. Low-valent W sulfides, however, are more soluble in an aqueous solution, and therefore play an important role in biology in anaerobic highly reducing environments, like those of early Earth (40, 102). It is thought that the role of W and Mo in biological systems began to change, however, with the cooling of the Earth's crust and with the development of oxygenic photosynthesis more than 3.5 billion years ago, and specifically with the accumulation of oxygen in the atmosphere between 1 and 2 billion years ago (92). In the

presence of an aerobic atmosphere, insoluble MoS_2 would be oxidized to soluble MoO_4^{2-} and would be readily available for cellular uptake and incorporation into enzymes. Furthermore, not only is Mo more suitable for the more positive redox reactions present in aerobic organisms, the analogous W compounds are typically oxygen sensitive (52).

Molybdenum, Tungsten and Pterin

The catalytic site of both Mo- and W-containing enzymes (with the exception of nitrogenase) contains one atom of the metal and an organic moiety called pterin. The pterin cofactor was first identified in 1982 by Johnson and Rajagopalan (77) using fluorescence and mass spectroscopy after estimation from a number of molybdoenzymes. More than a decade later the first structural determination of the pterin cofactor, previously referred to as molybdopterin (MPT) or Moco, was evident from the crystal structure of the aldehyde ferredoxin oxidoreductase (AOR) from *Pyrococcus furiosus* (21). The structure of this tungsten-containing enzyme illustrated that the metal atom, in this case W, is coordinated by dithiolene sidechains as originally proposed by Rajagopalan (76). There was one significant difference, however, in that the cofactor has a tricyclic structure as opposed to the bicyclic structure as originally thought (Fig. 1.4). To date, there are over 50 known enzymes that contain molybdopterin (41). The core of the pterin structure is conserved in all organisms examined, and within this wide range of organisms, the biosynthesis of the pterin cofactor is accomplished via a pathway consisting of at least twelve gene products (64).

The role of the pterin cofactor in the reaction mechanisms of the mononuclear molybdo- and tungstoenzymes is unclear. While the pterin is an indispensable component of the metal center in these enzymes, and in many cases constitutes the only means by which the poly-

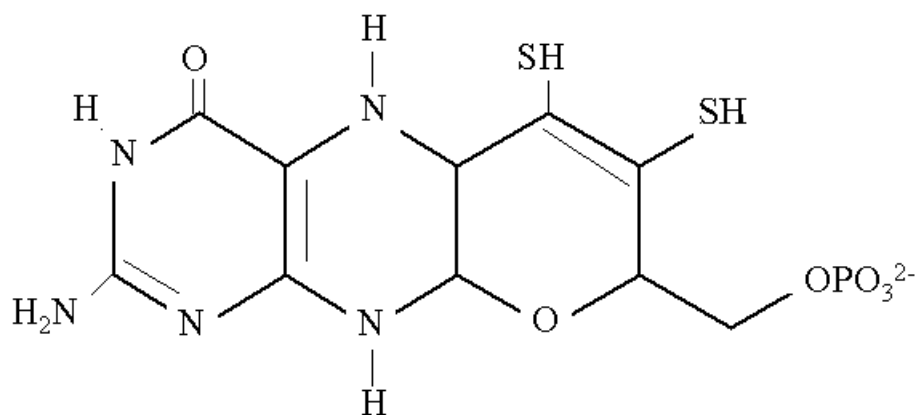


Fig. 1.4. Structural model of the pyranopterin cofactor. The structure is that of the tungsten center revealed in the crystal structure of AOR from *P. furiosus* (21), and is found in other W-containing and Mo-containing enzymes. Figure was adapted from (51).

peptide binds and retains the Mo or W center; it is very unlikely that the pterin itself participates directly in catalysis. This is because, in many cases, the pterin structure is deeply buried, and is not exposed to the channel in which the substrate enters the catalytic site. However, based on the structure of xanthine oxidase-related aldehyde oxidoreductase from *Desulfovibrio gigas* (78), two roles for the pterin related to catalysis have been postulated. First, the cofactor may have a role in the pathway of electron transfer into or out of the metal center once it has been reduced by the substrate, and second, the cofactor may play a part in modulating the properties of the metal center, in particular, its reduction potential.

In molybdoenzymes from eukaryota, the pterin cofactor has a terminal phosphate on the pterin sidechain (Fig.1.4), while in prokaryotic enzymes, the pterin cofactor usually has a dinucleotide of either cytosine, guanine, adenosine or inosine on the sidechain. This is not true, however, for the majority of tungstoenzymes, which so far have only been characterized from prokaryotes. The pterin structures of W-containing enzymes that have been characterized so far contain pterin cofactors without a dinucleotide, except for the formylmethanofuran dehydrogenase (FMDH II) from *Methanobacterium wolfei* (89) and the acetylene hydratase (AH) from *Pelobacter acetylenicus* (79).

Classification of Molybdoenzymes. Based on their catalytic properties, active site structures and amino acid sequences, molybdoenzymes can be categorized into three distinct families. They are the molybdenum hydroxylases (the xanthine oxidase family), the eukaryotic oxotransferases (the sulfite oxidase family), and the prokaryotic oxotransferases (the DMSO family) (Table 1.3) (30, 42, 110). A brief and general description of the molybdenum

hydroxylases and the eukaryotic oxotransferases follows along with a more detailed account of the prokaryotic oxotransferases, as the two enzymes of this study fall into this family.

The Molybdenum Hydroxylases - Xanthine Oxidase Family

The molybdenum hydroxylases, represented by xanthine oxidase, catalyze the hydroxylation of carbon centers of a diverse range of aldehydes and aromatic heterocycles. Carbon monoxide dehydrogenase, a member of this family, is an exception, as it oxidizes CO to CO₂. These enzymes use water rather than dioxygen as the source of oxygen, which is incorporated into the product. Furthermore, the electrons that are generated, rather than consumed, are transferred to various external acceptors. These enzymes contain one pterin cofactor coordinated to Mo, which in the oxidized form is MoOS(OH) (Table 1.3). In addition to the Mo, all of the enzymes in this family have various redox-active centers, such as Fe-S clusters and flavins (30, 42).

The Eukaryotic Oxotransferases - The Sulfite Oxidase Family

The family of eukaryotic oxotransferases includes sulfite oxidase, which is ubiquitous among animals, and the assimilatory nitrate reductase, which is found in fungi, algae and higher plants. These enzymes catalyze the net transfer of oxygen to or from a lone pair of electrons on the substrate. In the Mo hydroxylases, there is also a single pterin cofactor in the active site coordinated via its dithiolene side chain, but in this family, the coordination is to a Mo^{IV}O₂(S-Cys) component (Table 1.3). Both sulfite oxidase and assimilatory NR possess redox-active centers in addition to Mo in the form of a heme domain, specifically a *b*-type cytochrome. These

Table 1.3. Molybdenum Enzyme Families.[¶]

Enzyme Family	Examples	Active site Structure [¶]
Molybdenum Hydroxylases	Xanthine oxidase Xanthine dehydrogenase Aldehyde oxidase Aldehyde oxidoreductase Quinoline-2-oxidoreductase Nicotinic acid hydroxylase NADH - formate dehydrogenase CODH ±	
Eukaryotic Oxotransferases	Sulfite oxidase‡ Sulfite oxidoreductase‡ Assimilatory nitrate reductase	
Prokaryotic Oxotransferases	DMSO reductase* Nitrate reductase Formate dehydrogenase TMAO reductase§ Polysulfide reductase Formylmethanofuran dehydrogenase Arsenite reductase	

[¶]Data from (30, 41, 42). Structures were created using ChemDraw.

± CODH, carbon monoxide dehydrogenase. The significant differences in the active site of this enzyme, the presence of MoO₂ instead of MoOS and a selenylcysteine residue, set this protein apart. Yet, the overall homology of the structure is consistent.

‡ Both enzymes are found in vertebrates and plants.

* DMSO reductase, dimethyl sulfoxide reductase

§ TMAO reductase, trimethylamine-N-oxide reductase

domains are homologous in the enzymes but the position of the heme domain is N-terminally located to the Mo-binding portion of sulfite oxidase and C-terminally located in NR. Assimilatory NR also utilizes FAD as an additional redox-active center (30, 42).

The Prokaryotic Oxotransferases - The DMSO Reductase Family

Dissimilatory nitrate reductase and formate dehydrogenase are members of the third family of Mo-containing enzymes, the prokaryotic oxotransferases. Enzymes in this family primarily catalyze reactions involving oxygen-atom transfer and dehydrogenation. This family is the most diverse of the three, both in structure and in function. DMSOR is used as the primary representative of this family of molybdoenzymes as its crystal structure was the first to be determined, using the enzyme from *Rhodobacter sphaeroides* (87). Two significant differences in catalytic site structure are evident between the DMSO family and the xanthine oxidase and sulfite oxidase families. First, unlike the other two families, the active site of the prokaryotic oxotransferases contains two pterin cofactors, termed bispterin, bound to the metal. The coordination of the Mo with the two pterins is usually completed with a single Mo=O group and a sixth ligand that can be either a serine (DMSO), cysteine (NR), selenocysteine (FDH-H) or a hydroxide and/or water molecule (arsenite oxidase), rendering the configuration Mo^{IV}O (ser, cys, Se-cys, -OH) (Table 1.3) (40, 42). Second, and most interestingly, three enzymes in this family, DMSOR from *Rhodobacter* (87), and trimethylamine-N-oxide reductase (TMAOR) (58) and biotin sulfoxide reductase (74) from *E. coli*, possess a Mo center as their sole redox-active site. *E. coli* DMSOR, however, utilizes Fe-S clusters that are located in another subunit (106). Further, NR and FDH have Fe-S centers located in the same polypeptide as the Mo (17, 29).

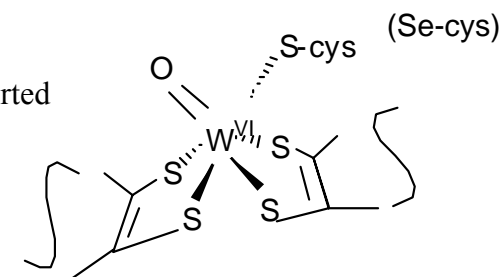
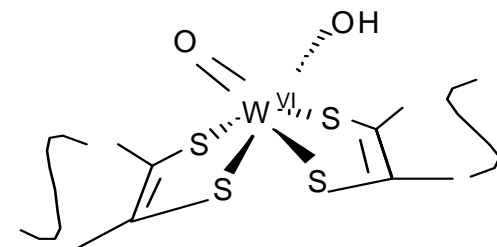
Classification of Tungstoenzymes. "True" W-containing enzymes or tungstoenzymes are defined here as those that are inactive when Mo replaces W. In 1983, the first active enzyme with W as a natural component, FDH from *C. thermoaceticum*, a thermophilic bacteria, was reported (113). Such tungstoenzymes are found in many types of prokaryotes, but they are not ubiquitous, and have yet to be identified in a eukaryote. Tungstoenzymes have been isolated from gram-positive and gram-negative bacteria, sulfate-reducing bacteria, methanogenic archaea and hyperthermophilic archaea. Interestingly, all of the W-containing enzymes identified to date are from anaerobic microorganisms and all are cytosolic; none has been isolated from membranes. Currently, there are more than a dozen known tungstoenzymes, and they can be divided into three general classes based on phylogenetic and functional differences (Table 1.4) (52). They are the aldehyde ferredoxin oxidoreductase (AOR) family, the formate dehydrogenase and formylmethanofuran dehydrogenase (F(M)DH) family and the acetylene hydratase (AH) family.

The AOR family

Members of the AOR family of W-containing enzymes include three ferredoxin-dependent oxidoreductases, termed AOR, FOR and GAPOR. They have been isolated from species belonging to the hyperthermophilic archaea *Pyrococcus*, and *Thermococcus* (66-68, 70), AOR from *P. aerophilum* (37) and two mesophilic enzymes, carboxylic acid reductase (CAR), found in *Clostridium thermoaceticum* (109) and *C. formicoaceticum* (107) and aldehyde dehydrogenase (ADH) from *D. gigas* (39) (Table 1.4). AOR from *P. furiosus* is the most extensively studied tungstoenzyme, and is the first W- and the first pterin-containing enzyme for which a crystal

Table 1.4. Tungsten Enzyme Families.

Family / Enzyme	Organism	Metal Content /Cofactor §	Structure†
AOR Family			
AOR	<i>P. furiosus</i> <i>Pyrococcus</i> sp. ES-4 <i>Thermococcus</i> sp. ES-1 <i>D. gigas</i>	2 W / 2 [4Fe-4S] / 1 Fe / 1Mg	MPT
FOR	<i>P. aerophilum</i> <i>P. furiosus</i> <i>T. litoralis</i>	2 W / 2 [4Fe-4S] 4 W / 4 [4Fe-4S]	MPT MPT
GAPOR	<i>P. furiosus</i>	1 W / 1 [4Fe-4S]	MPT
CAR I	<i>C. thermoaceticum</i>	1 W / ~29 Fe / ~25 S	MPT
CAR II	<i>C. thermoaceticum</i>	3 W / ~82 Fe / ~54 S / FAD	MPT
CAR	<i>C. formicoaceticum</i>	2 W / ~11 Fe / ~16 S	MPT
ADH	<i>D. gigas</i>	2 W / 2 [4Fe-4S]	Not Reported
F(M)DH Family			
FDH	<i>C. thermoaceticum</i> <i>D. gigas</i>	2 W / 20-40 Fe / 2 Se 1 W / 4 [4Fe-4S]‡	Not Reported MGD
FMDH II	<i>M. wolfei</i>	1 W / 2-5 Fe	MGD
FMDH II	<i>M. thermoautotrophicum</i>	1 W / ~ 8 Fe	MGD
AH Family			
AH	<i>Pelobacter acetylenicus</i>	1 W / 1 [4Fe-4S]	MGD Not Known



§ The metal content is per mole of enzyme. The abbreviations are: MPT molybdopterin, MGD molybdopterin guanine dinucleotide.

† Data from (52, 56). Note that the exact coordination of the metal site is not known. Structures made using ChemDraw.

‡ The large subunit contains one [Fe₄S₄], the small subunit contains three [Fe₄S₄], and potentially a fourth.

structure was determined. The AOR family of enzymes is distinct in that they exhibit high sequence similarity with each other, yet none of these enzymes are homologous (at the amino acid sequence level) to any known molybdoenzyme. This includes Mo-AOR, which is a Mo-containing CAR produced when *Clostridium formicoaceticum* is grown with Mo rather than W (108). AOR, FOR and GAPOR catalyze the oxidation of aldehydes to carboxylic acids, with the reducing equivalents being transferred to ferredoxin. CAR and ADH catalyze the same type of reaction but their physiological electron acceptors are not known. As the names of the enzymes indicate, they differ in their substrate specificities and in their roles in metabolism. The active site of AOR has a W atom symmetrically coordinated with four dithiolene sulfur atoms from two pterin cofactors (bispterin) that are bound to each subunit of the dimer and an oxo ligand. No ligand is contributed by the polypeptide (21). The exact type of ligands near the W atom is not known. It has been suggested (40) that in the oxidized form, there is most likely one $W^{VI}=O$ and one $W^{VI}-OH$, which is similar to the molybdoenzyme, arsenite oxidase (Table 1.4).

The F(M)DH Family

The second family of tungstoenzymes includes the formate dehydrogenases from *Clostridium thermoaceticum* and *Desulfovibrio gigas* and the formylmethanofuran dehydrogenases (FMDH) from *Methanobacterium wolfei* (13) and *M. thermoautotrophicum* (89). Physiologically, both of these enzymes reduce CO_2 , FDH to formate and FMDH to *N*-formylmethanofuran. Another difference between this family and the AOR family, in addition to the fact that both enzymes utilize the same substrate, is that both enzymes have amino acid sequence similarity to their Mo-containing counterparts. In fact, these enzymes not only have sequence similarity to FDH, but also to dissimilatory NR. FDH from *C. thermoaceticum*, the first tungstoenzyme to be isolated

and characterized (6, 113), uses NADP as an electron acceptor (Eq. 3) and like most anaerobic FDHs, is extremely oxygen sensitive.



The second W-containing FDH that has been isolated and characterized is from *D. gigas* (3) (Table 1.4). This FDH is quite different from the first W-containing FDH. Specifically, although activity is lost in the presence of air, the enzyme is stable, and most importantly activity can be restored under anaerobic conditions. Interestingly, even when *D. gigas* is grown in a Mo-containing medium, the FDH maintains its W center, and yet another enzyme that contained W, aldehyde oxidase, under these conditions becomes a Mo-containing enzyme. The active site of FDH from both *C. thermoaceticum* and *D. gigas* is located in the alpha subunit. Both are heterodimers, with two W per holoenzyme, but *C. thermoaceticum* also contains selenium in the form of a selenocysteine.

The second member of this family of W-containing enzymes is FMDH (Table 1.4). FMDH catalyzes the first step of a multi-step process in the conversion of CO₂ to methane in methanogens. This first step is the reversible formation of *N*-formylmethanofuran from CO₂ and methanofuran. The formyl group generated by FMDH is further reduced to methane in methanogenesis via a complex series of enzymatic reactions utilizing various cofactors that are in large part unique to methanogens (52, 56). As with FDH, FMDH is specific for CO₂ as the carbon substrate, yet unlike FDH, the physiological electron donor is unknown. FMDH is typically a molybdoenzyme, but the FMDHs from *Methanobacterium wolfei* and *M. thermoautotrophicum* contain one Mo-containing FMDH (FMDH I) and one W-containing

FMDH (FMDH II). As discussed above, the expression of these two forms of FMDH differs when the organisms are grown in the presence of either W or Mo.

The AH Family

Acetylene hydratase (AH) is the only member of this third family of tungstoenzymes. The enzyme catalyzes the conversion of acetylene to acetaldehyde through a hydration reaction. The enzyme has only been purified from *Pelobacter acetylenicus*, an anaerobic acetylene-utilizing bacterium (79). The enzyme is a monomer containing one W coordinated to a MGD and one Fe₄S₄ cluster (Table 1.4). The justification for this third family of tungstoenzymes is two-fold. First, although AH is similar to AOR in its molecular properties, there is no sequence similarity between AH and any known W- or Mo-containing enzyme. Second, the enzyme catalyzes a hydration reaction, which is in contrast to the oxidation and reduction reactions of all other tungsto- and molybdoenzymes. The physiological electron donor for AH is unknown and it has not been characterized spectroscopically. It is known, however, that AH is catalytically active only in the presence of strong reducing agents. This lends to supposition that the initial reaction might involve reduction of acetylene, followed by hydration and then oxidation, involving the W and the FeS cluster in the enzyme (79).

Mo- and W-substituted enzymes. The role of Mo in biological systems has been known for over 70 years (103), and W has been utilized as an antagonist of Mo in biological function experiments. Mo is found in enzymes involved in both aerobic and anaerobic reactions exhibiting catalytic function over a wide biological range. Although ubiquitous in biological systems, these complexes are less stable at high temperature than are W complexes (52, 56).

Further, W complexes generally react more slowly and have reduction potentials 300-400 mV lower than their Mo counterparts have (52). Coupled with the fact that reduced W complexes are very sensitive to oxygen (52), it becomes easy to see why naturally occurring, W-utilizing organisms are limited in biological systems, and so far have been identified only in microorganisms that live in high temperature anaerobic environments.

In 1973, the first W-stimulated growth of a microorganism was reported with *Clostridium thermoaceticum*, a thermophilic bacterial anaerobe (5). When *C. thermoaceticum* cells were grown on W, FDH activity was higher than when cells were grown on Mo. Interestingly, FDH activity was the highest when cells were grown on both W and Mo. It was proposed that Mo actually increased the incorporation of W into the active enzyme (5). A decade later, the first active enzyme with W as a natural component was reported, FDH from *C. thermoaceticum* (113). This finding is especially relevant to the current research, as growth of the hyperthermophilic archaeon, *Pyrobaculum aerophilum*, at hyperthermophilic temperatures (98 °C) was inhibited by equal concentrations of Mo and W present in the medium (Chapter 2), yet growth of *P. aerophilum* at thermophilic temperatures (78 °C) was enhanced in the presence of both W and Mo (Chapter 2).

E. coli cells grown in the presence of tungstate produce inactive forms of both NR and FDH (93). In the same study, it was shown that both enzymes could be subsequently activated upon the incubation of cells with molybdate. Further studies with *E. coli* illustrated that in the presence of tungstate, normal amounts of an inactive demolybdo-form of NR were produced that was not only stable but also identical to the Mo-containing active form in subunit composition (34). The lack of intracellular Mo had an adverse effect on FDH, in that production and stability of the functional enzyme was greatly decreased, and in the presence of tungstate, the α subunit

was either not produced at all or was very unstable rendering an atypical subunit composition (34). Thus, in *E. coli*, the absence of Mo and/or the presence of W result in no insertion of Mo into either NR or FDH. Furthermore, the presence of Mo is far more essential for the production and stability of functional FDH than for NR, as it was shown that in the presence of W the FDH α subunit was either not produced or was very unstable (34).

Numerous other studies have been conducted that focused on the replacement of W with Mo into the active site of enzymes. Most relevant are studies of dimethylsulfoxide reductase (DMSOR) from *Rhodobacter capsulatus*, (101), and the trimethylamine N-oxide reductase (TMAOR) from *E. coli* (19), both of which exhibit catalytic activity with W or Mo at the active site. TMAOR from *E. coli*, which is a molybdoenzyme that catalyzes the reduction of TMAO to trimethylamine (TMA) with a redox potential of +130 mV, is also active as a tungsto-TMAOR (19). This is the first example of W replacing Mo in an enzyme that is functional at catalyzing reactions at a high redox potential. Thus, the W-TMAOR is capable of catalyzing the reduction of TMAO to TMA with a redox potential of +130 mV, although it is kinetically slower than the Mo-TMAOR (a decrease in k_{cat} of $\sim 50\%$), catalytic efficiency was increased approximately two-fold (19). Furthermore, the substitution of W for Mo in TMAOR resulted in a change in substrate specificity of the enzyme. The Mo-TMAOR can only utilize TMAO as a substrate, but the W-TMAOR can also utilize DMSO, which is reduced to DMS with a redox potential of +160 mV (Mo-DMSOR, a homologous enzyme, can utilize both substrates) (19). The changes in substrate specificity of the W-TMAOR is most likely based on small structural changes in the active metal center, and thus in the substrate binding site and nature of the metal center, and secondly, on changes in the coordination of the Mo and W by pterins (19). To the contrary, there are no significant changes in the structure of the protein and the nature of the binding site when

W is substituted for Mo in DMSOR from *R. capsulatus*, (38, 101). Moreover, the W-DMSOR catalyzes the reduction of DMSO to DMS ($E_o' +160$ mV) approximately 17 times faster than the Mo-DMSOR, but in contrast to Mo-DMSOR cannot catalyze the oxidation of DMS to DMSO (38, 101). Thus, the differences in the redox potentials of Mo- and W-containing enzymes and the reactions that they catalyze illustrate the variability of organisms that use Mo, those that use W and those that are able to use both.

Another and a most interesting example of the usage of W vs. Mo in the active site of enzymes can be found in the methanogens *Methanobacterium wolfei* and *M. thermoautotrophicum*, in which case each of the organisms contain two distinct formylmethanofuran dehydrogenases (FMDH). FMDH I is the Mo-containing isozyme, while FMDH II contains W. The α and β subunits are identical in the two enzymes, but molecular weights for the γ subunit differ. Their catalytic properties differ in that FMDH I exhibits optimal activity at a higher pH than FMDH II (pH 7.9 vs. 7.4), and has no activity at a pH (pH 6.5) at which FMDH II still maintains 70 % of its activity (13, 89). In both organisms, the W-isozyme is constitutively expressed, while the Mo-isozyme is induced by molybdate (43). The organisms themselves differ in expression of FMDH I and II in response to changes in concentration of W and Mo in the growth medium. In *M. wolfei*, only FMDH I is expressed if cells are grown on Mo only, and both FMDH I and FMDH II are expressed in active and W-containing forms when cells are grown on W only. Moreover, in *M. thermoautotrophicum*, the opposite is true. FMDH I and FMDH II are both expressed, contain Mo and are active in cells grown in the presence of Mo only, but in W-grown cells, only the W-containing FMDH II is expressed (13, 89).

On the other hand, *Pyrococcus furiosus*, a W-dependent hyperthermophilic archaeon, was grown in a medium containing only added Mo in order to replace the W in three previously

characterized tungstoenzymes, aldehyde ferredoxin oxidoreductase (AOR), formaldehyde ferredoxin oxidoreductase (FOR), and glyceraldehyde-3-phosphate ferredoxin oxidoreductase (GAPOR). However, Mo did not replace W in these enzymes, and very low levels of activity were still detected. This activity was attributed to the residual W present in the enzyme that originated from the contaminating W content present in the growth medium (69).

These studies illustrate that the inability of pterin-containing molybdo- and tungstoenzymes to form active enzymes varies with the organism and the enzyme involved. It might reflect on the organism's ability to take up and incorporate the metal, but more likely is due to the differences in the chemical properties of the specific W and Mo active sites. These might include redox potential and stability at high temperature. Furthermore, combined with detailed structural, spectroscopic and kinetic data, these metal substitution studies will help to understand the roles in biological systems that W and Mo have today and have had throughout evolution.

Crystal Structures and Model of Formate-Nitrate Respiration in *E. coli*. The most well-studied and defined formate-nitrate respiration pathway is that from *E. coli*, and as such, serves as the model system for other organisms, in this case *Pyrobaculum aerophilum*, for studies focusing on this respiration pathway in general, and the primary enzymes, NR and FDH. Detailed structural data, such as the crystal structures of the respiratory NR and FDH from *E. coli*, thus help in more clearly defining the nitrate respiratory pathway in prokaryotes, but also in the understanding of the roles that Mo plays in the catalytic activity. The recent determination of the structures of NarGH (53), NarGHI (12), and NarGHI in complex with a quinol binding inhibitor (11) from *E. coli* have demonstrated for the first time, the presence of a [4Fe-4S] cluster

and the coordination of the Mo ion in the catalytic domain. Furthermore, the chain of electron transfer in NR is confirmed. In conjunction with the recent determination of the structure of *E. coli* FdhGHI (54) the overall characterization of the formate-nitrate respiratory chain in *E. coli* has been elucidated at the molecular level.

Crystal Structure of NarGHI

The NarGHI heterotrimer is significantly larger than any previously solved enzyme containing a Mo-*bis*MGD, with dimensions of 128 Å along the electron transfer chain, and 80 Å along the membrane perpendicular in monomer form (53) or 143 Å in dimer form. The enzyme appears in dimer form in the bacterial membrane *in situ*. The formation of the dimer, however, does not seem to have a mechanistic role as the closest distance between the redox centers of the two electron transfer chains in the complexes is ~ 33 Å (12) (Fig. 1.5).

Stability of the heterotrimer is provided through interactions between cytoplasmic subunits NarG and NarH that have a buried interface of ~ 11,500 Å and further through the integral membrane NarI subunit, which anchors the NarGH subunit to the membrane, with a primarily hydrophobic interface with both subunits (12). A phosphatidylglycerol molecule that is bound in a pocket formed by residues from all of the subunits contributes to even further stabilization of NarGHI. Interaction between the subunits, however, is centered on the N-terminal tail of NarG (Fig. 1.5). This unique feature of NarG is comprised of two α -helices separated by a β -hairpin. The longer of the two helices is completely engulfed by NarH, and the β -hairpin hydrogen bonds with the β -strand of the C-terminal of NarI. A β -hairpin from NarH joins with the β -hairpin from NarG and the β -strand from NarI to form a twisted β -sheet with extensive interactions between all three subunits through main chain hydrogen bonding (12).

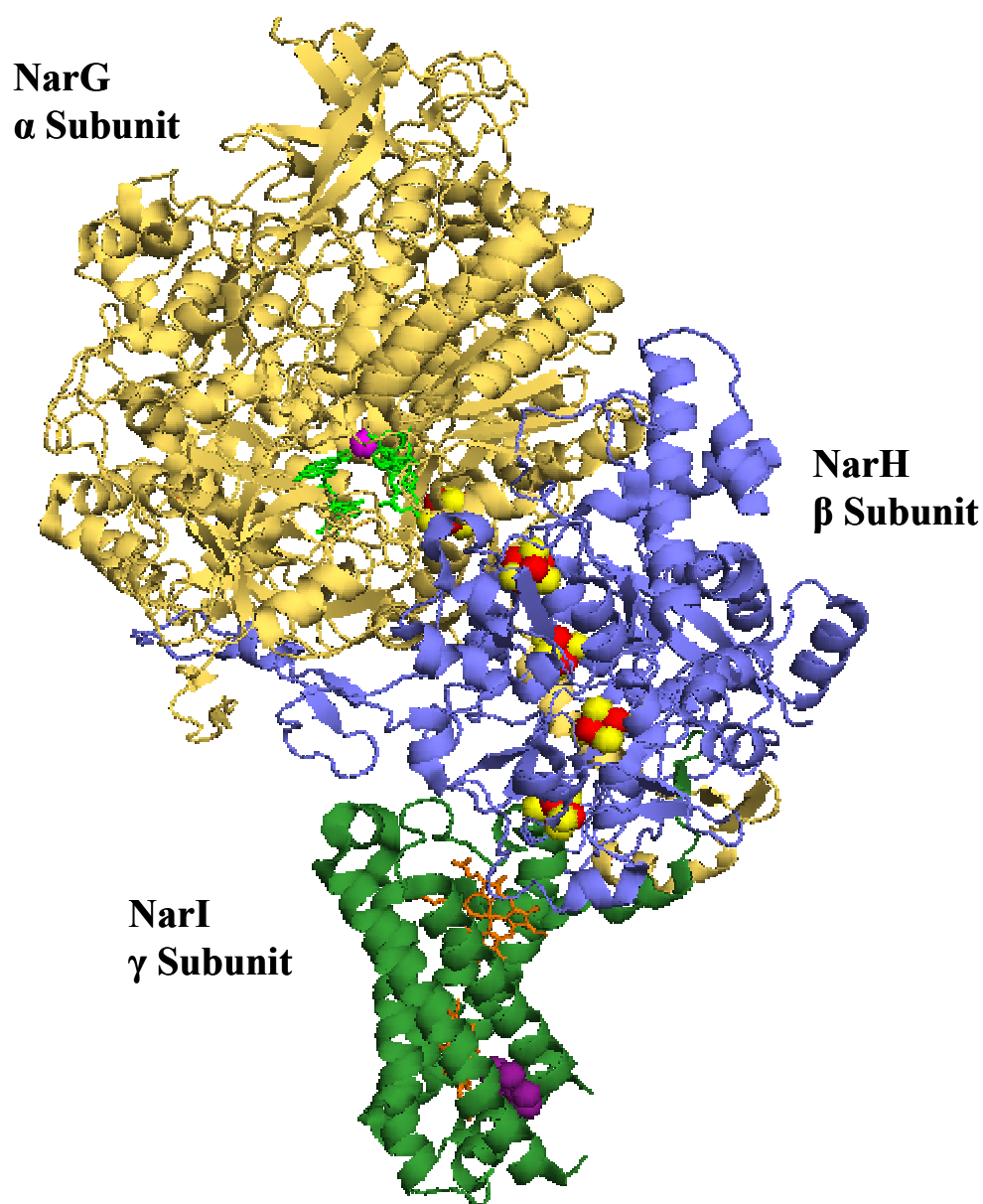


Fig. 1.5. The Crystal structure of the respiratory nitrate reductase Nar from *E. coli*. The structure was resolved at 1.9 Å (12). The α , β , and γ subunits are shown in gold, blue and forest green, respectively. Heme groups and MGD cofactors are shown in orange and green, respectively. Mo is shown in magenta and pentachlorophenol (PCP, a menaquinone analog and potent enzyme inhibitor) in purple. The four [4Fe-4S] and the [3Fe-4S] clusters show Fe atoms in red and S atoms in yellow. The figure was generated using PyMol from coordinates deposited in the Protein Data Bank (accession code 1Q16).

The structure of NarG is similar, albeit larger, to other members of the DMSO reductase family whose structures have been solved recently, including the previously mentioned Nap (29), FDH-N (54), FDH-H (17), and arsenite oxidase (31) from *E. coli*, FDH-H (75) from *D. gigas*, and the DMSO reductases from *Rhodobacter sphaeroides* (87) and *R. capsulatus* (9, 90). These similarities are based in the core architecture of the catalytic site of these Mo-*bis*MGD enzymes. This consists of four conserved α - β domains grouped around the cofactor, which form the active site in the form of a cleft between two α/β sandwiches (12, 53).

Domain I of NarG is comprised of three helices, two mixed β -sheets, the aforementioned unique N-terminal tail and a highly conserved loop structure. This loop structure contains three Cys sidechains and one His sidechain, which ligate a [4Fe-4S] cluster, termed FeS-0. Prior to solving the crystal structure of NarGHI, this Fe-S cluster was undetected and unknown as part of the electron transfer chain (12, 53). Another residue in this conserved loop region is Asn⁵², which is located at the interface of the FeS-0 and the Mo-*bis*MGD cofactor. This residue is thought to be involved in substrate binding.

The active site is located in NarG at the bottom of a cleft of α/β sandwiches formed by Domains II and III. Domain II coordinates one MGD, and Domain III the second MGD (12, 53). The molybdenum is coordinated by six ligands: four *cis*-dithiolene sulfur atoms of the Mo-*bis*MGD and, depending on the two structures reported, either by both side chain oxygen atoms in the carboxylate group of Asp²²² (12), or with one carboxylate oxygen from of Asp²²² and a Mo=O group (53). The molybdenum ion is presumed to be in the oxidized Mo(VI) state as both structures were crystallized aerobically. The contrasting findings between the two crystal structures are proposed to be due to a transition of Mo(V) between low-pH and high-pH states. Specifically, in the low-pH Mo(V) state, Asp²²² is hydrogen-bonded to His⁵⁴⁶, and this His

residue becomes deprotonated during the transition to the high-pH Mo(V) state (no strongly coupled proton) causing a rotation of the carboxylate group of Asp²²² resulting in a bidentate ligand. It is also possible that the different crystal structures represent structural flexibility of the active site (53). It is important to point out that the Asp-Mo coordination is so far unique in the family of molybdoenzymes (12, 53). As shown in Table 1.3, previously only Ser, Cys, SeCys, OH or oxo groups have been seen as ligands to the Mo atom, in addition to the dithiolene sulfurs.

Another novel finding in the Nar structure stemmed from the electron density of one of the MGD cofactors, which indicated a bicyclic dihydropterin structure (12). The other MGD cofactor, as well as other MGD cofactors in crystal structures solved of Mo-bisMGD enzymes, shows a typical tricyclic pyranopterin form (Fig. 1.4). While the tricyclic pyranopterins are completely bound by the enzyme via extensive hydrogen-bonding, this bicyclic form suggests that NarGHI not only is able to bind both forms, but also that the cofactor may be directly involved in the enzymatic mechanism through reactions of the pyran ring that participate in handling of the protons necessary for nitrate reduction (12).

Domain IV of NarG includes a β -barrel and set of four His residues that are highly conserved in all NarGs (53). A fifth domain, which was also observed in Fdh-N (54), is a large irregular structure which forms a cap on top of the subunit. A narrow channel with negatively-charged and hydrophobic residues in the center of Domain V leads to the active site. This channel is proposed to function in substrate specificity and acts as a filter to exclude large substrates (53).

NarH contains three [4Fe-4S] clusters (FS1, FS2, and FS3) and one [3Fe-4S] cluster (FS4), which classifies it in a distinct superfamily of bacterial oxidoreductase electron transfer subunits that contain four [4Fe-4S] and [3Fe-4S] clusters. NarH is distinct, however, in that it

contains other highly ordered motifs on the surface of the subunit that are not found in other members of this superfamily (Fig. 1.5). These motifs not only function in defining subunit-subunit interactions, but also in protecting the clusters from the aqueous environment (12). The core structure of NarH is divided into two domains (A and B), each consisting of two clusters that are packed between two helices and a β -sheet, and are associated by two-fold rotational symmetry. The redox centers form a single chain, and are all thought to have a direct role in the electron transfer pathway (Fig. 1.6) (12). The Fe-S clusters are divided into two classes: a high-potential class (FS1 and FS4) with midpoint potentials of +130 and +180 mV, and a low-potential class (FS2 and FS3) with midpoint potentials of -420 and -55 mV (60, 82). Each domain contains one high- and one low-potential cluster (12, 53). The midpoint potentials are regulated by hydrophobic residues, accessibility to solvent and electrostatic interactions. In particular, the low-potential clusters are located in a hydrophobic environment shielding the cluster from the solvent and only two (FS2) or three (FS3) sulfur atoms are hydrogen bonded to main chain nitrogen atoms. Following, the high-potential clusters are in a polar environment with all of the sulfur atoms forming hydrogen bonds with nitrogen atoms from main chain nitrogen atoms and Arg residues (12).

NarI, the transmembrane subunit, anchors NarGH to the membrane and provides the site of quinol binding and oxidation. This subunit contains five transmembrane helices and coordinates two hemes, heme b_p and heme b_D , named proximal and distal based on their proximity to the active site (Fig. 1.5). The first transmembrane helix aids in dimer formation, and the other four form a bundle around the heme groups. The C-terminal tail of NarI interacts with NarG and NarH as it extends towards the cytoplasm. This region of the C-terminus contains highly conserved charged residues and is key in forming the NarGHI heterotrimer (12).

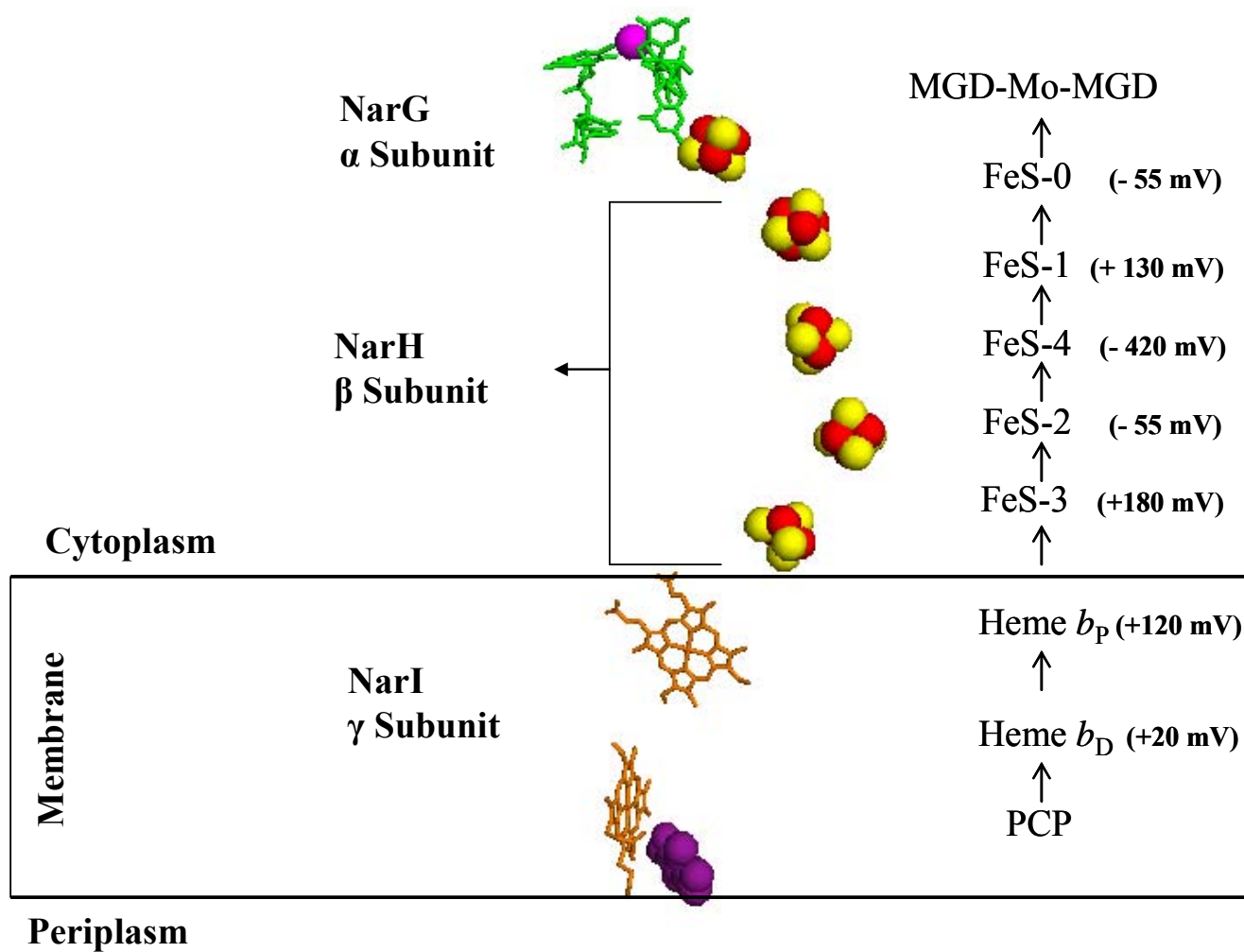


Fig. 1.6 Cofactors forming the electron transfer chain of Nar in *E. coli*. Mo is shown in magenta and MGD cofactors in green. Heme groups and pentachlorophenol (PCP, a menaquinone analog and potent enzyme inhibitor) are shown in orange and in purple, respectively. The four [4Fe-4S] and the [3Fe-4S] clusters show Fe atoms in red and S atoms in yellow. The figure was generated using PyMol from coordinates deposited in the Protein Data Bank (accession code 1Q16). Midpoint redox potentials were taken from (61, 80-82).

Two His residues coordinate the Fe atom in each heme. Heme b_P has a midpoint potential of +120 mV and heme b_D has a midpoint potential of +20 mV (Fig. 1.6). Both menaquinone and ubiquinol serve as physiological electron donors in NarGHI. Pentachlorophenol (PCP) is an inhibitor of the enzyme, and was crystallized in complex with NarGHI (11). This structure revealed that the quinone binding pocket is located between transmembrane helices II and III, close to heme b_D in predominantly nonpolar environment, replicating the physiological binding site (Fig. 1.5 and Fig. 1.6) (11).

Crystal Structure of Fdh-N

The crystal structure of the membrane-bound nitrate-inducible FDH, Fdh-N, from *E. coli* was recently solved at 1.6 Å (54). Fdh-N is a mushroom-shaped trimer with a molecular mass of 510 kDa whose monomers form a three-fold axis. The Fdh-N has dimensions of 150 Å along the electron transfer chain, and 60 Å along the membrane perpendicular in monomer form or 125 Å in trimer form (54). FdhG, the α subunit, and FdhH, the β subunit, are located on the periplasmic side of the membrane. FdhI, the γ subunit, is located on the opposite side of the membrane on the cytoplasmic side (Fig 1.7).

FdhG contains the active site. This subunit consists of the four domains conserved in the MGD enzymes, but additionally contains a fifth domain like NarG, which is organized around the Mo-*bis*MGD cofactor in each monomer. A single Mo atom is coordinated in a triangular prism pattern by two dithiolate groups from each of the MGD cofactors, by a selenate group from Se-Cys¹⁹⁶ and by a hydroxide ion. Domain I is the [4Fe-4S] cluster-binding domain. The site of formate oxidation is at the bottom of a cleft formed by Domains II and III. His¹⁹⁷ is directly involved via the removal of the α-proton from formate, analogous to the formate

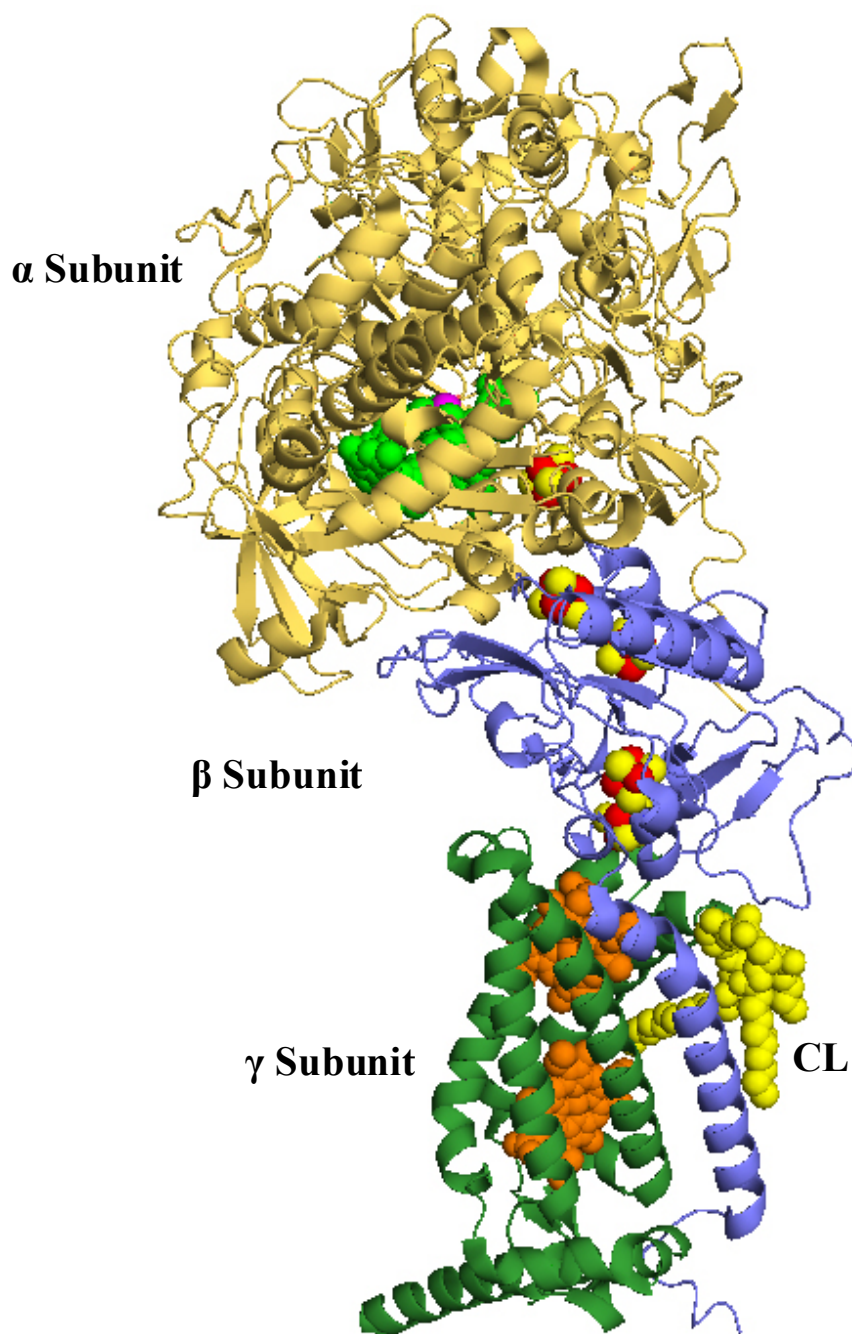


Fig. 1.7. The Crystal structure of the nitrate-inducible FDH (Fdh-N) from *E. coli*. The structure was resolved at 1.6 Å (54). The α , β , and γ subunits are shown in gold, blue and forest green, respectively. Mo is shown in magenta and MGD cofactors are shown in green. Heme groups and cardiolipin (CL) are shown in orange and in yellow, respectively. The five [4Fe-4S] show Fe atoms in red and S atoms in yellow. The figure was generated using PyMol from coordinates deposited in the Protein Data Bank (accession code 1KQF).

oxidation site in the W-FDH from *D. gigas* (75). Domain V of FdhG forms a cap-like structure, as in NarG, on the surface of enzyme toward the outer membrane and at the trimer interface. Similar to NarG, a hole in the middle of Domain V connects with the aforementioned cleft. The channel in FdhG however, is a wider funnel shaped structure lined with positively charged residues, unlike the narrow negatively charged channel of NarG. Additionally, the positively charged, wide funnel in FdhG is important in the attraction of the substrate, formate (54).

The β subunit of FdhGHI, as in NarGHI, is also classified in the distinct superfamily of bacterial oxidoreductase electron transfer subunits that contain four [4Fe-4S] clusters. In addition to the four [4Fe-4S] clusters, FdhH also consists of a transmembrane helix in the C-terminal section. The four [4Fe-4S] clusters occupy two different environments within the subunit. FeS1 and FeS3 are located close to the surface, and are only hydrogen-bonded to the main-chain amide groups. FeS2 and FeS4, however, are buried in the external domain of the β subunit, and are hydrogen-bonded to various positively charged residues leading to modulation of the redox potentials of the clusters.

The membrane-bound γ subunit is a cytochrome *b* and contains two heme *b* groups, four transmembrane helices and a reduction site for menaquinone. In addition to the transmembrane helices, this tightly packed trimer is associated with a cardiolipin molecule (a phospholipid derived from the original *E. coli* membrane) that is hydrogen bonded to the extended N-terminal structure of FdhH and to the loop structure in FdhI (Fig. 1.7). These hydrogen bonds between the β transmembrane helix (His²⁷⁵) and the γ IV transmembrane helix (Tyr¹⁷¹) and Leu⁹⁶ in the main chain of the γ subunit appear to be essential for stabilizing the association between the β and γ subunits. All four transmembrane helices maintain the two heme *b* groups, but only three of them provide the ligands (I, II and IV). Two His residues coordinate the Fe atom in each

heme. The heme on the periplasmic side receives electrons from the β subunit and the heme on the cytoplasmic side transfers electrons to the menaquinone (Fig. 1.8) (54). HQNO (2-heptyl-4-hydroxyquinoline-*N*-oxide), an analog of menaquinone, was used to determine the quinone binding site in FdhI. The structure of the Fdh-N-HQNO complex was determined at 2.8 Å resolution (54). The binding site is located on the cytoplasmic side of the membrane, and formed by transmembrane helices II, III and the loop structure (Fig. 1.7 and Fig. 1.8).

Model of Formate-Nitrate Respiration in *E. coli*

The induction of Fdh-N and Nar in *E. coli* occurs during anaerobic growth in the presence of nitrate. Formate is oxidized by Fdh-N and is the primary electron donor to nitrate, which is reduced by Nar. The determination of the structures of Nar and Fdh-N and their respective menaquinone binding sites has led to the elucidation of the electron transfer pathway in this multienzyme system. The Fdh-N and Nar form a respiratory system through a quinol pool (Fig. 1.9). The coupling of electron transfer from formate to nitrate, to the translocation of protons across the cytoplasmic membrane, generates a proton motive force (PMF) by a redox loop (12, 36, 53, 54). A redox loop is formed as electrons from the site of Fdh-N formate oxidation in the periplasm are transferred to the nitrate reduction site of NarGHI in the cytoplasm via the lipid soluble quinol pool, driving the translocation of protons (one per electron) in the opposite direction from the cytoplasmic side of the membrane to the periplasmic side. This mechanism generates a membrane potential that is equivalent to a 2H^+ translocation per mole of formate oxidized (54).

The transfer of electrons in Fdh-N occurs through the single chain of redox centers that extends through the enzyme (54). The electrons that directly reduce the Mo atom in the catalytic

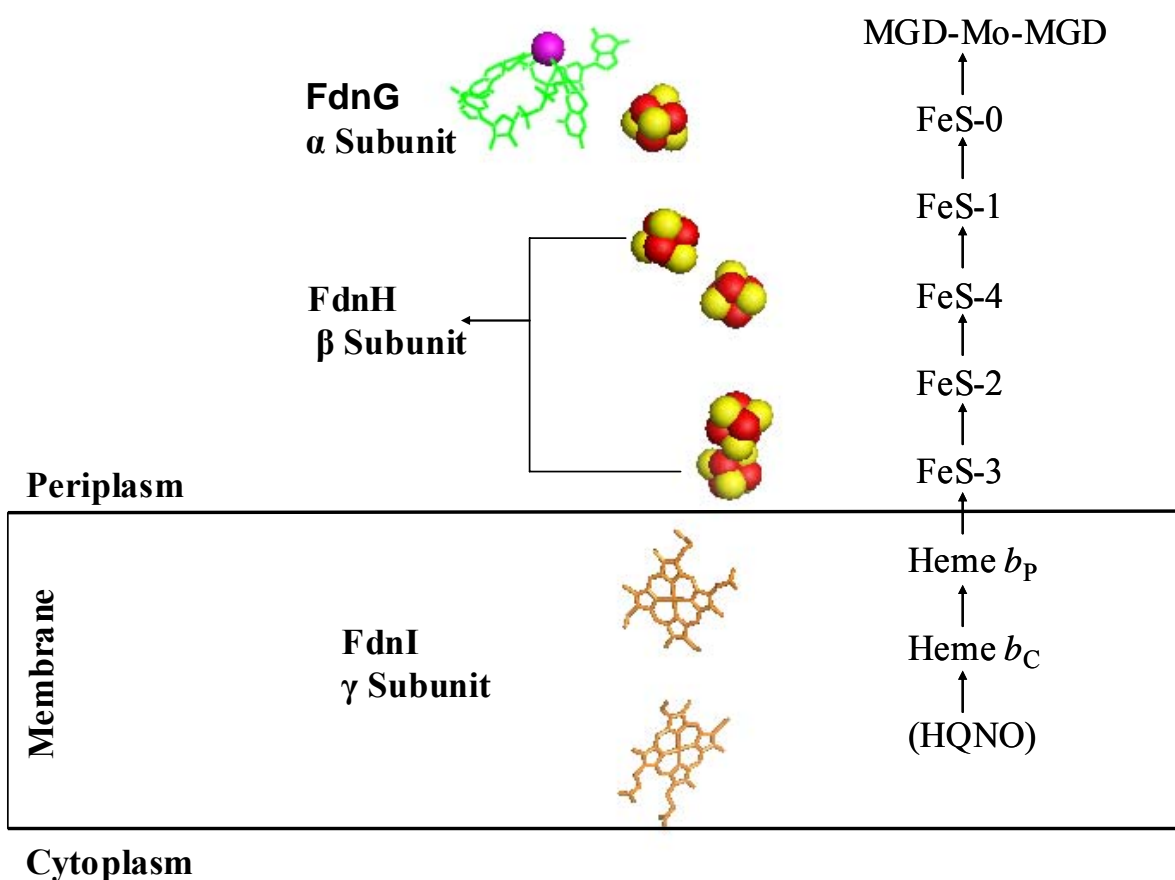


Fig. 1.8. Cofactors forming the electron transfer chain of FDH-N in *E. coli*. Mo is shown in magenta and MGD cofactors in green. Heme b_p (periplasmic) and Heme b_C (cytoplasmic) are shown in orange. The five [4Fe-4S] clusters show Fe atoms in red and S atoms in yellow. HQNO, a quinone analog, is not shown, but was used in defining the quinone binding pocket in FdnI. The figure was generated using PyMol from coordinates deposited in the Protein Data Bank (accession code 1Q16).

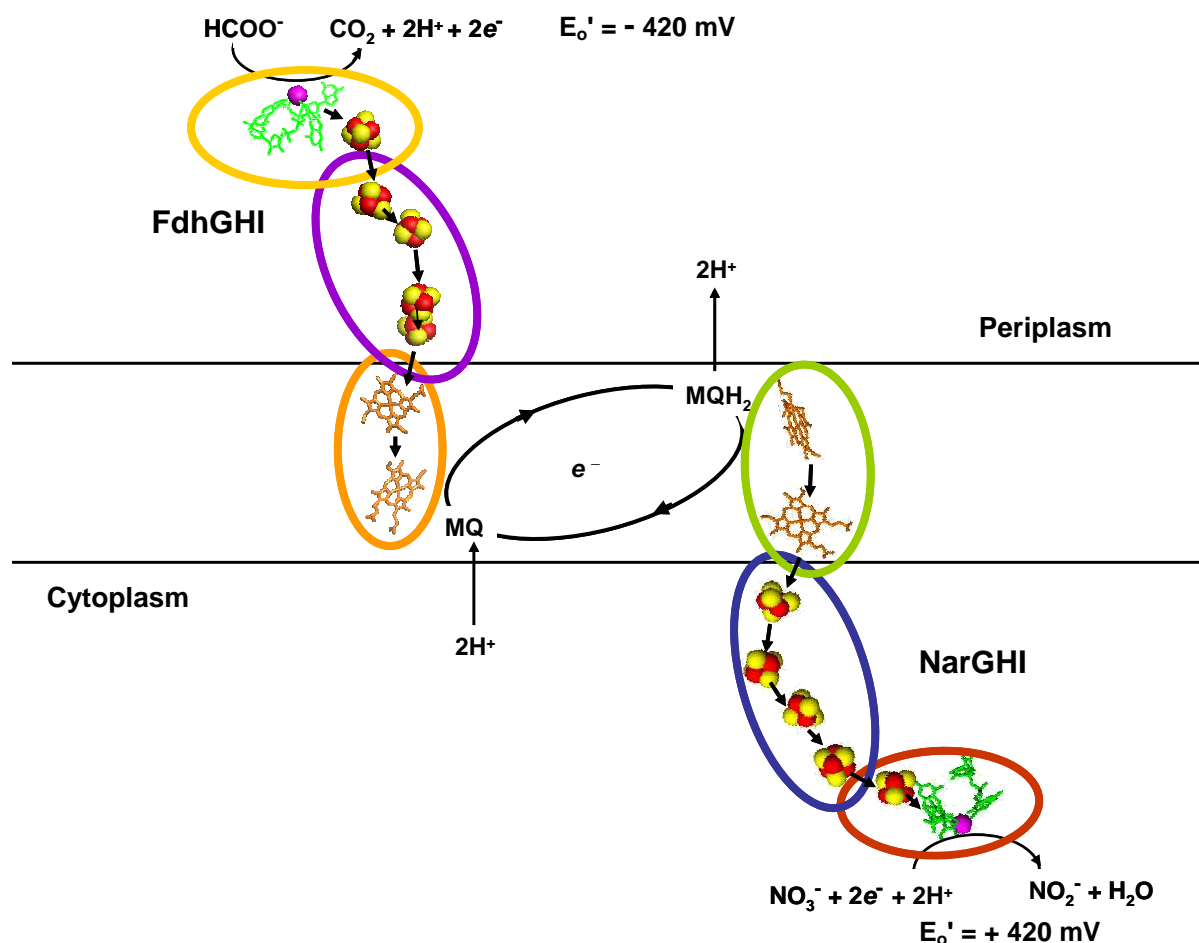


Fig. 1.9. Proposed model of the Fdh-N/Nar respiratory chain in *E. coli*. FdhGHI subunits are encircled in yellow, purple, and orange, respectively. NarGHI subunits are encircled in red, blue and lime, respectively. Arrows indicate the path of the electrons. In both enzymes Mo is shown in magenta and MGD cofactors in green. Heme groups are shown in orange. The [4Fe-4S] and [3Fe-4S] clusters show Fe atoms in red and S atoms in yellow. The electron transfer components were generated using PyMol from coordinates deposited in the Protein Data Bank (accession code 1KQF and 1Q16). This model of the FDH-N/NR respiratory chain in *E. coli* was proposed by Jormakka and coworkers (54) and Bertero and coworkers (12).

site from formate oxidation are transferred to the [4Fe-4S] cluster in the α subunit and then to the four [4Fe-4S] clusters in the β subunit. These clusters connect the α and γ subunits, and consequently electrons are transferred to the periplasmically-located heme in the γ subunit and then across the membrane to the cytoplasmically located heme. His¹⁶⁹ in this heme provides the ligand for menaquinone binding. The first of two electrons is transferred to the menaquinone upon binding, and a proton is taken up from the cytoplasmic space to neutralize the charge, forming a menasemiquinone. Reduction of menasemiquinone to menaquinol occurs with the transfer of the second electron. A proton is taken up from His¹⁶⁹ resulting in the release of menaquinol to the membrane, and immediately protonated through a water channel. The transfer of electrons from formate (-420 mV) to menaquinone (-75 mV) occurs against the membrane potential due to this highly exergonic reaction (54).

The fully reduced menaquinol or ubiquinol molecule binds to NarI, and one electron is transferred to the periplasmically located heme forming a semiquinone intermediate, as one proton is shuttled towards the periplasm (11). Oxidation of the quinol to a quinone is completed with the transfer of the second electron. A second proton is released, and the oxidized menaquinone or ubiquinone is dissociated for further enzyme turnover (11). The redox centers in NarGHI are located in a single chain as in Fdh-N. The transfer of electrons continues to the cytoplasmically located heme and then to the [3Fe-4S] cluster in the β subunit through an extensive network of hydrogen bonding. Electrons are subsequently transferred through the three [4Fe-4S] clusters in NarH and the [4Fe-4S] cluster in the cytoplasmically located catalytic α subunit to the Mo-*bis*MGD active site, where nitrate is reduced to nitrite (Fig. 1.9) (11, 12, 53).

The *E. coli* Fdh-N/Nar respiratory pathway is the perfect model system for studying a wide variety of aspects, including the role of Mo, the electron transfer pathways, and the

structure-function relationships of FDH and NR. As such, this system serves as the model system for the research conducted in this study of Mo and W and their role in the growth of *P. aerophilum*, and in the formate-nitrate respiration pathway and key enzymes, NR and FDH, in this hyperthermophilic archaeon.

Proposed Research. The goal of this project is to evaluate the role tungsten (W) and molybdenum (Mo) in the nitrate reduction pathway of *Pyrobaculum aerophilum*. The isolation of *Pyrobaculum aerophilum* approximately a decade ago, led to the discovery of the first nitrate reducer and the first facultative anaerobe in the phylum *Thermoproteales*. Other than that it is a true denitrifier and a microaerophile, relatively little is known about its respiratory pathway. This is a very important issue because other members of this genus, and hyperthermophiles in general, grow by either sulfur reduction, sulfur respiration or fermentation.

The fundamental issue addressed by this research is how and why do organisms choose to use Mo or W at the catalytic sites of key enzymes. The model organism is *Pyrobaculum aerophilum*, and the model system is nitrate reduction. Nitrate reductase (NR) catalyzes a high potential reaction ($E_o' + 420$ mV), while in organisms such as *E. coli* the physiological electron donor is formate via formate dehydrogenase (FDH) ($E_o' - 430$ mV) in the formate-nitrate respiratory chain. Both of these enzymes are molybdoenzymes in *E. coli*. However, FDH has also been purified as a naturally-occurring tungstoenzyme from various thermophilic bacteria, but NR has not been previously purified from a thermophilic organism, let alone one growing at 100 °C. So, does *P. aerophilum* produce a W-containing NR or a W-containing FDH? This might be expected (in terms of thermal stability), but perhaps not in the case of NR, in terms of how the redox chemistry will be carried out. In order to address these fundamental questions a

defined medium will be established for reproducible growth and high yields of *P. aerophilum*. The use of media supplemented with W only, Mo only and both W and Mo will determine the uptake of these metals by the organism and provide material for analysis of incorporation of the metals into the active site of both NR and FDH (Chapter 2). Once accomplished, purification of specific enzymes in the respiration pathway will be carried out. The purification and characterization of NR (Chapter 3) and of FDH (Chapter 4) will enable determination of their metal centers. The role of W and Mo in the metabolism of *P. aerophilum* can then be assessed by comparing the results with the properties of the molybdoenzymes and tungstoenzymes in *P. aerophilum* with analogous enzymes in *E. coli* and *P. furiosus*. *E. coli* is used as the reference microorganism for of Mo-containing enzymes, and *P. furiosus* is used as the representative organism with W-containing enzymes. This comparison (Chapter 5) gives insight to how *P. aerophilum* fits into what is currently known about how these two metals are utilized in the active sites of enzymes in anaerobic metabolism.

REFERENCES

1. **Adams, M. W. W.** 1999. The biochemical diversity of life near and above 100 degrees C in marine environments. *Journal of Applied Microbiology* **85**:108S-117S.
2. **Adams, M. W. W.** 1993. Enzymes and proteins from organisms that grow near and above 100 degrees C. *Annu. Rev. Microbiol.* **47**:627-58.
3. **Almendra MJ, B. C., Gavel O, Pereira AS, Tavares P, Bursakov S, Duarte R, Caldeira J, Moura JJ, Moura I.** 1999. Purification and characterization of a tungsten-containing formate dehydrogenase from *Desulfovibrio gigas*. *Biochemistry* **38**:16366-72.

4. **Amo, T., M. L. Paje, A. Inagaki, S. Ezaki, H. Atomi, and T. Imanaka.** 2002. *Pyrobaculum calidifontis* sp. nov., a novel hyperthermophilic archaeon that grows in atmospheric air. *Archaea* **1**:113-21.
5. **Andreesen, J. R., and L. G. Ljungdahl.** 1973. Formate dehydrogenase of *Clostridium thermoaceticum*: incorporation of selenium-75, and the effects of selenite, molybdate, and tungstate on the enzyme. *J Bacteriol.* **116**:867-73.
6. **Andreesen, J. R., and L. G. Ljungdahl.** 1974. Nicotinamide adenine dinucleotide phosphate-dependent formate dehydrogenase from *Clostridium thermoaceticum*: purification and properties. *J Bacteriol* **120**:6-14.
7. **Antipov, A. N., N. N. Lyalikova, T. V. Khijniak, and P. L'Vov N.** 1998. Molybdenum-free nitrate reductases from vanadate-reducing bacteria. *FEBS Lett* **441**:257-60.
8. **Antipov AN, S. D., L'Vov NP, Kuenen JG.** 2003. New enzyme belonging to the family of molybdenum-free nitrate reductases. *Biochem J.* **369**:185-9.
9. **Bailey, S., A. S. McAlpine, E. M. Duke, N. Benson, and A. G. McEwan.** 1996. Preliminary crystallographic studies of dimethylsulfoxide reductase from *Rhodobacter capsulatus*. *Acta Crystallogr D Biol Crystallogr* **52**:194-6.
10. **Bell, L. C., D. J. Richardson, and S. J. Ferguson.** 1990. Periplasmic and membrane-bound respiratory nitrate reductases in *Thiosphaera pantotropha*. The periplasmic enzyme catalyzes the first step in aerobic denitrification. *FEBS Lett* **265**:85-7.
11. **Bertero, M. G., R. A. Rothery, N. Boroumand, M. Palak, F. Blasco, N. Ginet, J. H. Weiner, and N. C. Strynadka.** 2005. Structural and biochemical characterization of a quinol binding site of *Escherichia coli* nitrate reductase A. *J Biol Chem* **280**:14836-43.

12. **Bertero, M. G., R. A. Rothery, M. Palak, C. Hou, D. Lim, F. Blasco, J. H. Weiner, and N. C. Strynadka.** 2003. Insights into the respiratory electron transfer pathway from the structure of nitrate reductase A. *Nat Struct Biol* **10**:681-7.
13. **Bertram, P. A., R. A. Schmitz, D. Linder, and R. K. Thauer.** 1994. Tungstate can substitute for molybdate in sustaining growth of *Methanobacterium thermoautotrophicum*. Identification and characterization of a tungsten isoenzyme of formylmethanofuran dehydrogenase. *Arch Microbiol* **161**:220-8.
14. **Bintrim, S. B., T. J. Donohue, J. Handelsman, G. P. Roberts, and R. M. Goodman.** 1997. Molecular phylogeny of Archaea from soil. *Proc Natl Acad Sci U S A* **94**:277-82.
15. **Bloch, E., R. Rachel, S. Burggraf, D. Hafenbradl, H. W. Jannasch, and K. O. Stetter.** 1997. *Pyrolobus fumarii*, gen. and sp. nov., represents a novel group of archaea, extending the upper temperature limit for life to 113 degrees C. *Extremophiles* **1**:14-21.
16. **Bonnefoy, V., and J. A. Demoss.** 1994. Nitrate reductases in *Escherichia coli*. *Antonie Van Leeuwenhoek* **66**:47-56.
17. **Boyington, J., V. Gladyshev, S. Khangulov, T. Stadtman, and P. Sun.** 1997. Crystal structure of formate dehydrogenase H: catalysis involving Mo, molybdopterin, selenocysteine, and an Fe₄S₄ cluster. *Science* **275**:1305-8.
18. **Brons H.J. and Zehnder, A. J. B.** 1990. Aerobic nitrate and nitrite reduction in continuous cultures of *Escherichia coli* E4. *Archives of Microbiology* **153**:531-536.
19. **Buc, J., C. L. Santini, R. Giordani, M. Czjzek, L. F. Wu, and G. Giordano.** 1999. Enzymatic and physiological properties of the tungsten-substituted molybdenum TMAO reductase from *Escherichia coli*. *Mol Microbiol* **32**:159-68.

20. **Burggraf, S., H. Huber, and K. O. Stetter.** 1997. Reclassification of the crenarchaeal orders and families in accordance with 16S rRNA sequence data. *Int J Syst Bacteriol* **47**:657-60.
21. **Chan, M. K., S. Mukund, A. Kletzin, M. W. Adams, and D. C. Rees.** 1995. Structure of a hyperthermophilic tungstopterin enzyme, aldehyde ferredoxin oxidoreductase. *Science* **267**:1463-9.
22. **Chang, L., L. I. Wei, J. P. Audia, R. A. Morton, and H. E. Schellhorn.** 1999. Expression of the *Escherichia coli* NRZ nitrate reductase is highly growth phase dependent and is controlled by RpoS, the alternative vegetative sigma factor. *Mol Microbiol* **34**:756-66.
23. **Chaudhry, G. R., and C. H. MacGregor.** 1983. *Escherichia coli* nitrate reductase subunit A: its role as the catalytic site and evidence for its modification. *J Bacteriol* **154**:387-94.
24. **Davies KJ, L. D., Boddy L.** 1989. The effect of oxygen on denitrification in *Paracoccus denitrificans* and *Pseudomonas aeruginosa*. *J Gen Microbiol.* **135**:2445-51.
25. **Deamer, D. W.** 1997. The first living systems: a bioenergetic perspective. *Microbiol Mol Biol Rev.* **61**:239-61.
26. **DeLong, E. F.** 1992. Archaea in coastal marine environments. *Proc Natl Acad Sci U S A* **89**:5685-9.
27. **DeLong, E. F., L. L. King, R. Massana, H. Cittone, A. Murray, C. Schleper, and S. G. Wakeham.** 1998. Dibiphytanyl ether lipids in nonthermophilic crenarchaeotes. *Appl Environ Microbiol* **64**:1133-8.

28. **DeLong, E. F., K. Y. Wu, B. B. Prezelin, and R. V. Jovine.** 1994. High abundance of Archaea in Antarctic marine picoplankton. *Nature* **371**:695-7.
29. **Dias, J. M., M. E. Than, A. Humm, R. Huber, G. P. Bourenkov, H. D. Bartunik, S. Bursakov, J. Calvete, J. Caldeira, C. Carneiro, J. J. Moura, I. Moura, and M. J. Romao.** 1999. Crystal structure of the first dissimilatory nitrate reductase at 1.9 Å solved by MAD methods. *Structure Fold Des* **7**:65-79.
30. **Dobbek, H., and R. Huber.** 2002. The molybdenum and tungsten cofactors: a crystallographic view. *Met Ions Biol Syst.* **39**:227-63.
31. **Ellis, P. J., T. Conrads, R. Hille, and P. Kuhn.** 2001. Crystal structure of the 100 kDa arsenite oxidase from *Alcaligenes faecalis* in two crystal forms at 1.64 Å and 2.03 Å. *Structure (Camb)* **9**:125-32.
32. **Enoch, H. G., and R. L. Lester.** 1975. The purification and properties of formate dehydrogenase and nitrate reductase from *Escherichia coli*. *J Biol Chem* **250**:6693-705.
33. **Fuchs, T., H. Huber, S. Burggraf, and K. O. Stetter.** 1996. 16S rDNA-based phylogeny of the archaeal order *Sulfolobales* and reclassification of *Desulfurolobus ambivalens* as *Acidianus ambivalens* comb nov. *Systematic and Applied Microbiology* **19**:56-60.
34. **Giordano, G., B. A. Haddock, and D. H. Boxer.** 1980. Molybdenum-limited growth achieved either phenotypically or genotypically and its effect on the synthesis of formate dehydrogenase and nitrate reductase by *Escherichia coli* K12. *FEMS Microbiol Lett* **8**:229-235.
35. **Giordano, R., C. L. Medani, M. A. Mandrand-Berthelot, and D. H. Boxer.** 1983. Formate dehydrogenases from *E. coli*. *FEMS Microbiol Lett* **17**:171-177.

36. **Grimaldi, S., P. Lanciano, P. Bertrand, F. Blasco, and B. Guigliarelli.** 2005. Evidence for an EPR-detectable semiquinone intermediate stabilized in the membrane-bound subunit NarI of nitrate reductase A (NarGHI) from *Escherichia coli*. *Biochemistry* **44**:1300-8.
37. **Hagedoorn, P. L., T. Chen, I. Schroder, S. R. Piersma, S. de Vries, and W. R. Hagen.** 2005. Purification and characterization of the tungsten enzyme aldehyde:ferredoxin oxidoreductase from the hyperthermophilic denitrifier *Pyrobaculum aerophilum*. *J Biol Inorg Chem* **10**:259-69.
38. **Hagedoorn, P. L., W. R. Hagen, L. J. Stewart, A. Docrat, S. Bailey, and C. D. Garner.** 2003. Redox characteristics of the tungsten DMSO reductase of *Rhodobacter capsulatus*. *FEBS Lett* **555**:606-10.
39. **Hensgens, C. M., W. R. Hagen, and T. A. Hansen.** 1995. Purification and characterization of a benzylviologen-linked, tungsten-containing aldehyde oxidoreductase from *Desulfovibrio gigas*. *J Bacteriol* **177**:6195-200.
40. **Hille, R.** 2002. Molybdenum and tungsten in biology. *Trends Biochem. Sci.* **27**:360-367.
41. **Hille, R.** 2002. Molybdenum enzymes containing the pyranopterin cofactor: an overview. *Met Ions Biol Syst* **39**:187-226.
42. **Hille, R.** 1996. The Mononuclear Molybdenum Enzymes. *Chem Rev* **96**:2757-2816.
43. **Hochheimer, A., R. Hedderich, and R. K. Thauer.** 1998. The formylmethanofuran dehydrogenase isoenzymes in *Methanobacterium wolfei* and *Methanobacterium thermoautotrophicum*: induction of the molybdenum isoenzyme by molybdate and constitutive synthesis of the tungsten isoenzyme. *Arch Microbiol* **170**:389-93.

44. **Hochstein, L. I., and F. Lang.** 1991. Purification and properties of a dissimilatory nitrate reductase from *Haloferax denitrificans*. Arch Biochem Biophys **288**:380-5.
45. **Huber, C., and G. Wächtershauser.** 1997. Activated acetic acid by carbon fixation on (Fe,Ni)S under primordial conditions [see comments]. Science **276**:245-7.
46. **Huber, R., J. K. Kristjansson, and K. O. Stetter.** 1987. *Pyrobaculum* gen. nov., a new genus of neutrophilic, rod-shaped archaeobacteria from continental solfataras growing optimally at 100 °C. Arch Microbiol **149**:95-101.
47. **Huber, R., M. Sacher, A. Vollmann, H. Huber, and D. Rose.** 2000. Respiration of arsenate and selenate by hyperthermophilic archaea. Syst. Appl. Microbiol. **23**:305-14.
48. **Huber, R., T. Wilharm, D. Huber, A. Trincone, S. Burggraf, H. König, R. Rachel, I. Rockinger, H. Fricke, and K. O. Stetter.** 1992. *Aquifex Pyrophilus* gen-nov sp-nov represents a novel group of marine hyperthermophilic hydrogen-oxidizing bacteria. Syst. Appl. Microbiol. **15**:340-351.
49. **Iobbi-Nivol, C., C. L. Santini, F. Blasco, and G. Giordano.** 1990. Purification and further characterization of the second nitrate reductase of *Escherichia coli* K12. Eur J Biochem **188**:679-87.
50. **Iwabe, N., K. Kuma, M. Hasegawa, S. Osawa, and T. Miyata.** 1989. Evolutionary relationship of archaeobacteria, eubacteria, and eukaryotes inferred from phylogenetic trees of duplicated genes. Proc Natl Acad Sci U S A **86**:9355-9.
51. **Johnson, J. L., K. V. Rajagopalan, S. Mukund, and M. W. Adams.** 1993. Identification of molybdopterin as the organic component of the tungsten cofactor in four enzymes from hyperthermophilic Archaea. J. Biol. Chem. **268**:4848-52.

52. **Johnson, M. K., D. C. Rees, and M. W. W. Adams.** 1996. Tungstoenzymes. *Chem. Rev.* **96**:2817-2839.
53. **Jormakka, M., D. Richardson, B. Byrne, and S. Iwata.** 2004. Architecture of NarGH reveals a structural classification of Mo-*bis*MGD enzymes. *Structure (Camb)* **12**:95-104.
54. **Jormakka, M., S. Tornroth, B. Byrne, and S. Iwata.** 2002. Molecular basis of proton motive force generation: structure of formate dehydrogenase-N. *Science* **295**:1863-8.
55. **Kelly, R. M., and M. W. W. Adams.** 1994. Metabolism in Hyperthermophilic Microorganisms. *Antonie Van Leeuwenhoek International Journal of General and Molecular Microbiology* **66**:247-270.
56. **Kletzin, A., and M. W. Adams.** 1996. Tungsten in biological systems. *FEMS Microbiol. Rev.* **18**:5-63.
57. **Knappe, J., and G. Sawers.** 1990. A radical-chemical route to acetyl-CoA: the anaerobically induced pyruvate formate-lyase system of *Escherichia coli*. *FEMS Microbiol Rev* **6**:383-98.
58. **Li, H.-K., C. K. Temple, K. V. Rajagopalan, and H. Schindelin.** 2000. The 1.3 Å Crystal Structure of *Rhodobacter sphaeroides* Dimethyl Sulfoxide Reductase Reveals Two Distinct Molybdenum Coordination Environments. *J. Am. Chem. Soc.* **122**:7673 - 7680.
59. **Madigan, M. T., J. M. Martinko, and J. Parker.** 1997. *Brock Biology of Microorganisms*, 8th ed. Prentice Hall.
60. **Magalon, A., M. Asso, B. Guigliarelli, R. A. Rothery, P. Bertrand, G. Giordano, and F. Blasco.** 1998. Molybdenum cofactor properties and [Fe-S] cluster coordination in

- Escherichia coli* nitrate reductase A: investigation by site-directed mutagenesis of the conserved his-50 residue in the NarG subunit. *Biochemistry* **37**:7363-70.
61. **Magalon, A., R. A. Rothery, D. Lemesle-Meunier, C. Frixon, J. H. Weiner, and F. Blasco.** 1998. Inhibitor binding within the NarI subunit (cytochrome bnr) of *Escherichia coli* nitrate reductase A. *J Biol Chem.* **273**:10851-6.
62. **Mahne, I., and J. M. Tiedje.** 1995. Criteria and methodology for identifying respiratory denitrifiers. *Applied and Environmental Microbiology* **61**:1110-1115.
63. **Martinez Murillo, F., T. Gugliuzza, J. Senko, P. Basu, and J. F. Stolz.** 1999. A heme-C-containing enzyme complex that exhibits nitrate and nitrite reductase activity from the dissimilatory iron-reducing bacterium *Geobacter metallireducens*. *Arch Microbiol* **172**:313-20.
64. **Mendel, R. R., and R. Hansch.** 2002. Molybdoenzymes and molybdenum cofactor in plants. *J Exp Bot.* **53**:1689-98.
65. **Moreno-Vivian, C., P. Cabello, M. Martinez-Luque, R. Blasco, and F. Castillo.** 1999. Prokaryotic nitrate reduction: molecular properties and functional distinction among bacterial nitrate reductases. *J Bacteriol* **181**:6573-84.
66. **Mukund, S., and M. W. W. Adams.** 1993. Characterization of a novel tungsten-containing formaldehyde ferredoxin oxidoreductase from the hyperthermophilic archaeon, *Thermococcus litoralis*. A role for tungsten in peptide catabolism. *J. Biol. Chem.* **268**:13592-600.
67. **Mukund, S., and M. W. W. Adams.** 1990. Characterization of a tungsten-iron-sulfur protein exhibiting novel spectroscopic and redox properties from the hyperthermophilic archaeobacterium *Pyrococcus furiosus*. *J. Biol. Chem.* **265**:11508-16.

68. **Mukund, S., and M. W. W. Adams.** 1995. Glyceraldehyde-3-phosphate ferredoxin oxidoreductase, a novel tungsten-containing enzyme with a potential glycolytic role in the hyperthermophilic archaeon *Pyrococcus furiosus*. *J. Biol. Chem.* **270**:8389-92.
69. **Mukund, S., and M. W. W. Adams.** 1996. Molybdenum and vanadium do not replace tungsten in the catalytically active forms of the three tungstoenzymes in the hyperthermophilic archaeon *Pyrococcus furiosus*. *J. Bacteriol.* **178**:163-7.
70. **Mukund, S., and M. W. W. Adams.** 1991. The novel tungsten-iron-sulfur protein of the hyperthermophilic archaebacterium, *Pyrococcus furiosus*, is an aldehyde ferredoxin oxidoreductase. Evidence for its participation in a unique glycolytic pathway. *J. Biol. Chem.* **266**:14208-16.
71. **Munson, M. A., D. B. Nedwell, and T. M. Embley.** 1997. Phylogenetic diversity of Archaea in sediment samples from a coastal salt marsh. *Appl Environ Microbiol* **63**:4729-33.
72. **Peck, H. D., Jr. and H. Gest.** 1957. Formic dehydrogenase and the hydrogenlyase enzyme complex in *coli-aerogenes* bacteria. *Journal of Bacteriology* **73**:706-721.
73. **Philippot, L., and O. Hojberg.** 1999. Dissimilatory nitrate reductases in bacteria. *Biochim Biophys Acta* **1446**:1-23.
74. **Pollock, V. V., and M. J. Barber.** 2001. Kinetic and mechanistic properties of biotin sulfoxide reductase. *Biochemistry* **40**:1430-40.
75. **Raaijmakers, H., S. Teixeira, J. M. Dias, M. J. Almendra, C. D. Brondino, I. Moura, J. J. Moura, and M. J. Romao.** 2001. Tungsten-containing formate dehydrogenase from *Desulfovibrio gigas*: metal identification and preliminary structural data by multi-wavelength crystallography. *J Biol Inorg Chem.* **6**:398-404.

76. **Rajagopalan, K. V., and J. L. Johnson.** 1992. The pterin molybdenum cofactors. *J Biol Chem* **267**:10199-202.
77. **Rajagopalan, K. V., J. L. Johnson, and B. E. Hainline.** 1982. The pterin of the molybdenum cofactor. *Fed Proc* **41**:2608-12.
78. **Romao, M. J., M. Archer, I. Moura, J. J. Moura, J. LeGall, R. Engh, M. Schneider, P. Hof, and R. Huber.** 1995. Crystal structure of the xanthine oxidase-related aldehyde oxido-reductase from *D. gigas*. *Science* **270**:1170-6.
79. **Rosner, B. M., and B. Schink.** 1995. Purification and characterization of acetylene hydratase of *Pelobacter acetylenicus*, a tungsten iron-sulfur protein. *J Bacteriol.* **177**:5767-72.
80. **Rothery, R. A., M. G. Bertero, R. Cammack, M. Palak, F. Blasco, N. C. Strynadka, and J. H. Weiner.** 2004. The catalytic subunit of *Escherichia coli* nitrate reductase A contains a novel [4Fe-4S] cluster with a high-spin ground state. *Biochemistry* **43**:5324-33.
81. **Rothery, R. A., F. Blasco, A. Magalon, M. Asso, and J. H. Weiner.** 1999. The hemes of *Escherichia coli* nitrate reductase A (NarGHI): potentiometric effects of inhibitor binding to narI. *Biochemistry* **38**:12747-57.
82. **Rothery, R. A., A. Magalon, G. Giordano, B. Guigliarelli, F. Blasco, and J. H. Weiner.** 1998. The molybdenum cofactor of *Escherichia coli* nitrate reductase A (NarGHI). Effect of a mobAB mutation and interactions with [Fe-S] clusters. *J Biol Chem* **273**:7462-9.
83. **Sako, Y., N. Nomura, A. Uchida, Y. Ishida, H. Morii, Y. Koga, T. Hoaki, and T. Maruyama.** 1996. *Aeropyrum pernix* gen nov, sp nov, a novel aerobic hyperthermophilic

- archaeon growing at temperatures up to 100 degrees C. *Int. J. Syst. Bacteriol.* **46**:1070-1077.
84. **Sako, Y., T. Nunoura, and A. Uchida.** 2001. *Pyrobaculum oguniense* sp. nov., a novel facultatively aerobic and hyperthermophilic archaeon growing at up to 97 degrees C. *Int. J. Syst. Evol. Microbiol.* **51**:303-9.
85. **Sawers, G.** 1994. The hydrogenases and formate dehydrogenases of *Escherichia coli*. *Antonie Van Leeuwenhoek* **66**:57-88.
86. **Sawers G, H. J., Zehelein E, Bock A.** 1991. Expression and operon structure of the sel genes of *Escherichia coli* and identification of a third selenium-containing formate dehydrogenase isoenzyme. *J Bacteriol.* **173**:4983-93.
87. **Schindelin, H., C. Kisker, J. Hilton, K. V. Rajagopalan, and D. C. Rees.** 1996. Crystal structure of DMSO reductase: redox-linked changes in molybdopterin coordination. *Science* **272**:1615-21.
88. **Schleper, C., W. Holben, and H. P. Klenk.** 1997. Recovery of crenarchaeotal ribosomal DNA sequences from freshwater-lake sediments. *Appl Environ Microbiol* **63**:321-3.
89. **Schmitz, R. A., S. P. Albracht, and R. K. Thauer.** 1992. A molybdenum and a tungsten isoenzyme of formylmethanofuran dehydrogenase in the thermophilic archaeon *Methanobacterium wolfei*. *Eur J Biochem* **209**:1013-8.
90. **Schneider, F., J. Lowe, R. Huber, H. Schindelin, C. Kisker, and J. Knablein.** 1996. Crystal structure of dimethyl sulfoxide reductase from *Rhodobacter capsulatus* at 1.88 Å resolution. *J Mol Biol* **263**:53-69.
91. **Schönheit, P., and T. Schafer.** 1995. Metabolism of hyperthermophiles. *World J. Microb. Biot.* **11**:26-57.

92. **Schopf, J. W., Packer BM.** 1987. Early Archean (3.3-billion to 3.5-billion-year-old) microfossils from Warrawoona Group, Australia. *Science* **237**:70-3.
93. **Scott RH, S. G., DeMoss JA.** 1979. In vitro incorporation of molybdate into demolybdoproteins in *Escherichia coli*. *J Bacteriol.* **137**:719-26.
94. **Segerer, A. H., S. Burggraf, G. Fiala, G. Huber, R. Huber, U. Pley, and K. O. Stetter.** 1993. Life in Hot-Springs and Hydrothermal Vents. *Origins of Life and Evolution of the Biosphere* **23**:77-90.
95. **Silva, J. R. R. F. d., and R. J. P. Williams.** 1991. The biological chemistry of the elements : the inorganic chemistry of life, vol. xxi. Oxford University Press Clarendon Press, Oxford [England] New York.
96. **Spector MP, G. d. P. F., Bearson SM, Mahmud A, Magut M, Finlay BB, Dougan G, Foster JW, Pallen MJ.** 1999. The rpoS-dependent starvation-stress response locus stiA encodes a nitrate reductase (narZYWV) required for carbon-starvation-inducible thermotolerance and acid tolerance in *Salmonella typhimurium*. *Microbiology* **145**:3035-45.
97. **Stetter, K. O.** 1996. Hyperthermophilic procaryotes. *Fems Microbiol. Rev.* **18**:149-158.
98. **Stetter, K. O.** 1989. Order III. *Sulfolobales* ord. nov., p. 2250-2253. *In* M. P. B. J. T. Staley, N. Pfennig, and J.G. Holt (ed.), *Bergey's manual of systematic bacteriology*, vol. 3. Williams & Wilkins, Baltimore, MD.
99. **Stetter, K. O., R. Huber, E. Blochl, M. Kurr, R. D. Eden, M. Fielder, H. Cash, and I. Vance.** 1993. Hyperthermophilic archaea are thriving in deep north-sea and alaskan oil-reservoirs. *Nature* **365**:743-745.

100. **Stetter, K. O., A. Seegerer, W. Zillig, G. Huber, G. Fiala, R. Huber, and H. König.** 1986. Extremely thermophilic sulfur-metabolizing archaeobacteria. *Syst. Appl. Microbiol.* **7**:393-397.
101. **Stewart, L. J., S. Bailey, B. Bennett, J. M. Charnock, C. D. Garner, and A. S. McAlpine.** 2000. Dimethylsulfoxide reductase: an enzyme capable of catalysis with either molybdenum or tungsten at the active site. *J Mol Biol* **299**:593-600.
102. **Stiefel, E. I.** 2002. The biogeochemistry of molybdenum and tungsten. *Met Ions Biol Syst.* **39**:1-29. Review.
103. **Stiefel, E. I., D. Coucouvanis, W. E. Newton, American Chemical Society. Division of Inorganic Chemistry., and American Chemical Society. Meeting.** 1993. Molybdenum enzymes, cofactors, and model systems : developed from a symposium sponsored by the Division of Inorganic Chemistry at the 204th National Meeting of the American Chemical Society, Washington, DC, August 23-28, 1992. American Chemical Society, Washington, DC.
104. **Uchimura, H., H. Enjoji, T. Seki, A. Taguchi, N. Takaya, and H. Shoun.** 2002. Nitrate reductase-formate dehydrogenase couple involved in the fungal denitrification by *Fusarium oxysporum*. *J Biochem (Tokyo)* **131**:579-86.
105. **Völkl, P., R. Huber, E. Drobner, R. Rachel, S. Burggraf, A. Trincone, and K. O. Stetter.** 1993. *Pyrobaculum aerophilum* sp. nov., a novel nitrate-reducing hyperthermophilic archaeum. *Appl. Environ. Microbiol.* **59**:2918-26.
106. **Weiner JH, R. R., Sambasivarao D, Trieber CA.** 1992. Molecular analysis of dimethylsulfoxide reductase: a complex iron-sulfur molybdoenzyme of *Escherichia coli*. *Biochim Biophys Acta* **1102**:1-18.

107. **White, H., R. Feicht, C. Huber, F. Lottspeich, and H. Simon.** 1991. Purification and some properties of the tungsten-containing carboxylic acid reductase from *Clostridium formicoaceticum*. *Biol Chem Hoppe Seyler* **372**:999-1005.
108. **White, H., C. Huber, R. Feicht, and H. Simon.** 1993. On a reversible molybdenum-containing aldehyde oxidoreductase from *Clostridium formicoaceticum*. *ARCH MICROBIOL* **159**:244-249.
109. **White, H., G. Strobl, R. Feicht, and H. Simon.** 1989. Carboxylic acid reductase: a new tungsten enzyme catalyses the reduction of non-activated carboxylic acids to aldehydes. *Eur J Biochem* **184**:89-96.
110. **Williams, R. J., and Frausto da Silva JJ.** 2002. The involvement of molybdenum in life. *Biochem Biophys Res Commun.* **292**:293-9.
111. **Woese, C. R.** 1994. There must be a prokaryote somewhere: microbiology's search for itself. *Microbiol Rev* **58**:1-9.
112. **Woese, C. R., O. Kandler, and M. L. Wheelis.** 1990. Towards a natural system of organisms: proposal for the domains Archaea, Bacteria, and Eucarya. *Proc. Natl. Acad. Sci. U S A* **87**:4576-9.
113. **Yamamoto, I., T. Saiki, S. M. Liu, and L. G. Ljungdahl.** 1983. Purification and properties of NADP-dependent formate dehydrogenase from *Clostridium thermoaceticum*, a tungsten-selenium-iron protein. *J. Biol. Chem.* **258**:1826-1832.
114. **Yoshimatsu, K., T. Sakurai, and T. Fujiwara.** 2000. Purification and characterization of dissimilatory nitrate reductase from a denitrifying halophilic archaeon, *Haloarcula marismortui*. *FEBS Lett* **470**:216-20.

115. **Zillig, W.** 1989. Order II. *Thermoproteales*, p. 2240-2246. In M. P. B. J. T. Staley, N. Pfenning, and J.G. Holt (ed.), *Bergey's manual of systematic bacteriology*, vol. 3. Williams & Wilkins, Baltimore, MD.

CHAPTER 2

UPTAKE AND INCORPORATION OF MOLYBDATE AND TUNGSTATE DURING GROWTH OF *PYROBACULUM AEROPHILUM*¹

¹ Feingold, L.E. and M.W.W. Adams. 2006. To be submitted to *Journal of Bacteriology*.

ABSTRACT

The hyperthermophilic archaeon, *Pyrobaculum aerophilum*, respire either anaerobically via denitrification utilizing nitrate as the terminal electron acceptor, or aerobically, but only in the presence of low concentrations of oxygen. In this study, *P. aerophilum* was grown at 98 °C, representing its optimum high temperature environment, and at 78 °C, representing its low temperature threshold of growth. In general, hyperthermophilic organisms are known to utilize tungsten rather than its counterpart molybdenum, which is utilized by mesophilic and often by moderately thermophilic organisms. Consequently, variable concentrations and combinations of molybdate and tungstate were added to the growth medium of *P. aerophilum* to evaluate uptake of the oxyanions under the two temperature extremes. It was shown that growth of *P. aerophilum* at 98 °C in the presence of nitrate requires tungstate (WO_4^{2-}) and is inhibited by the presence of molybdate (MoO_4^{2-}) in higher or equimolar concentrations. However, both WO_4^{2-} and MoO_4^{2-} support growth at the low (78 °C) temperature. Notwithstanding the difference in effect of the presence of the oxyanions under the two growth temperatures, elemental analyses showed that both oxyanions were taken up by the organism under both of these conditions. Nitrate reductase (NR) and formate dehydrogenase (FDH) are two key enzymes involved in the respiratory pathway of *P. aerophilum*. NR is a ubiquitous molybdoenzyme, and FDH has been purified from a variety of organisms, usually as a naturally-occurring molybdoenzyme. Both enzymes were found to be membrane-bound in *P. aerophilum*. The specific activity of NR and of FDH on WO_4^{2-} -grown cells were each approximately the same in the two cell types grown at the different temperatures, while the activity in cells grown only on MoO_4^{2-} at 78 °C was slightly lower than in the cells grown only on WO_4^{2-} . Highest specific activity for both enzymes was found in cells grown with both oxyanions (1.5 μM) at 78 °C. Anaerobic growth of the organism

was highly dependent upon pH, with slight changes greatly affecting cell yield and doubling time. Furthermore, the addition of formate during growth greatly enhanced the specific activity of both NR and FDH, and also increased growth rate and cell yield.

INTRODUCTION

The hyperthermophile *Pyrobaculum aerophilum* was discovered less than a decade ago. It represents the first nitrate-reducing hyperthermophile and the first facultative anaerobe in the phylum *Thermoproteales* (29). Other than that it is a true denitrifier and a microaerophile, relatively little was known about its respiratory pathway. Other members of this genus, and hyperthermophiles in general, obtain energy for growth either by sulfur respiration or fermentation. Moreover, when this research began, nothing was known about the enzymes of the denitrification pathway in hyperthermophiles.

The denitrification pathway carries out the reduction of nitrate to dinitrogen predominately through anaerobic respiration involving the terminal oxidases nitrate reductase (NR), nitrite reductase, nitric oxide reductase and nitrous oxide reductase. The reduction of nitrate to nitrite catalyzed by NR is a high potential reaction ($E_o' + 420$ mV), and the physiological electron donor is often formate, which, is oxidized by formate dehydrogenase (FDH) in the formate-nitrate respiratory chain. The FDH complex catalyzes the oxidation of formate to carbon dioxide ($E_o' - 430$ mV) coupled with the transfer of reducing equivalents to nitrate in an energy-conserving pathway (23). The formate-nitrate reductase respiratory pathway is exclusively membrane-associated, and also involves quinones (5, 15). The respiratory coupling of the dissimilatory enzymes FDH and NR is common in prokaryotic denitrification.

Both NR and FDH are ubiquitous molybdenum-containing enzymes in mesophilic nitrate-reducing organisms, such as *Escherichia coli* (1). FDH, however, has also been purified as a naturally-occurring tungstoenzyme from the thermophilic bacterium, *Clostridium thermoaceticum*, and was the first tungstoenzyme to be purified (30). The role of molybdenum (Mo) in biological systems has been known for over 70 years (28), and tungsten (W) has routinely been utilized as an antagonist in experiments designed to investigate the role of Mo. Mo is found in enzymes involved in both aerobic and anaerobic reactions, and in these enzymes exhibits a wide range of catalytic function, including sulfate oxidation, DMSO reduction and arsenate oxidation. Although ubiquitous in biological systems, Mo complexes are less stable at high temperature than are W complexes (11). Furthermore, W complexes generally react more slowly and have reduction potentials 300 to 400 mV lower than their Mo counterparts (11). In addition, reduced W complexes are typically very sensitive to oxygen, in contrast to corresponding Mo complexes. Such properties may explain why W-utilizing enzymes are limited in biological systems, and so far are predominantly identified in microorganisms, such as *C. thermoaceticum* (30), *Pyrococcus furiosus* and *Thermococcus litoralis* (16-18, 20) which live in high temperature, anaerobic environments. Moreover, W has been found to stimulate the growth of certain thermophilic (3) and hyperthermophilic organisms (6).

In the current study, *P. aerophilum* was grown near its optimum temperature, and near its minimum growth temperature, in the presence of various combinations and concentrations of tungstate and molybdate. The objective was to investigate the differential uptake and the effect that these two metals have on the growth of the organism. It was also assumed that one or both metals would be assimilated into the active sites of metalloenzymes, such as FDH and NR. Consequently, the activities of these two enzymes, under all conditions, were also investigated to

determine the role of these metals in the formate-nitrate reductase respiratory pathway. Unfortunately, the methods described in the original description of *P. aerophilum* (29) did not result in reproducible growth of the organism. Thus, protocols were established to achieve this and also to obtain significant cell densities to enable the study of its metal metabolism.

MATERIALS AND METHODS

Strain. *P. aerophilum* (DSM 7523) was obtained from Deutsche Sammlung von Mikroorganismen und Zellkulturen in Braunschweig, Germany.

Culture conditions. *P. aerophilum* was cultured anaerobically in marine medium as originally described by Völkl et al. (1993) with the modifications described below. 10 mM PIPES (piperazine-*N,N'*-bis (2-ethanesulfonic acid)-HCl) was used as the buffering agent in small-scale closed system growth (20 mL - 500 mL) instead of the NaCO₃ - CO₂ buffer system in the original medium and NH₄Cl was omitted. Peptone (0.05%, w/v) was used to supplement the yeast extract (0.05%, w/v) as carbon sources. The final concentrations of oxyanions were routinely 1.5 μM WO₄²⁻ and/or MoO₄²⁻ rather than 0.5 μM WO₄²⁻ and 0.3 μM MoO₄²⁻ as in the original medium. Other concentrations of WO₄²⁻ and MoO₄²⁻ were used as described in the text. In order to remove the need for overpressure as required in the original medium [300 kPa N₂/CO₂ (80:20)], 10 mM sodium formate was added to the growth medium. The final modification of the original medium was the omission of a reducing agent. However, KNO₃, the terminal electron acceptor, was added at a concentration of 0.1% w/v (10 mM initial concentration) as described in the original medium.

Small-scale cultures, 50 mL and 500 mL, were grown anaerobically in 120 mL serum vials and 1 L culture bottles, respectively. Cultures were bubbled with N₂/CO₂ (80:20) for 1 hr / 100 mL medium and inoculated with a 10 % volume of culture grown at same WO₄²⁻ and/or MoO₄²⁻ concentration and at the same temperature. Cultures were grown at 98 °C or 78 °C.

Additional modifications were made when *P. aerophilum* was grown in gassed large-scale cultures (16 L and 450 L). PIPES was not added to the large-scale medium, resulting in a final concentration of 1 mM PIPES due to the presence of PIPES in the inoculum. 16 L cultures were grown without shaking in 20 L carboys and were continuously bubbled with N₂/CO₂ (80:20) during growth at 98 °C or 78 °C. 450 L cultures were grown at 95 °C in a 600 L custom stainless steel fermentor (W. B. Moore, Inc.) stirring at 50 rpm. The medium was sparged with Ar while heating it to the growth temperature, and N₂/CO₂ (80:20) was continually flushed through the headspace throughout the growth phase. Because this is a gassed system, and the primary buffering agent was removed, cells were pH controlled (6.8 - 7.0) with either 0.1N HCl or 0.5 M formic acid. Growth was determined by direct cell counts using a 0.020 mm deep Petroff-Hausser counting chamber (Hausser Scientific Partnership, Horsham, PA) and by optical density at 600 nm (OD₆₀₀) using a Spectronic 501 (Milton Roy, Inc.) spectrophotometer.

Preparation of cell free extracts and membrane fractions. Cells grown in 16 L carboys were used for all analyses. Three carboys were used for each growth treatment and cells were harvested in mid-logarithmic growth phase, rapidly frozen with liquid nitrogen and stored at -80 °C until use. To prepare extracts of *P. aerophilum* cells, all procedures were carried out under strictly anaerobic conditions. Cells were thawed under Ar, resuspended (1 g/3 mL) in anaerobic lysis buffer (50 mM Tris, pH 8.0, containing 2 mM dithionite (DT) and 50 µg of DNase) and

were stirred at 37°C for 2 hours. The extract was then passed twice through a French pressure cell under anaerobic conditions. The cell suspension was spun at 8,000 x *g* for 10 min to remove unbroken cells and precipitate. The supernatant represents the cell-free extract. For experiments requiring further fractionation, the supernatant was centrifuged again at 100,000 x *g* for 1.5 h to separate the membrane and cytoplasmic fractions. The membrane pellet was resuspended in 50 mM Tris, pH 8.0, containing 4 M NaCl and 2 mM DT, homogenized in a glass tissue grinder and centrifuged at 100,000 x *g* for 1 h. The remaining membrane pellet was again resuspended in the same buffer but without salt, homogenized and centrifuged (100,000 x *g* for 1 h). The membrane fraction was finally resuspended in solubilization buffer (50 mM Tris, pH 8.0, containing 2 mM DT, 2.0% n-octyl β -glucoside, 100 mMol PMSF) at a protein concentration of 14-16 mg/mL. This was stirred for 2 h, and centrifuged again for 1 h at 100,000 x *g*. The supernatant represents the solubilized membrane fraction.

Enzyme assays. NR activity was determined with reduced methyl viologen (MV) as an artificial electron donor at 90 °C. Anaerobic serum-stoppered cuvettes contained 2 mL of anaerobic assay buffer (50 mM HEPES, pH 7.0) and methyl viologen (MV) (0.5 mM). To this, sufficient dithionite was added from a stock solution (100 mM in 50 mM HEPES, pH 7.0) to reduce the MV to an OD of 2.0 at 600nm. The enzyme sample was then added and the cuvettes were heated for 3 min at 90 °C in a custom Spectronic 501 spectrophotometer. The reaction was initiated by the addition of KNO₃ (10 mM). A molar absorbance coefficient, ϵ_{600} , of 12,000 M⁻¹ cm⁻¹ was used to follow the oxidation of reduced MV.

FDH activity was determined by measuring the reduction of benzyl viologen (BV) (3 mM) in anaerobic buffer (50 mM Ches, pH 8.5) under the same anaerobic conditions as

described above. The reaction was initiated by the addition of sodium formate (5 mM). A molar absorbance coefficient, ϵ_{600} , of $7,400 \text{ M}^{-1} \text{ cm}^{-1}$ was used to follow reduced BV.

Aldehyde oxidoreductase (AOR) activity was measured spectrophotometrically at $80 \text{ }^\circ\text{C}$ with crotonaldehyde (0.25 mM) as the substrate and BV (5 mM) as the electron acceptor. Anaerobic serum-stoppered cuvettes contained 100 mM EPPS buffer, pH 8.4, and were incubated for 3 min and then were slightly prereduced by the addition of a small amount of DT (100 mM). The reaction was initiated by the addition of crotonaldehyde (0.25 mM), and the reduction of BV was followed and 580 nm (molar absorbance, $7,400 \text{ M}^{-1} \text{ cm}^{-1}$). Formaldehyde oxidoreductase (FOR), and glyceraldehyde-3-phosphate (GAPOR) activity were measured under the same conditions (GAPOR was measured at $70 \text{ }^\circ\text{C}$) with formaldehyde (50 mM) as the substrate for FOR activity, and glyceraldehyde-3-phosphate (0.4 mM) as the substrate for GAPOR activity.

Glutamate dehydrogenase (GDH) activity was determined at $85 \text{ }^\circ\text{C}$ by the reduction of NADP^+ at 340 nm. The assay reaction mixture (2 mL) included 100 mM EPPS buffer, pH 8.0, and 80 mM glutamate in anaerobic cuvettes. These were heated at $85 \text{ }^\circ\text{C}$ for two min and the protein sample was then added. After heating for an additional minute, the reaction was initiated by the addition of 8 mM NADP^+ . All specific enzymatic activities are expressed as μmoles of substrate oxidized or reduced/min/mg of protein for NR, FDH, AOR, FOR, GAPOR and GDH.

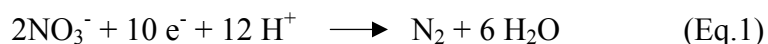
Protein measurement. Protein concentration was determined using a detergent-compatible modified Lowry assay (*DC Protein Assay*, Bio-Rad). Bovine serum albumin was used as the protein standard.

Metal analysis. Tungsten and molybdenum concentrations were measured using inductively coupled plasma emission spectroscopy (ICP) performed at the Chemical Analysis Laboratory of the University of Georgia. Measurements were repeated using inductively coupled plasma mass spectroscopy (ICP-MS). This analysis was performed at the Skidaway Institute of Oceanography of the University of Georgia in Savannah, GA.

Other methods. Formate was measured on a Waters 2690 Alliance high performance liquid chromatography (HPLC) system with a photodiode array detector using an Aminex HPX-87H column (300 x 7.8 mm) that was eluted with a linear gradient (30 mL) from 0 to 30 % of sulfuric acid, 0.01 N (Buffer A) to acetonitrile (Buffer B) at a flow rate of 1 mL/min. The genome of *P. aerophilum* that was used was taken from the GenBank database, accession number AE009441. Amino acid sequences of W- and Mo- containing enzymes were analyzed with MacVector (Accelrys Software Inc.). Phylogenetic tree analysis was compiled using Vector NTI, Suite 9.0.0 (InforMax, Inc.).

RESULTS

Cell yield and doubling time are dependent upon pH during anaerobic growth. Growth of *P. aerophilum* is greatly affected by pH, as explained by the overall electron balance of growth on nitrate:



As illustrated, two additional H^+ are needed, and therefore the medium becomes basic during growth. The equation can also be written:



Therefore, preliminary studies focused on optimizing the buffering capacity of the medium to maintain a high-temperature (98 °C) pH of between 6.6 - 6.8. Initial growth of *P. aerophilum* cultures were obtained in a pH range from 5.0 to 9.0 with an optimum around pH 7.0 (29). In our laboratory, for small-scale (20 – 500 mL) closed-system growth, 10 mM PIPES (pKa = 6.76) was found to be a more effective buffering agent than bicarbonate (pKa = 6.86), which was the buffering agent in the original medium (29) and also than phosphate buffer (pKa = 6.86). Growth of *P. aerophilum* cells in medium at pH below 6.5 or above 8.5 resulted in cell lysis, which was observed as a loss of turbidity in the culture, and as broken cells in the light microscope. Furthermore, at pH around 8.0 and during stationary and late log phase, spherical bodies began to form at the end of the rods, referred to as ‘golf clubs’ (Fig. 1.2b, Chapter 1). Using the PIPES based medium, doubling times of 3-5 hours were routinely obtained. For large-scale cultures, using 20 L carboys and the 600 L fermentor, only the PIPES in the inoculum was present, and this resulted in final concentrations of 1 mM and 0.1 mM, respectively. Concentrations higher than this caused substantial precipitation during growth. Consequently, cells were pH-controlled with either 0.1 N HCl or 0.5 M formic acid. Cultures grown under these conditions attained final cell densities ranging from 1.5×10^8 to 7×10^8 cells/mL with doubling times ranging from 4.5 h to 11 h depending upon growth temperature. Optimum growth conditions were obtained when yeast extract (YE) (0.05%) plus peptone (0.05%) were used as carbon sources. The cell yields were higher than when YE (0.1% or 0.2%), peptone (0.05% or 0.1%) or tryptone (0.05%) were used individually or in combination with YE (0.05%).

The addition of formate during growth enhances cell yield and activity of respiratory enzymes. Initial small-scale growth of *P. aerophilum* (29) was reported to require an overpressure of 300 kPa N₂/CO₂ (80:20). In our laboratory this condition was easily and satisfactorily reproduced for cultures up to and including 500 mL. Larger cultures (16 L), however, were continually sparged with N₂/CO₂ during growth. In order to remove the need for overpressure at small scale, 10 mM sodium formate was added to the growth medium. The addition of formate to the growth medium allows additional substrate for FDH, and thus an increased production of CO₂ in the medium which serves to increase pressure in the growth vessel. HPLC analysis confirmed that approximately 64% of added formate was utilized during growth. Experiments using Ar in place of N₂/CO₂ as an alternative gas phase with the addition of formate were also performed. Surprisingly, no growth occurred under Ar. However, if the medium was gas-exchanged with Ar until the growth temperature was reached, and then N₂/CO₂ was flushed and retained in the headspace, growth yields were comparable to yields obtained using N₂/CO₂ alone (data not shown). While the addition of formate to the growth medium improved growth rates and cell density only slightly, the specific activities of both NR and FDH were approximately doubled in the presence of formate in small- and large-scale cultures (Fig. 2.1). Specific activities in both the membrane fraction and the cytosolic fraction were determined. As expected, the activities of both NR and FDH were localized to the membrane fraction with only residual activity in the cytosolic fraction (Fig. 2.1).

Growth of *P. aerophilum* at 98 °C requires tungstate and is inhibited by molybdate. Growth experiments were carried out with the addition to the media of WO₄²⁻ only, of MoO₄²⁻ only, and

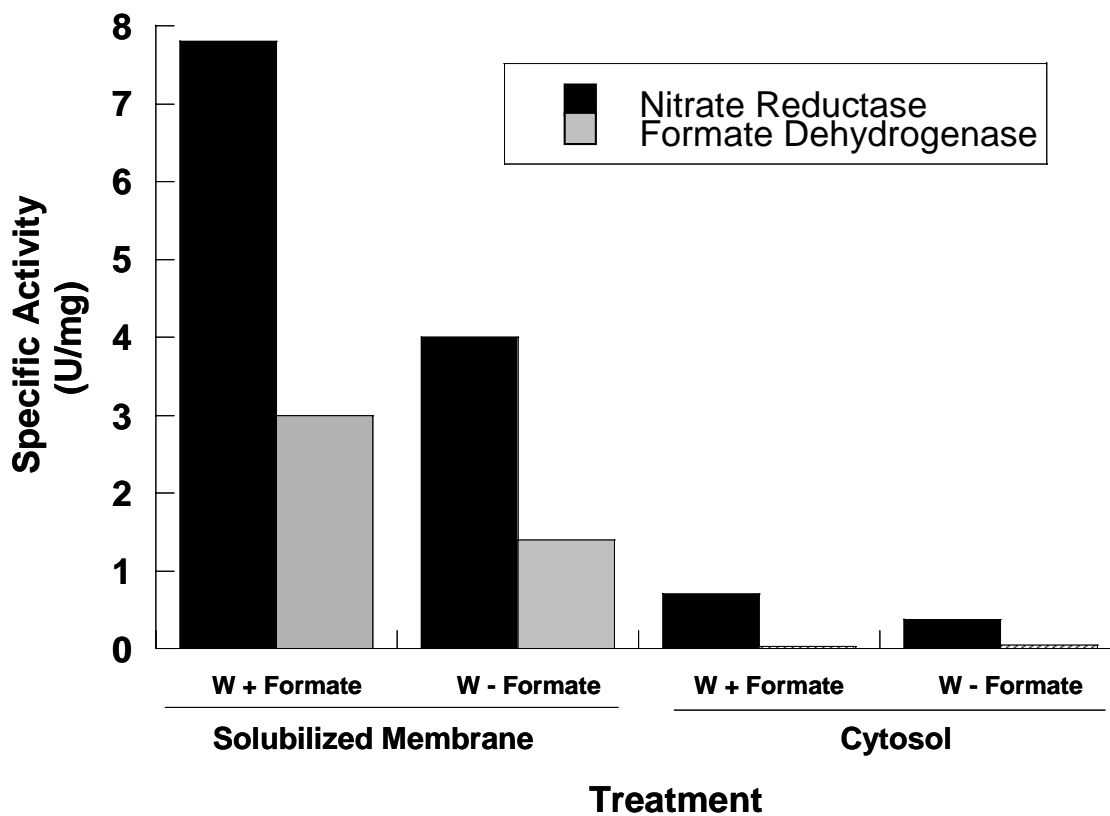


Figure 2.1. Specific activities of nitrate reductase and formate dehydrogenase in *P. aerophilum*. Solubilized membrane and cytosolic fractions from cells grown with $1.5 \mu\text{M WO}_4^{2-}$ at 98°C with and without formate added to the growth medium. Extracts were prepared as described in the Materials and Methods. The results were obtained with three sets of cultures grown under the same conditions. The standard deviation is less than 0.5%.

with the addition of both oxyanions at concentrations of 0.3 μM , 0.9 μM , 1.5 μM and 2.1 μM . These cultures were grown at 98 °C. Preliminary experiments demonstrated that four transfers were necessary to limit contamination of residual metals in the inoculum. Based on these conditions, optimum growth, both in terms of yield and reproducibility, was obtained with 1.5 μM WO_4^{2-} , and slightly lower yields were supported by the addition of 0.3 μM . Interestingly, growth was inhibited by the presence of MoO_4^{2-} at all concentrations when supplied as the only oxyanion and also when equal molar amounts of WO_4^{2-} and MoO_4^{2-} were present. A low concentration of MoO_4^{2-} (0.3 μM) in combination with a high WO_4^{2-} concentration (1.5 μM), however, did successfully support growth at 98°C (Fig. 2.2). No growth was obtained, however, beyond two transfers without the addition of WO_4^{2-} at 98 °C (Fig. 2.2).

Both molybdate and tungstate support growth at the minimal growth temperature (78 °C).

Because molybdate had such a strong inhibitory effect on high temperature growth, and molybdenum has been found to replace tungsten in many thermophilic microorganisms, such as *C. thermoaceticum* (3), analogous growth studies were conducted at 78°C, which is near the minimum growth temperature for *P. aerophilum*. *P. aerophilum* cells grew at 78°C in the presence of either WO_4^{2-} or MoO_4^{2-} , and in the presence of both metals (Fig. 2.2). Optimum growth was obtained with an oxyanion concentration of 1.5 μM , and approximately equal yields in the presence of 0.3 μM concentrations. Further, no growth was obtained beyond two transfers without the addition of either WO_4^{2-} or MoO_4^{2-} at 78 °C (Fig.2.2). As expected, the doubling times (11 to 17 h) of cultures grown at 78 °C were much longer in comparison with cultures grown at 98 °C (doubling times of 3 to 5 h). Additionally, cells grown at 78 °C experienced a

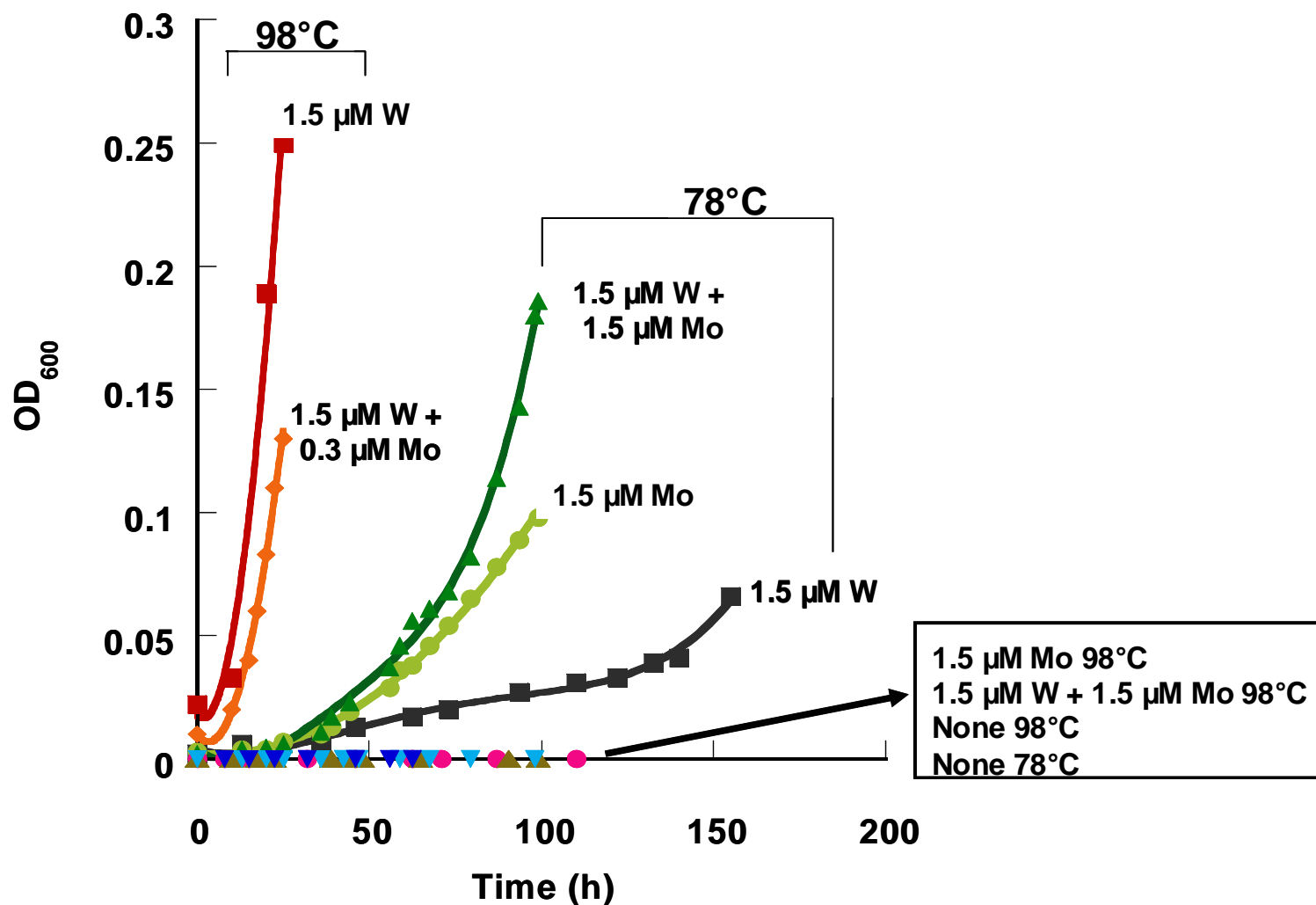


Fig. 2.2. Growth of *P. aerophilum* cells at 98 °C and 78 °C. Growth was in the presence of 1.5 μM WO_4^{2-} , 1.5 μM MoO_4^{2-} , 1.5 μM WO_4^{2-} and 1.5 μM MoO_4^{2-} , or without any WO_4^{2-} or MoO_4^{2-} added to the medium. The W/Mo treatment at 98 °C, however, is 1.5 μM WO_4^{2-} and 0.3 μM MoO_4^{2-} . Cell growth was measured by optical density at 600 nm (OD₆₀₀). The final time point represents the time of harvest of cultures. The inset indicates which metal was added (W or Mo) and the growth temperature (78 or 98 °C).

lag phase ranging between 13 h (1.5 μM WO_4^{2-} and MoO_4^{2-}) and 25 h (1.5 μM MoO_4^{2-}), unlike cultures grown at the high temperature (Fig. 2.2).

Cell size is more variable than cell number between growth temperatures. Growth was measured by both optical density and by direct cell counts. Cell densities reached at least 1×10^8 cells/mL at both temperatures under all conditions in which growth was supported through a minimum of four transfers (Fig. 2.3). Growth yields based on optical density (OD_{600}), however, exhibited a wide range (0.066 to 0.250). This reflects the differences in cell size under the different growth conditions (Fig. 2.2). Observations using Phase/Contrast Microscopy revealed that cells grown under low temperature conditions were in general smaller (2 to 5 μm in length), as compared to cells grown under high temperature conditions (4 to 10 μm). Moreover, V-shaped and raft-shaped aggregates of cells were more prominent in cultures grown at the high temperature.

Intracellular concentrations of W and Mo. ICP analyses were conducted on media prior to the addition of YE, peptone and nitrate, after they were added, after the addition of WO_4^{2-} and/or MoO_4^{2-} , and after growth using the supernatant and pellet after cells were centrifuged. The results indicate that both Mo and W are incorporated into *P. aerophilum* cells, even when no additional WO_4^{2-} or MoO_4^{2-} are added to the growth medium (Table 2.1). This is indicative of residual amounts of W and Mo present in the medium from the added YE and peptone. For example, with no WO_4^{2-} or MoO_4^{2-} added, the medium contained 0.04 μM Mo and from 0.02 to 0.05 μM W. At 78 °C, when cells were grown in the presence of added MoO_4^{2-} only, the accumulation of MoO_4^{2-} in cells was more than double that of WO_4^{2-} . In the presence of both

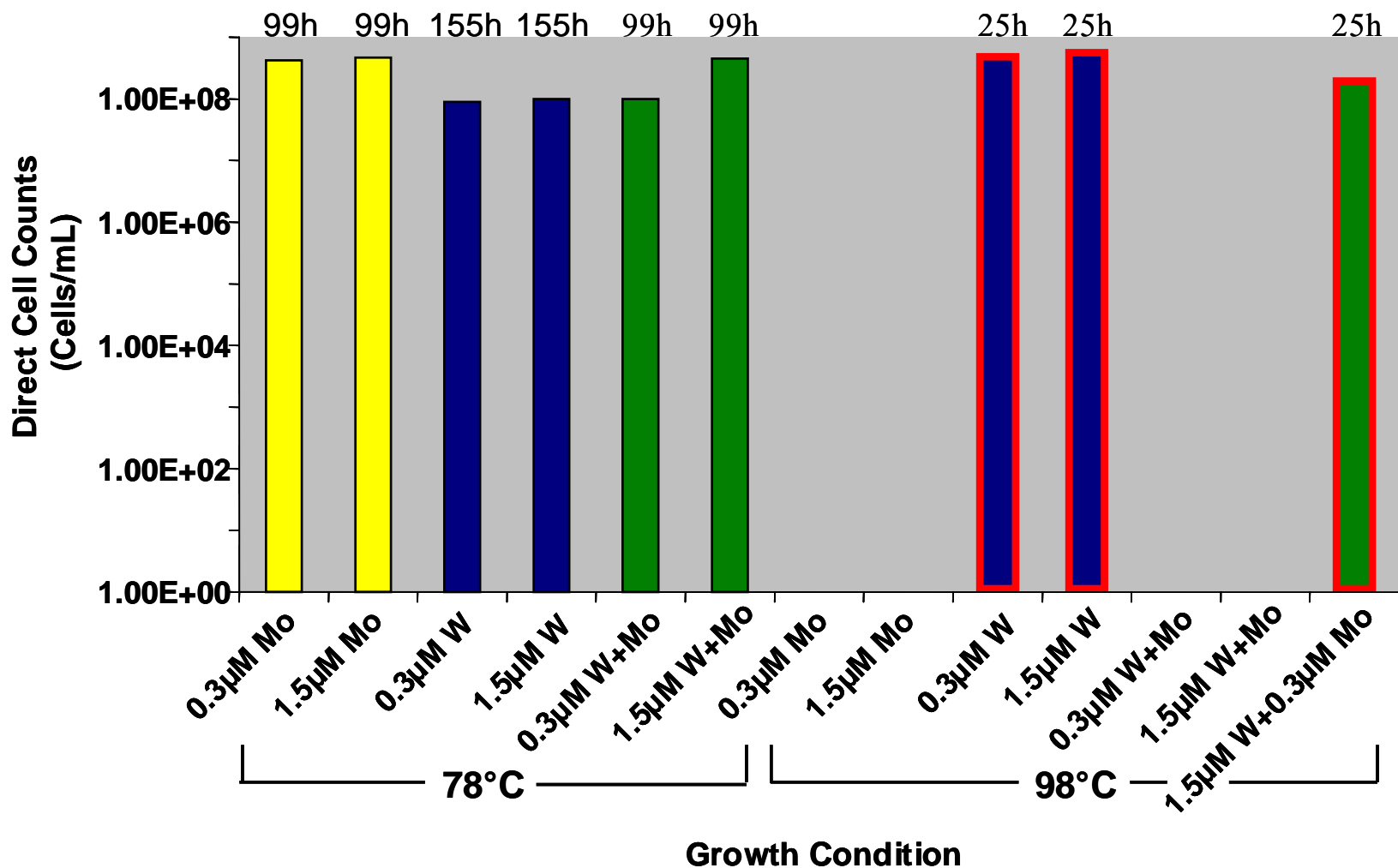


Fig. 2.3. Direct cell counts of *P. aerophilum* cultures at time of harvest. Cells were grown at 98 °C and 78 °C in the presence of 0.3 μM and 1.5 μM WO_4^{2-} (blue bars), 0.3 μM and 1.5 μM MoO_4^{2-} (yellow bars), or 0.3 μM and 1.5 μM WO_4^{2-} and MoO_4^{2-} (green bars). The W/Mo treatment at 98 °C, however, is 1.5 μM WO_4^{2-} and 0.3 μM MoO_4^{2-} (green-red bar). Cells grown at 98 °C are outlined in red. No growth was exhibited in cultures at 98 °C in the presence of only MoO_4^{2-} or equal molar amounts of WO_4^{2-} and MoO_4^{2-} . All other cultures reached at least 1×10^8 cells / mL, and were harvested at the time in hours that is denoted above each bar.

Table 2.1. Intercellular Concentrations of W and Mo in *P. aerophilum* growth media and cells under variable conditions[§].

Cell Growth Conditions	Media		Cells	
	Mo	W (μM)	Mo (pmoles / mg cells)	W
0.3 μM Mo 78 °C	0.59	0.05	14.6	7.07
1.5 μM Mo 78 °C	2.55	0.02	15.6	7.07
1.5 μM W 78 °C	0.04	2.28	3.13	4.35
0.3 μM Mo/W 78 °C	0.64	0.46	3.13	2.72
1.5 μM Mo/W 78 °C	2.66	2.25	5.21	3.81
0.3 μM W 98 °C	0.04	0.76	2.08	2.28
1.5 μM W 98 °C	0.04	2.23	2.08	5.44

[§] Determined by ICP analysis.

added oxyanions, the accumulation was approximately the same. Cells grown in the presence of added WO_4^{2-} only, accumulated approximately equal amounts of MoO_4^{2-} and WO_4^{2-} except for the 1.5 μM culture grown at 98 °C.

Cellular localization of NR and FDH. After separation of the membrane and soluble fractions by ultracentrifugation, virtually all of the NR and FDH activity remained in the membrane fraction, indicating that both enzymes are membrane associated. In order to further determine association with the membrane, cells were homogenized, resuspended, centrifuged and assayed sequentially in 0.5 M, 1 M, 2 M and 4 M NaCl. NR had a specific activity of 4 U/mg in the cell free extract and a specific activity of 3.5 U/mg after the 4 M NaCl wash (88%). FDH had a specific activity of 1.1 U/mg in the cell free extract and a specific activity of 0.83 U/mg after the 4 M NaCl wash (76%). Again, virtually all of the NR and FDH activity remained in the membrane fraction, indicating that the enzymes are at least partially embedded in the membrane. Based on these initial results, further characterization of the enzymes used membranes after they had been washed with 4 M NaCl.

Specific activity of NR and FDH in solubilized membranes. In order to compare enzyme activities under the different growth conditions, solubilized membranes were prepared from 16 L cultures (Table 2.2). Glutamate dehydrogenase (GDH) activity, determined from cell free extracts, was used as the control because it is neither a membrane bound protein nor does it contain Mo or W. Thus, it should be expressed at the same level under all conditions. Specific activities were determined using cells from each growth treatment where growth was sustained

Table 2.2. Specific Activities* of NR, FDH, and GDH at 90 °C in Solubilized Membranes under various growth conditions of *P. aerophilum*.

Enzyme	78 °C			98.5 °C	
	Mo 1.5 µM	W 1.5 µM	W/Mo 1.5 / 1.5µM	W 1.5 µM	W/Mo 1.5 / 0.3 µM
Nitrate Reductase	2.80 ± 0.060	3.70 ± 0.016	7.66 ± 0.140	3.98 ± 0.040	4.53 ± 0.030
Formate Dehydrogenase	0.26 ± 0.004	0.80 ± 0.005	1.36 ± 0.011	0.89 ± 0.040	0.52 ± .020
Glutamate Dehydrogenase [§]	0.102 ± 0.008	0.101 ± 0.012	0.096 ± 0.003	0.110 ± 0.017	0.099 ± 0.006

* Defined as one µmole of substrate utilized min⁻¹ mg⁻¹ protein.

[§] Activity in Cell Free Extracts.

through the fourth transfer. The specific activity of GDH, approximately 0.1 U/mg, was the same under all growth conditions tested, as shown in Table 2.2. The specific activities of NR and FDH in WO_4^{2-} -grown cells were approximately the same at both growth temperatures, but those in MoO_4^{2-} -grown cells (only at 78°C) were slightly lower than that of WO_4^{2-} -grown cells. The specific activity of NR in cells grown in the presence of both WO_4^{2-} (1.5 μM) and MoO_4^{2-} (0.3 μM) at 98°C was similar to that in cells grown in the presence of WO_4^{2-} alone. FDH activity, however, was slightly lower (Table 2.2). The highest specific activity for both NR and FDH was achieved at 78°C when both WO_4^{2-} and MoO_4^{2-} were added in equal molar amounts (Table 2.2).

Other W- and Mo-containing enzymes in *P. aerophilum*. Amino acid sequence analysis of the open reading frames (ORFs) in the genome of *P. aerophilum* reveals that, in addition to NR and FDH, there are eleven other ORFs which potentially encode molybdo- or tungstoenzymes (Fig 2.4). Of these eleven, there are four AOR-type enzymes, including one aldehyde ferredoxin oxidoreductase (AOR), one formaldehyde ferredoxin oxidoreductase (FOR), one glyceraldehyde-3-phosphate ferredoxin oxidoreductase (GAPOR), and one distantly-related tungsten-containing oxidoreductase (WOR-X). These enzymes are cytosolic in organisms such as *P. furiosus* (21), and are not known to utilize Mo (19). Specific activities of AOR, FOR and GAPOR in the cytosolic fraction of *P. aerophilum* cells grown in the presence of 1.5 μM WO_4^{2-} at 98 °C were determined to be 0.0326 U/mg \pm 0.003, 0.104 U/mg \pm 0.024, and 0.00914 U/mg \pm 0.009, respectively. These enzymes presumably account for some of the requirement for W of the organism, yet, do not help to explain the presence of W in the membrane fraction. In addition to NR and FDH and the four AOR-type enzymes, there are seven ORFs in the genome

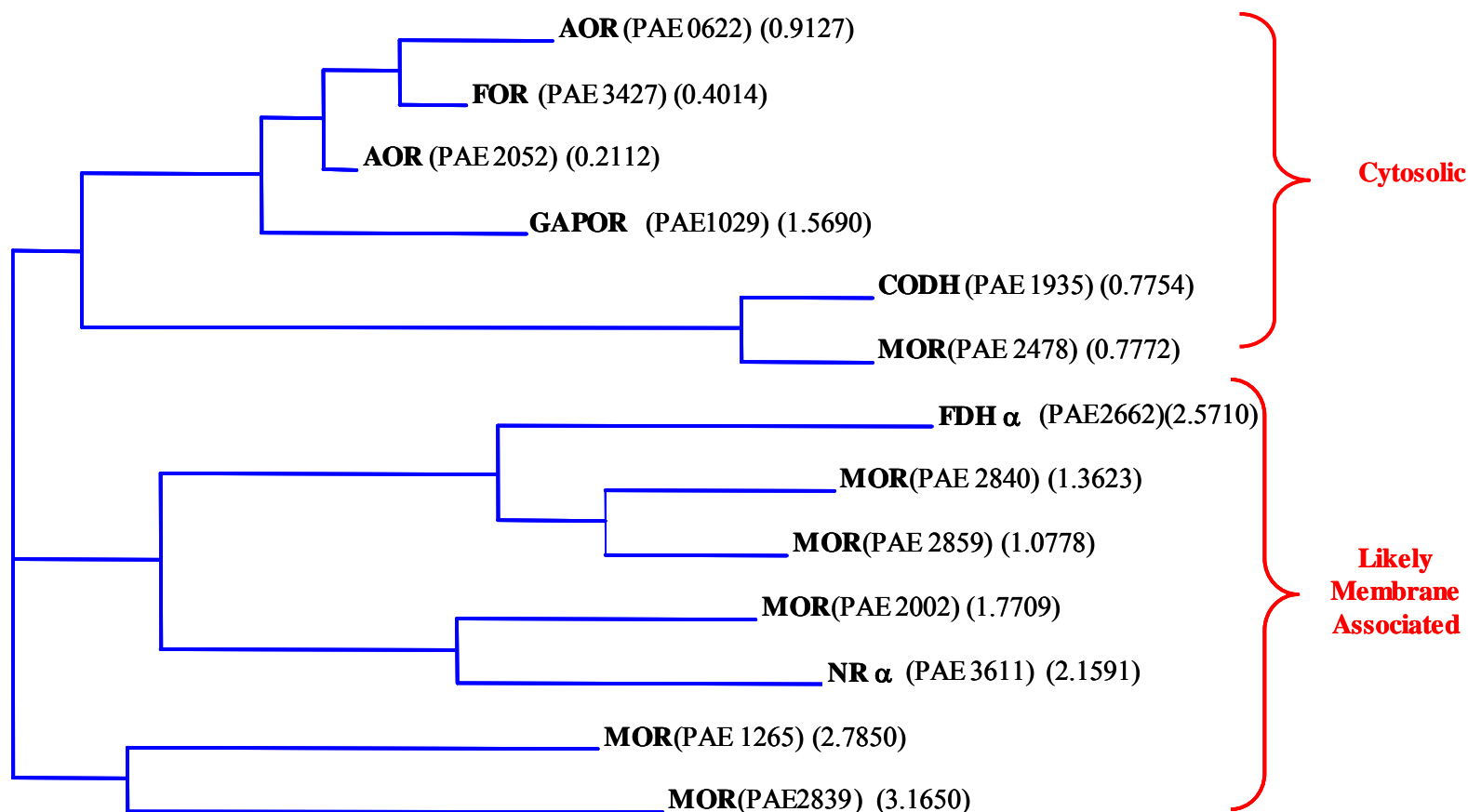


Fig. 2.4. Phylogenetic tree of all W- and Mo-containing enzymes found in *P. aerophilum*, as determined by genomic sequence analysis. The tree was constructed using Vector NTI, Suite 9.0.0 (InforMax, Inc.). The corresponding locus for each enzyme is presented within the bold parentheses. The second set of parentheses contain the calculated sequence distance utilizing the neighbor joining method (22) and Kimura's correction factor (13). Brackets indicate the likelihood that the predicted proteins will be located in the cytosol or associated with the membrane, based amino acid sequence analysis and transmembrane helixes predictions.

that are predicted to encode molybdoenzymes, or molybdopterin oxidoreductases (MOR) (Fig. 2.4). Based on BLAST searches, two of these seven proteins, which show the highest similarity to carbon monoxide dehydrogenase (PAE1935), and xanthine dehydrogenase (PAE2478), are assumed to be cytosolic proteins, as they exhibited no transmembrane domains from sequence analysis, unlike the remaining 5 proteins that are likely to be membrane associated. Of these remaining MOR (PAE2840 and PAE2859) have a high similarity to FDH (Fig. 2.4) and also contain the twin arginine translocation (TAT) sequence for protein export. PAE2840 has a greater than 45% similarity to FDH in *Archaeoglobus fulgidus* and *C. thermoaceticum*. PAE2859 also has a high similarity (~ 55%) to FDH in *C. thermoaceticum*, but in addition has greater than 50% similarity to dimethyl sulfoxide reductase (DMSOR) in *Aquifex aeolicus*, *E. coli* and *Haloarcula marismortui*, to thiosulfate reductase in *Thermus thermophilus*, *Wolinella succinogenes* and several *Salmonella* species, and to putative oxidoreductases in numerous other bacteria and archaea. PAE2002 has from 50 to 60% similarity to dehydrogenase α subunits (the amino end fragment), including FDH, from numerous organisms including *Pyrococcus* species, *Thermococcus kodakaraensis*, and *Sulfolobus solfataricus*. PAE1265 has approximately 50% similarity to tetrathionate reductase in *Vibrio*, *Thiobacillus*, *Azoarcus* bacterial species, and approximately 80% to MOR in the archaea *Aeropyrum pernix* and *A. fulgidus*. To the contrary, PAE2839 has no high similarity to other MOR in particular, but rather to putative oxidoreductases that contain the TAT sequence, and thus is most likely a membrane attached protein. Therefore, many of the MOR identified in *P. aerophilum* are membrane-bound in other organisms, and could account for some of the requirement of Mo and/or W in the membranes of *P. aerophilum* cells.

DISCUSSION

P. aerophilum was isolated in strongly-gassed marine water holes in the tidal zones off of the coast of Ischia, Italy (29). This archaeon thrives in an extreme temperature environment, at or above 90 °C, and is therefore a hyperthermophile. While most organisms (bacteria, archaea, and eukaryotes, including humans) are dependent on Mo for their existence, only hyperthermophilic archaea are known to require W. This requirement for the two metals stems from their presence in the active sites of metalloenzymes. Although the abundance of Mo and W in nature is equal in the earth's crust (15 g/metric ton), Mo is the most abundant transition metal in the oceans. The concentration of Mo in seawater is approximately 11 µg/L; which is about two orders of magnitude higher than the concentration of W (0.12 µg/L). Most significantly, however, the abundance of W in hyperthermophilic environments such as hot springs (15-300 µg/kg) and vent flanges (180-585 mg/kg) is far greater than that of Mo (3-60 µg/kg and 47 mg/kg, respectively) (26). *P. aerophilum* was grown near its optimum temperature (98 °C), representative of its natural hyperthermophilic environment, and near its minimum growth temperature (78 °C), representative of mesophilic environments, in the presence of various combinations and concentrations of tungstate and molybdate. Protocols were established to achieve growth with significant cell densities under these conditions to enable the study of its metal metabolism.

Anaerobic growth of *P. aerophilum* on nitrate is greatly affected by slight variations in pH. Maintaining a pH of 6.6 to 7.3 in the culture medium during growth is essential, as cell lysis was observed in cultures with pH below 6.5 and above 8.5. Furthermore, at pH around 8.0 and during stationary and late log phase, spherical bodies began to form at the end of the rods. This tremendous pH effect could originate from the dependency of *P. aerophilum* on WO_4^{2-} and/or MoO_4^{2-} . Specifically, as in *E. coli* (10), pH could critically affect the affinity of the uptake

system for the oxyanions (pKa of MoO_4^{2-} is 3.8 and 4.7 for WO_4^{2-}), and thus limit the availability of these metals for NR and FDH, and consequently for growth. Since the medium becomes basic during growth, an adequate buffering system must be employed. This was accomplished by the use of PIPES in small-scale cultures, and by pH maintenance by the addition of HCl and formic acid throughout growth in large-scale cultures. The addition of formate to the culture medium also aided in pH-control during growth, and this resulted in increased cell yield and an increased growth rate. In addition, the specific activity of NR and FDH increased by approximately two-fold in formate-grown cells. By supplying cells with formate in combination with YE and peptone, there appears to be a surplus source of carbon and reductant, resulting in enhanced growth. In *E. coli*, formate is known as a key intermediate in anaerobic metabolism, and is produced from the CoA-dependent cleavage of pyruvate by the pyruvate formate-lyase (PFL) enzyme (14). PFL is catalytically active only in anaerobic cells. Further, *E. coli* mutants unable to synthesize PFL exhibit little growth anaerobically, and instead perform lactic acid fermentation, unless the growth medium is supplemented with formate, nitrate and acetate (23). Nitrate functions to repress the fermentative pathway by removing formate (the inducer). In essence, formate, which is excreted by the cell at neutral pH, is localized on the periplasmic side of the cytoplasmic membrane, where it is efficiently oxidized by the nitrate-inducible FDH (FDH-N) or by FDH-O, which oxidizes formate in the presence of oxygen and also nitrate (23). Consequently when nitrate is present in *E. coli* cells, there is a low intracellular concentration of formate. However, when nitrate becomes limiting, the extracellular formate concentration increases with a simultaneous decrease in the pH of the culture medium, thus shifting the accumulation of formate to the cytoplasm. Most likely, it is in this manner that the addition of formate to the growth medium of anaerobically growing *P. aerophilum* cells functions as a

substrate for FDH and consequently supplies electrons for nitrate reduction. Thus, this results in an increase growth rate and cell yield as well as increased activities of NR and FDH. The addition of formate to the growth medium resulted in increased FDH activity and induction of NR activity in anaerobically growing *Paracoccus denitrificans* cells (8), suggesting a similar mechanism.

The most crucial element necessary for growth of *P. aerophilum*, however, is WO_4^{2-} near the optimum growth temperature (98 °C) and WO_4^{2-} or MoO_4^{2-} near the minimum growth temperature (78 °C). WO_4^{2-} not only had a stimulatory effect on anaerobic growth of *P. aerophilum*, it was required for growth at high temperature (98 °C). MoO_4^{2-} , on the other hand, inhibited growth at this temperature when present in the growth medium without and WO_4^{2-} and also when equal molar concentrations of MoO_4^{2-} and WO_4^{2-} were added. When WO_4^{2-} (1.5 μM) was present in higher concentrations than that of MoO_4^{2-} (0.3 μM), growth at 98 °C was maintained beyond four transfers. While this work was in progress, another group (2) reported growth studies of *P. aerophilum*. Their data support the findings presented herein. They also found that no growth occurred (96 °C) when MoO_4^{2-} alone was added to the medium and that up to 1 μM MoO_4^{2-} had no affect on cell growth when WO_4^{2-} was also added to the medium (2). However, they did not study metal requirements at the minimal growth temperature.

We show here that growth of *P. aerophilum* at the minimum growth temperature (78 °C) also required the presence of WO_4^{2-} but MoO_4^{2-} was easily substituted in this role. Although growth rate was much slower and cell size was much smaller, the cell density was similar to that reached under optimum temperature conditions.

Numerous growth studies have been conducted with other organisms that focus on the requirement of WO_4^{2-} and MoO_4^{2-} . The organisms include *Methanobacterium*

thermoautotrophicum and *M. wolfei*, *E. coli*, *Methylobacterium* sp. RXM, *Azotobacter chroococcum*, *P. furiosus*, *P. denitrificans*, *Rhodobacter capsulatus*, and *C. thermoaceticum* (4, 7, 8, 19, 24, 25, 27, 30). However, all of these studies investigated oxyanion requirement near the optimal growth temperature. This is an important distinction because the results presented herein are the first to show a temperature-dependent difference in W and Mo requirements. In addition, all but one of the aforementioned studies have been conducted on mesophilic or moderately thermophilic organisms. The exception was the hyperthermophile *Pyrococcus furiosus*, which was grown at 95 °C, near its optimal growth temperature (100 °C) in the presence MoO_4^{2-} and without WO_4^{2-} (19). The growth yield and rate were unchanged compared to cells in W-supplemented medium. More importantly, although the specific activities of the W-containing oxidoreductases (AOR, FOR, GAPOR) of *P. furiosus* did decrease, the enzymes did not incorporate Mo into their active site. Unfortunately, the cellular concentrations of W and Mo were not measured, so it is not known if Mo was taken up into the cells. These experiments were conducted using *P. furiosus* cells grown in a complex medium and the required W is available from the added YE.

Contrary to *P. furiosus*, *P. aerophilum* took up both W and Mo oxyanions into cells at both optimal and minimal growth temperatures. Furthermore, the mechanism by which WO_4^{2-} and MoO_4^{2-} were taken up and incorporated appears not to discriminate between the two oxyanions. Perhaps, as in *E. coli*, the molybdate transporter of *P. aerophilum* binds MoO_4^{2-} and WO_4^{2-} with similar affinities (10) and uptake is dependent on the concentration of the oxyanion in the medium. Based on the measured intracellular concentrations, when MoO_4^{2-} alone was added to the medium concentrations of Mo were much higher than those of W. When both oxyanions were added to the medium, the intracellular concentration of Mo and W was

approximately the same. When only WO_4^{2-} was added to the medium, the concentration of W was slightly higher than that of Mo. In *E. coli*, cells can accumulate up to thirty times more Mo than is present in the medium. Furthermore, cells grown in the absence of MoO_4^{2-} can accumulate levels of WO_4^{2-} up to six times greater than the normal physiological concentration of MoO_4^{2-} (27). This is possible because the molybdate transporter (encoded by the *modABCD* operon) is repressed by the *modE* gene product. ModE is activated by MoO_4^{2-} , and is six times less sensitive to WO_4^{2-} (9). *C. thermoaceticum* was also found to concentrate W intracellularly (30). Furthermore, there is only one homolog for each of the gene products of the *modABCD* operon in *P. aerophilum*, and are conserved enough to assume similar structure and function, yet different enough to be organism and environmentally specific. A detailed comparison of cofactor biosynthesis and metal transport in *E. coli* and *P. aerophilum* is discussed in Chapter 5.

We show here that WO_4^{2-} has a stimulatory affect on the growth of *P. aerophilum*. Conversely, one would expect that a ready supply of MoO_4^{2-} would be required for optimal growth considering that NR is expected to be dependent on the element, especially given the high reduction potential of the NR reaction. Either oxyanion, however, could potentially be used for catalysis by FDH. The specific activities of NR and FDH were approximately the same in cells grown in the presence of WO_4^{2-} alone, both at high (3.98 U/mg for NR and 0.89 U/mg for FDH) and low temperatures (3.70 U/mg for NR and 0.80 U/mg for FDH), and decreased slightly in the presence of MoO_4^{2-} only (2.80 U/mg for NR and 0.26 U/mg for FDH). An oxyanion concentration of 1.5 μM yielded the highest specific activities under all conditions. This is in contrast to the reported small-scale growth studies of *P. aerophilum* where the highest NR (FDH was not studied) specific activities were found in the presence of 0.1 μM and 0.3 μM WO_4^{2-} (1.36 and 1.10 U/mg, respectively) with a fourfold decrease in activity in the presence of 1.5 μM

WO_4^{2-} (0.35 U/mg) (2). The differences between these results are most likely due to the fact that one procedure used intact cells (2) rather than solubilized membranes (this study), as well as differences in time of harvest, i.e. late logarithmic (2) or early logarithmic phase (this study). Regardless of these differences, the highest specific activities for both enzymes, however, were found in this study in cells grown at 78 °C in the presence of both oxyanions (Table 2.2).

Results of specific activity measurements using *P. aerophilum* grown at 78 °C resemble results from a growth study of *C. thermoaceticum*, a thermophilic organism that grows at approximately 60 °C and has a W-containing FDH. When *C. thermoaceticum* cells were grown on W, FDH activity was higher than when grown on Mo. Interestingly, FDH activity was the highest when cells were grown in media containing both W and Mo (3). Perhaps, as the authors speculated, MoO_4^{2-} serves as an "inducer" in that it increases production of FDH and actually helps incorporate WO_4^{2-} into the active site (30). It is also possible that the NR and FDH from *P. aerophilum* contain both metals as exemplified by the purified FDH from *Methanococcus vannielii*. This enzyme appears to contain a mixed population of enzyme molecules with some containing Mo and some containing W, coordinated into their active site (12).

In contrast, the specific activities of *P. aerophilum* cells grown at 98 °C show that MoO_4^{2-} inhibits activity, and presumably directly competes with WO_4^{2-} for incorporation into the active site, illustrating a preference of one metal versus the other. Analogous situations have been reported in mesophilic bacteria such as in *Methylobacterium* sp. RXM, in which W has a positive role in the stimulation of FDH activity in the absence of Mo, but in the presence of both metals, there is an antagonistic action of W on the enzyme activity. Likewise, in the mesophilic bacterium *A. chroococcum*, W and Mo compete for the same site in NR, yet the enzyme is active only when it has incorporated Mo. This has also been demonstrated with *R. capsulatus* cells

grown with equal concentrations of the two metals. In this case, purified dimethylsulfoxide reductase (DMSOR) contained Mo and W in a 2:1 ratio (27). This enzyme, like the trimethylamine N-oxide reductase (TMAOR) from *E. coli* (7), exhibits catalytic activity with either W or Mo at the active site. In *M. wolfei* and *M. thermoautotrophicum*, however, both a W-containing and a Mo-containing isozyme of formylmethanofuran dehydrogenase are present. In both organisms, the W-isozyme is constitutively expressed, while the Mo-isozyme is induced by molybdate (4, 24).

P. aerophilum cells grown at 78 and 98 °C contained active forms of both NR and FDH and also incorporated both Mo and W oxyanions. It remains unknown, however, if W or Mo or both are incorporated into the active sites of one or both enzymes, and which forms are active. TMAOR from *E. coli* incorporates either metal and is active, but as expected the characteristics of the enzymes are different. The W-TMAOR is more sensitive to pH and oxygen, more resistant to high temperature and high salt concentration, and is kinetically slower in oxygen atom transfer reactions than the Mo-TMAOR. Such properties of W-containing enzymes as compared to Mo-containing enzymes were predicted (11). The W-TMAOR can also utilize DMSO as substrate in addition to TMAO, but the Mo-TMAOR cannot (7). This enzyme was the first example where W was able to replace Mo and catalyze a reaction with a high redox potential (TMAO/TMA, redox potential +130mV; DMSO/DMS, redox potential +160mV). This is obviously relevant to the ability of W to substitute for Mo in the NR in *P. aerophilum*. On the other hand, W-DMSOR and Mo-DMSOR isolated from *R. capsulatus* exhibit differences in activity. W-DMSOR is significantly more active than Mo-DMSOR in catalyzing the reduction of DMSO, but it cannot catalyze the oxidation of DMS like Mo-DMSOR. These differences can be attributed to the differences in redox potentials of the Mo and W centers of the DMSOR, with

W(IV) being a stronger reductant than Mo(IV) and W(VI) being a weaker oxidant than Mo(VI) (27).

In addition to the requirement of WO_4^{2-} and MoO_4^{2-} for biosynthesis of NR and FDH, or any of the other W- or Mo-containing enzymes in *P. aerophilum*, the W and Mo oxyanions may provide or enhance the expression or stability of these enzymes to different extents, and may also differentially affect the biosynthesis of molybdopterin. Considering the differences in the redox potentials of the reactions catalyzed by FDH and NR, it is surprising that both enzymes are active when cells are grown in the presence solely of either WO_4^{2-} or MoO_4^{2-} . It was therefore of great interest to determine which metal was incorporated into which enzyme under the various growth conditions, and to what extent the different forms of the enzymes (Mo- or W-containing), if they exist, are catalytically active. Such questions are addressed in the subsequent chapters.

REFERENCES

1. **Adams, M. W. W., and L. E. Mortenson.** 1985. Mo-reductases: nitrate reductase and formate dehydrogenase, p. 519-593. *In* T. G. Spiro (ed.), Molybdenum enzymes, vol. 7. Wiley, New York.
2. **Afshar, S., C. Kim, H. G. Monbouquette, and I. Schroder.** 1998. Effect of tungstate on nitrate reduction by the hyperthermophilic archaeon *Pyrobaculum aerophilum*. *Appl. Environ. Microb.* **64**:3004-3008.
3. **Andreesen, J. R., and L. G. Ljungdahl.** 1973. Formate dehydrogenase of *Clostridium thermoaceticum*: incorporation of selenium-75, and the effects of selenite, molybdate, and tungstate on the enzyme. *J Bacteriol.* **116**:867-73.

4. **Bertram, P. A., R. A. Schmitz, D. Linder, and R. K. Thauer.** 1994. Tungstate can substitute for molybdate in sustaining growth of *Methanobacterium thermoautotrophicum*. Identification and characterization of a tungsten isoenzyme of formylmethanofuran dehydrogenase. Arch Microbiol **161**:220-8.
5. **Bonnefoy, V., and J. A. Demoss.** 1994. Nitrate reductases in *Escherichia coli*. Antonie Van Leeuwenhoek **66**:47-56.
6. **Bryant, F. O., and M. W. W. Adams.** 1989. Characterization of hydrogenase from the hyperthermophilic archaeobacterium, *Pyrococcus furiosus*. J. Biol. Chem. **264**:5070-9.
7. **Buc, J., C. L. Santini, R. Giordani, M. Czjzek, L. F. Wu, and G. Giordano.** 1999. Enzymatic and physiological properties of the tungsten-substituted molybdenum TMAO reductase from *Escherichia coli*. Mol Microbiol **32**:159-68.
8. **Burke, K. A., K. Calder, and J. Lascelles.** 1980. Effects of molybdenum and tungsten on induction of nitrate reductase and formate dehydrogenase in wild type and mutant *Paracoccus denitrificans*. Arch Microbiol **126**:155-9.
9. **Grunden, A. M., W. T. Self, M. Villain, J. E. Blalock, and K. T. Shanmugam.** 1999. An analysis of the binding of repressor protein ModE to *modABCD* (molybdate transport) operator/promoter DNA of *Escherichia coli*. J Biol Chem **274**:24308-15.
10. **Imperial, J., M. Hadi, and N. K. Amy.** 1998. Molybdate binding by ModA, the periplasmic component of the *Escherichia coli* mod molybdate transport system. Biochim Biophys Acta. **1370**:337-46.
11. **Johnson, M. K., D. C. Rees, and M. W. W. Adams.** 1996. Tungstoenzymes. Chem. Rev. **96**:2817-2839.

12. **Jones, J. B., and T. C. Stadtman.** 1981. Selenium-dependent and selenium-independent formate dehydrogenases of *Methanococcus vannielii*. Separation of the two forms and characterization of the purified selenium-independent form. *J Biol Chem* **256**:656-63.
13. **Kimura, A., and Y. Takagi.** 1983. A frameshift addition causes silencing of the δ -globin gene in an old world monkey, an annubis (*Papio doguera*). *Nucleic Acids Res* **11**:2541-50.
14. **Knappe, J., and G. Sawers.** 1990. A radical-chemical route to acetyl-CoA: the anaerobically induced pyruvate formate-lyase system of *Escherichia coli*. *FEMS Microbiol Rev* **6**:383-98.
15. **Moreno-Vivian, C., P. Cabello, M. Martinez-Luque, R. Blasco, and F. Castillo.** 1999. Prokaryotic nitrate reduction: molecular properties and functional distinction among bacterial nitrate reductases. *J Bacteriol* **181**:6573-84.
16. **Mukund, S., and M. W. W. Adams.** 1993. Characterization of a novel tungsten-containing formaldehyde ferredoxin oxidoreductase from the hyperthermophilic archaeon, *Thermococcus litoralis*. A role for tungsten in peptide catabolism. *J. Biol. Chem.* **268**:13592-600.
17. **Mukund, S., and M. W. W. Adams.** 1990. Characterization of a tungsten-iron-sulfur protein exhibiting novel spectroscopic and redox properties from the hyperthermophilic archaeobacterium *Pyrococcus furiosus*. *J. Biol. Chem.* **265**:11508-16.
18. **Mukund, S., and M. W. W. Adams.** 1995. Glyceraldehyde-3-phosphate ferredoxin oxidoreductase, a novel tungsten-containing enzyme with a potential glycolytic role in the hyperthermophilic archaeon *Pyrococcus furiosus*. *J. Biol. Chem.* **270**:8389-92.

19. **Mukund, S., and M. W. W. Adams.** 1996. Molybdenum and vanadium do not replace tungsten in the catalytically active forms of the three tungstoenzymes in the hyperthermophilic archaeon *Pyrococcus furiosus*. *J. Bacteriol.* **178**:163-7.
20. **Mukund, S., and M. W. W. Adams.** 1991. The novel tungsten-iron-sulfur protein of the hyperthermophilic archaeobacterium, *Pyrococcus furiosus*, is an aldehyde ferredoxin oxidoreductase. Evidence for its participation in a unique glycolytic pathway. *J. Biol. Chem.* **266**:14208-16.
21. **Roy, R., and M. W. W. Adams.** 2002. Tungsten-dependent aldehyde oxidoreductase: A new family of enzymes containing the pterin cofactor. *Met. Ions Biol. Syst.* **39**:673-697.
22. **Saitou, N., and M. Nei.** 1987. The neighbor-joining method: a new method for reconstructing phylogenetic trees. *Mol Biol Evol* **4**:406-25.
23. **Sawers, G.** 1994. The hydrogenases and formate dehydrogenases of *Escherichia coli*. *Antonie Van Leeuwenhoek* **66**:57-88.
24. **Schmitz, R. A., S. P. Albracht, and R. K. Thauer.** 1992. A molybdenum and a tungsten isoenzyme of formylmethanofuran dehydrogenase in the thermophilic archaeon *Methanobacterium wolfei*. *Eur J Biochem* **209**:1013-8.
25. **Scott RH, S. G., DeMoss JA.** 1979. In vitro incorporation of molybdate into demolybdoproteins in *Escherichia coli*. *J Bacteriol.* **137**:719-26.
26. **Silva, J. R. R. F. d., and R. J. P. Williams.** 1991. The biological chemistry of the elements : the inorganic chemistry of life, vol. xxi. Oxford University Press Clarendon Press, Oxford [England] New York.

27. **Stewart, L. J., S. Bailey, B. Bennett, J. M. Charnock, C. D. Garner, and A. S. McAlpine.** 2000. Dimethylsulfoxide reductase: an enzyme capable of catalysis with either molybdenum or tungsten at the active site. *J Mol Biol* **299**:593-600.
28. **Stiefel, E. I., D. Coucouvanis, W. E. Newton, American Chemical Society. Division of Inorganic Chemistry., and American Chemical Society. Meeting.** 1993. Molybdenum enzymes, cofactors, and model systems : developed from a symposium sponsored by the Division of Inorganic Chemistry at the 204th National Meeting of the American Chemical Society, Washington, DC, August 23-28, 1992. American Chemical Society, Washington, DC.
29. **Völkl, P., R. Huber, E. Drobner, R. Rachel, S. Burggraf, A. Trincone, and K. O. Stetter.** 1993. *Pyrobaculum aerophilum* sp. nov., a novel nitrate-reducing hyperthermophilic archaeum. *Appl. Environ. Microbiol.* **59**:2918-26.
30. **Yamamoto, I., T. Saiki, S. M. Liu, and L. G. Ljungdahl.** 1983. Purification and properties of NADP-dependent formate dehydrogenase from *Clostridium thermoaceticum*, a tungsten-selenium-iron protein. *J. Biol. Chem.* **258**:1826-1832.

CHAPTER 3

PURIFICATION AND CHARACTERIZATION OF THE RESPIRATORY NITRATE REDUCTASE FROM THE HYPERTHERMOPHILIC ARCHAEON *PYROBACULUM* *AEROPHILUM*.¹

¹ Feingold, L.E. and M.W.W. Adams. 2006. To be submitted to *Journal of Bacteriology*.

ABSTRACT

Pyrobaculum aerophilum is a facultative anaerobic hyperthermophile and uses nitrate as a terminal electron acceptor. Nitrate reductase is the primary enzyme in the denitrification respiratory chain. It has been well-studied in mesophilic nitrate-reducing organisms in which it is a molybdoenzyme. Molybdoenzymes, however, are rarely found in hyperthermophiles, which utilize the analogous metal, tungsten. To date, tungstoenzymes that have been characterized typically catalyze only low potential redox reactions ($E_o' < -420$ mV), but nitrate reduction to nitrite is a high potential reaction ($E_o' = +420$ mV). The goals of this study were therefore to purify and characterize the nitrate reductase from *P. aerophilum* and determine its metal content. The results show that the majority of the purified enzyme contains molybdenum, yet, there is a significant portion of active nitrate reductase that contains tungsten. Possible mechanisms of nitrate-reduction by a tungsten active site are discussed.

INTRODUCTION

Hyperthermophiles are defined as organisms that can grow at or above 90 °C (79). Some of the most metabolically versatile among them are species of the genus *Pyrobaculum*, as they are able to use oxygen, nitrate, nitrite, S^0 , thiosulfate, sulfite, arsenate and selenate as terminal electron acceptors (6, 37, 71, 84, 86). An organism that couples the oxidation of a growth substrate to the reduction of nitrate (NO_3^-) to N_2O or N_2 leading to energy conservation can be termed a respiratory denitrifier (50). *P. aerophilum*, classified as a true denitrifier, reduces nitrate to N_2 through respiratory dissimilatory nitrate reduction (86). Analogous to its bacterial counterparts, *P. aerophilum* is also a facultative anaerobe. In contrast, however, *P. aerophilum* is a microaerophile utilizing between 0.6 and 3.0 % oxygen. Most importantly, growth of *P.*

aerophilum at optimal temperatures of 100 °C is dependent upon tungsten (W) and inhibited by molybdenum (Mo) [Chapter 2 and (3)]. W, however, is a known antagonist to the growth of many mesophilic microorganisms, especially those that respire anaerobically with nitrate, which are dependent on Mo.

Denitrification is widespread in bacteria as an anaerobic process to conserve energy, and it also occurs in archaea, such as *Pyrolobus* (17) and *Haloferax* (36), as well as in eukaryotes, in particular fungi and yeast. Interestingly, in these eukaryotic organisms, the site of denitrification is intact mitochondria and microaerophilic conditions are needed (81). In prokaryotic denitrification, the source of electrons for nitrate reduction is often formate, which is oxidized by formate dehydrogenase (FDH). Like all respiratory systems, the formate-nitrate reductase respiratory pathway is membrane-associated, and electron transfer between the nitrate reductase (NR) and the FDH is coupled by quinones (19, 53). Hence, this multienzyme complex catalyzes the oxidation of formate to carbon dioxide coupled with the transfer of reducing equivalents to nitrate in an energy-conserving pathway.

In addition to their coupled role in nitrate respiration, both NR and FDH are traditionally molybdoenzymes. Growth is inhibited when the essential Mo is replaced with W in these mesophilic microorganisms, resulting in inactive demolybdo NRs. As discussed in Chapter 4, this is usually the case with the FDHs as well (31, 73). Hyperthermophilic microorganisms, however, typically require tungsten rather than molybdenum at the active sites of key oxidoreductase-type enzymes, and particularly those that catalyze low potential reactions, such as formate oxidation to carbon dioxide ($E_o' = -420$ mV) (4, 55-57, 59). Whether tungstoenzymes can catalyze reactions of high potential, such as nitrate reduction ($E_o' = +420$ mV) is not known. Until recently, all purified nitrate reductases have been found to contain Mo in their active sites,

but two membrane-bound nitrate reductases (respiratory) have now been identified that contain no metal at all in their active sites. One contains a subunit composition typical of membrane-bound NRs (7) as described below, while the other is a distinctive heterotetramer that utilizes heme-*c* groups to catalyze nitrate reduction (51). Additionally, the presence of W or Mo did not inhibit growth or enzyme activity of the organism containing this Mo-free NR (51). Moreover, two soluble nitrate reductases (periplasmic) have been purified that contain vanadium (V) rather than Mo in their active sites (7, 8). These enzymes also do not contain any pterin cofactors, but do contain subunit composition equivalent to other NRs.

The membrane-bound respiratory nitrate reductase, Nar, encoded by *narGHJI* and referred to as NRA, has been well characterized from bacterial sources (19, 38, 40, 53, 61). The most extensively studied is the NR enzyme in *E. coli*. It is a heterotrimer ($\alpha\beta\gamma$) and the catalytic α subunit, NarG, (140 kDa) contains a Mo ion and a [4Fe-4S] cluster (40). The Mo atom is coordinated by *bis*-molybdopterin guanine dinucleotide (Mo-*bis*MGD). The β subunit, NarH, (60 kDa) contains one [3Fe-4S] and three [4Fe-4S] clusters (40), which function in electron transfer. The membrane-bound γ subunit, NarI, (30 kDa) functions to bind the $\alpha\beta$ complex to the membrane and to transfer electrons to the complex via two heme *b* groups (13). An additional (fourth) subunit, δ (NarJ, 26 kDa), is encoded in the operon of *E. coli*, but has not been associated with any purified NR. It is assumed to function in the stabilization or in the assembly of the $\alpha\beta$ complex prior to their interaction with the γ subunit (19, 38, 61).

A second membrane-bound respiratory NR, NRZ, is also found in *E. coli* and in *Salmonella typhimurium*. NRZ is encoded by *narZYWV* and the purified enzyme has also been well characterized (19, 53, 78). Both NRA and NRZ have the same subunit composition, with similar molecular masses, and contain the same cofactors. In cells lacking NRA, NRZ catalyzes

the same reaction with the same physiological substrates as electron donors. When both enzymes are present, it has been proposed that NRZ assists *E. coli* in the transition from an aerobic to an anaerobic metabolism. Interestingly, NRZ is constitutively expressed, while NRA needs anaerobiosis and the presence of nitrate to be expressed (19, 38). New contradictory evidence, however, indicates the expression of NRZ is highly dependent on growth phase and is stress-induced (22).

The availability of the genomic sequences of *P. aerophilum* (28) and *E. coli* (15, 16) has allowed comparison between their respective nitrate reductases. The high identity and similarity between these NRs (Fig. 3.1) led to the prediction that *P. aerophilum* would contain one *E. coli*-like nitrate reductase. The genomic sequence of *P. aerophilum* confirms only one copy of the Nar operon, as opposed to the two, *narGHJI* and *narZYWV*, found in *E. coli*. This prediction was the initial basis for this research and raises two important questions. One, does the NR in *P. aerophilum* contain W rather than Mo? And two, does *P. aerophilum* also contain a non-conventional NR not recognized in the genome analysis? The goal of this study was to answer these questions by the purification and characterization of the respiratory nitrate reductases from *P. aerophilum*. The results further provide insight into the similarities and differences between this enzyme in mesophiles and hyperthermophiles and in archaea and bacteria.

MATERIALS AND METHODS

Growth conditions. *P. aerophilum* (DSM 7523) was grown anaerobically in the marine medium originally reported (86) but with the following modifications. NH_4Cl , NaCO_3 , MoO_4^{2-} , and the reductant were omitted from the medium; and 10 mM sodium formate, 1.5 μM WO_4^{2-} , yeast extract (0.05%, w/v), peptone (0.05%, w/v), and 10 mM KNO_3 were added. An additional

Nitrate Reductase Operon

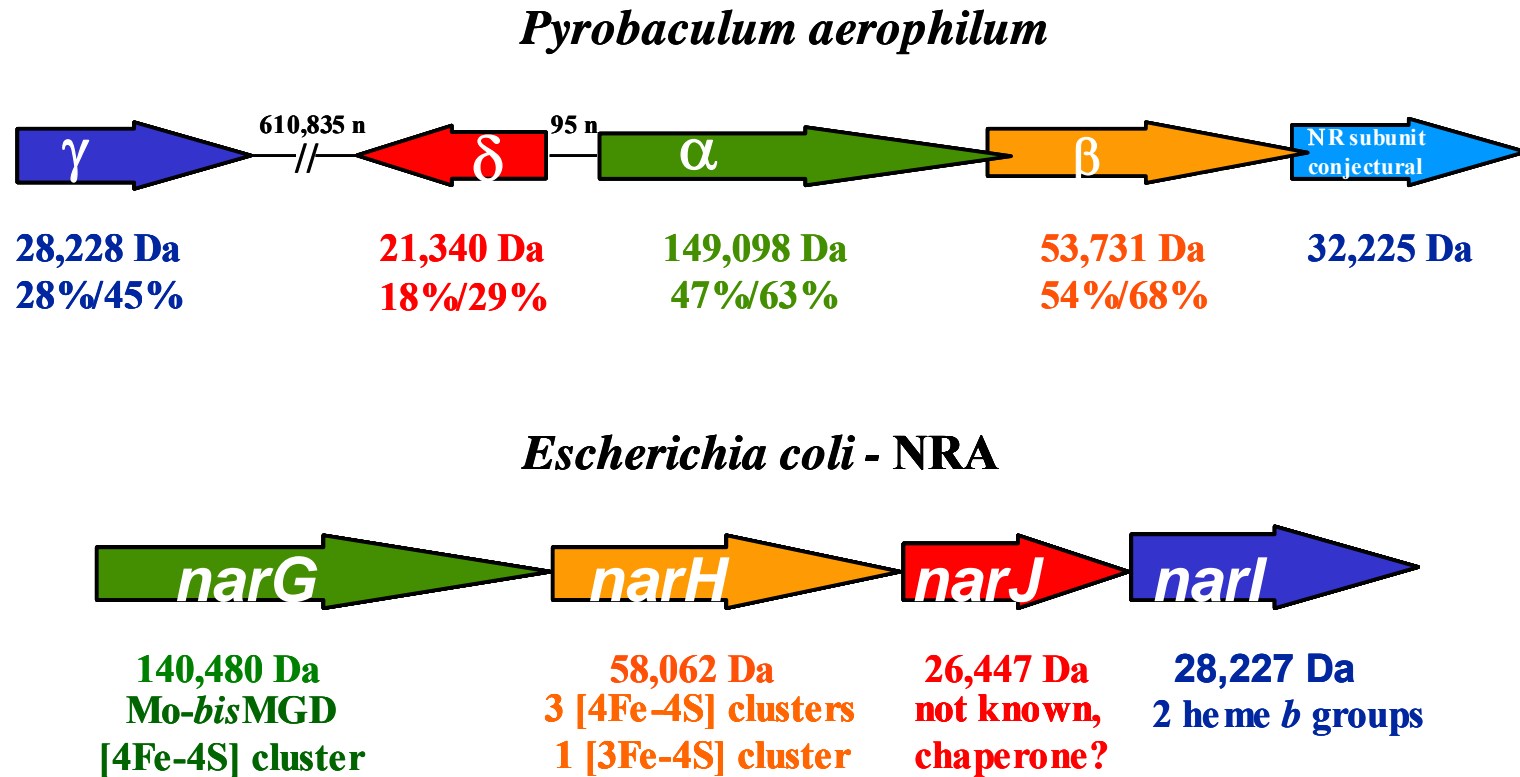


Fig. 3.1. Respiratory nitrate reductase operons from *P. aerophilum* and *E. coli* (NRA). The size of the gene products is shown for both organisms. Metal components shown for *E. coli* also represent the metal components expected in *P. aerophilum*. There are 95 nucleotides (95 n) between NR δ and α in the *P. aerophilum* operon. Percents represent percentage of amino acid sequence identity and percentage of sequence similarity respectively. Sequences were retrieved from NCBI, (<http://www.ncbi.nlm.nih.gov/>) and identity and similarity alignments were performed using MacVector.

5 mM KNO₃ was added midway through the growth phase (which corresponded to the first doubling, approximately 2×10^7 cells/mL). Large-scale cultures (450 L) were grown at 95 °C in a 600 L custom stainless steel fermentor (W. B. Moore, Inc.) under pH-controlled conditions (pH 6.8 - 7.0) with either 0.1N HCl or 0.5 M formic acid while stirring at 50 rpm. The medium was sparged with Argon (Ar) while heating it to the growth temperature and N₂/CO₂ (80:20) was then continually flushed through the headspace throughout the growth phase. Cells were harvested during mid-logarithmic growth at a density of approximately 3×10^8 cells/mL, with a Sharples AS16 centrifuge. The cells (approximately 250 g, wet weight) were immediately frozen in liquid N₂, and stored at -80 °C.

Preparation of membrane fractions. Approximately 50 g of frozen *P. aerophilum* cells were used for each purification. Cells were thawed under Ar, and suspended in approximately 150 mL of anaerobic lysis buffer (50 mM Tris pH 8.0, 2 mM sodium dithionite (DT), and 50 µg of DNase) and stirred at 37 °C for 3 h. The extract was then passed two times through a French pressure cell at 15,000 psi under anaerobic conditions. The cell suspension was frozen and stored at -80 °C overnight, thawed under Ar and centrifuged at 8,000 x g for 7 min to remove cell debris. The cell-free extract (supernatant) was centrifuged at 100,000 x g for 2 h to separate the membrane and soluble fractions. In an anaerobic chamber, membranes were resuspended in buffer containing 100 mM potassium phosphate (pH 7.0), 50 mM NaCl and 2 mM DT, and homogenized in a glass tissue grinder. The protein concentration was adjusted to 24 – 28 mg/mL by adding anaerobic buffer. Solubilization of the membrane-bound proteins was conducted in two steps. First, 0.5% (w/v) n-octyl β-glucoside and 100 µM phenylmethylsulfonyl fluoride (PMSF) was added to the cell suspension, which was then stirred for 0.5 h and centrifuged at

110,000 x g for 1 h. This supernatant represents the first (0.5% n-octyl β -glucoside) solubilized membrane fraction. The pellet was resuspended in the same buffer containing 4.0% (w/v) n-octyl β -glucoside and 100 μ M PMSF. This membrane suspension was stirred for 2 h and then centrifuged for 1 h at 110,000 x g. This supernatant represents the second (4.0% n-octyl β -glucoside) solubilized membrane fraction. The solubilized membrane fractions that were not used immediately were frozen as pellets and stored in liquid N₂.

Protein purification. Purification of nitrate reductase was performed under strictly anaerobic conditions at room temperature. In each purification (~50g of cells), approximately 400 mg of protein was obtained from the first extraction of the membranes using 0.5% n-octyl β -glucoside, and approximately 400 mg of protein was obtained from the remaining membrane fraction by extraction with 4.0% n-octyl β -glucoside. For the first column only, each 400 mg fraction was separately loaded and eluted in equal parts (200 mg each) (Fig. 3.2). Subsequent columns contained combined fractions with NR activity from the total 400 mg of protein from each solubilized membrane fraction. Purification with the first 0.5% n-octyl β -glucoside membrane fraction was completed, and then purification was repeated in the same manner with the second 4.0% n-octyl β -glucoside membrane fraction (Fig. 3.2).

Approximately 200 mg of protein from each solubilized membrane fraction were loaded onto a column (5.0 x 9.5 cm) of Q Sepharose High Performance (QHP, Amersham Pharmacia Biotech Inc.). The QHP column was previously equilibrated with 50 mM Tris/HCl, pH 8.0, containing 2 mM DT (Buffer A) and washed with one column volume of Buffer A containing 0.5% n-octyl β -glucoside. Membranes were diluted with 9 volumes of Buffer A as they were

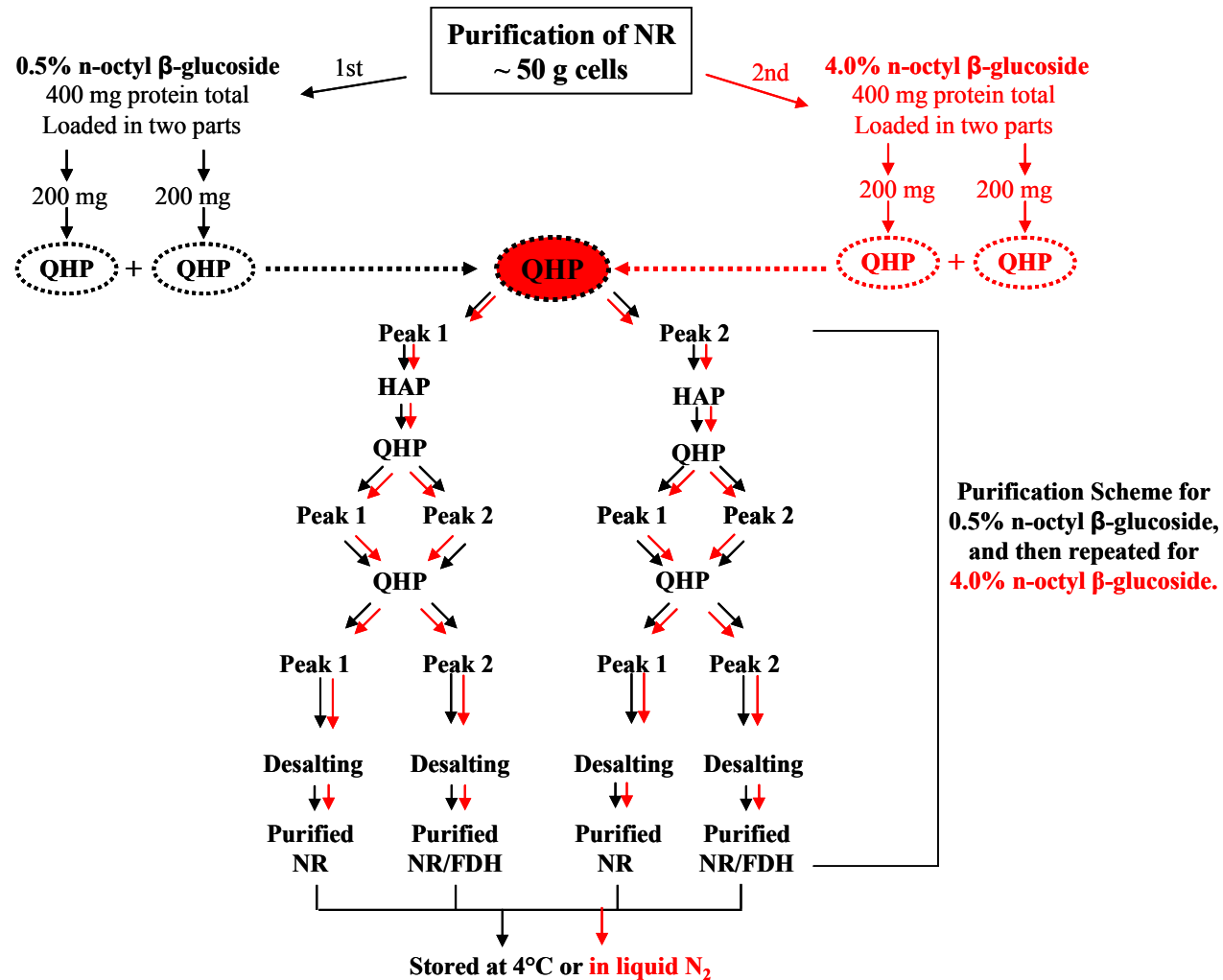


Fig. 3.2. Generalized schematic of the methodology of purification of NR from 50 g of cells. The QHP column encircled with the dashed lines represents the first column in the purification for both solubilized membrane fractions. Details of the methodology are as described in the text. A more detailed schematic of the purification including the results is shown in Fig. 3.3, and described in the text.

loaded, and the column was washed with Buffer A until protein could not be detected in the eluate based on the absorption at 405 nm. The QHP column was then washed with two column volumes of Buffer A containing 0.1% (v/v) Triton X-100. Adsorbed proteins were eluted with a linear gradient (750 mL) from 100 to 400 mM NaCl in Buffer A containing 0.1% Triton. NR activity eluted as two separate peaks. The first peak was collected during the second column volume of the 0.1% Triton wash for both solubilizations, and the second peak as 160 – 220 mM NaCl was applied for 0.5% n-octyl β -glucoside solubilized membranes and as 140 – 180 mM NaCl was applied for 4.0% n-octyl β -glucoside solubilized membranes (Fig. 3.2). Fractions from each peak were combined and concentrated anaerobically by ultrafiltration with a YM-100 membrane (Amicon) and applied separately to a column (5.0 x 15.0 cm) of Hydroxyapatite (Bio-Rad) previously equilibrated with 10 mM sodium phosphate, pH 6.9, containing 2 mM DT and 0.1% Triton. A linear gradient (2100 mL) from 10 to 250 mM sodium phosphate was applied. Fractions containing NR activity eluted in 75 – 100 mM sodium phosphate. These fractions were combined and concentrated anaerobically by ultrafiltration with a XM-50 membrane (Amicon) and applied to a column (5.0 x 3.5 cm) of QHP (Amersham Pharmacia Biotech Inc.) previously equilibrated with 50 mM Bis-Tris, pH 6.8, 2 mM DT and 0.1% Triton. Adsorbed proteins were eluted with a linear gradient (500 mL) from 100 to 400 mM NaCl. Fractions containing NR activity again eluted in two peaks, one in the pass through and the second as 130 mM NaCl was applied (Fig. 3.2). Active fractions from each peak of activity were combined, concentrated with a PM30 membrane (Amicon) and loaded separately onto a column (2.6 x 2.8 cm) of QHP previously equilibrated with Buffer A containing 0.1% Triton X-100. Adsorbed proteins were eluted with a linear gradient (105 mL) from 100 to 300 mM KCl. Fractions containing NR activity eluted in the pass through (Peak 1), or when 130 mM KCl (Peak 2, 0.5%

n-octyl β -glucoside) and 140 mM KCl (Peak 2, 4.0% n-octyl β -glucoside) was applied (Fig. 3.2). Peak 1 and peak 2 fractions were loaded separately onto a Hi Prep Desalting column (2.6 x 10 cm) (Pharmacia) to exchange the buffer with Buffer A containing 0.1% (w/v) n-octyl β -glucoside. Purified protein from Peak 1 and Peak 2 were combined from both membrane solubilizations, concentrated with a YM100 membrane, and stored at 4 °C for immediate use or as pellets in liquid N₂ (Fig. 3.2).

Enzyme assays. NR activity was determined with reduced methyl viologen (MV) as an artificial electron donor at 90 °C. Two mL of anaerobic assay buffer (50 mM HEPES pH 7.0), MV (0.5 mM), enough dithionite (100 mM stock) to reduce the MV to an OD₆₀₀ of 2.0, and the fraction to be assayed were added to anaerobic serum-stoppered cuvettes. The cuvettes were heated for 3 minutes at 90 °C in a Spectronic 501 spectrophotometer. The reaction was initiated by the addition of KNO₃ (10 mM). A molar absorbance coefficient, ϵ_{600} , of 12,000 M⁻¹ cm⁻¹ was used to follow the oxidation of reduced MV. The specific activity of NR is expressed as one micromole of nitrate oxidized (U) per minute per milligram of protein.

Protein measurement. Protein concentrations were determined using the detergent-compatible modified Lowry assay (*DC Protein Assay*, Bio-Rad). Bovine serum albumin was used as the protein standard.

Gel electrophoresis. Molecular weights were estimated by SDS-PAGE using a 4 – 12% Bis-Tris acrylamide gel (NuPage, Invitrogen Corp.) with MOPS Running Buffer (NuPage, Invitrogen Corp.) under reducing conditions. Protein samples were diluted 4:1 with 30 mM Tris-HCl buffer

(pH 6.8) containing 5% SDS, 5% β -mercaptoethanol, 10% glycerol and 0.025% bromphenol blue and heated for 15 min at 100 °C. Molecular weights were estimated using the AlphaImager IS-2200 with AlphaEase v5.5 software. Calculations were based on molecular weight standards of the BenchMark Protein Ladder (Invitrogen Corp.). This ladder consists of 15 engineered proteins with the molecular weights ranging from 220 kDa to 10 kDa.

Electrophoresis under non-denaturing conditions and in-gel activity measurements were carried out in 3 - 8% Tris-Acetate gels (NuPage, Invitrogen Corp.) with Tris – Glycine buffer (25 mM Tris Base and 192 mM Glycine, pH 8.3). Protein samples were diluted 4:1 with 30 mM Tris-HCl buffer (pH 6.8) containing 10% glycerol and 0.025% bromphenol blue. Triton X-100 (0.1% v/v) was added to the cathode buffer and gels were run for 30 min at 100 mV prior to loading the samples. Proteins were stained with Coomassie Blue R250. NR activity was detected at room temperature by adding the gel to a tray containing 20 mL Hepes (50 mM), pH 7.0, and adding 10 mM MV, enough DT to maintain reducing conditions, and 10 mM KNO₃ or 10 mM NaClO₃. NR activity was detected as a clear band in a dark-blue background. FDH activity was detected by adding the gel to a tray containing 20 mL CHES (50 mM), pH 8.5, and adding 0.08 mM 2,6-dichlorophenolindophenol, 0.25 mM phenazine methosulphate, and 10 mM sodium formate. The tray was then heated for 5 to 15 min in a 95 °C incubator, at which time clear bands representing FDH activity appeared in a light blue background.

Metal analysis. Tungsten and molybdenum contents were determined using inductively coupled plasma emission mass spectroscopy (ICP-MS) performed at the Environmental Analysis Laboratory of the University of Georgia. Sodium molybdate and sodium tungstate were used as standards. All values were corrected for the W and Mo contents of the control samples

containing only buffer. Iron content was determined colorimetrically as previously described (44), with the exception that the acid treatment was conducted at 100 °C in a dry bath for 1 hour.

pH and temperature optima. The effect of pH on nitrate reductase activity was estimated using buffers with low $\Delta\text{pH}/\Delta\text{T}$ (°C) ratios (ranging from -0.0085 to -0.015) due to the high temperature requirement of the activity assay. Buffers included MES, Bis-Tris, PIPES, MOPS, HEPES, EPPS, and CHES at a concentration of 50 mM ranging from pH 6.0 to pH 9.0 in 0.5 unit increments under the assay conditions described above. Nitrate reductase activity was also measured at 10 °C increments from 30 to 100 °C using purified enzymes and cell-free extracts as described above.

UV-Visible and EPR Spectroscopy. Optical spectra were recorded using a Shimadzu UV-2501PC recording spectrophotometer. Samples were oxidized by treatment with chlorate (10 mM) at 80 °C, and were reduced by adding sodium dithionite. All measurements were conducted at room temperature. All EPR spectra were recorded by Richard Cammack at the Department of Life Sciences, King's College, London SE1 9NN, U.K in the laboratory of Professor Michael K. Johnson, Department of Chemistry, University of Georgia, Athens, GA. They were recorded on a Bruker ER 300E spectrometer equipped with an Oxford Instruments ITC flow cryostat and interfaced to an ESP 3220 computer. Instrument conditions and temperatures are described in the Results.

Other methods. In order to identify individual subunits, purified enzymes were separated by electrophoresis in the presence of SDS and electroblotted on to a polyvinylidene difluoride

membrane (PVDF membrane). The transfer was carried out at 200 mA for 3 h in 10 mM CAPS, pH 11 at 4 °C. Methanol was not added to the buffer, due to observations in early experiments that it prevented transfer of the high molecular weight proteins. N-terminal sequence analysis was determined by direct Edman sequencing using an automated sequencer (PE-Biosystems 491 A Pulsed-Liquid Sequencer) equipped with a PE-Biosystems 140S PTH Analyzer at the Emory University Winship Cancer Center Microchemical Facility. Mass spectroscopy using an Applied Biosystems 4700 Proteomics Analyzer at the Proteomics Resource Facility at the University of Georgia was used to analyze fragments of in-gel coomassie-stained protein digested with trypsin according to protocols previously described (74). Observed masses were compared with sequences from Archaea and human genomes deposited in the National Center for Biotechnology Information (NCBI) database (<http://www.ncbi.nlm.nih.gov/>). The genomic and amino acid sequences of *P. aerophilum* (28) and of *E. coli* (15, 16) were analyzed using MacVector (Accelrys Software Inc.) and Vector NTI (Invitrogen Corporation) from sequences retrieved from the NCBI database.

RESULTS

Purification of NR. Nitrate reductase from *P. aerophilum* was purified from cells grown anaerobically in a fermentor (450 L) in marine medium supplemented with nitrate, formate and tungstate. No molybdate was added to the medium; although residual amounts were present in the yeast extract and peptone (see Chapter 2). Given that nitrate reductase activity has been previously shown to be localized in the membrane fraction (Chapter 2), several concentrations of different detergents were used to evaluate the efficiency in extracting the enzyme from cytoplasmic membranes. Membranes were disrupted anaerobically by two passes through a

French press and one freeze-thaw cycle prior to solubilization. Proteins in the membrane fraction of *P. aerophilum* comprise almost 50% of the total protein in the lysed cells, and 73% of the total nitrate reductase (NR) activity in the cell-free extract (Table 3.1). Nitrate reductase and formate dehydrogenase (FDH) co-purify in *P. aerophilum* during membrane solubilization and chromatography. The release of both of these enzymes was accomplished by sequential solubilization of the membranes. Membranes were initially solubilized with 0.5% n-octyl β -glucoside, which contained about 30% of the total NR activity, while extraction of the precipitated membranes with 4.0% n-octyl β -glucoside contained the majority (64%) of NR activity (Table 3.1). As described in Chapter 4, the opposite was true for FDH, as the majority of the FDH activity was extracted by 0.5% n-octyl β -glucoside. Consequently, approximately 95% of total nitrate reductase activity was solubilized from the membrane fraction by the two detergent treatments. The membranes solubilized with 4.0% n-octyl β -glucoside had a specific activity of 74 U/mg, and those solubilized in the initial 0.5% n-octyl β -glucoside treatment had a specific activity of 33 U/mg (Table 3.1). By comparison, earlier experiments showed nitrate reductase that was solubilized from membranes with Triton X-100 (0.5% to 4.0%) ranged from 26% to 66% of the total activity, with specific activities ranging from 6 to 11 U/mg. Further, concentrations of SDS ranging from 0.5% to 2%, extracted 1% or less of the nitrate reductase activity with a high specific activity of only 13 U/mg.

Membranes solubilized with 0.5% n-octyl β -glucoside and 4.0% n-octyl β -glucoside were loaded separately onto a Q-Sepharose column so that the concentration of the detergent was 0.5% (Fig. 3.3). The column was also equilibrated using buffer containing this detergent concentration. In order to elute all fractions containing nitrate reductase activity in all columns,

Table 3.1. Solubilization of nitrate reductase from *P. aerophilum* cells with n-octyl β -glucoside.

Fractions	Total Protein (mg)	Total Activity (U)	Specific Activity (U/mg)	Protein Yield (%)	Activity Yield (%)
French Pressed Cells ^a	4111	68,594	17	100	100
Cell Free Extract	3570	78,533	22	86.8	114
Cytosolic	2074	8,743	4	50.5	12.7
Membranes	2006	50,158	25	48.8	73.1
0.5% Solubilized Membranes ^b	460	15,056	33	11.2	21.9
4.0% Solubilized Membranes ^b	436	32,092	74	10.6	46.8

^a Using 50g (wet weight) of frozen cells.

^b The percentage indicates the concentration (w/v) of n-octyl β -glucoside that was used to solubilize the membrane fraction.

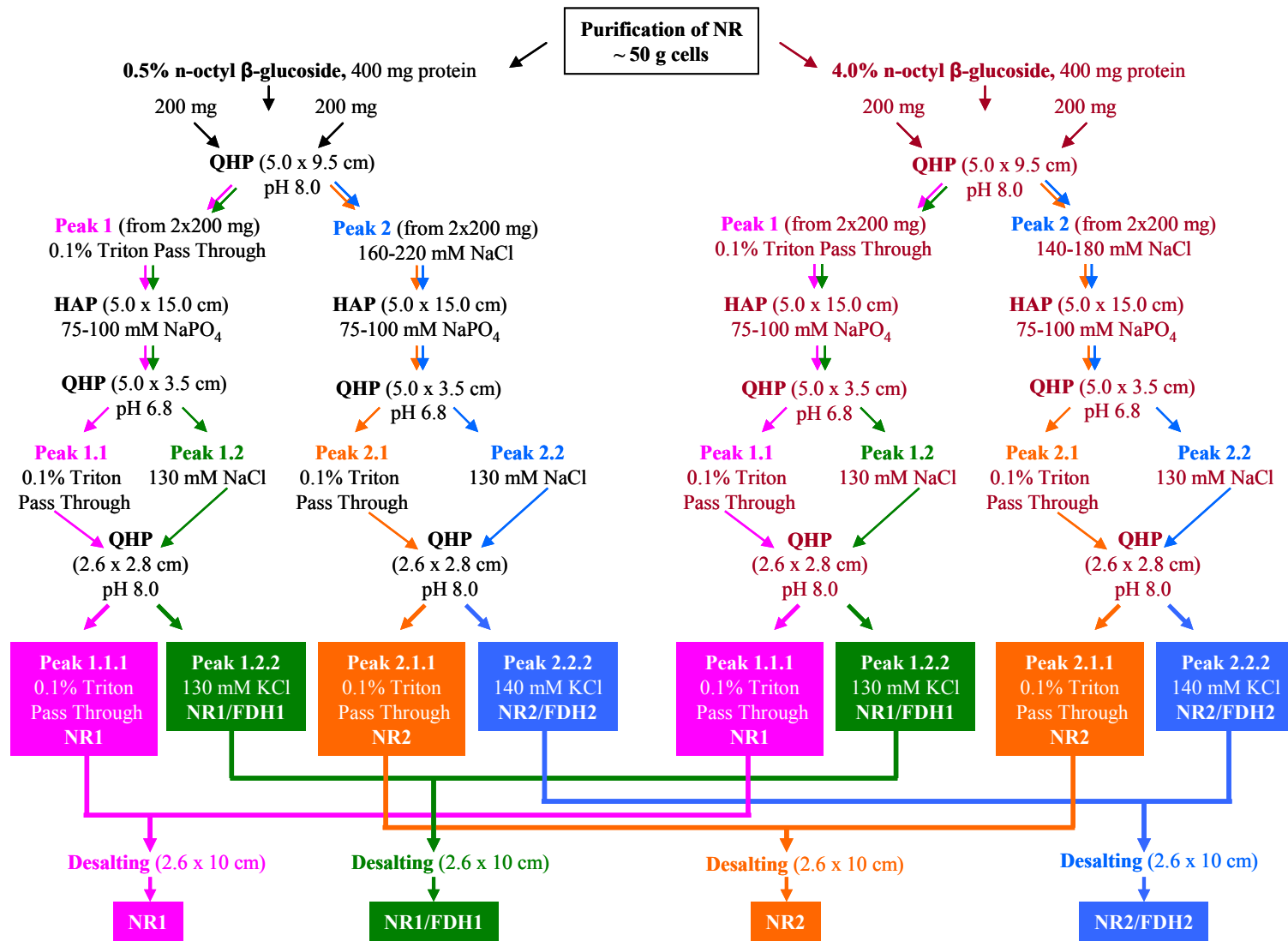


Fig. 3.3. Purification of NR from 50 g of cells. NR purified from membranes solubilized with n-octyl β -glucoside from *P. aerophilum* cells results in two forms of NR, NR1 and NR2, and two forms of NR in complex with FDH, NR1/FDH1, and NR2/FDH2.

0.1% Triton was added to all elution buffers. N-octyl β -glucoside was also effective in eluting fractions containing nitrate reductase activity, but only in concentrations above 0.5% (w/v).

Final purification of NR was accomplished by combining fractions from each peak of activity from the second QHP column (pH 6.8) and applying the distinct peaks (one from the through, peak 1, and one as 0.13 M NaCl was applied, peak 2) to a QHP column equilibrated at pH 8.0 and eluting with KCl (Fig. 3.3 and Table 3.2). Elution of peak 1 yielded a purified NR fraction in the pass through and a NR fraction also containing FDH activity with 130 mM KCl. These are now termed NR1 and NR1/FDH1, respectively. Elution of peak 2 also resulted in a purified NR fraction, again in the pass through and a second containing both NR and FDH activity, which eluted at 140 mM KCl. These fractions are now termed as NR2 and NR2/FDH2, respectively (Fig. 3.3). Throughout the purification, peak 1 and peak 2 fractions were separated and analyzed with respect to their catalytic activities measured by the standard anaerobic assays and by the in-gel assays, metal content, chromatographic elution profile, and by subunit composition.

Purified NR samples (NR1 and NR2) and the enzyme complexes (NR1-FDH1 and NR2-FDH2) each gave rise to a single protein band after nondenaturing PAGE (Fig. 3.4 D). In agreement with the direct FDH assays (Chapter 4), when the gels were stained with formate, the same protein bands from NR1-FDH1 and NR2-FDH2 exhibited FDH activity as well as NR activity, suggesting that both enzymes were within the same native complex (Fig. 3.4 A and C). Although NR1 shows a slight activity when stained with formate (Fig. 3.4C), no FDH activity was measurable in the standard assays using benzyl viologen. The purified NRs and the NR-FDH complexes exhibited nitrate reductase activity when stained with either nitrate or chlorate (Fig. 3.4 A and B). The ability of the NR from *P. aerophilum* to reduce chlorate, further

Table 3.2. Purification of nitrate reductase from *P. aerophilum* membranes.

Purification Step		Total Protein (mg)	Total Activity (U)	Specific Activity (U/mg)	Protein Yield (%)	Activity Yield (%)	Purification (-fold)
Membrane fraction		2006	50,158	25	100	100	1
Solubilized fraction*		896	47,148	53	45	94	2.1
Q-Sepharose pH 8.0		456	30,819	68	23	61	2.7
Hydroxyapatite		105	29,081	277	5	58	10.8
Q-Sepharose pH 6.8		64	28,181	440	3	56	17.6
Q-Sepharose pH 8.0							
Peak 1	NR1	20	10,868	534	1.0	22	21.4
	NR1/FDH1	19	13,534	712	0.95	27	28.5
Peak 2	NR2	7	1,553	223	0.35	3	8.9
	NR2/FDH2	10	3,883	373	0.50	8	14.9

* Denotes combined fractions from 0.5% and 4.0% n-octyl β -glucoside solubilized membrane fractions.

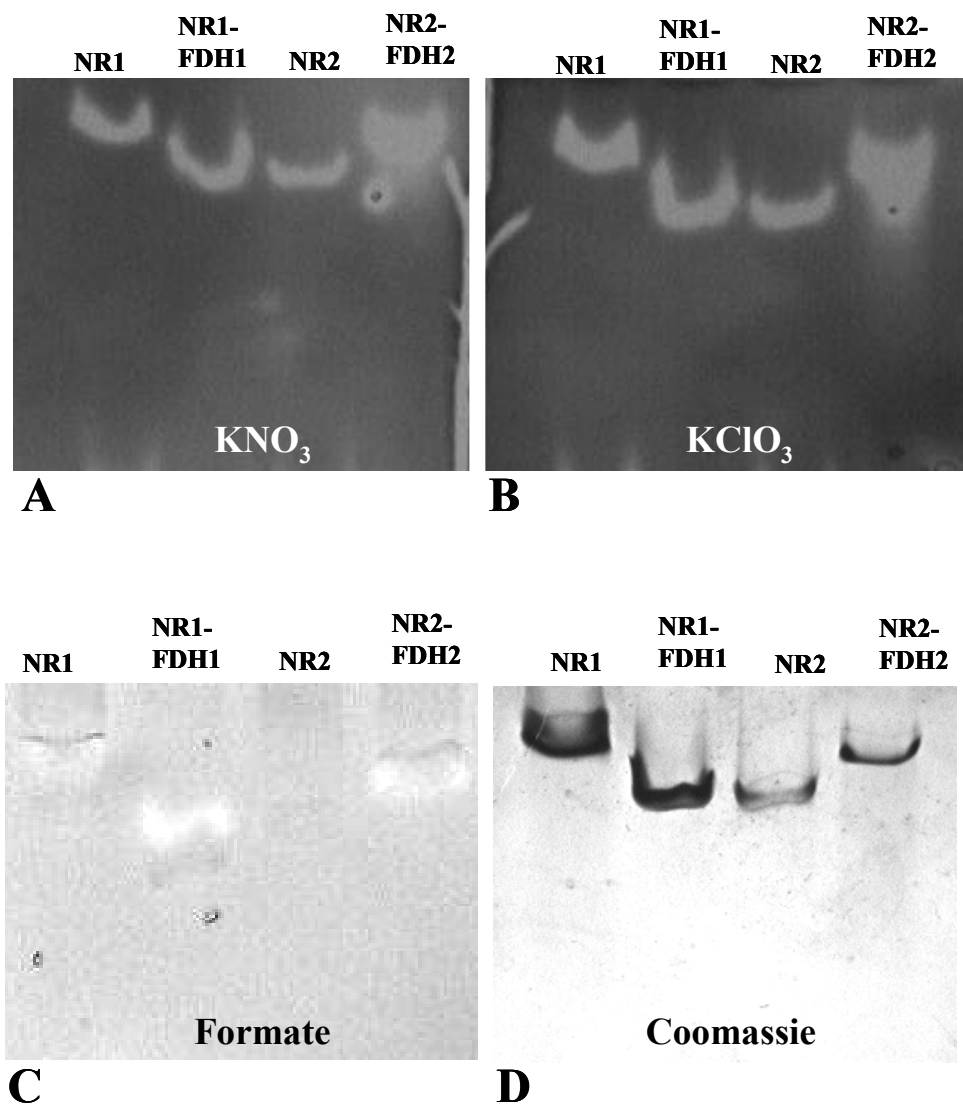


Fig. 3.4. Nitrate reductase and formate dehydrogenase activity-stained gels. 15 μg of each protein was run on 3-8% Tris-Acetate gels under non-denaturing conditions. Nitrate reductase activity was measured at room temperature, and formate dehydrogenase was heated at 98 °C until bands appeared (approximately 10 min.). (A) Developed with nitrate, (B) developed with chlorate, (C) developed with formate, and (D) stained with Coomassie blue R-250.

reinforces its identification as a membrane-bound active Mo-containing NarGHI enzyme, as this is one of the traits that distinguishes this classification of NR from the periplasmic NRs often found in conjunction with Nar enzymes (9, 64, 80).

In the standard assays, the specific activity of NR1 was approximately 40% higher than NR2, while NR1/FDH1 exhibited over 50% higher activity than NR2/FDH2 (Table 3.2). Approximately 70% of the total purified NR was present in the first peak, constituting 82% of the total NR activity. Purified NR1 exhibited a lower NR specific activity (534 U/mg) than the enzyme complex, NR1/FDH1, (712 U/mg). Overall, the NR purified in the first peak yielded 2% of the protein in the membrane fraction and represented a 21.4- (NR1) and 28.4- (NR1/FDH1) fold purification over the membrane fraction (Table 3.2).

Conversely, the second NR peak constituted only 18% of the total NR activity, corresponding to 30% of the total purified NR. Similarly, the specific activity of purified NR in the second peak was lower (223 U/mg) than the corresponding NR2/FDH2 complex (373 U/mg). The second peak of NR activity contained less than 1% of the total protein in the membrane fraction, representing an 8.4- (NR2) and 14.9- (NR2/FDH2) fold purification (Table 3.2).

The total activity in the final purified samples (NR1, NR1/FDH1, NR2 and NR2/FDH2) was higher than the total activity in peak 1 and peak 2 fractions from the final QHP column (Table 3.2). This increase in activity was achieved by exchanging the elution buffer, which contained 0.1% Triton X-100 with Buffer A containing 0.1% (w/v) n-octyl β -glucoside in the final samples. Triton X-100 (0.1%) was found to have an inhibitory effect (by 6 to 10%) on enzyme activity. This effect was also reported in studies of the NR of *Bacillus halodenitrificans* (41).

Kinetic properties of NR1. The kinetic properties of the purified nitrate reductase, NR1, were determined using reduced methyl viologen as the electron donor and nitrate as the electron acceptor. Classical Michaelis-Menten kinetics were observed when nitrate concentrations were varied between 5 and 500 μM (see inset Fig. 3.5). The apparent K_m for nitrate was 200 μM , and the calculated maximum activity (V_{max}) was 3333 U/mg (Fig. 3.5). The apparent K_m for nitrate against substrate concentrations ranging from 30 μM to 2.5 mM was 40 μM with a V_{max} of 267 U/mg.

The effect of pH on the activity of NR1 was examined over the range 6.0 to 9.0 (Fig. 3.6). The pH optimum was pH 7.0 (using HEPES buffer). In the presence of Bis-Tris buffer (pH 7.0), however, the specific activity decreased from 156 to 113 U/mg, and in PIPES buffer at pH 7.0 the activity decreased to 135 U/mg. Other buffers used were MES (pH 6.0 and 6.5), Bis-Tris also at pH 6.0 and 6.5, MOPS (pH 7.0, 7.5 and 8.0), PIPES also at pH 7.5, HEPES also at pH 6.5, 7.5 and 8.0, EPPS (pH 8.0 and 8.5), and CHES (pH 8.5 and 9.0).

The effect of temperature on the various forms of *P. aerophilum* NR is shown in Fig. 3.7. Cell-free extracts, the purified enzymes and the NR/FDH enzyme complexes all exhibited maximal activity at 90 °C, as determined by the reduction of methyl viologen (Fig. 3.7). Interestingly, no activity was detected in cell-free extracts at 30 °C or 40 °C, but in purified NR1 and NR2, 16% and 18% of optimal activity was present at 30 °C, respectively, and 20% and 34% at 40 °C. The NR-FDH complex, however, while still active at these temperatures, exhibited lower specific activity. NR1/FDH1 and NR2/FDH2 both retained 6% of optimal activity at 30 °C, but at 40 °C, NR1/FDH1 exhibited only 8% of optimal activity and NR2/FDH2 displayed higher specific activity, maintaining 18% of optimal. Moreover, as shown by the in-gel activity assays (Fig. 3.4), activity could be detected using all of the forms of purified *P. aerophilum* NR

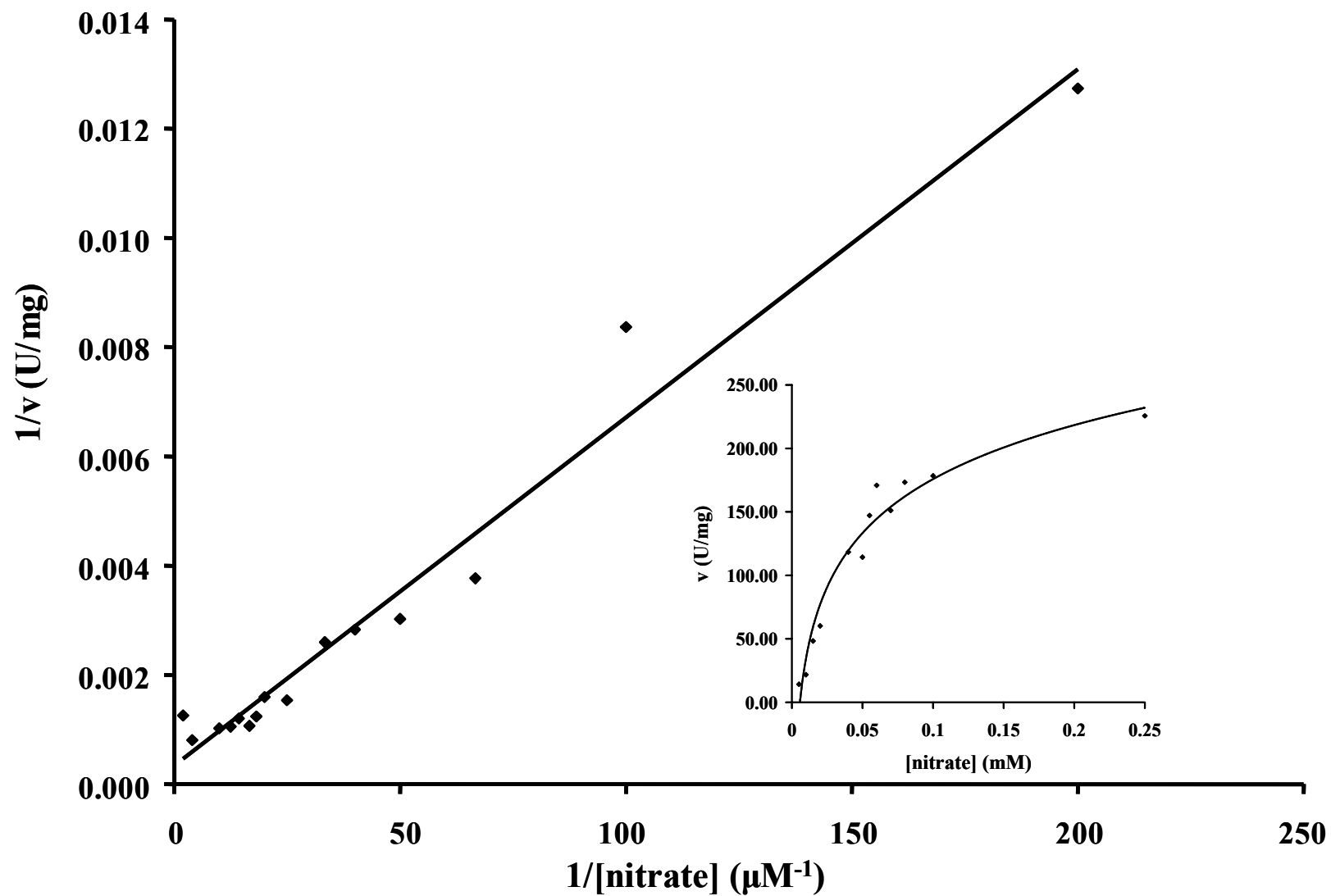


Fig. 3.5. Kinetic parameters of NR1. Lineweaver-Burke plot of the dependence of NR activity on nitrate concentration. Assays were carried out under standard conditions at 90 °C as described in the Methods section. The inset shows the relationship between nitrate concentration and NR activity.

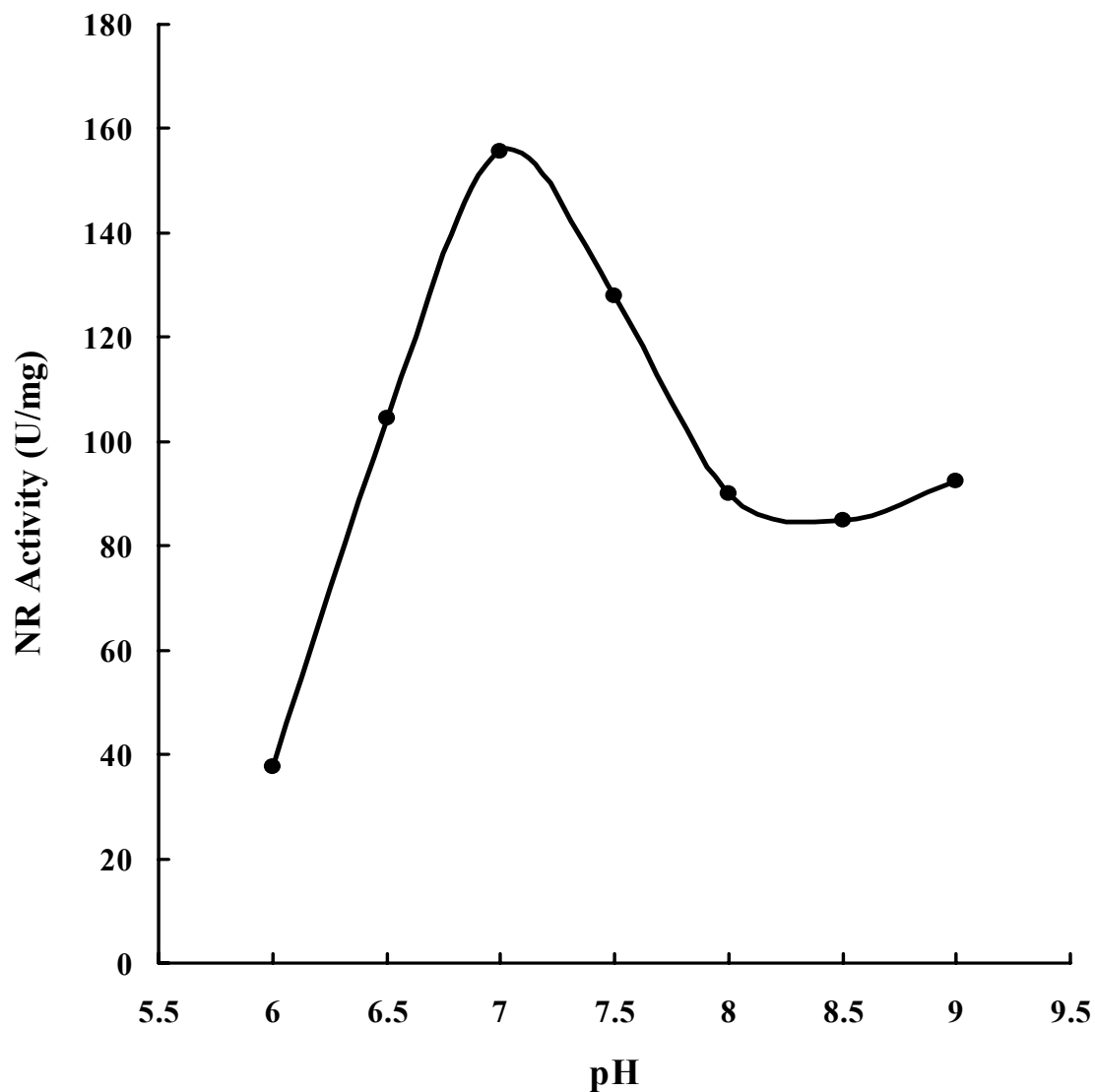


Fig. 3.6. The effect of pH on the nitrate reductase activity of NR1. Activity was determined at 90 °C under standard conditions except that the following buffers at the indicated pH were used: MES (pH 6.0 and 6.5), Bis-Tris (pH 6.0, 6.5 and 7.0), HEPES (pH 6.5, 7.0, 7.5 and 8.0), PIPES (pH 7.0 and 7.5), MOPS (pH 7.0, 7.5 and 8.0), EPPS (pH 8.0 and 8.5), and CHES (pH 8.5 and 9.0).

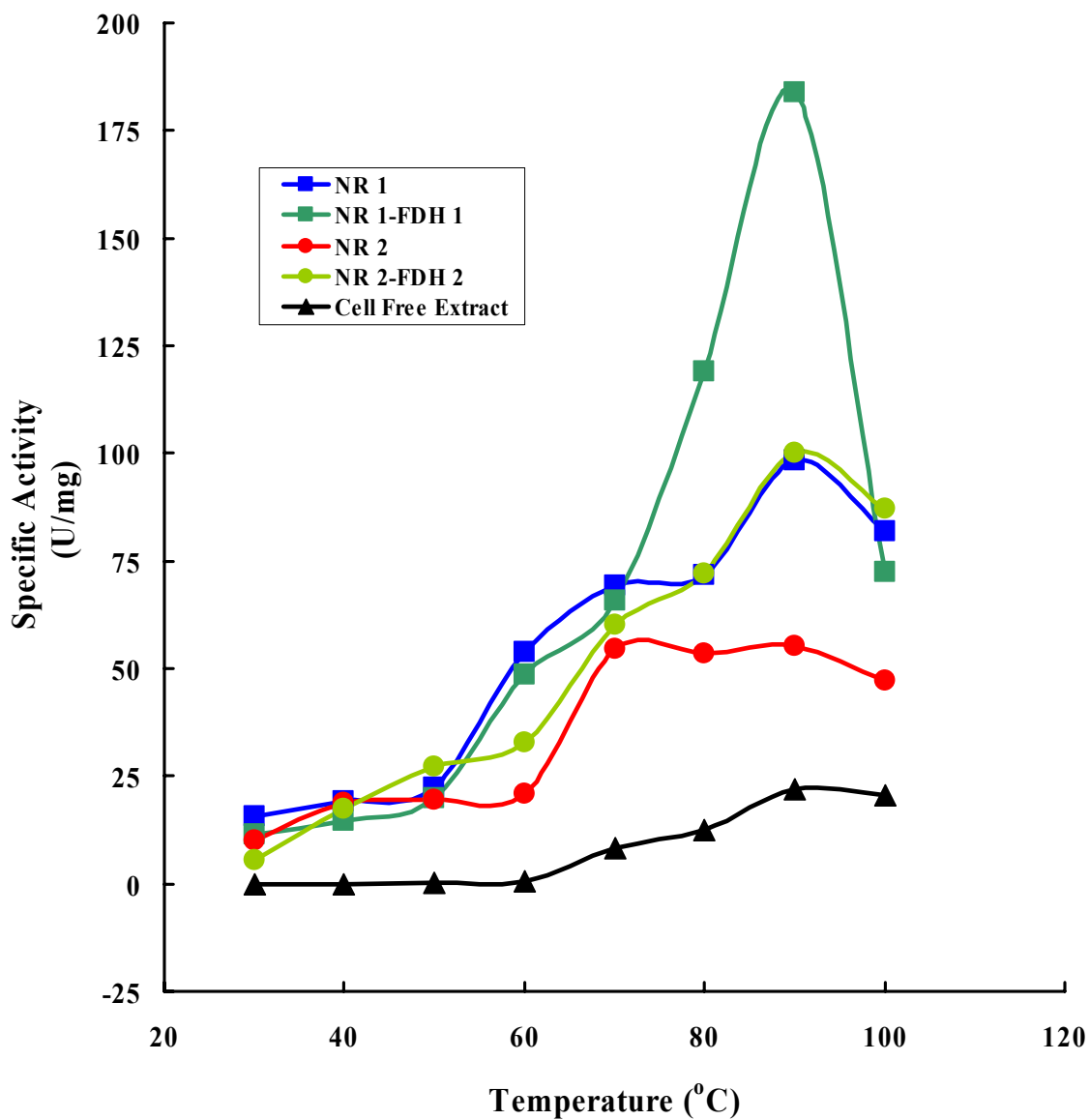


Fig. 3.7. Effect of temperature on various forms of nitrate reductase in *P. aerophilum*. The assays were carried out under standard conditions, except that the temperature was varied as indicated. The amount of protein added to each assay was 10 μg except for NR2, which was 5 μg .

at room temperature. Note, however, that the time factor in the spectrophotometric assay is seconds, while at least a minute was required to observe activity in the in-gel assay.

Molecular mass and subunit composition of NR. The two purified forms of nitrate reductase, NR1 and NR2, and the two nitrate reductase-formate dehydrogenase complexes, NR1/FDH1 and NR2/FDH2, were analyzed by SDS-PAGE. In addition, the protein band from nondenaturing PAGE of NR1, which was excised, crushed, suspended in SDS-PAGE sample buffer, and then analyzed by SDS-PAGE, shows the three polypeptides, α , β and γ , of NR1 in *P. aerophilum* (Fig. 3.8). The α , β , and γ subunits of NR were assigned according to their molecular weights predicted from the gene sequences, encoded by genes PAE3611, PAE3612, and PAE3614 respectively, identified in the *P. aerophilum* genome (28). The identities of the nitrate reductase subunits were confirmed by N-terminal sequencing, mass spectroscopy, and in some cases by visible spectroscopy and activity assays (Fig. 3.9 and Table 3.3). N-terminal sequencing (MNVRAQITMAMN) was successful in identifying all monomer and some dimer forms of the β subunits. Neither N-terminal amino acid sequence analysis, nor internal amino acid analysis of blotted polypeptide fragments, however, could identify the high molecular weight protein bands of the purified NRs or the NR/FDH complexes (137 to 146 kDa). These subunits were identified, however, by mass spectroscopy (MS) of in-gel, coomassie-stained protein digested with trypsin. In cases that did not result in an unambiguous identification, resultant polypeptides from the tryptic digest were subjected to further MS (MS/MS), which resulted in derived internal sequences based on BLAST results of observed peak masses that were used for identification.

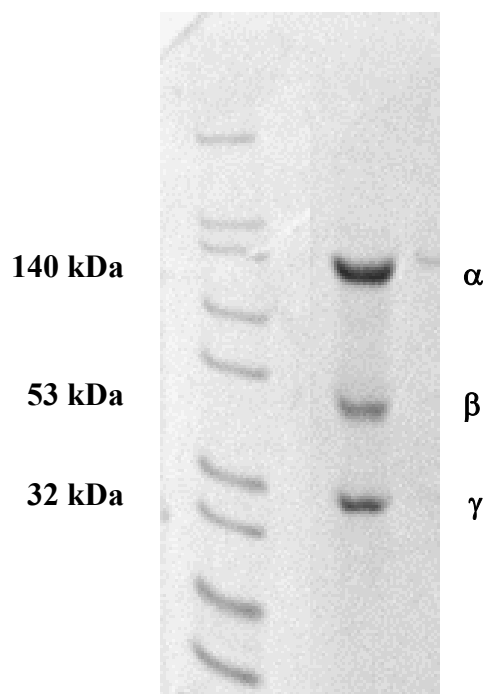


Fig. 3.8. SDS-PAGE of NR1 from nondenaturing gel band. The protein band corresponding to NR1 (15 ug) from a 3-8% Tris-Acetate gel which was run under non-denaturing conditions, was cut out, mashed, and boiled for 15 min in the presence SDS sample buffer. The resultant sample was analyzed using SDS-PAGE, which shows the three subunits of NR1 in *P. aerophilum*.

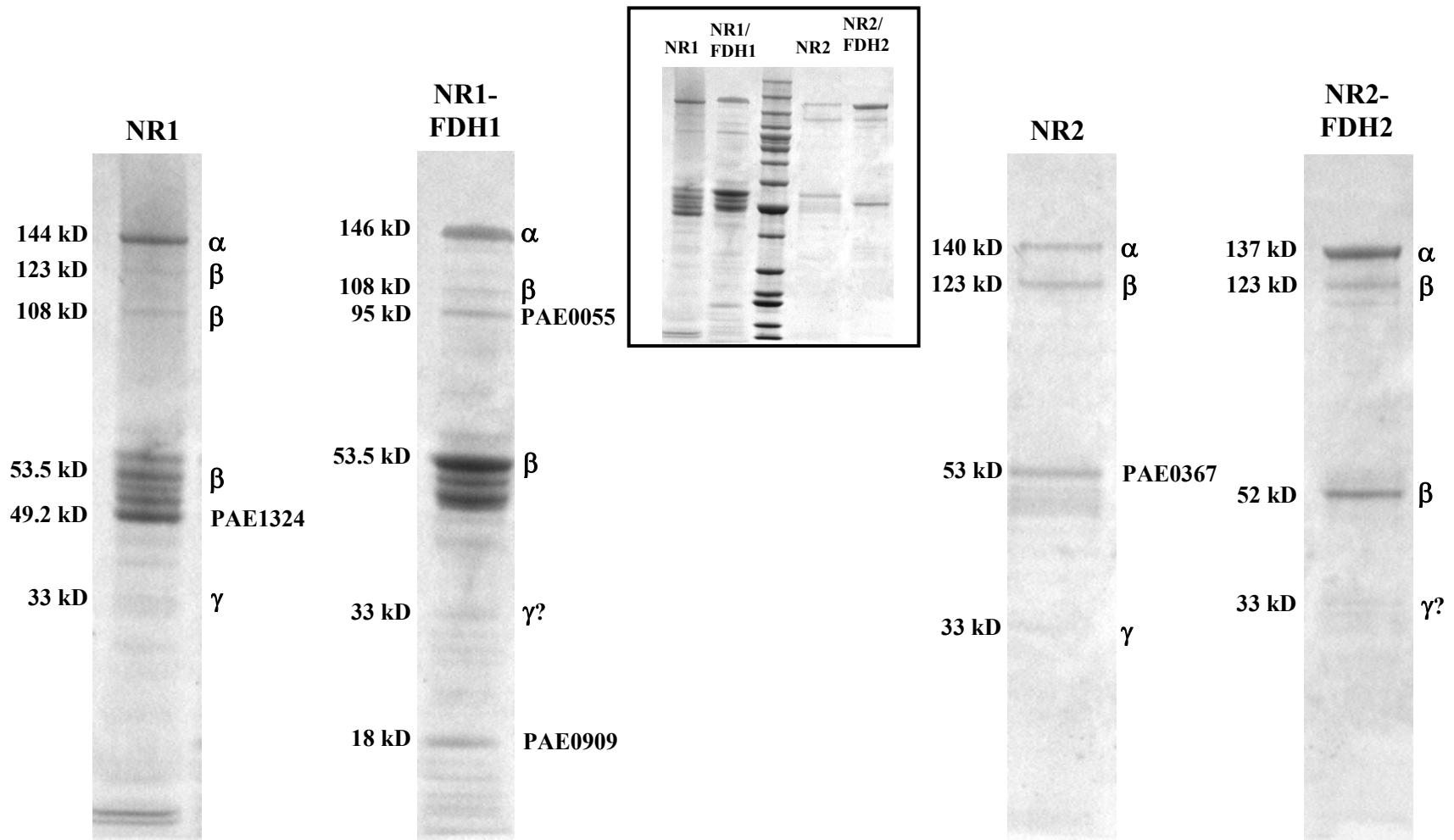


Fig. 3.9. SDS-PAGE analysis of the two peaks of nitrate reductase activity from *P. aerophilum*. Proteins were separated in a 4-12% Bis-Tris acrylamide gel and stained with Coomassie blue R-250. Each lane contains 10 μ g of protein. Active NR, peak 1 and 2 (see Fig. 3.3 for details), each consisted of purified NR (NR1 and NR2) and the enzyme complex (NR1-FDH1 and NR2-FDH2), respectively. The inset is the gel as run with the samples and the standards that were used (BenchMark Protein Ladder; Invitrogen Corp.) which consisted of 15 engineered proteins with the molecular weights ranging from 220 kDa to 10 kDa.

Table 3.3. Method of and identification of subunits and additional proteins in the purified nitrate reductases in *P. aerophilum* identified from SDS-PAGE analysis.

NR Subunit/Protein Identified		Gene	Estimated M _r (SDS-PAGE) (Da)	Predicted M _r (genomic sequence) (Da)	Method of identification
α	NR1	PAE3611	144,000	146,322	MS/MS [§]
	NR1-FDH1		146,000		MS*
	NR2		140,000		Activity Assays
	NR2-FDH2		137,000		MS
β	NR1	PAE3612	123,000	53,735	N-terminal [¶]
			108,000		N-terminal
			53,500		N-terminal
	NR1-FDH1		108,000		N-terminal
			53,500		MS
	NR2		123,000		N-terminal
	NR2-FDH2		123,000		MS
			52,000		N-terminal and MS
γ	NR1, NR2, NR1-FDH1, NR2-FDH2	PAE2614	~33,000	28,229	Visible spectroscopy and genomic sequences

Hypothetical ABC Transporter	PAE1324	50,000	49,200	N-terminal
Conserved Hypothetical; Transport and Binding cations	PAE0367	53,000	48,773	MS/MS
Hypothetical protein	PAE0055	95,000	67,871	MS/MS
Conserved region	PAE0909	18,000	14,439	MS/MS

§ Mass spectroscopy

* Mass spectroscopy/Mass spectroscopy, tandem mass spectroscopy

¶ N-terminal amino acid sequencing

The γ subunits for all forms of NR in *P. aerophilum*, NR1, NR2, NR1/FDH1 and NR2/FDH2, were identified by visible spectroscopy (Table 3.3, Fig. 3.9). Results for the analyses of FDH subunits will be presented in Chapter 4.

Purified NR, NR1 and NR2, as predicted by genomic sequence, consisted of three major polypeptides as shown by SDS-PAGE analysis (Fig. 3.9). NR1 α had an approximate M_r value of 144 kDa. The β subunit was present as major polypeptide in monomer form as 53.5 kDa and as a dimer with M_r values of 123 kDa and 108 kDa (Fig. 3.9 and Table 3.3). The γ subunit in NR1 appeared only as a faint band when analyzed by SDS-PAGE with an approximate M_r value of 33 kDa. In addition to the proteins predicted by gene sequences, a putative extracellular solute binding protein (PAE1324) with a molecular weight of 49.2 kDa was identified by N-terminal sequencing (MASRIGIIGVIVL) as seen in the lane loaded with NR1 (Fig. 3.9). The predicted M_r values for the α and β subunits of NR2 were 140 kDa and 123 kDa, respectively. The 123 kDa polypeptide in NR2, confirmed by N-terminal amino acid sequence analysis as the β subunit, was present only in dimer form. Neither MS, nor MS/MS analysis of the 140 kDa polypeptide from NR2, however, yielded an irrefutable result, but based on activity and peak matches that were observed in MS, is presumed to be NR α subunit. The γ subunit for NR2 also appeared only as a faint band when analyzed by SDS-PAGE with an approximate M_r value of 33 kDa. In addition to the α , β and γ subunits, a 53 kDa protein present in NR2 (Fig. 3.9) was identified using MS/MS analysis as a conserved hypothetical protein in *P. aerophilum*, encoded by gene PAE0367, with a calculated molecular weight of 48.7 kDa. This protein showed sequence similarity (45% to 53%) to iron (III) ABC transporter proteins in numerous hyperthermophiles and other archaea as well as several bacteria.

The two nitrate reductase-formate dehydrogenase complexes (NR1-FDH1 and NR2-FDH2) also contained the three predicted major NR polypeptides. The α subunits were identified by MS as the 146 kDa band in NR1-FDH1 and the 137 kDa band in NR2-FDH2 (Fig. 3.9). The 53.5 kDa and 108 kDa (NR1-FDH1), and the 52 kDa and 123 kDa (NR2-FDH2) bands were all identified as monomer and dimer forms of the β subunit by N-terminal amino acid sequence analysis and MS (Table 3.3). Two additional proteins were also identified in NR1-FDH1 complex. One was a 95 kDa polypeptide that was identified by MS/MS analysis as a hypothetical protein (PAE0055) with a molecular weight of 67.8 kDa. The remaining major band present in NR1/FDH1, an 18 kDa protein, was identified as a conserved region within *P. aerophilum* (PAE0909) with a calculated molecular weight of 14.4 kDa. This locus (PAE0909) is surrounded by genes encoding five hypothetical proteins both upstream and downstream.

The additional bands around the β subunit present in the lanes loaded with NR1 and NR1-FDH1 (Fig. 3.9) represent degradation products of the β subunit. The β subunit was found to undergo proteolysis and break down into smaller peptides during storage at 4°C. Studies with *E. coli* (25, 45, 46), *B. halodenitrificans* (41) and in *Haloferax denitrificans* (36) also report the breakdown of the NR β subunit during storage, as revealed by SDS-PAGE. Furthermore, variability among subunit size in SDS-PAGE is in part a reflection of the interaction between detergent present in the protein from purification and the denaturing detergents used in analysis. This variability is not uncommon in SDS-PAGE analysis of integral membrane proteins, especially those with heteromultimeric structures like NR (25, 36, 45, 46).

The presence of the γ subunits of NR1, NR1-FDH1, NR2 and NR2-FDH2 could not be confirmed by N-terminal sequence analysis or MS because the concentrations were too low in SDS-PAGE. However, this subunit is predicted to contain cytochrome *b*, by analogy with *E. coli*

NR (27), and the presence of a *b*-type cytochrome in the *P. aerophilum* NR samples was confirmed by visible spectroscopy (Fig. 3.10). There were differences, however, between the four forms of *P. aerophilum* NR. Absorption maxima at 527 and 562 nm (β and α bands, respectively) of reduced NR1 (300 $\mu\text{g/mL}$) and at 526 and 555 nm of reduced NR1-FDH1 (300 $\mu\text{g/mL}$) are indicative of the presence of a *b*-type cytochrome (23, 27, 41, 49). While no distinct peak was visible in NR2 (40 $\mu\text{g/mL}$), a broad shoulder of increasing absorption was observed between 507 - 539 nm, and reduced NR2-FDH2 (65 $\mu\text{g/mL}$) exhibited a low absorption α band at 555 nm. It is possible that NR2 does not contain a cytochrome *b* in purified form. Purification of NR from *E. coli* also resulted in two forms of the enzyme, one with *cytb* and one without (23). These two forms of the enzyme also eluted from an ion-exchange column at different salt concentrations. The first form, which eluted at a low salt concentration, had absorption maxima for *cytb* at 427, 529 and 558 nm upon complete reduction. The second form of the enzyme with no *cytb* had an absorption peak at 412 nm when oxidized and showed a general decrease in the visible range when reduced, similar to that seen with NR2. Furthermore, in NRs purified from other mesophilic bacteria, the γ subunit was lost during purification. For example, in *Bacillus stearothermophilus*, NR was also solubilized from the membranes with *n*-octyl β -glucoside, and cytochrome *b*₁, while present during the early stages of the purification, was lost in the final step (24). Moreover, even when spectral studies of nitrate reductase Z from *E. coli* revealed the presence of a *b*-type cytochrome, no polypeptide corresponding to the γ subunit was detected in coomassie-stained SDS-PAGE (38). In this case, the γ subunit was lost due to irreversible aggregation when the sample was heated at 100 °C for 5 min in the presence of SDS. Similar conditions were used in the present study. Loss of the γ subunit is also common

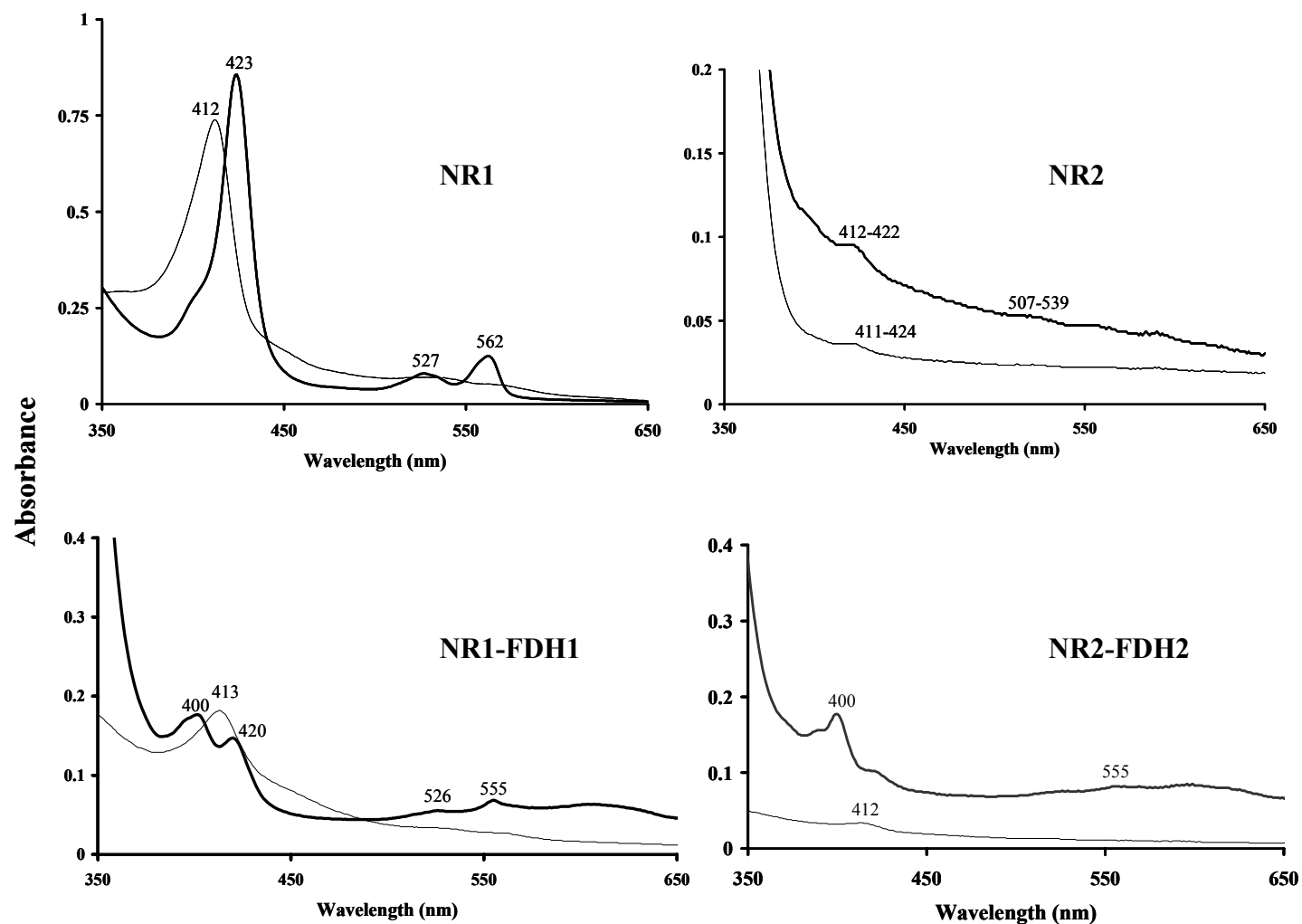


Fig. 3.10. UV-Visible spectra of nitrate reductase. Samples were oxidized by treatment with chlorate (10 mM) at 80 °C, and were reduced with sodium dithionite. The presence of a *b*-type heme in the reduced enzyme is indicated by an α -band maximum at approximately 560 nm, and a γ -band maximum at approximately 420 nm. The thin lines are the spectra of the oxidized enzyme, and the heavy solid lines represent the reduced form. Protein concentrations are NR1 (300 $\mu\text{g}/\text{mL}$), NR1-FDH1 (300 $\mu\text{g}/\text{mL}$), NR2 (40 $\mu\text{g}/\text{mL}$), and NR2-FDH2 (65 $\mu\text{g}/\text{mL}$).

in NRs when purified with deoxycholate, as seen with the enzymes from *E. coli* (26), *Klebsiella aerogenes* (82), and in *B. licheniformis* (83).

Metal content. NR1 contained 0.8 ± 0.2 g-atoms Mo and 0.02 ± 0.01 g-atoms W per mol of complex, based on a M_r value of 235,000 for NR $\alpha\beta\gamma$. NR2 contained 0.03 ± 0.05 g-atoms Mo and 0.7 ± 0.1 W g-atoms per mol of NR2 complex when analyzed by plasma emission spectroscopy. Thus, the principal nitrate reductase, NR1, in *P. aerophilum* is a Mo-containing enzyme with a specific activity of 534 U/mg (Table 3.2). The secondary form of nitrate reductase present, NR2, however, contains primarily W with a specific activity of 223 U/mg. Iron was present in NR1 at 20 ± 0.1 g-atoms per mol of enzyme, and at 16 ± 0.5 g-atoms per mol of NR2 as determined by colorimetric analysis. The metal content of NR1-FDH1 and NR2-FDH2 will be presented in Chapter 4.

EPR spectra were recorded for whole cells and NR1. Whole cells and purified NR1 prepared under dithionite-reducing conditions exhibited EPR signals at $g = 2.06$ and 1.95 at 12K, but not above 30K, (Fig. 3.11), which is characteristic of reduced $S = \frac{1}{2} [4Fe-4S]^{1+}$ clusters. Furthermore, the EPR spectra of the oxidized enzyme at 12K (Fig. 3.12A) showed a peak at $g = 2.02$ and a trough at 1.99 , which is characteristic of an oxidized $S = \frac{1}{2} [3Fe-4S]^{1+}$ cluster. These spectra are similar to those reported for membranes of nitrate grown *E. coli* cells and for purified, overexpressed NarGH (48). Comparison of the spectra of whole cells and purified NR, which both contain characteristics indicative of Fe-S clusters, suggests that NR is the major Fe-S containing protein in *P. aerophilum* cells and a major protein in this organism.

At 100K, in the reduced state, signals from NR1 at $g = 1.986$ and 1.959 were observed, which are indicative of $S = \frac{1}{2} Mo(V)$ (Fig. 3.12A). This spectrum is similar to that seen from

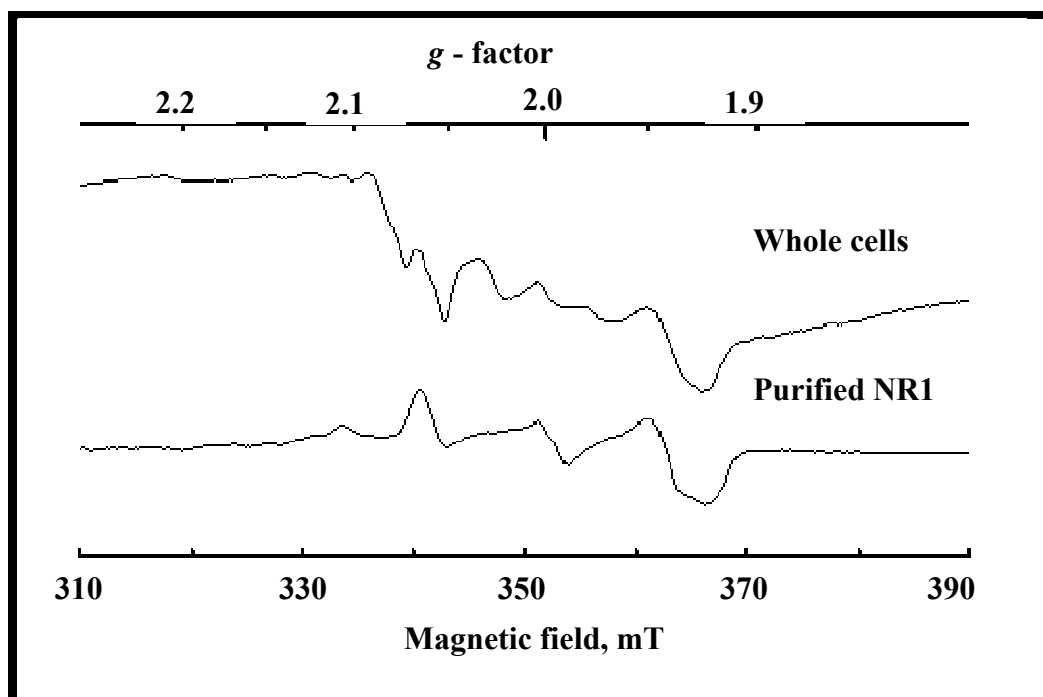


Fig. 3.11. EPR spectra of whole cells and purified NR1 of *P. aerophilum*. EPR spectrometer conditions: temperature, 12K; microwave power, 20 mW at 9.605 GHz; and modulation amplitude 1 mT. Spectra were recorded by Richard Cammack of the Department of Life Sciences, King's College, London SE1 9NN, U.K in the laboratory of Professor Michael K. Johnson, Department of Chemistry, University of Georgia, Athens, GA.

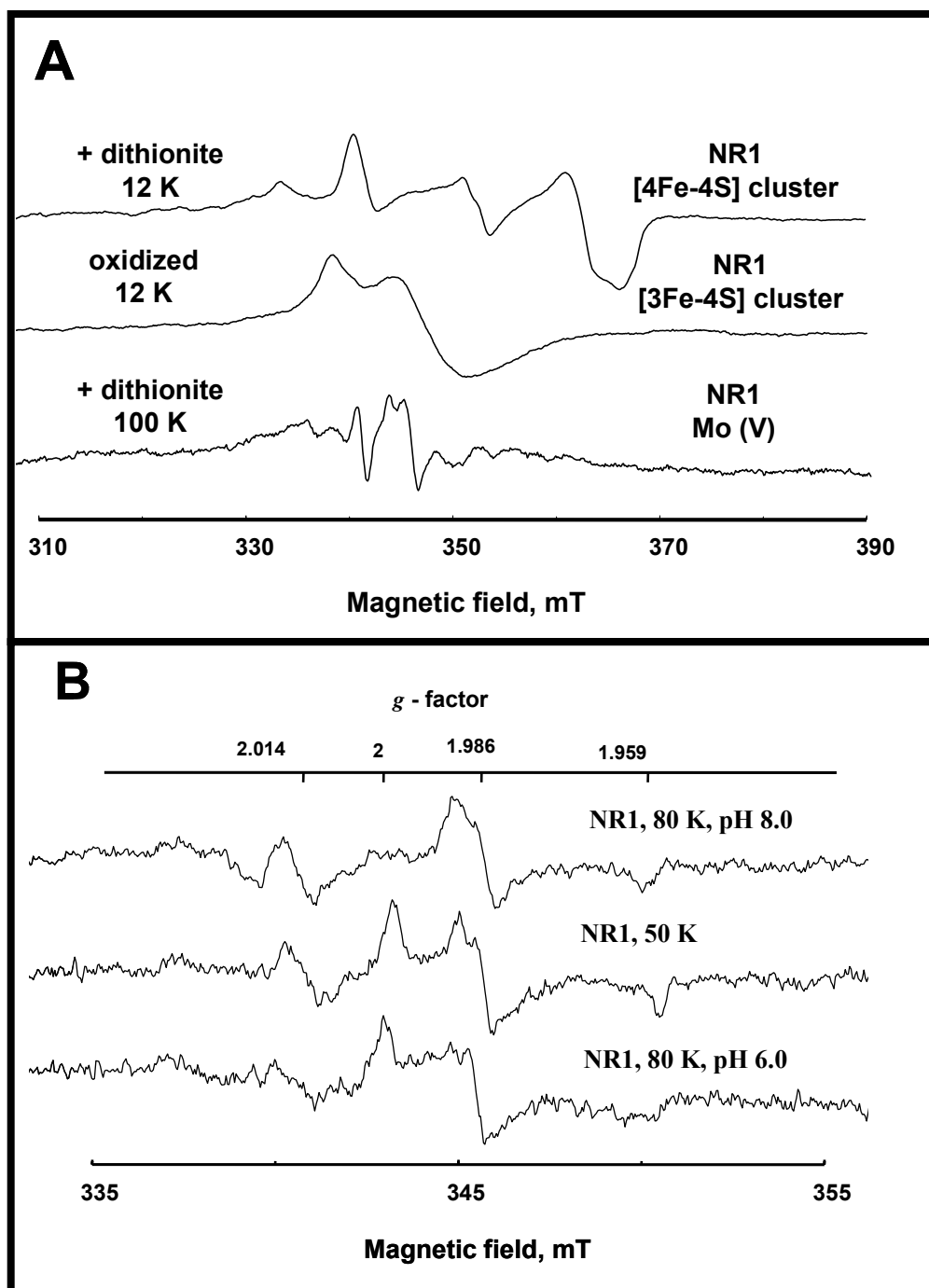


Fig. 3.12. EPR spectra of *P. aerophilum* nitrate reductase. (A) Signals of Fe-S clusters in NR1 reduced with dithionite (2 mM) at 12K, of Mo (V) at 100K in the reduced state, and of Fe-S clusters in the oxidized state at 12K. (B) Three forms of Mo (V) present in NR1 at 80K (pH 8.0 and 6.0) and 50K. Temperature is as indicated, microwave power 20 mW, frequency 9.605 GHz and modulation amplitude 2 mT. Spectra were recorded by Richard Cammack of the Department of Life Sciences, King's College, London SE1 9NN, U.K in the laboratory of Professor Michael K. Johnson, Department of Chemistry, University of Georgia, Athens, GA.

the NR of the denitrifying halophilic archaeon *Haloarcula marismortui* (88), and from the high-pH form of the *E. coli* NR (30). NR1 at 80K (pH 8.0 and pH 6.0) and at 50K (Fig. 3.12B) also exhibited these signals from Mo, and additional peaks at $g = 2.00$ and 2.014 were seen in some preparations. EPR absorption at these g values are indicative of radicals from an intermediate as seen in an extensive EPR study of *E. coli* membranes, overexpressed NarGH and NarGH mutants (48). The radicals appeared in membranes and in purified protein concomitant with the addition of nitrate to dithionite-reduced membranes, and in samples with a quinone-analog inhibitor. No signals indicative of W(V) were obtained from the samples analyzed in this study, which was expected. Unfortunately, insufficient quantities of purified W-containing NR2 and NR2-FDH2 were available for EPR analysis.

Sequence comparisons. Comparison of the gene arrangement and amino acid sequences of the NR from *P. aerophilum* and NRA from *E. coli* (Fig. 3.1) reveal high similarity suggesting that *P. aerophilum* contains a conventional NR that is homologous to *E. coli* NRA. Further, *P. aerophilum* does not appear to contain another NR, at least one that could be recognized in the genomic sequence, as is the case with *E. coli*, namely NRZ. Specifically, the α and β subunits of the *P. aerophilum* enzyme (PAE3611 and PAE3612, respectively) show high sequence identity and similarity with the homologous subunits of NRA in *E. coli* (b1224 and b1225, respectively), and are thought to contain the same cofactors. Although the γ subunit (PAE2614, b1227) has a lower sequence similarity overall (Fig. 3.1), the subunit of the *P. aerophilum* enzyme is assumed to contain the same heme cofactors, as the His ligands for the heme cofactors are also conserved in *P. aerophilum*, and the cofactor was identified by visible spectroscopy. The lower similarity between the γ and δ subunits (PAE3610, b1226) of the two enzymes reflects their involvement in

binding the proteins to the membranes. This might be due to the differences between the ester-linked fatty acid membranes of bacteria and the ether-linked phospholipids and isoprenoids in archaeal membranes. There are differences in the operons encoding NRA of *E. coli* and NR of *P. aerophilum*, notably that they differ in gene order, the δ subunit of *P. aerophilum* is transcribed in the opposite direction to the other three, and the gene encoding the γ subunit of the *P. aerophilum* NR is located over 600,000 nucleotides upstream from the operon (Fig. 3.1). Furthermore, the NR operon of *P. aerophilum* contains an additional gene (PAE3613), which is annotated as a conjectural NR subunit. This gene has homology to the γ subunit of the selenate reductases of *Aeropyrum pernix* (60%) and *Haloarcula marismortui* (44%), and to the γ subunit of the ethylbenzene dehydrogenase of *Azoarcus* sp. EbN1 (44%). Hence, while this gene shows no similarity to the γ subunit of *E. coli* NR, it may function as an alternative γ subunit in *P. aerophilum* NR. In addition, there are also small differences in the sizes of the corresponding subunits. For example, the α and γ subunits of *P. aerophilum* are approximately 9 kDa and 4 kDa larger, respectively, while the β (4 kDa) and δ (5 kDa) subunits are smaller than the corresponding subunits in NRA of *E. coli*.

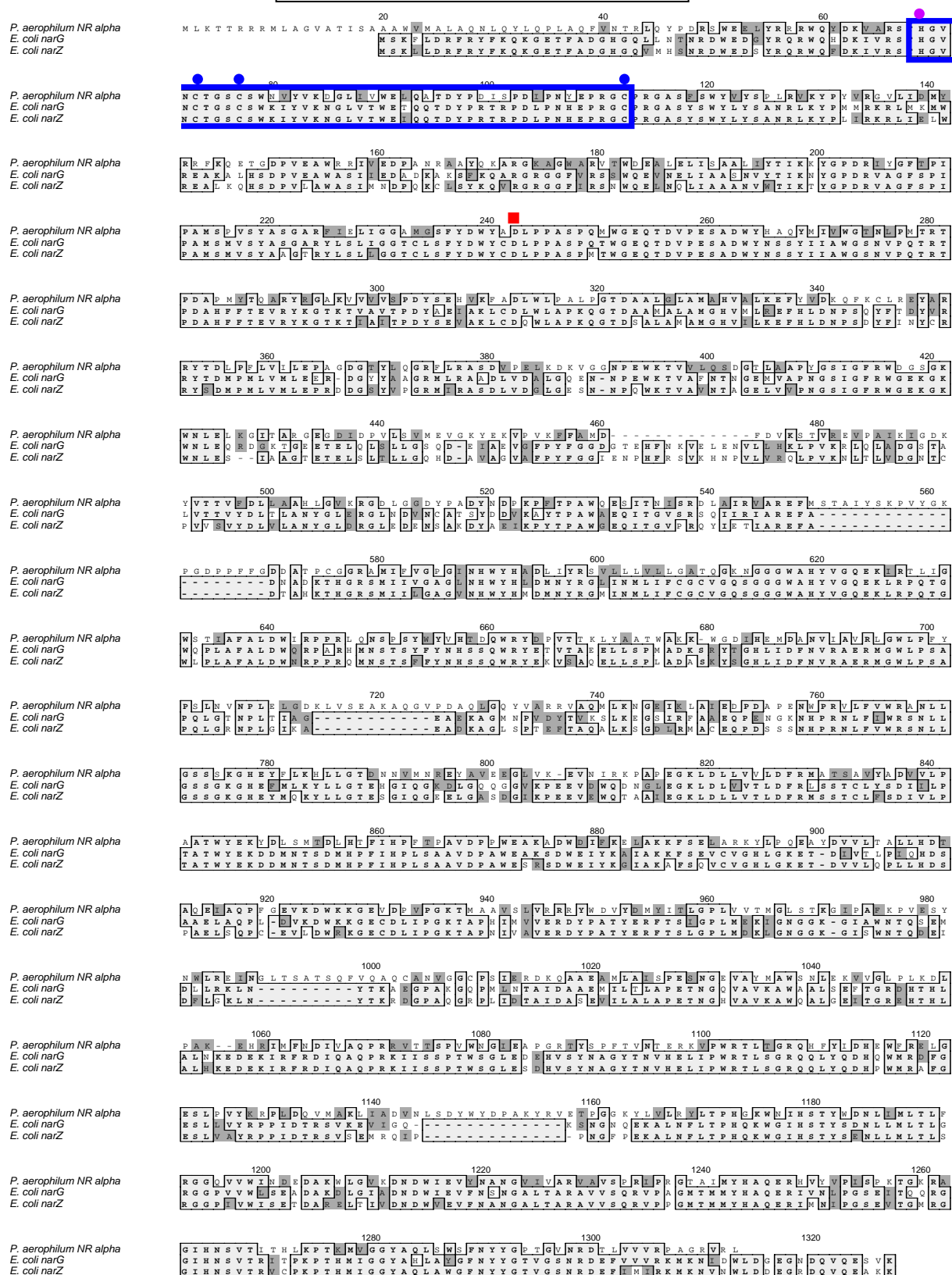
The catalytic α subunits of most multimeric respiratory molybdoenzymes contain a CX₂-₃CX₃CX₂₆₋₃₄C region in the amino-terminal that coordinates a [4Fe-4S] cluster, with the exception of the α subunits of nitrate reductases, NarG and NarZ (10, 11, 14-16, 18, 42, 43, 52, 62, 63, 65, 75, 76, 89). In these cases a His residue replaces the first Cys residue. Replacement of the expected Cys residue with a His in coordinating a [4Fe-4S] cluster is also found in the [Ni-Fe] hydrogenase from *Desulfovibrio gigas* (85) and the Fe-only hydrogenase from *Clostridium pasteurianum* (60). Recently, from crystal structures of *E. coli* NRA (13, 40), it was discovered that the His and Cys residues in NarG also coordinate a [4Fe-4S] cluster. Alignment of the

corresponding protein sequences shows that this alternative motif is also found in *P. aerophilum* α (Fig. 3.13A) (28), as well as in the membrane-bound respiratory nitrate reductases (NRA and NRZ) of *E. coli* (15, 16). Another unique finding revealed by the crystal structures was the identification of Asp²²² (NarG) as a ligand coordinating Mo in the active site. This residue is also conserved in the sequence of *P. aerophilum* NR α (Fig. 3.13A) and in NarZ. In addition to the [4Fe-4S] in the α subunit, Cys residues known as binding sites for a [3Fe-4S] and three additional [4Fe-4S] clusters in *E. coli* NarH (33) are also conserved in the β subunit of *P. aerophilum* and in *E. coli* NarY (Fig. 3.13B).

In *E. coli* NRA, the γ subunit (NarI) contains two *b*-type hemes named according to their location relative to the active site. The ligands of both the proximal and the distal hemes, heme *b_P* and heme *b_D*, respectively, have also recently been determined based on recent crystal structures of the respiratory NR from *E. coli* (12, 13). These His ligands are also conserved in the sequence of the γ subunit of *P. aerophilum* NR and in NarV from NRZ (Fig. 3.13C). In *E. coli* NRA, His⁵⁶ and His²⁰⁵ coordinate the high potential heme ($E_m \sim 120$ mV) located towards the cytoplasmic side of NarI; and His⁶⁶ and His¹⁸⁷ coordinate the low potential heme ($E_m \sim 20$ mV) located towards the periplasmic side of NarI (48, 69).

The δ subunit of NRA in *E. coli* (NarJ), which anchors NarGHI to the membrane, does not contain any cofactors. As expected, alignment of *P. aerophilum* and *E. coli* sequences of the NR δ subunit (Fig. 3.13D) show a low similarity (Fig. 3.1). This may be due to the aforementioned difference in membrane structure between bacteria and archaea, but could also reflect sequence divergence.

As many of the W-containing enzymes characterized to date are from hyperthermophiles and their pterin cofactors do not contain a dinucleotide side-chain, it was interesting to see if NR,

A. NR α subunit

B. NR β subunit

P. aerophilum NR beta
E. coli narH
E. coli narY

```

MNVVRAQLITMA MNLDCICIGCHTCSVTC NVWVTNRRAAGAEYMWNNVETRPGFGYPRQWEDQNKYNGGWA LDG
MKIRSQVGMVNLNLDCCICIGCHTCSVTC NVWVTSREGV EYAWFNNVETKPGQGFPTDWEQEKYKGGWIRKI
MKIRSQVGMVNLNLDCCICIGCHTCSVTC NVWVTGREGMEYAWFNNVETKPGIGYPKNWEDQEQWQGGWIRDV
  
```

P. aerophilum NR beta
E. coli narH
E. coli narY

```

G-----KLLKLELTKNYKPPSLKDYEPWTDYEA LFSDDKQ-TDQQPVARPLSLITD EPMDEVAY-
NGKILQPRMGNRAMLLGKIFANPHLPGLIDDYEPFDYDYNLHTEAPEGSRSGPILARPRSLITGERMAKLEK
NGKILRPRLGNKMGIITKIFANPVVPIQIDDYEPFTFDYELHSAPE-GKHIP TARPRSLIDGKRRMDKVIW
  
```

P. aerophilum NR beta
E. coli narH
E. coli narY

```

GPNWNDDLGLGTDYILE-DPNDLGLQR ELYAQFKDVFMMYLPRICNHCLNPSCLAAAC RKA IYKREEDGIV
GPNWEDDLGGEFDKLAKDKNFDNIQKAMYSQFENTFMMYLPR LCEHCLNPA CVATC SGAIYKREEDGIV
GPNWEELGGEFELKRLARDRNFBAMQKEMYGQFENTFMMYLPR LCEHCLNPSCVATC SGAIYKREEDGIV
  
```

P. aerophilum NR beta
E. coli narH
E. coli narY

```

LIDQNIJCRGMRYCVAAACIYKKNVYNWKGKSEKCI LCYPSVEAGQPTVCSLITC GRIYRMLGVLLYDADK V
LIDQDCRGMRCITGCIYKKIYFNWKS GSKSEKCI FCPRIEAGQPTVCS ETC GRIRYLGVLLYDADA I
LIDQDCRGMRLCISGCIYKKIYFNWKS GSKSEKCI FCPRIE SGOPTVCS ETC GRIRYLGVLLYDADRI
  
```

P. aerophilum NR beta
E. coli narH
E. coli narY

```

LDVAAATPDPALVRRFIDEVLLDPFDFAVIEAARKNGIPDYWTITAAQRSPVYKLVKRWKVGFP LRPFRFRV
ERRAASTENEKDLYQRQLD-VFLDPNDPKVIEQAIKDGIPLSVIEAAQQLSPVYKMMAMEWKLALPLHPEYRT
EEAASTEREVLDYERQCE-VFLDPHDPSEVIEEALKOGIPQNVIDAAQRSPVYKMMAMDWKLALPLHPEYRT
  
```

P. aerophilum NR beta
E. coli narH
E. coli narY

```

LPMVFIYVPLSPVVTTFEKTYGAIADLFPKVS ELRIPILKYLANMFTSGDTALLESALKKLI AVRIYVBR
LPMVWYVPLSPIQSAADAGELG SNG-ILPDVESLRIPVQYLANLLTAGDTK FVLRALKRMLAMRHYKRA
LPMVWYVPLSPIQSYADAGELPKSEGLPAI ESLRIPVQYLANMLSAGDTG FVLRALKRMMAMRHYMRS
  
```

P. aerophilum NR beta
E. coli narH
E. coli narY

```

KNVAEPGLADKAKAALAEAGLSEADAEEMYRLFALAR YEDRFVIPTNPKRYAAQPQIMRGTVGLP
ETVDG---KVDTRALEEVLGTEAQAQ EMYRYLAIANYEDRFVVPSSHRELAR EAFPERNGCGFTFGDGC
QTVEG---VTDTRALIDEVGLSV AQVEEMYRYLAIANYEDRFVIPTSHREMA GDAPFA ERNGCGFTFGDGC
  
```

P. aerophilum NR beta
E. coli narH
E. coli narY

```

HGSDTKFNLFNSRIDAI DVTSKTEPH P
HGSDSKFNLFNSRIDAI NIT EVRDKAEGE
  
```

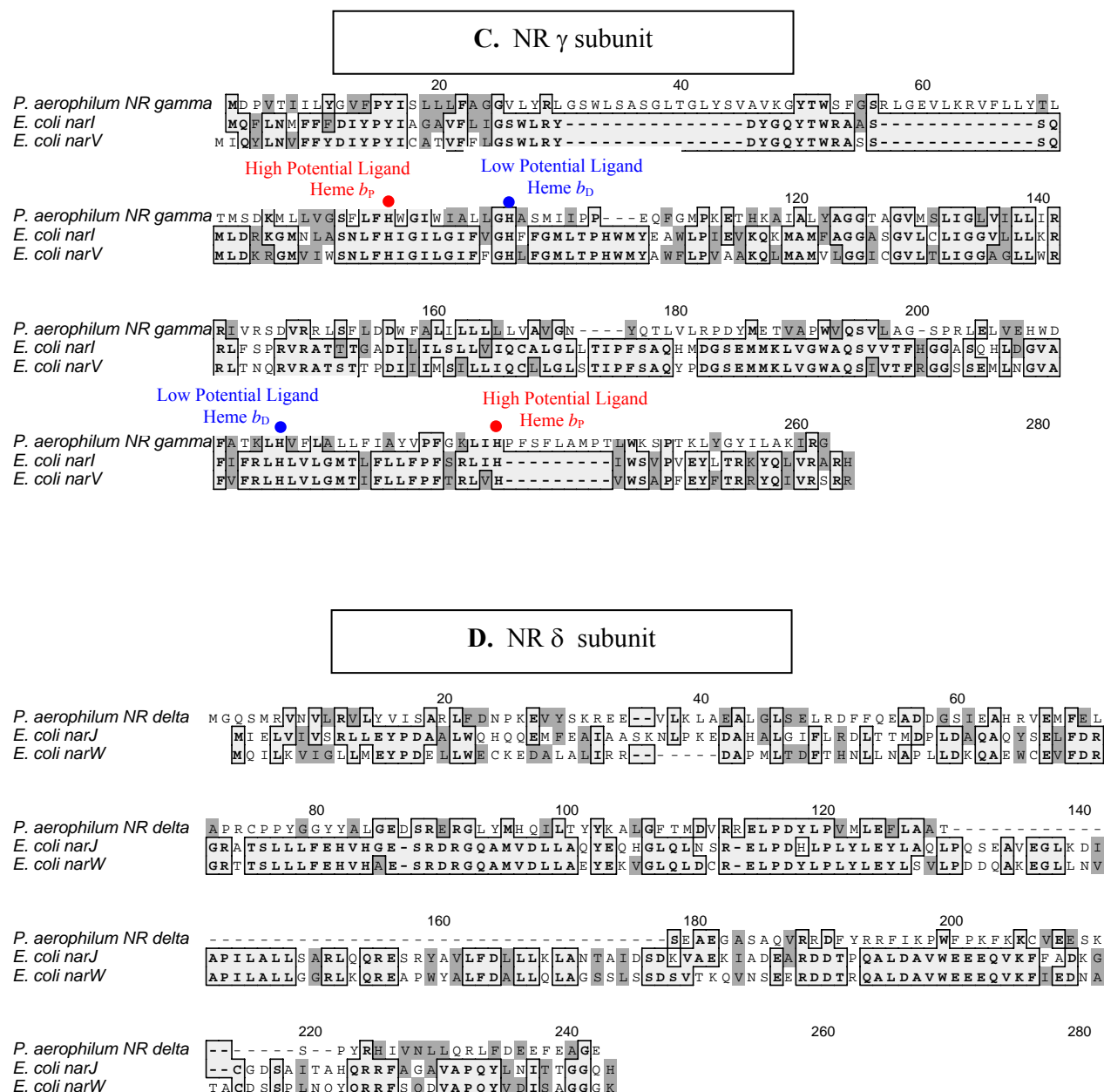


Fig. 3.13. Alignment of sequences of the α , β , γ , and δ subunits of the respiratory NR from *Pyrobaculum aerophilum*, and *Escherichia coli* NRA (*narGHJI*) and NRZ (*narZYWV*). Identical amino acids are boxed and shaded light gray. Similar amino acids are shaded dark gray. (A) NR α subunit. Residues that bind Fe-S clusters are boxed in blue with purple and blue dots denoting ligands. Mo binding site is denoted by red box as identified in (13, 40). (B) NR β subunit. Fe-S cluster binding sites are boxed in blue and blue dots denote ligands. (C) NR γ subunit. High potential ligands of heme b_p (proximal) are denoted by red dots. Low potential His ligands of heme b_D (distal) are denoted by blue dots. Heme ligand identification from (69). (D) NR δ subunit. Amino acid sequences of *P. aerophilum* and of *E. coli* were aligned using MacVector (Accelrys Software Inc.) from sequences retrieved from the NCBI database.

and also FDH, from *P. aerophilum* could be aligned with the NR (and FDH) of *E. coli* and other molybdoenzymes to indicate the possible nature of the pterin. Such enzymes include the *Rhodobacter sphaeroides* DMSO reductase, for which crystal structure is available (72). As shown in Fig. 3.14, most of the residues that bind the dinucleotide in these two enzymes are conserved in *P. aerophilum* NR, or are replaced by residues with similar properties. It therefore appears that the NR from *P. aerophilum* may have a dinucleotide attached to the pterin cofactor.

DISCUSSION

The natural high-temperature environments of hyperthermophiles typically contain an abundance of W, whereas mesophilic environments contain an abundance of the analogous heavy metal, Mo (77). The incorporation of Mo into the active sites of enzymes such as the extensively-studied mesophilic enzyme, NR (31, 73), or of W into enzymes such as the aldehyde ferredoxin oxidoreductase (AOR) in hyperthermophilic microorganisms (58), are essential for catalytic activity. Furthermore, growth of mesophilic microorganisms, such as NR-containing *E. coli*, is inhibited when W is present in the medium due to the production of an inactive demolybdo-form of NR, even though enzyme stability is maintained and subunit composition is identical to the active Mo-containing enzyme (31, 73). Conversely, it has been shown in Chapter 2 and in another study (3) that growth of *P. aerophilum* under nitrate-reducing conditions at high temperatures is dependent upon the presence of W. Moreover, it was shown that both W and Mo were taken up by *P. aerophilum* during anaerobic growth on nitrate, and the NR was membrane-bound (Chapter 2). The purification and characterization of NR in *P. aerophilum* was undertaken as part of this study in order to determine the nature of the NR or NRs, in this organism and the composition of cofactors that they contain.

NR and FDH co-purify during solubilization and column chromatography in *P. aerophilum* resulting in two forms of purified NR (NR1 and NR2) and two forms of a NR-FDH complex (NR1-FDH1 and NR2-FDH2). The NR-FDH complexes will be discussed in more detail in Chapter 4. Each form was characterized with respect to the metal composition of the pterin cofactor, catalytic activity measured in a standard anaerobic assay, activity in an in-gel assay, and apparent molecular weight of the subunits. Of the approximately 95% of NR activity solubilized from the membrane fraction, NR1 comprises 36 % of the total protein purified, constituting 82% of the total NR activity. NR1 is a Mo-containing enzyme (0.8 atoms Mo and 0.02 atoms W per mol of enzyme) and resembles that of *E. coli* as well as other respiratory NRs found in mesophilic microorganisms, including metal content and subunit composition (19, 53). Likewise, cytochrome *b* was established as an integral cofactor of *P. aerophilum* NR1 and had the ability to reduce chlorate in addition to nitrate, as is the case in *E. coli* NR. EPR spectra of [Fe-S] clusters and Mo (V) of *P. aerophilum* NR1 also demonstrate a cofactor composition similar to that of NRA from *E. coli* (30, 48). Residues identified in cofactor binding in *E. coli* (13, 40) were conserved in *P. aerophilum* and the overall high identity of sequences between the subunits, including the regions that bind the MGD cofactor, further confirm the high similarity between *P. aerophilum* NR1 and *E. coli* NRA.

NR1 from *P. aerophilum* is distinct, however, from corresponding mesophilic NRs in that it exhibits its highest activity at extreme temperatures (90 °C). Surprisingly, the enzyme has significant catalytic activity at mesophilic temperatures; in fact, its specific activity at mesophilic temperatures is comparable to that of mesophilic NRs. Yet, at its optimal temperature (90 °C), the specific activity of NR1 (534 U/mg) is 7 - 28 times higher than specific activities of corresponding mesophilic enzymes from bacterial sources, such as *E. coli* and *B. licheniformis*

(1, 45, 46, 83), and from 9 to over 20,000 times higher than NRs from the halophilic archaea *Haloferax denitrificans* (36) and *Haloarcula marismortui* (88), respectively. Furthermore, NR1 displays an apparent affinity for nitrate (40 μM) that is 5 to 95 – fold higher than the values reported for other mesophilic nitrate reductases (29, 36). For comparison, the reported kinetic properties of nitrate reductase from *P. aerophilum* (2) were a K_m of 58 μM , with a V_{max} of 326 U/mg. Archaeal NR from the halophiles *Haloferax denitrificans* had a K_m of 190 μM nitrate (V_{max} was not reported) (36) and that from *Haloferax mediterranei* had a K_m of 2.5 mM and a V_{max} of 0.142 U/mg at a salt concentration of 0.4 M NaCl, and a K_m of 6.7 mM and V_{max} of 0.109 U/mg in the presence of 3.4 M NaCl (5). In *E. coli*, NRA has reported K_m values of 420 μM (54) and 470 μM with a calculated V_{max} of 85 U/mg (1), and NRZ has a reported K_m of 500 μM (38).

Results from this study also share similarities and differences to those found in a previous study of *P. aerophilum* (2), which was published while this work was in progress. The most important difference is that in the previous study, only one form of NR was identified, which corresponds in this study to NR1. In addition, the scale of the purification was much larger in this study (2006 mg vs. 78 mg protein in the membrane fraction) resulting in 20 mg purified NR1 versus 1 μg purified protein in the previous study. Furthermore, extraction and solubilization of the membrane fraction was conducted with n-octyl β -glucoside in the current study, and Triton X-100 was used in the earlier published work (2). The scale of the study is important, as in early experiments and purifications in this research, small-scale purifications of NR1 were easily obtained, however, the second peak of NR activity (NR2) was difficult to measure because of the low quantity. Therefore, in the small-scale experiments, purification of NR2 beyond the first column was not possible. Thus, the purification of NR on a larger scale described herein allowed

for the identification of both the Mo-containing (NR1) and the W-containing (NR2) nitrate reductases in *P. aerophilum*. Also in these initial small-scale studies Triton X-100 was used to solubilize the membrane fraction, but the solubilization agent was consequently changed to n-octyl β -glucoside for the large scale purifications, as detergent curves using both detergents showed a more efficient extraction of NR and FDH from the membrane, and a more consistent and higher activity with n-octyl β -glucoside. Furthermore, FDH was neither identified nor measured in the previous published study (2). EPR studies conducted in the present research, which further confirms the presence of cofactors and metal content, were not conducted previously by others (2). Similarities between the two studies lie in comparison between NR1 and the NR identified in the previous study. Both studies identified the three subunits of NR, although the M_r of the α subunit reported previously (2) was smaller (130 kDa vs. 144 kDa). The metal content of NR was also virtually the same (0.8 mol Mo/mol NR complex, and 0.06 mol W from the previous study, and 0.02 mol W in the present study, per mol NR), as was the identification of cyt *b* in the γ subunit by visible spectroscopy. Schröder and coworkers (2) reported the specific activity of NR as 326 U/mg, which was measured at 75 °C, and further estimates that activity at 95 °C would be 526 U/mg. Specific activity of NR1 measured at 90 °C in the present study was 534 U/mg. Furthermore, NR1 maintained over 30% of optimum activity at 40 °C, while NR from the previous study maintained approximately 10%. Another difference between the two studies was a reported optimal pH at 6.5 as compared to an optimal pH of 7.0 found in this study.

The primary distinction between the NRs in *P. aerophilum* and all reported NRs to date, is however, the presence of NR2, which contains W (0.7 g-atoms W per mol enzyme). While it is not surprising that NR is able to take up and incorporate W into the active site, it is surprising

to find a level of activity (223 U/mg) that is comparable to that of the Mo-containing NR1 (534 U/mg), and to other Mo-only containing enzymes. NR2 represents 30% of the total purified NR, and constitutes 18% of the total NR activity. There is the possibility, however, that the NR2 specific activity is from the Mo present in the active site, and that the W which is present in the active site of NR2 is simply present but not active. Further experimentation, such as EPR analysis, would fully confirm the activity of the NR2-W site.

Although Mo appears to be the preferable metal utilized in *P. aerophilum* NR, the incorporation of W into the NR active site does lead to a highly active enzyme. Partial purification of *P. aerophilum* cells grown in Mo-only media at 78 °C did not contain a second peak of NR activity, in other words, there was no NR2 (data not shown). Thus, it seems that if Mo is no longer available, W is utilized in *P. aerophilum* NR. Furthermore, the genomic sequence of *P. aerophilum* confirms only one copy of NarGHJI (28) suggesting that NR1 and NR2 are the same enzyme with the exception of the metal incorporated into the active site.

A W-containing NR raises a primary mechanistic question of how a high potential redox reaction ($\text{NO}_3^-/\text{NO}_2$, $E_o' = +420$ mV) is catalyzed by an active site containing W, which typically catalyzes redox reactions of low potential ($E_m < -400$ mV). The mid-point potentials of the redox centers (hemes, [Fe-S] clusters or the W) in *P. aerophilum* NR are not known, yet the great similarity with the *E. coli* NR may provide some possible answers.

In the simplest terms, the NR from *P. aerophilum* has to function with Mo or W coordinated into its active site. In both cases, electron transfer from Mo^{IV} ($\sim +220$ mV) to NO_3^- (+420 mV) and from W^{IV} (~ -200 mV) to NO_3^- (+420 mV) is a thermodynamically favorable reaction. The ability of W-mediated nitrate reduction by direct atom transfer has been shown by Jiang and Holm (39) using synthetic chemical analogues of the reactant complexes of

bis(dithiolene)tungsten (W^{IV}) and their oxidation products bis(dithiolene)tungsten (W^{VI}). To the contrary, while the transfer of electrons in the overall reaction of nitrate reduction from menaquinone (-80 mV) to the Mo site in NR ($\sim +220$ mV) is a favorable reaction, as illustrated by the NR in *E. coli* (Fig. 3.15), the transfer of electrons from menaquinone to the W site in NR (-80 mV to -200 mV) is not. The real question then becomes not whether nitrate can be reduced at a W site, but rather how does the W site become reoxidized so that catalysis can continue. In the case of Mo, electron transfer proceeds favorably to the active site, and for NR2, a W-containing NR, there are two suggested possibilities for favorable electron transfer from menaquinone to the W-NR active site in *P. aerophilum*. One, is the case in which the midpoint potential of the coordinated W (operating between the IV and VI redox states) is more positive than would be expected from inorganic model W chemistry, thus allowing for a thermodynamically favorable reaction and functioning with the same mechanism as the Mo-NR; and two, in which there is a variation in the redox potentials of the electron carriers forming a favorable reaction to the W site with a redox potential of ~ -200 mV.

In support of the first possibility, the trimethylamine *N*-oxide (TMAO) reductase (TMAOR) of *E. coli*, which is a molybdoenzyme that catalyzes the reduction of TMAO to trimethylamine (TMA) with a redox potential of +130 mV, is also active as a tungsto-TMAOR (20). Thus, the W-TMAOR is capable of catalyzing the reduction of TMAO to TMA with a redox potential of +130 mV, challenging the model that tungstoenzymes catalyze reactions of extremely low potential. However, the redox potentials for the W^{VI}/W^V and W^V/W^{IV} couples were not determined in this study. Therefore there is no direct evidence for a high positive potential for a W active site. But by analogy with the W-TMAOR, as shown by the structural

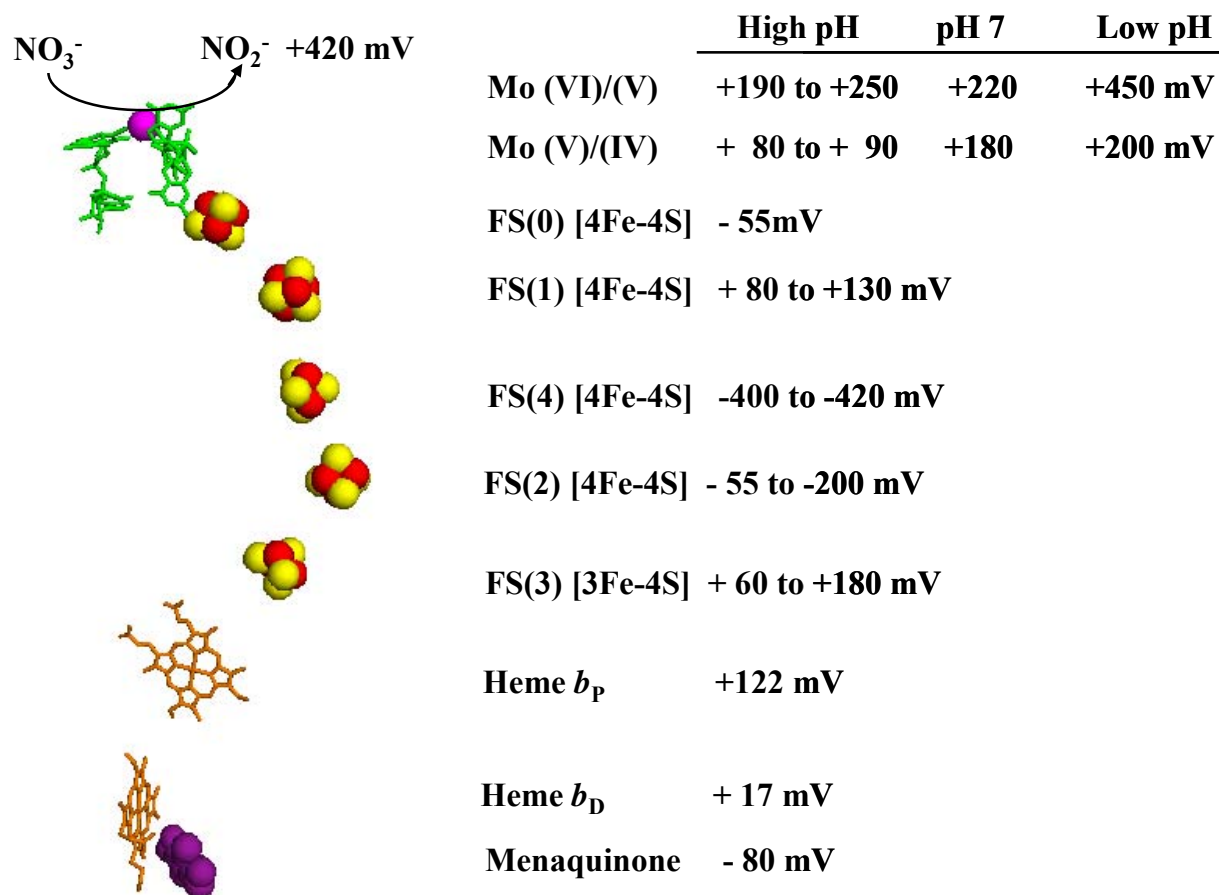


Fig. 3.15. Redox potentials of the cofactors in NRA from *E. coli*. Mo is shown in magenta and MGD cofactors in green. Heme groups and Menaquinone are shown in orange and in purple, respectively. The four [4Fe-4S] and the [3Fe-4S] clusters show Fe atoms in red and S atoms in yellow. The figure was generated using PyMol from coordinates deposited in the Protein Data Bank (accession code 1Q16). Midpoint redox potentials of the cofactors were taken from (32, 47, 48, 68, 70).

changes that occur when W is substituted for Mo in the active site (described below), it is possible that the W-NR in *P. aerophilum* catalyzes the high potential redox reaction of NO_3^- to NO_2 ($E_0' = +420$ mV).

One of the structural changes in the TMAOR from *E. coli* that occurred upon substitution of W for Mo in its active site was in substrate specificity of the enzyme. The Mo-TMAOR can only utilize TMAO as a substrate, but the W-TMAOR can also utilize DMSO, which is reduced to DMS with a redox potential of +160 mV (Mo-DMSOR, a homologous enzyme, can utilize both substrates) (20). The changes in substrate specificity of the W-TMAOR is most likely based on small structural changes in the active metal center, and thus in the substrate binding site and nature of the metal center, and secondly, on changes in the coordination of the Mo and W by pterins (20). The metal center of the Mo-DMSOR (Fig. 3.14) shows that the conserved residue Tyr¹¹⁴ is hydrogen bonded to one of the oxo-groups that serves as a ligand to the Mo ion, and may play a role in the oxygen atom transfer from DMSO to water (72). This Tyr residue or an equivalent residue is not present in the active site of TMAOR ((20) and references therein). Furthermore, there are differences in the charges in the tunnel leading to the active site of the two enzymes, with TMAOR containing substantially less charged residues. The Ser¹⁴⁷ and the Q pterin of Mo-DMSOR (Fig. 3.14) are also thought to participate interactions with the Mo ion influencing the electronic properties of Mo (or W) (72). Thus, there seems to be a different coordination sphere in the W-TMAOR, and a change in the substrate binding site (20). Accordingly, by analogy, changes in the active site of the NR in *P. aerophilum* could occur allowing for small structural changes and a chemically different composition of the metal center, which would allow for coordination of a W ion in an active enzyme. Specifically, in the NR from *E. coli* the molybdenum is coordinated by six ligands: four *cis*-dithiolene sulfur atoms of

the Mo-*bis*MGD and, depending on the two structures reported, either by a bidentate ligand of both side chain oxygen atoms in the carboxylate group of Asp²²² (13) or with one carboxylate oxygen from Asp²²² and a Mo=O group (40). This Asp residue is conserved in *P. aerophilum* (Fig. 3.13). The molybdenum ion is presumed to be in the oxidized Mo(VI) state in both crystal structures, and therefore the contrasting findings between the two crystal structures are proposed to be due to a transition of Mo(V) between low-pH and high-pH states (13, 40). Specifically, in the low-pH Mo(V) state, Asp²²² is hydrogen bonded to His⁵⁴⁶, and this His residue becomes deprotonated during the transition to the high-pH Mo(V) state (no strongly coupled proton) causing a rotation of the carboxylate group of Asp²²² resulting in a bidentate ligand. It is also possible that the different crystal structures represent structural flexibility of the active site (40). It is important to point out that the observation of an Asp-Mo coordination is unique in the family of molybdoenzymes (13, 35, 40) (see Table 1.3, Chapter 1), and that so far, that W is not coordinated by an amino acid in the protein in the tungstoenzymes like AOR and FOR (21).

Additionally, in the *E. coli* NR structure, a bicyclic dihydropterin structure was indicated for one of the coordinating MGD cofactors, and the other MGD cofactor, as well as other MGD cofactors in crystal structures solved of Mo-*bis*MGD enzymes, shows a typical tricyclic pyranopterins form (13) (See Fig. 1.4, Chapter 1). While the tricyclic pyranopterins are completely bound by the enzyme, via extensive hydrogen bonding, this bicyclic form suggests that NarGHI not only is able to bind both forms, but also that the cofactor may be directly involved in the enzymatic reaction (13). The tricyclic pyranopterins is also more common in other W-molybdopterins and Mo-*bis*MGD structures that have been solved (21, 35). Furthermore, in the W-containing FDH of *D. gigas*, which also contains a *bis*MGD cofactor (66), one of the pterins (MGD) is involved in the electron transfer. This has also been seen with the

xanthine oxidase from *D. gigas* (67). Moreover, the pterin cofactors that have been associated with hyperthermophilic W-containing enzymes do not contain a dinucleotide attached to the molybdopterin (21), thus distinguishing the W-NR, NR2 from *P. aerophilum* from a typical W-containing hyperthermophilic enzyme. Consequently, the potential participation of pterin in catalysis by *P. aerophilum* NR may facilitate the use of W and its efficient replacement of Mo.

Taking into account the extensive homology of the Mo-NR in *P. aerophilum* to that of the NR from *E. coli*, which includes amino acid sequence and conserved residues, metal content and subunit structure, it seems likely that the findings in the crystal structures of *E. coli* NR, such as the structural flexibility of the active site, and the participation of the MGD cofactors in catalysis, also apply to the NR from *P. aerophilum*. The likelihood of this relationship, combined with the similarities to the model of an active W-substituted molybdoenzyme that can catalyze a reaction with a redox potential of +160 mV, provided by W-TMAOR, lends itself to a possible explanation of how the reduction of nitrate to nitrite ($E_o' = +420$ mV) is aided by the catalysis of a W-NR (NR2) in *P. aerophilum*. Thus, there is the possibility that W functions the same as Mo, yet with less efficient catalytic properties and lower enzyme turnover.

With regard to the first possible explanation of how W functions in the *P. aerophilum* NR, it is possible that the W site has a more positive potential than would be expected, closer to the potential of the $\text{NO}_3^-/\text{NO}_2$ couple. This could be determined by EPR spectroscopy if the signal from the W(V) site can be observed, which was not possible with the experiments reported here due to the low quantity of NR2 available. The second possibility is that it is the redox potentials of the other redox components in *P. aerophilum* NR that allows the W site to function at the expected negative potentials. For example, contrary to the W-TMAOR in *E. coli*, the homologous W-substituted DMSOR in *Rhodobacter capsulatus* contains redox potentials for

W^{VI}/W^V and W^V/W^{IV} couples of -194 mV and -134 mV, respectively. Moreover, this W-DMSOR catalyzes reduction of DMSO to DMS, but cannot catalyze the oxidation of DMS to DMSO (34). No possible explanation was proposed of how this W-DMSOR reduces DMSO to DMS ($E_o' = +160$ mV). An explanation of this reaction may be similar to a second possibility of the catalysis of W-NR in *P. aerophilum*. This second possibility involves the variation in the potentials of the redox carriers in the electron transport chain, which has been established in the Ni-Fe hydrogenase from *D. gigas* (85).

Specifically for the W-NR in *P. aerophilum*, this possible explanation is that the [Fe-S] clusters function at different potentials in the W- and Mo-containing sites of the homologous enzymes, or that different clusters have different roles depending on the metal bound in the active site. The redox potentials of the Mo site and the [4Fe-4S] in NarG, FS(0), and the Fe-S clusters in *E. coli* NarH, identified as FS(1) to FS(4), have been determined from redox titrations monitored by EPR (Fig. 3.15). The midpoint potential for the Mo (VI)/(V) couple at high pH ranges from +190 to +250 mV and the Mo (V)/(IV) couple from +80 to +90 mV (32, 47, 70). At neutral pH, midpoint potentials for the Mo (VI)/(V) couple are +220 mV and +180 mV for the Mo (V)/(IV) couple (32, 47). The midpoint potential for the Mo (VI)/(V) couple at low pH is +450 mV and +200 mV for the Mo (V)/(IV) couple (30). The high spin [4Fe-4S] cluster in NarG, FS(0), has a redox potential of -55 mV at pH 8 (68). At pH 8.3, the midpoint potentials for the NarH clusters are +80, -200 and -400 mV for the [4Fe-4S] clusters and +60 mV for the [3Fe-4S] cluster (32). At pH 8.0, reported midpoint potentials are +180 mV for the [3Fe-4S] cluster and for the [4Fe-4S] centers FS1, 2 and 4, +130, -55 and -420 mV, respectively (Fig. 3.15) (48, 70). The Fe-S clusters are divided into two classes: a high-potential class with midpoint potentials of +130 and +180 mV ([3Fe-4S]), and a low-potential class with midpoint

potentials of -420 and -55 mV (47). Each domain contains one high- and one low-potential cluster (13, 40). The midpoint potentials are regulated by hydrophobic residues, accessibility to solvent and electrostatic interactions. In particular, the low-potential clusters are located in a hydrophobic environment shielding the cluster from the solvent and only two (FS2) or three (FS3) sulfur atoms are hydrogen bonded to main chain nitrogen atoms. In contrast, the high-potential clusters are in a polar environment with all of the sulfur atoms forming hydrogen bonds with nitrogen atoms from main chain nitrogen atoms and Arg residues (13). Because the redox centers form a line from the quinone binding site to the Mo active site, all of them are thought to have a direct role in electron transfer (13, 40). In spite of this, it has also been strongly suggested that in order to achieve efficient electron transfer, the redox potentials of the clusters must vary during the transfer of electrons (40), which is due to the increased distance and thus unfavorable electron transfer, if FeS(4) with a redox potential of -400 mV was skipped. Other studies have also suggested that there could be multiple pathways for electron flow through the clusters in the NarH subunit (33). Interestingly, observations in EPR studies on the NarGHI holoenzyme and the NarGH dimer led to the suggestion that the FeS(4) cluster, which remains oxidized in membranes reduced with dithionite, has a redox potential of approximately -500 mV at pH 7, or that in the NR holoenzyme this cluster is redox isolated from the other Fe-S clusters, hemes and MGDs (48). This redox isolated Fe-S cluster was therefore proposed to have a structural role (48). The role of FeS(4), is extremely pertinent to electron transfer of NR in *P. aerophilum*. The possibility of redox isolation in NR1, a Mo-containing enzyme consisting of NarGHI, and the participation of FeS(4) in the electron flow of NR2, a W-containing enzyme which appears to be NarGH dimer, would provide efficient electron transfer to the W active site. Moreover, the crystal structure of NR from *E. coli* revealed that NR forms a dimer, yet the distances between

the redox centers of the electron transport chain of the monomers precludes any mechanistic role of monomer-monomer interactions within the dimer (13). It is possible that in *P. aerophilum* the formation of the dimer is more closely packed allowing for interactions between multiple β subunits, and therefore multiple Fe-S clusters, thus playing a role in NR2 activity. Therefore, while the NRs of *P. aerophilum* and *E. coli* share high sequence identity in their respective NarG and NarH subunits, the environments of their Fe-S clusters may be very different, thus allowing a wide range of different redox potentials.

P. aerophilum contains two forms of purified NR. The majority of the purified enzyme contains Mo (534 U/mg), yet there is a significant portion of active NR that contains tungsten (223 U/mg). On the one hand, it is very interesting that a hyperthermophilic organism contains a highly active Mo-containing enzyme, instead of a W-containing one that is most often found. However, an active W-containing NR is unprecedented, as this enzyme usually contains Mo. The possibility that the Mo-NR (NR1) functions in promoting catalysis in the same manner as the NR from *E. coli* is highly likely. The W-NR (NR2), however, could possibly function in this manner as well, which would mean that the redox potential of the W couples would be more positive as seen in the W-TMAOR from *E. coli*, but is not typical of tungstoenzymes. Another possibility is that there is a wide range in the different redox potentials of the electron carriers in the transport chain, as seen in the hydrogenase from *D. gigas*. In order to establish these mechanisms, however, future experiments focusing on the redox potentials of the Mo and W active sites, as well as the Fe-S clusters and hemes would need to be determined, and structural analysis would of course help in resolving the speculation of the mechanism of the NRs in *P. aerophilum*.

REFERENCES

1. **Adams, M. W. W., and L. E. Mortenson.** 1982. The Effect of Cyanide and Ferricyanide On the Activity of the Dissimilatory Nitrate Reductase of *Escherichia coli*. Journal of Biological Chemistry **257**:1791-1799.
2. **Afshar, S., E. Johnson, S. de Vries, and I. Schroder.** 2001. Properties of a thermostable nitrate reductase from the hyperthermophilic archaeon *Pyrobaculum aerophilum*. J. Bacteriol. **183**:5491-5.
3. **Afshar, S., C. Kim, H. G. Monbouquette, and I. Schroder.** 1998. Effect of tungstate on nitrate reduction by the hyperthermophilic archaeon *Pyrobaculum aerophilum*. Appl. Environ. Microb. **64**:3004-3008.
4. **Almendra MJ, B. C., Gavel O, Pereira AS, Tavares P, Bursakov S, Duarte R, Caldeira J, Moura JJ, Moura I.** 1999. Purification and characterization of a tungsten-containing formate dehydrogenase from *Desulfovibrio gigas*. Biochemistry **38**:16366-72.
5. **Alvarez-Ossorio, M. C., F. J. G. Muriana, F. F. de la Rosa, and A. M. Relimpio.** 1992. Purification and Characterization of Nitrate Reductase from the Halophile Archaeobacterium *Haloferax mediterranei*. Z Naturforsch [C] **47**:670-676.
6. **Amo, T., M. L. Paje, A. Inagaki, S. Ezaki, H. Atomi, and T. Imanaka.** 2002. *Pyrobaculum calidifontis* sp. nov., a novel hyperthermophilic archaeon that grows in atmospheric air. Archaea **1**:113-21.
7. **Antipov, A. N., N. N. Lyalikova, T. V. Khijniak, and P. L'Vov N.** 1998. Molybdenum-free nitrate reductases from vanadate-reducing bacteria. FEBS Lett **441**:257-60.
8. **Antipov AN, S. D., L'Vov NP, Kuenen JG.** 2003. New enzyme belonging to the family of molybdenum-free nitrate reductases. Biochem J. **369**:185-9.

9. **Bell, L. C., D. J. Richardson, and S. J. Ferguson.** 1990. Periplasmic and membrane-bound respiratory nitrate reductases in *Thiosphaera pantotropha*. The periplasmic enzyme catalyzes the first step in aerobic denitrification. FEBS Lett **265**:85-7.
10. **Berg, B. L., J. Li, J. Heider, and V. Stewart.** 1991. Nitrate-inducible formate dehydrogenase in *Escherichia coli* K-12. I. Nucleotide sequence of the *fdnGHI* operon and evidence that opal (UGA) encodes selenocysteine. J Biol Chem. **266**:22380-5.
11. **Berks, B. C., D. J. Richardson, A. Reilly, A. C. Willis, and S. J. Ferguson.** 1995. The napEDABC gene cluster encoding the periplasmic nitrate reductase system of *Thiosphaera pantotropha*. Biochem J **309**:983-92.
12. **Bertero, M. G., R. A. Rothery, N. Boroumand, M. Palak, F. Blasco, N. Ginet, J. H. Weiner, and N. C. Strynadka.** 2005. Structural and biochemical characterization of a quinol binding site of *Escherichia coli* nitrate reductase A. J Biol Chem **280**:14836-43.
13. **Bertero, M. G., R. A. Rothery, M. Palak, C. Hou, D. Lim, F. Blasco, J. H. Weiner, and N. C. Strynadka.** 2003. Insights into the respiratory electron transfer pathway from the structure of nitrate reductase A. Nat Struct Biol **10**:681-7.
14. **Bilous, P. T., S. T. Cole, W. F. Anderson, and J. H. Weiner.** 1988. Nucleotide sequence of the dmsABC operon encoding the anaerobic dimethylsulphoxide reductase of *Escherichia coli*. Mol Microbiol. **2**:785-95.
15. **Blasco, F., C. Iobbi, G. Giordano, M. Chippaux, and V. Bonnefoy.** 1989. Nitrate reductase of *Escherichia coli*: completion of the nucleotide sequence of the nar operon and reassessment of the role of the alpha and beta subunits in iron binding and electron transfer. Mol Gen Genet **218**:249-56.

16. **Blasco, F., C. Iobbi, J. Ratouchniak, V. Bonnefoy, and M. Chippaux.** 1990. Nitrate reductases of *Escherichia coli*: sequence of the second nitrate reductase and comparison with that encoded by the narGHJI operon. *Mol Gen Genet* **222**:104-11.
17. **Bloch, E., R. Rachel, S. Burggraf, D. Hafenbradl, H. W. Jannasch, and K. O. Stetter.** 1997. *Pyrolobus fumarii*, gen. and sp. nov., represents a novel group of archaea, extending the upper temperature limit for life to 113 degrees C. *Extremophiles* **1**:14-21.
18. **Bokranz, M., M. Gutmann, C. Kortner, E. Kojro, F. Fahrenholz, F. Lauterbach, and A. Kroger.** 1991. Cloning and nucleotide sequence of the structural genes encoding the formate dehydrogenase of *Wolinella succinogenes*. *Arch Microbiol.* **156**:119-28.
19. **Bonnefoy, V., and J. A. Demoss.** 1994. Nitrate reductases in *Escherichia coli*. *Antonie Van Leeuwenhoek* **66**:47-56.
20. **Buc, J., C. L. Santini, R. Giordani, M. Czjzek, L. F. Wu, and G. Giordano.** 1999. Enzymatic and physiological properties of the tungsten-substituted molybdenum TMAO reductase from *Escherichia coli*. *Mol Microbiol* **32**:159-68.
21. **Chan, M. K., S. Mukund, A. Kletzin, M. W. Adams, and D. C. Rees.** 1995. Structure of a hyperthermophilic tungstopterin enzyme, aldehyde ferredoxin oxidoreductase. *Science* **267**:1463-9.
22. **Chang, L., L. I. Wei, J. P. Audia, R. A. Morton, and H. E. Schellhorn.** 1999. Expression of the *Escherichia coli* NRZ nitrate reductase is highly growth phase dependent and is controlled by RpoS, the alternative vegetative sigma factor. *Mol Microbiol* **34**:756-66.

23. **Chaudhry, G. R., and C. H. MacGregor.** 1983. Cytochrome b from *Escherichia coli* nitrate reductase. Its properties and association with the enzyme complex. *J Biol Chem* **258**:5819-27.
24. **Chikwem, J. O., and R. J. Downey.** 1982. Purification and characterization of the respiratory nitrate reductase of *Bacillus stearothermophilus*. *Anal Biochem.* **126**:74-80.
25. **Clegg, R. A.** 1976. Purification and some properties of nitrate reductase (EC 1.7.99.4) from *Escherichia coli* K12. *Biochem J* **153**:533-41.
26. **Demoss, J. A., T. Y. Fan, and R. H. Scott.** 1981. Characterization of subunit structural alterations which occur during purification of nitrate reductase from *Escherichia coli*. *Arch Biochem Biophys.* **206**:54-64.
27. **Enoch, H. G., and R. L. Lester.** 1975. The purification and properties of formate dehydrogenase and nitrate reductase from *Escherichia coli*. *J Biol Chem* **250**:6693-705.
28. **Fitz-Gibbon, S. T., H. Ladner, U. J. Kim, K. O. Stetter, M. I. Simon, and J. H. Miller.** 2002. Genome sequence of the hyperthermophilic crenarchaeon *Pyrobaculum aerophilum*. *Proc. Natl. Acad. Sci. U S A* **99**:984-9.
29. **Frunzke, K., B. Heiss, O. Meyer, and W. G. Zumft.** 1993. Molybdopterin guanine dinucleotide is the organic moiety of the molybdenum cofactor in respiratory nitrate reductase from *Pseudomonas stutzeri*. *FEMS Microbiol Lett* **113**:241-245.
30. **George, G. N., N. A. Turner, R. C. Bray, F. F. Morpeth, D. H. Boxer, and S. P. Cramer.** 1989. X-ray-absorption and electron-paramagnetic-resonance spectroscopic studies of the environment of molybdenum in high-pH and low-pH forms of *Escherichia coli* nitrate reductase. *Biochem J.* **259**:693-700.

31. **Giordano, G., B. A. Haddock, and D. H. Boxer.** 1980. Molybdenum-limited growth achieved either phenotypically or genotypically and its effect on the synthesis of formate dehydrogenase and nitrate reductase by *Escherichia coli* K12. *FEMS Microbiol Lett* **8**:229-235.
32. **Guigliarelli, B., M. Asso, C. More, V. Augier, F. Blasco, J. Pommier, G. Giordano, and P. Bertrand.** 1992. EPR and redox characterization of iron-sulfur centers in nitrate reductases A and Z from *Escherichia coli*. Evidence for a high-potential and a low-potential class and their relevance in the electron-transfer mechanism. *Eur J Biochem* **207**:61-8.
33. **Guigliarelli, B., A. Magalon, M. Asso, P. Bertrand, C. Frixon, G. Giordano, and F. Blasco.** 1996. Complete coordination of the four Fe-S centers of the beta subunit from *Escherichia coli* nitrate reductase. Physiological, biochemical, and EPR characterization of site-directed mutants lacking the highest or lowest potential [4Fe-4S] clusters. *Biochemistry* **35**:4828-36.
34. **Hagedoorn, P. L., W. R. Hagen, L. J. Stewart, A. Docrat, S. Bailey, and C. D. Garner.** 2003. Redox characteristics of the tungsten DMSO reductase of *Rhodobacter capsulatus*. *FEBS Lett* **555**:606-10.
35. **Hille, R.** 2002. Molybdenum enzymes containing the pyranopterin cofactor: an overview. *Met Ions Biol Syst* **39**:187-226.
36. **Hochstein, L. I., and F. Lang.** 1991. Purification and properties of a dissimilatory nitrate reductase from *Haloferax denitrificans*. *Arch Biochem Biophys* **288**:380-5.
37. **Huber, R., M. Sacher, A. Vollmann, H. Huber, and D. Rose.** 2000. Respiration of arsenate and selenate by hyperthermophilic archaea. *Syst. Appl. Microbiol.* **23**:305-14.

38. **Iobbi-Nivol, C., C. L. Santini, F. Blasco, and G. Giordano.** 1990. Purification and further characterization of the second nitrate reductase of *Escherichia coli* K12. *Eur J Biochem* **188**:679-87.
39. **Jiang, J., and R. H. Holm.** 2005. Reaction systems related to dissimilatory nitrate reductase: nitrate reduction mediated by bis(dithiolene)tungsten complexes. *Inorg Chem* **44**:1068-72.
40. **Jormakka, M., D. Richardson, B. Byrne, and S. Iwata.** 2004. Architecture of NarGH reveals a structural classification of Mo-*bis*MGD enzymes. *Structure (Camb)* **12**:95-104.
41. **Ketchum, P. A., G. Denariáz, J. LeGall, and W. J. Payne.** 1991. Menaquinol-nitrate oxidoreductase of *Bacillus halodenitrificans*. *J Bacteriol* **173**:2498-505.
42. **Krafft, T., M. Bokranz, O. Klimmek, I. Schroder, F. Fahrenholz, E. Kojro, and A. Kroger.** 1992. Cloning and nucleotide sequence of the *psrA* gene of *Wolinella succinogenes* polysulphide reductase. *Eur J Biochem.* **206**:503-10.
43. **Lin, J. T., B. S. Goldman, and V. Stewart.** 1993. Structures of genes *nasA* and *nasB*, encoding assimilatory nitrate and nitrite reductases in *Klebsiella pneumoniae* M5a1. *J Bacteriol.* **175**:2370-8.
44. **Lovenberg, W., B. B. Buchanan, and J. C. Rabinowitz.** 1963. Studies on the chemical nature of Clostridial ferredoxin,. *J. Biol. Chem.* **238**:3899-3913.
45. **Lund, K., and J. A. DeMoss.** 1976. Association-dissociation behavior and subunit structure of heat-released nitrate reductase from *Escherichia coli*. *J Biol Chem* **251**:2207-16.
46. **MacGregor, C. H., C. A. Schnaitman, and D. E. Normansell.** 1974. Purification and properties of nitrate reductase from *Escherichia coli* K12. *J Biol Chem* **249**:5321-7.

47. **Magalon, A., M. Asso, B. Guigliarelli, R. A. Rothery, P. Bertrand, G. Giordano, and F. Blasco.** 1998. Molybdenum cofactor properties and [Fe-S] cluster coordination in *Escherichia coli* nitrate reductase A: investigation by site-directed mutagenesis of the conserved his-50 residue in the NarG subunit. *Biochemistry* **37**:7363-70.
48. **Magalon, A., R. A. Rothery, G. Giordano, F. Blasco, and J. H. Weiner.** 1997. Characterization by electron paramagnetic resonance of the role of the *Escherichia coli* nitrate reductase (NarGHI) iron-sulfur clusters in electron transfer to nitrate and identification of a semiquinone radical intermediate. *J Bacteriol.* **179**:5037-5045.
49. **Magalon, A., R. A. Rothery, D. Lemesle-Meunier, C. Frixon, J. H. Weiner, and F. Blasco.** 1998. Inhibitor binding within the NarI subunit (cytochrome bnr) of *Escherichia coli* nitrate reductase A. *J Biol Chem.* **273**:10851-6.
50. **Mahne, I., and J. M. Tiedje.** 1995. Criteria and methodology for identifying respiratory denitrifiers. *Applied and Environmental Microbiology* **61**:1110-1115.
51. **Martinez Murillo, F., T. Gugliuzza, J. Senko, P. Basu, and J. F. Stolz.** 1999. A heme-C-containing enzyme complex that exhibits nitrate and nitrite reductase activity from the dissimilatory iron-reducing bacterium *Geobacter metallireducens*. *Arch Microbiol* **172**:313-20.
52. **Mejean, V., C. Iobbi-Nivol, M. Lepelletier, G. Giordano, M. Chippaux, and M. C. Pascal.** 1994. TMAO anaerobic respiration in *Escherichia coli*: involvement of the tor operon. *Mol Microbiol.* **11**:1169-79.
53. **Moreno-Vivian, C., P. Cabello, M. Martinez-Luque, R. Blasco, and F. Castillo.** 1999. Prokaryotic nitrate reduction: molecular properties and functional distinction among bacterial nitrate reductases. *J Bacteriol* **181**:6573-84.

54. **Morpeth, F. F., and D. H. Boxer.** 1985. Kinetic analysis of respiratory nitrate reductase from *Escherichia coli* K12. *Biochemistry* **24**:40-6.
55. **Mukund, S., and M. W. W. Adams.** 1993. Characterization of a novel tungsten-containing formaldehyde ferredoxin oxidoreductase from the hyperthermophilic archaeon, *Thermococcus litoralis*. A role for tungsten in peptide catabolism. *J. Biol. Chem.* **268**:13592-600.
56. **Mukund, S., and M. W. W. Adams.** 1990. Characterization of a tungsten-iron-sulfur protein exhibiting novel spectroscopic and redox properties from the hyperthermophilic archaeobacterium *Pyrococcus furiosus*. *J. Biol. Chem.* **265**:11508-16.
57. **Mukund, S., and M. W. W. Adams.** 1995. Glyceraldehyde-3-phosphate ferredoxin oxidoreductase, a novel tungsten-containing enzyme with a potential glycolytic role in the hyperthermophilic archaeon *Pyrococcus furiosus*. *J. Biol. Chem.* **270**:8389-92.
58. **Mukund, S., and M. W. W. Adams.** 1996. Molybdenum and vanadium do not replace tungsten in the catalytically active forms of the three tungstoenzymes in the hyperthermophilic archaeon *Pyrococcus furiosus*. *J. Bacteriol.* **178**:163-7.
59. **Mukund, S., and M. W. W. Adams.** 1991. The novel tungsten-iron-sulfur protein of the hyperthermophilic archaeobacterium, *Pyrococcus furiosus*, is an aldehyde ferredoxin oxidoreductase. Evidence for its participation in a unique glycolytic pathway. *J. Biol. Chem.* **266**:14208-16.
60. **Peters, J. W., W. N. Lanzilotta, B. J. Lemon, and L. C. Seefeldt.** 1998. X-ray crystal structure of the Fe-only hydrogenase (CpI) from *Clostridium pasteurianum* to 1.8 angstrom resolution. *Science* **282**:1853-8.

61. **Philippot, L., and O. Hojberg.** 1999. Dissimilatory nitrate reductases in bacteria. *Biochim Biophys Acta* **1446**:1-23.
62. **Pierson, D. E., and A. Campbell.** 1990. Cloning and nucleotide sequence of bisC, the structural gene for biotin sulfoxide reductase in *Escherichia coli*. *J Bacteriol.* **172**:2194-8.
63. **Plunkett, G. I., V. Burland, D. L. Daniels, and F. R. Blattner.** 1993. Analysis of the *Escherichia coli* genome. III. DNA sequence of the region from 87.2 to 89.2 minutes. *Nucleic Acids Res.* **21**:3391-3398.
64. **Polcyn, W., and R. Lucinski.** 2003. Aerobic and anaerobic nitrate and nitrite reduction in free-living cells of *Bradyrhizobium* sp. (Lupinus). *FEMS Microbiol Lett* **226**:331-7.
65. **Pollock, V. V., and M. J. Barber.** 1995. Molecular cloning and expression of biotin sulfoxide reductase from *Rhodobacter sphaeroides* forma sp. *denitrificans*. *Arch Biochem Biophys.* **318**:322-332.
66. **Raaijmakers, H., S. Teixeira, J. M. Dias, M. J. Almendra, C. D. Brondino, I. Moura, J. J. Moura, and M. J. Romao.** 2001. Tungsten-containing formate dehydrogenase from *Desulfovibrio gigas*: metal identification and preliminary structural data by multi-wavelength crystallography. *J Biol Inorg Chem.* **6**:398-404.
67. **Romao, M. J., M. Archer, I. Moura, J. J. Moura, J. LeGall, R. Engh, M. Schneider, P. Hof, and R. Huber.** 1995. Crystal structure of the xanthine oxidase-related aldehyde oxido-reductase from *D. gigas*. *Science* **270**:1170-6.
68. **Rothery, R. A., M. G. Bertero, R. Cammack, M. Palak, F. Blasco, N. C. Strynadka, and J. H. Weiner.** 2004. The catalytic subunit of *Escherichia coli* nitrate reductase A contains a novel [4Fe-4S] cluster with a high-spin ground state. *Biochemistry* **43**:5324-33.

69. **Rothery, R. A., F. Blasco, A. Magalon, M. Asso, and J. H. Weiner.** 1999. The hemes of *Escherichia coli* nitrate reductase A (NarGHI): potentiometric effects of inhibitor binding to narI. *Biochemistry* **38**:12747-57.
70. **Rothery, R. A., A. Magalon, G. Giordano, B. Guigliarelli, F. Blasco, and J. H. Weiner.** 1998. The molybdenum cofactor of *Escherichia coli* nitrate reductase A (NarGHI). Effect of a mobAB mutation and interactions with [Fe-S] clusters. *J Biol Chem* **273**:7462-9.
71. **Sako, Y., T. Nunoura, and A. Uchida.** 2001. *Pyrobaculum oguniense* sp. nov., a novel facultatively aerobic and hyperthermophilic archaeon growing at up to 97 degrees C. *Int. J. Syst. Evol. Microbiol.* **51**:303-9.
72. **Schindelin, H., C. Kisker, J. Hilton, K. V. Rajagopalan, and D. C. Rees.** 1996. Crystal structure of DMSO reductase: redox-linked changes in molybdopterin coordination. *Science* **272**:1615-21.
73. **Scott RH, S. G., DeMoss JA.** 1979. In vitro incorporation of molybdate into demolybdoproteins in *Escherichia coli*. *J Bacteriol.* **137**:719-26.
74. **Shevchenko, A., M. Wilm, O. Vorm, and M. Mann.** 1996. Mass spectrometric sequencing of proteins silver-stained polyacrylamide gels. *Anal Chem.* **68**:850-858.
75. **Shuber, A. P., E. C. Orr, M. A. Recny, P. F. Schendel, H. D. May, N. L. Schauer, and J. G. Ferry.** 1986. Cloning, expression, and nucleotide sequence of the formate dehydrogenase genes from *Methanobacterium formicicum*. *J Biol Chem* **261**:12942-7.
76. **Siddiqui, R. A., U. Warnecke-Eberz, A. Hengsberger, B. Schneider, S. Kostka, and B. Friedrich.** 1993. Structure and function of a periplasmic nitrate reductase in *Alcaligenes eutrophus* H16. *J Bacteriol.* **175**:5867-76.

77. **Silva, J. R. R. F. d., and R. J. P. Williams.** 1991. The biological chemistry of the elements : the inorganic chemistry of life, vol. xxi. Oxford University Press Clarendon Press, Oxford [England] New York.
78. **Spector MP, G. d. P. F., Bearson SM, Mahmud A, Magut M, Finlay BB, Dougan G, Foster JW, Pallen MJ.** 1999. The rpoS-dependent starvation-stress response locus stiA encodes a nitrate reductase (narZYWV) required for carbon-starvation-inducible thermotolerance and acid tolerance in *Salmonella typhimurium*. *Microbiology* **145**:3035-45.
79. **Stetter, K. O., A. Segerer, W. Zillig, G. Huber, G. Fiala, R. Huber, and H. Konig.** 1986. Extremely thermophilic sulfur-metabolizing archaeobacteria. *Syst. Appl. Microbiol.* **7**:393-397.
80. **Stewart, V.** 1988. Nitrate respiration in relation to facultative metabolism in enterobacteria. *Microbiol Rev* **52**:190-232.
81. **Uchimura, H., H. Enjoji, T. Seki, A. Taguchi, N. Takaya, and H. Shoun.** 2002. Nitrate reductase-formate dehydrogenase couple involved in the fungal denitrification by *Fusarium oxysporum*. *J Biochem (Tokyo)* **131**:579-86.
82. **van Riet, J., J. H. van Ed, R. Wever, B. F. van Gelder, and R. J. Planta.** 1975. Characterization of the respiratory nitrate reductase of *Klebsiella aerogenes* as a molybdenum-containing iron-sulfur enzyme. *Biochim Biophys Acta.* **405**:306-17.
83. **Van Riet, J., F. B. Wientjes, J. Van Doorn, and R. J. Planta.** 1979. Purification and Characterization of the Respiratory Nitrate Reductase of *Bacillus licheniformis*. *Biochim Biophys Acta* **572**:347-360.

84. **Vargas, M., K. Kashefi, E. L. Blunt-Harris, and D. R. Lovley.** 1998. Microbiological evidence for Fe(III) reduction on early Earth. *Nature* **395**:65-7.
85. **Volbeda, A., M. H. Charon, C. Piras, E. C. Hatchikian, M. Frey, and J. C. Fontecilla-Camps.** 1995. Crystal structure of the nickel-iron hydrogenase from *Desulfovibrio gigas*. *Nature* **373**:580-7.
86. **Völkl, P., R. Huber, E. Drobner, R. Rachel, S. Burggraf, A. Trincone, and K. O. Stetter.** 1993. *Pyrobaculum aerophilum* sp. nov., a novel nitrate-reducing hyperthermophilic archaeum. *Appl. Environ. Microbiol.* **59**:2918-26.
87. **Voorhorst, W. G., Y. Gueguen, A. C. Geerling, G. Schut, I. Dahlke, M. Thomm, J. van der Oost, and W. M. de Vos.** 1999. Transcriptional regulation in the hyperthermophilic archaeon *Pyrococcus furiosus*: coordinated expression of divergently oriented genes in response to beta-linked glucose polymers. *J. Bacteriol.* **181**:3777-83.
88. **Yoshimatsu, K., T. Sakurai, and T. Fujiwara.** 2000. Purification and characterization of dissimilatory nitrate reductase from a denitrifying halophilic archaeon, *Haloarcula marismortui*. *FEBS Lett* **470**:216-20.
89. **Zinoni, F., A. Birkmann, T. C. Stadtman, and A. Bock.** 1986. Nucleotide sequence and expression of the selenocysteine-containing polypeptide of formate dehydrogenase (formate-hydrogen-lyase-linked) from *Escherichia coli*. *Proc Natl Acad Sci U S A* **83**:4650-4.

CHAPTER 4

PURIFICATION AND CHARACTERIZATION OF THE NITRATE-INDUCIBLE FORMATE DEHYDROGENASE COMPLEX FROM THE HYPERTHERMOPHILIC ARCHAEON *PYROBACULUM AEROPHILUM*¹

¹ Feingold, L.E. and M.W.W. Adams. 2006. To be submitted to the *Journal of Bacteriology*.

ABSTRACT

Pyrobaculum aerophilum is a facultative anaerobic hyperthermophile and obtains energy by nitrate reduction. Formate dehydrogenase is an enzyme closely associated with nitrate reductase in the denitrification respiratory chain, and is a molybdoenzyme in mesophilic nitrate reducing organisms. Molybdoenzymes, however, are not ordinarily found among the hyperthermophiles. These enzymes usually contain the analogous metal, tungsten (W) in their active sites, rather than molybdenum (Mo). Tungstoenzymes typically catalyze low potential redox reactions, such as formate oxidation. Naturally-occurring tungsten-containing formate dehydrogenases have been isolated and purified among thermophilic bacteria. Herein we show that the formate dehydrogenase of *P. aerophilum* occurs in complex with nitrate reductase. Two forms of the complex were identified; one contained primarily Mo, and the other, primarily W.

INTRODUCTION

Anaerobic growth of the hyperthermophilic archaeon, *Pyrobaculum aerophilum*, can occur using nitrate as a terminal electron acceptor for respiration (32). During anaerobic growth of *Escherichia coli* cells in the presence of nitrate, a respiratory chain is synthesized in which nitrate reduction is coupled to the oxidation of formate (27). Formate is produced in *E. coli* from the acetyl-CoA-dependent cleavage of pyruvate (18), and serves as a primary electron donor for nitrate respiration. The coupling of formate oxidation to nitrate respiration in *E. coli* and other microorganisms is catalyzed by a major respiratory chain, the membrane-associated formate-nitrate reductase respiratory pathway. This energy-conserving system consists of formate dehydrogenase-N (FDH-N), quinone and nitrate reductase (NR) (16).

FDH-N is one of three genetically-distinct FDH isozymes that have been identified in *E. coli* (12, 28). These isozymes are named according to the growth condition that leads to their synthesis. Two are membrane associated and form part of the formate-nitrate respiratory chain, and are germane to this study. FDH-O is synthesized when cells are grown in the presence of oxygen or nitrate; and FDH-N is produced by nitrate and anaerobic conditions. The third, FDH-H, is produced during fermentation and is a soluble enzyme. All three enzymes contain Mo, Se, and Fe-S centers. *E. coli* FDH-N is encoded by *fdnGHI* and the purified enzyme consists of three subunits in the ratio of $\alpha_4\beta_4\gamma_2$. It has a total molecular weight of 608 kDa ($\alpha=112$ kDa, $\beta=32$ kDa and $\gamma=25$ kDa) (7). The crystal structure of *E. coli* FDH-N was recently solved (16). This shows that the α subunit, which is the site of formate oxidation, contains a molybdopterin cofactor, Se in the form of selenocysteine, and a [4Fe-4S] cluster. The β subunit functions in electron transfer and contains four [4Fe-4S] clusters, while γ subunit contains two heme *b* groups and is the site of menaquinone reduction.

Much less is known biochemically about the FDH-O isozyme, which is encoded by *fdoGHI*. It was reported to be structurally very similar to FDH-N (27). The molecular weights of its subunits ($\alpha=112$ kDa, $\beta=33$ kDa and $\gamma=24$ kDa) are also very similar to those of FDH-N (24). FDH-O is produced in aerobically-grown cells, and catalyzes the oxidation of formate where oxygen is the terminal electron acceptor of the respiratory chain. It is also synthesized during nitrate respiration by *E. coli* (28), and is thought to transfer electrons to the quinone pool (25, 28).

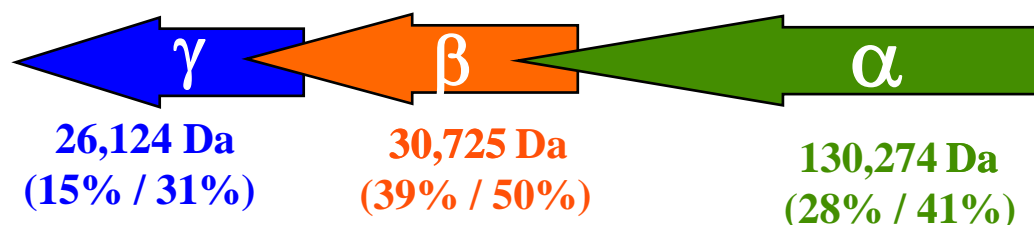
The two primary enzymes in the formate-nitrate respiratory chain of *E. coli*, FDH-N and NR, exhibit extensive similarity in charge, size and composition (7, 16). In fact, in this microorganism, these enzymes co-purify (7), and the enzyme preparation used to crystallize

FDH-N contained 50% NR (15). An essential difference between these two enzymes, however, is their ability to utilize Mo or W at their active sites. In mesophilic microbes, NR is always inactive when cells are grown in the presence of W (10, 29). Furthermore, until the present research (Chapter 3), which showed that NR of *P. aerophilum* is active with both W and Mo coordinated in the active site, the only NR characterized to date in a hyperthermophilic microbe had also been reported to solely coordinate Mo into its active site (1). FDH, on the other hand, has been found to be functional when W is incorporated into the active site in both mesophilic (26) and thermophilic microorganisms (3, 33).

Sequence comparisons between the NRs from *P. aerophilum* and *E. coli* exhibited a high identity and similarity (Chapter 3), which provided a basis for the initial investigation and characterization of the NRs from *P. aerophilum*. In order to further investigate nitrate respiration through a formate-nitrate respiratory pathway in *P. aerophilum*, the FDH sequence from *P. aerophilum* (8) was compared to the FDH-N (4) and FDH-O sequences (24) from *E. coli* (Fig. 4.1). As with NR, the genomic sequence of *P. aerophilum* contains only one operon encoding FDH, as opposed to the two respiratory, *fdnGHI* and *fdoGHI*, and the fermentative, *fdhF*, found in *E. coli*. Further, in the genomic sequence of *P. aerophilum* a gene corresponding to that which encodes the γ subunit of the *E. coli* enzymes has not been identified (8). There is however, a hypothetical protein which contains conserved residues that correspond to heme ligands in the γ subunits of both FDH-N and FDH-O, although the overall homology of the subunits is fairly low (Fig. 4.1). The α and β subunits from *P. aerophilum* FDH, however, exhibit a high similarity to the corresponding subunits of the *E. coli* FDHs, and are thought to contain the same metal cofactors. These comparisons raise the question of whether the enzyme

Formate Dehydrogenase Operon

Pyrobaculum aerophilum



Escherichia coli FDH-N and FDH-O

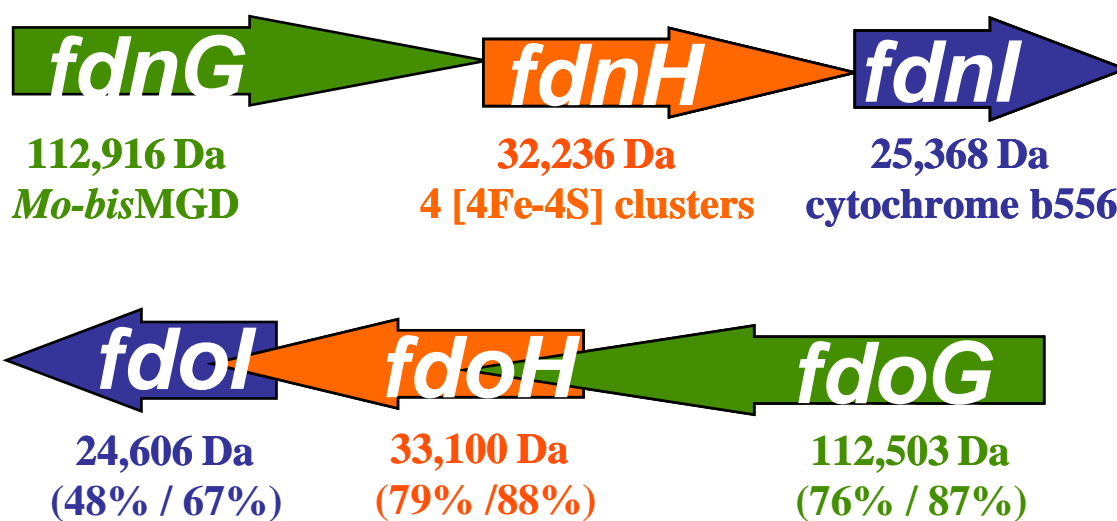


Fig. 4.1. Respiratory formate dehydrogenase operons from *P. aerophilum* and *E. coli*. The size of the gene products is shown for both organisms. Metal components shown for *E. coli* also represent the metal components expected in *P. aerophilum*. Percents represent percentage of sequence identity and percentage of sequence similarity respectively, from *P. aerophilum* and from *E. coli* FDH-O as compared to *E. coli* FDH-N. Sequences were retrieved from NCBI, (<http://www.ncbi.nlm.nih.gov/>) and identity and similarity alignments were performed using MacVector (Accelrys Software Inc.).

in *P. aerophilum* is a Mo-containing enzyme as in *E. coli*, or a W-containing enzyme, consistent with the hyperthermophilic nature of the organism. This study addresses this question by the purification and characterization of the respiratory formate dehydrogenase complexes from *P. aerophilum*.

MATERIALS AND METHODS

Growth conditions, preparation of the membrane fractions and purification of FDH from *P. aerophilum* (DSM 7523) are as reported in Chapter 3.

Enzyme assays. FDH activity was determined with benzyl viologen (BV) as an artificial electron acceptor at 90 °C. Two mL of anaerobic assay buffer (50 mM CHES pH 8.5), BV (0.5 mM), enough dithionite (100 mM stock) to ensure that the cuvette was anaerobic, and the fraction to be assayed were added to anaerobic serum-stoppered cuvettes. These cuvettes were heated for 3 minutes at 90 °C in a custom Spectronic 501 spectrophotometer. The reaction was initiated by the addition of sodium formate (10 mM). The reduction of BV was followed at 600 nm (molar absorbance $7,400 \text{ M}^{-1} \text{ cm}^{-1}$). The specific activity of FDH is expressed as one micromole of formate oxidized (U) per minute per milligram of protein.

Protein measurement. Protein concentrations were determined using the detergent compatible modified Lowry assay (*DC Protein Assay*, Bio-Rad). Bovine serum albumin was used as the protein standard.

Gel electrophoresis. Subunit molecular weights were estimated by SDS-PAGE using a 4 – 12% Bis-Tris acrylamide gel (NuPage, Invitrogen Corp.) with MOPS Running Buffer (NuPage, Invitrogen Corp.) under reducing conditions. Protein samples were diluted 4:1 with 30 mM Tris-HCl buffer (pH 6.8) containing 5% SDS, 5% β -mercaptoethanol, 10% glycerol and 0.025% bromphenol blue and heated for 15 min at 100 °C. The BenchMark Protein Ladder (Invitrogen Corp.) was used for the molecular weight standards. This ladder consists of 15 engineered proteins with the molecular weights ranging from 220 kD to 10 kD.

Electrophoresis under non-denaturing conditions and in-gel activity was carried out in 3 - 8% Tris-Acetate gels (NuPage, Invitrogen Corp.) with Tris – Glycine buffer (25 mM Tris Base and 192 mM Glycine, pH 8.3). Protein samples were diluted 4:1 with 30 mM Tris-HCl buffer (pH 6.8) containing 10% glycerol and 0.025% bromphenol blue. Triton X-100 (0.1%) was added to the cathode buffer and gels were run for 30 min at 100 mV prior to loading the samples. Proteins were stained with Coomassie Blue R250. FDH activity was detected by adding the gel to a tray containing 20 mL CHES (0.05 M), pH 8.5, and adding 0.08 mM 2,6-dichlorophenolindophenol (DCIP), 0.25 mM phenazine methosulphate (PMS), and 10 mM sodium formate. The tray was then heated for 10 to 15 min in a 95 °C incubator, at which time clear bands representing FDH activity appeared in a light blue background.

Metal analysis. Tungsten and molybdenum contents were determined using inductively coupled plasma emission mass spectroscopy (ICP-MS) performed at the Environmental Analysis Laboratory of the University of Georgia. Sodium molybdate and sodium tungstate were used as standards. All values were corrected for W and Mo metal content of the control samples

containing only buffer. Iron content was determined colorimetrically as previously described (19), with the exception that the acid treatment was conducted at 100 °C in a dry bath for 1 hour.

pH and temperature optima. The effect of pH on formate dehydrogenase activity was estimated using buffers with low $\Delta\text{pH} / \Delta^\circ\text{C}$ ratios (ranging from -0.0085 to -0.015) due to the high temperature requirement of the activity assay. Buffers included MES, Bis-Tris, PIPES, MOPS, HEPES, EPPS, and CHES at a concentration of 50 mM ranging from pH 6.0 to pH 9.0 in 0.5 unit increments under the assay conditions described above. Formate dehydrogenase activity was also measured at 10 °C increments from 30 °C to 100 °C using purified enzymes and cell-free extracts as described above.

UV-Visible Spectroscopy. Optical spectra were recorded using a Shimadzu UV-2501PC recording spectrophotometer. Samples were oxidized by treatment with formate at 80 °C and reduced with sodium dithionite. All measurements were conducted at room temperature.

Other methods. In order to analyze individual subunits, purified enzymes were separated by electrophoresis in the presence of SDS and electroblotted on to a polyvinylidene difluoride membrane. Transfer was carried out at 200 mA for 3 h in 10 mM CAPS, pH 11 at 4 °C. Methanol was not added to the buffer, as it prevented transfer of the high molecular weight proteins. N-terminal sequence analysis was determined by direct Edman sequencing using an automated sequencer (PE-Biosystems 491 A Pulsed-Liquid Sequencer) equipped with a PE-Biosystems 140S PTH Analyzer at the Emory University Winship Cancer Center Microchemical Facility. Mass spectroscopy using an Applied Biosystems 4700 Proteomics Analyzer at the

Proteomics Resource Facility at the University of Georgia was used to analyze fragments of in-gel coomassie-stained protein digested with trypsin according to protocols previously described (30). Observed masses were compared with sequences from Archaea and human genomes deposited in the National Center for Biotechnology Information (NCBI) database (<http://www.ncbi.nlm.nih.gov/>). Genomic sequence analyses of *P. aerophilum* (8) and of *E. coli* (4, 25) were compiled using MacVector (Accelrys Software Inc.) and Vector NTI (Invitrogen Corporation) from sequences retrieved from the NCBI database.

RESULTS

Purification of FDH. Formate dehydrogenase from *P. aerophilum* was purified from cells grown anaerobically in a fermentor (450 L) in marine medium supplemented with nitrate, formate and tungstate. No molybdate was added to the medium, although residual amounts were supplied in the medium through both the yeast extract and peptone (see Chapter 2). Given that formate dehydrogenase activity had been previously shown to be localized in the membrane fraction (Chapter 2), several concentrations of different detergents were used to evaluate whether they could extract formate dehydrogenase from the membranes. Cells were ruptured by two passes through a French press and one freeze-thaw cycle prior to solubilization. Proteins in the membrane fraction of *P. aerophilum* comprised almost 50% of the total protein in the lysed cells, and 88% of the total activity in the cell-free extracts (Table 4.1). Formate dehydrogenase (FDH) and nitrate reductase (NR) co-purify in *P. aerophilum*. The release of both of these enzymes was accomplished by sequential solubilization of the membranes. Membranes were initially solubilized with 0.5% n-octyl β -glucoside, which extracted the majority (61%) of the total FDH

Table 4.1. Solubilization of formate dehydrogenase from *P. aerophilum* cells with n-octyl β - glucoside.

Fractions	Total Protein (mg)	Total Activity (U)	Specific Activity (U/mg)	Protein Yield (%)	Activity Yield (%)
French Pressed Cells	4111	4,678	1.14	100	100
Cell Free Extract	3570	4,466	1.25	86.8	95.5
Cytosolic	2074	505	0.24	50.5	10.8
Membranes	2006	3,927	1.96	48.8	83.9
0.5% Solubilized Membranes	460	2,842	6.18	11.2	60.8
4.0% Solubilized Membranes	436	1,399	3.21	10.6	29.9

activity with a specific activity of 6.2 U/mg. The remaining FDH activity was extracted from the precipitated membranes with 4.0% n-octyl β -glucoside with a specific activity of 3.2 U/mg. Approximately 84% of the total FDH activity was solubilized from the membrane fraction by the two sequential detergent treatments. Less efficient extraction was obtained with solubilization using other detergents. For example, extraction of FDH from the membranes with Triton X-100 (0.5% to 4.0%) released from 4% to 48% of the total activity, with specific activities ranging from 0.6 to 2.75 U/mg. Similarly, extraction with SDS ranging from 0.5% to 2% yielded approximately 20% of the FDH activity with a high specific activity of 2.6 U/mg. Consequently, the enzyme extracted with n-octyl β -glucoside was used for further study.

Membranes solubilized with 0.5% n-octyl β -glucoside and 4.0% n-octyl β -glucoside were loaded separately onto a Q-Sepharose column so that the concentration of the detergent was maintained at 0.5% (Fig. 4.2). The column was also equilibrated with buffer containing this detergent concentration. However, to elute fractions, the buffer contained 0.1% Triton rather than n-octyl β -glucoside. The latter was also effective in eluting fractions containing FDH activity, but only when used at relatively high concentrations above 0.5% (w/v).

Further purification of FDH was accomplished by combining fractions from each peak of activity from the second QHP column (pH 6.8) and applying them (one from the pass through, peak 1, and one as 0.13 M NaCl was applied, peak 2) to a QHP column equilibrated at pH 8.0 and eluting with KCl (Fig. 4.2). Elution of peak 1 contained a pure NR fraction (in the pass through) and also a fraction containing NR and FDH (130 mM KCl), now termed NR1 and NR1/FDH1, respectively. Elution of peak 2 also resulted in a purified NR fraction, again in the pass through and a second containing both NR and FDH activity, which eluted at 140 mM KCl. These fractions are now termed as NR2 and NR2/FDH2, respectively (Fig.4.2). Throughout the

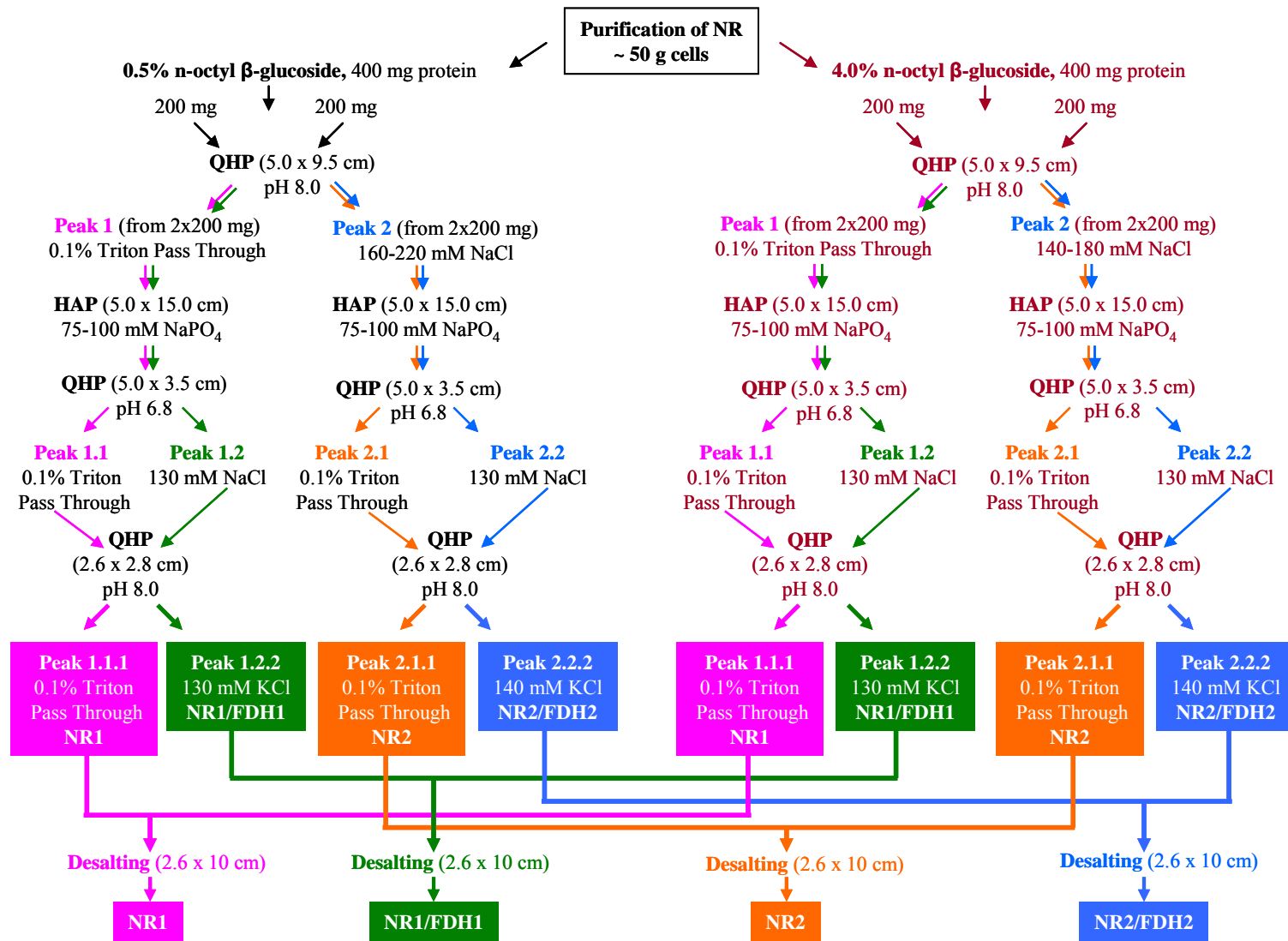


Fig. 4.2. Purification of NR and the FDH complex from 50 g of cells. NR purified from membranes solubilized with n-octyl β -glucoside from *P. aerophilum* cells results in two forms of purified NR, NR1 and NR2, and two forms of NR in complex with FDH, NR1/FDH1, and NR2/FDH2.

purification, peak 1 and peak 2 fractions were separated and analyzed with respect to their catalytic activities (measured by the standard anaerobic cuvette assays and by the in-gel assays), metal content, chromatographic elution profile, and molecular weight of the subunits that they contain.

The specific activity of FDH in NR1/FDH1 was 24 times higher than the specific activity in NR2/FDH2 (Table 4.2). Approximately 70% of the total purified FDH complex was present in the first peak, constituting 96% of the total FDH activity. The NR1/FDH1 complex yielded 1% of the protein in the membrane fraction and represented a 33-fold purification over the membrane fraction (Table 4.2). On the other hand, the second peak of FDH activity constituted only 4% of the total FDH activity, and approximately 30% of the total purified protein occurred in this peak. Freezing of the 4.0% n-octyl β -glucoside solubilized membranes in liquid N₂ resulted in a 42% loss of FDH activity when they were thawed and then assayed under standard conditions. Thus, the total FDH activity in the solubilized membrane fraction decreased from 2428 total units of activity to 1390 total units, which corresponds to a decrease from 5.6 U/mg to 3.2 U/mg. Preliminary purifications in the current study revealed that freezing and thawing samples adversely affected FDH activity, but often enhanced NR activity. Because the highest yield of NR activity was in the 4.0% detergent solubilized membranes, and these samples were utilized after purification of the 0.5% detergent solubilized membranes, freezing in liquid N₂ was necessary. While the NR2/FDH2 complex represented approximately 30% of the purified protein in *P. aerophilum*, it constituted less than 1% of the total protein in the membrane fraction (Table 4.2).

Table 4.2. Purification of formate dehydrogenase from *P. aerophilum* membranes*.

Purification Step	Total Protein (mg)	Total Activity (U)	Specific Activity (U/mg)	Protein Yield (%)	Activity Yield (%)	Purification (-fold)
Membrane fraction	2006	3,927	2	100	100	1
Solubilized fraction	896	4,241	5	45	108	2.1
Q-Sepharose pH 8.0	456	2,933	6	23	75	3
Hydroxyapatite	99	1,889	19	5	48	9.5
Q-Sepharose pH 6.8	46	1,617	35	2.3	41	17.5
Q-Sepharose pH 8.0						
Peak 1 NR1/FDH1	19	1,255	66	0.95	32	33
Peak 2 NR2/FDH2 [§]	10	52	5.2	0.50	1.3	2.6

* Denotes combined protein and activity from 0.5% and 4.0% n-octyl β - glucoside solubilized membrane fractions.

[§] Peak 2 fractions were frozen in liquid N₂ prior to the final chromatography steps, which adversely affected FDH activity, but often enhanced NR activity (see text for details).

Purified NR samples (NR1 and NR2) and the enzyme complexes (NR1-FDH1 and NR2-FDH2) each gave rise to a single protein band after nondenaturing PAGE (Fig. 4.3 D). In agreement with the direct FDH assays, when the gels were stained with formate, the same protein bands from NR1-FDH1 and NR2-FDH2 exhibited FDH activity as well as NR activity, suggesting that both enzymes were within the same native complex (Fig. 4.3 A and C). The purified NRs and the NR-FDH complexes exhibited nitrate reductase activity when stained with either nitrate or chlorate (Fig. 4.3 A and B). Although NR1 shows a slight activity when stained with formate (Fig. 4.3 C), no FDH activity was measurable in the standard assays. In this study, FDH activity throughout the solubilization and purification procedures was measured by the standard assay, the formate-dependent reduction of BV. Previous studies with *E. coli* (7, 27) have established that BV-linked formate dehydrogenase activity is primarily associated with FDH present in the soluble fraction, namely FDH-H, and that PMS(DCIP)-linked formate dehydrogenase activity, as was used in the in-gel assays, is diagnostic of FDH from the membrane fraction, namely FDH-N and FDH-O. However, a proportion of BV-linked activity is also found in the membrane fraction, which possesses both activities (7, 12). Differences in specific activity of FDH-N measured by the PMS-linked activity has been reported to be between 40 (7) and over 100 (12) times greater than that of the BV-linked activity. For *P. aerophilum*, PMS-linked FDH activity was also measured in this study on fractions during purification. However, while specific activities were much higher in most samples than those obtained with the BV-linked assay, the results were not consistent, even in triplicate measurements. Consequently, the BV-linked specific activity is reported here. Initially, the high temperature at which the assay was conducted was thought to be the problem, yet the assay worked in the in-gel

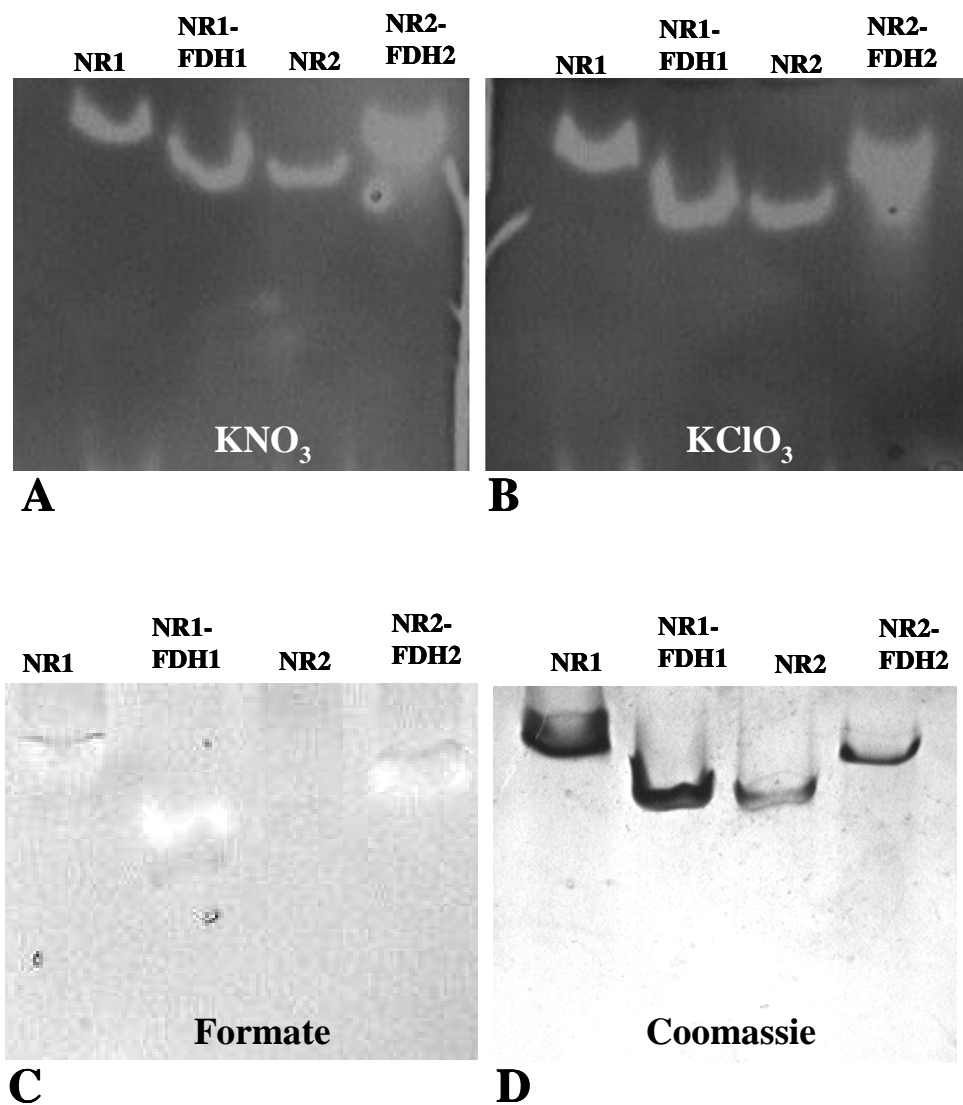


Fig. 4.3. Formate dehydrogenase and Nitrate reductase activity-stained gels. 15 ug of each protein sample (see Table 4.2) was run on a 3-8% Tris-Acetate gel under non-denaturing conditions. Nitrate reductase activity was measured at room temperature, and formate dehydrogenase was heated at 98 °C until bands appeared (approximately 10 min.). (A) Developed with nitrate, (B) developed with chlorate, (C) developed with formate, and (D) stained with Coomassie blue R-250.

assays. BV-linked activity, on the other hand, was inconsistent in the in-gel assays due to oxygen contamination.

Kinetic properties of FDH in the NR1/FDH1 complex. The effect of pH on the FDH activity of NR1/FDH1 was examined over the range of 6.5 to 9.0 (Fig. 4.4). The pH optimum was pH 8.5 using CHES buffer. In the presence of EPPS buffer (pH 8.5), the specific activity decreased from 20.5 to 17 U/mg, and in CHES buffer at pH 9.0 the activity decreased to 18 U/mg. Other buffers used were MES (pH 6.5), Bis-Tris (pH 6.5 and 7.0), PIPES and HEPES (pH 7.0), MOPS (pH 7.5), and EPPS (pH 8.0).

The effect of temperature on the two forms of the *P. aerophilum* FDH complex is shown in Fig. 4.5. The NR/FDH complexes exhibited maximal activity at 90 °C as determined by the reduction of benzyl viologen (Fig. 4.5). Both NR1/FDH1 and NR2/FDH2 exhibited no detectable activity at or below 40 °C, and while NR1/FDH1 exhibited only 4% of optimal activity at 50 °C, NR2/FDH2 still displayed no detectable activity. Further, at 100 °C, NR1/FDH1 maintained maximal activity and NR2/FDH2 exhibited a 52% decrease in activity from the maximum at 90 °C. Likewise, as shown by the in-gel activity assays (Fig. 4.3), formate dehydrogenase activity could only be detected after heating the gels for approximately 10 min in a 95 °C incubator.

Relative molecular mass and subunit composition of FDH. The two purified forms of nitrate reductase, NR1 and NR2, and the two nitrate reductase-formate dehydrogenase complexes, NR1/FDH1 and NR2/FDH2, were analyzed by SDS-PAGE. The α , β , and γ subunits of NR and of FDH were identified according to their molecular weights predicted from the corresponding

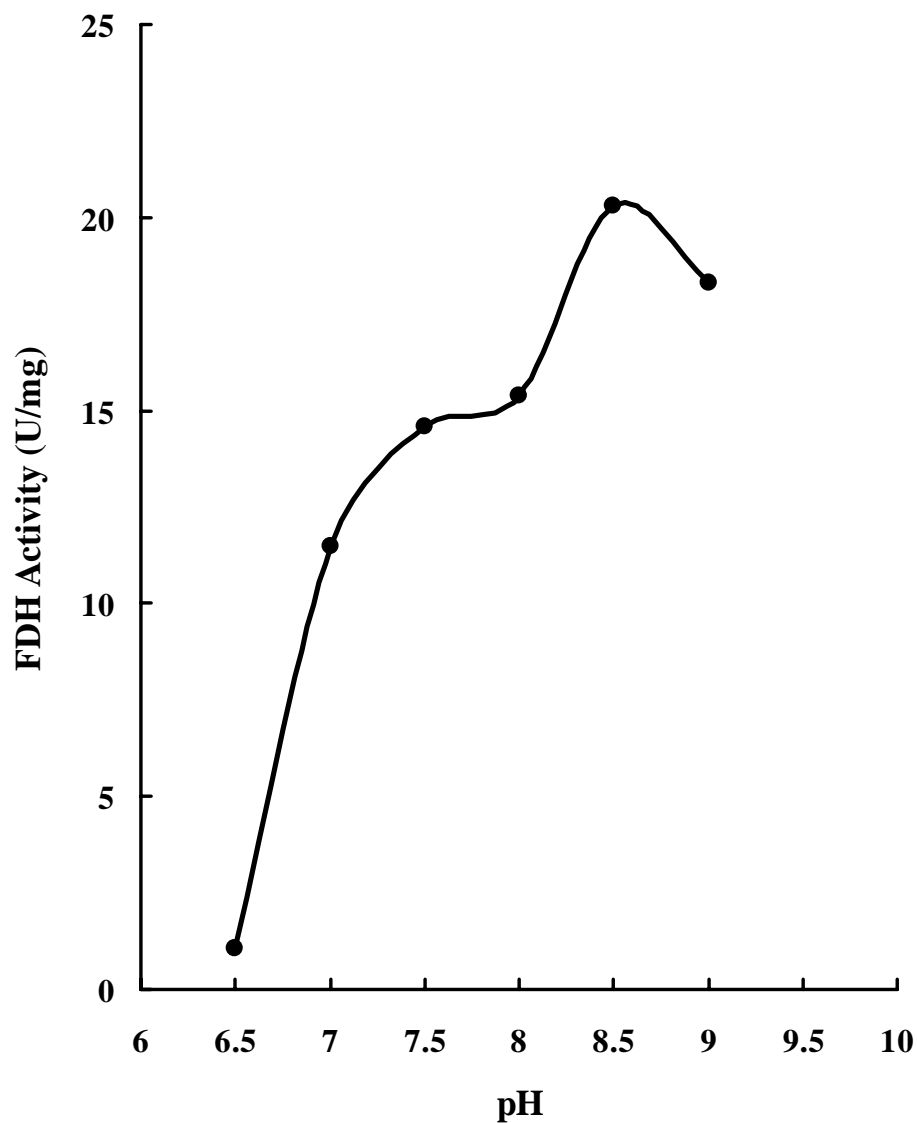


Fig. 4.4. The effect of pH on the formate dehydrogenase activity of the NR1/FDH1 complex. Activity was determined at 90 °C under standard conditions except that the following buffers at the indicated pH were used: MES (pH 6.5), Bis-Tris (pH 6.5 and 7.0), HEPES (pH 7.0), PIPES (pH 7.0), MOPS (pH 7.5), EPPS (pH 8.0 and 8.5), and CHES (pH 8.5 and 9.0).

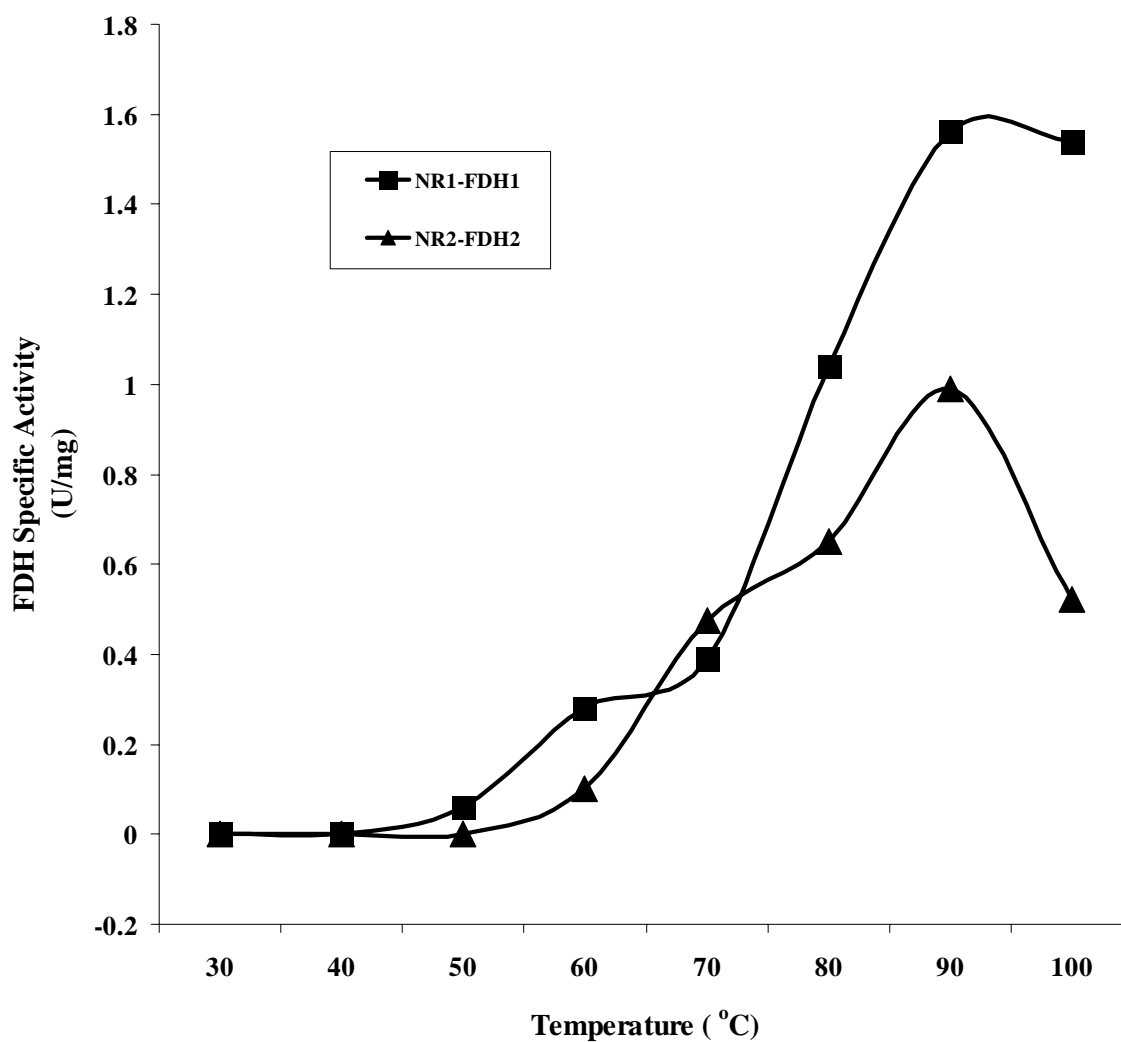


Fig. 4.5. Effect of temperature on the formate dehydrogenase complex in *P. aerophilum*. The assays were carried out under standard conditions, except that the temperature was varied as indicated. The amount of protein added to each assay was: NR1/FDH1, 20 μ g; NR2/FDH2, 10 μ g.

gene sequences in the *P. aerophilum* genome (8). The genes predicted to encode the α , β , and γ subunits of NR are encoded by PAE3611, PAE3612, and PAE3614, respectively, and the α and β subunits of FDH by PAE2662 and PAE2661, respectively. There is no gene predicted to encode the γ subunit of FDH in the original annotation of the genome. However, when the genome was searched with the sequence of the γ protein, it was found that gene PAE2660 encodes a protein with significant similarity (31%) and it contains conserved residues for the heme ligands in the *E. coli* γ subunit. PAE2660 is therefore assumed to encode the FDH γ subunit of *P. aerophilum*. The α and β subunits of NR in both purified forms and the complexes were identified by N-terminal sequencing and mass spectroscopy (MS), and the γ subunits by visible spectroscopy (Fig. 4.6 and Chapter 3, Fig. 3.9). The two complexes, NR1-FDH1 and NR2-FDH2, also consisted of the three predicted major NR polypeptides (Fig. 4.6). Attempts to identify the predicted polypeptides from FDH by N-terminal sequencing, internal sequencing (Fig. 4.7) or MS, however, were unsuccessful. Consequently, there was some uncertainty in the identification. For example, the faint bands at approximately 33 kDa (Fig. 4.6) in both lanes loaded with the NR1-FDH1 and NR2-FDH2 complexes could be either the γ subunit of NR or the β subunit of FDH. Visible spectroscopy verified the presence of cytochrome *b* in the complexes (Chapter 3), which, by analogy with *E. coli* NR (7), is indicative of the γ subunit. However, the 33 kDa bands in NR1-FDH1 and NR2-FDH2 identified by SDS-PAGE analysis were at a concentration that was too low to be characterized using N-terminal sequence analysis or MS.

Two additional proteins were also identified in NR1-FDH1 complex. A polypeptide with an apparent molecular weight of 95 kDa was identified by MS/MS analysis and subsequent genome analysis as a hypothetical protein (PAE0055) with a molecular weight of 67.8 kDa (Fig.

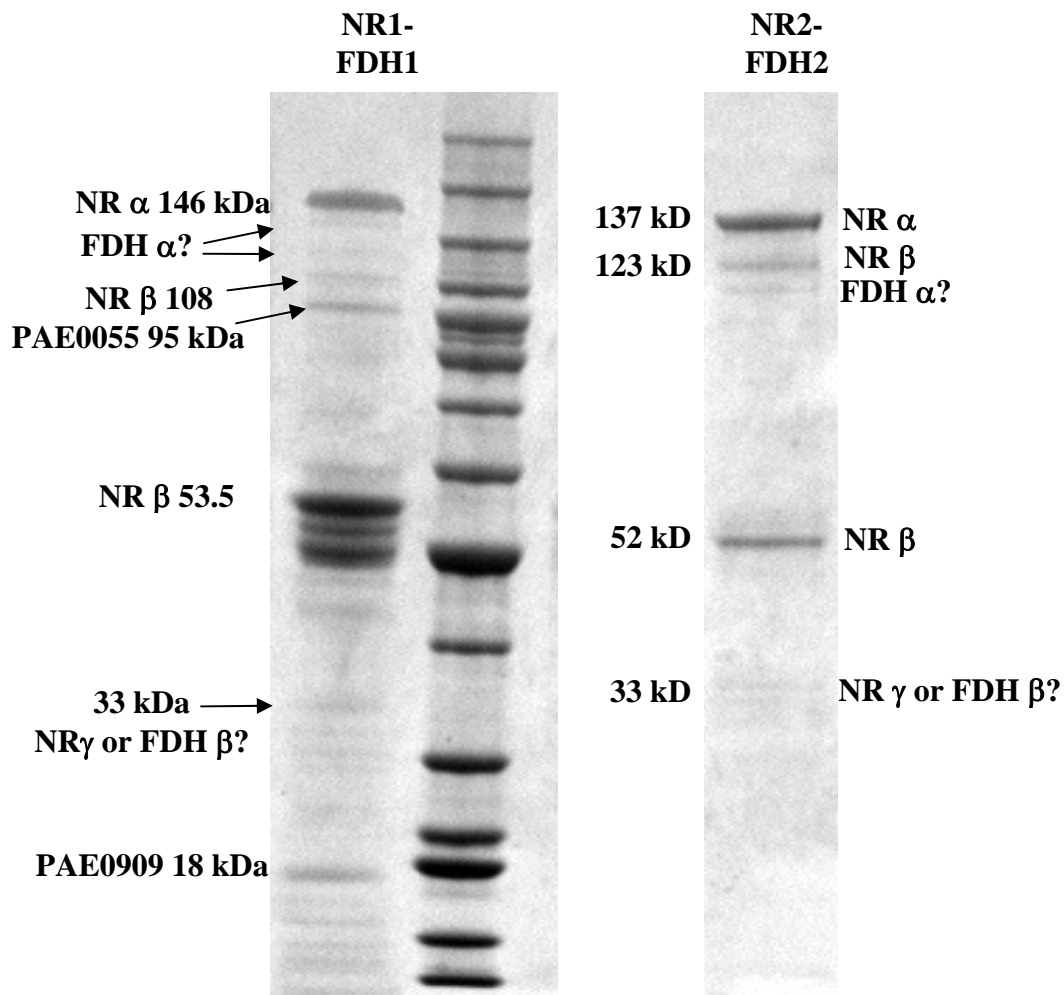


Fig. 4.6. SDS-PAGE analysis of the two formate dehydrogenase complexes from *P. aerophilum*. Proteins were separated in a 4-12% Bis-Tris acrylamide gel and stained with Coomassie blue R-250. Each lane contains 10 μ g of protein. Standards that were used (BenchMark Protein Ladder; Invitrogen Corp.) consisted of 15 engineered proteins with the molecular weights ranging from 220 kDa to 10 kDa.

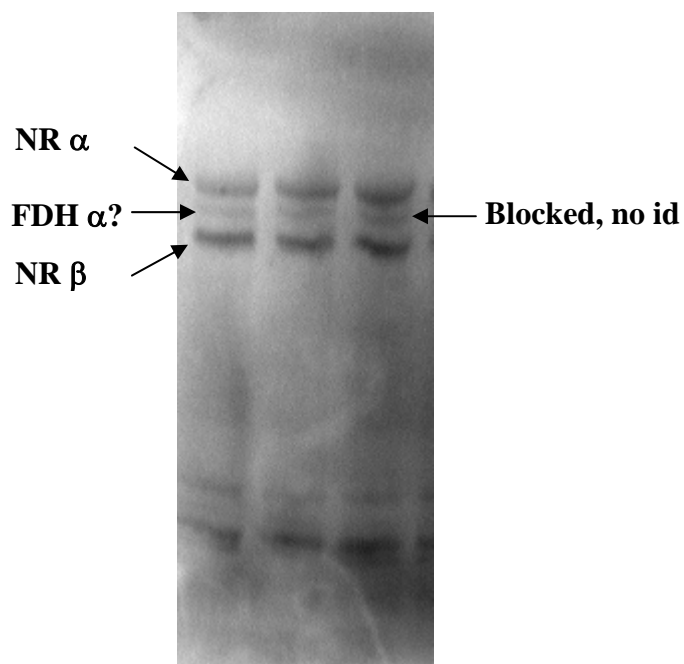


Fig. 4.7. Nitrate reductase/formate dehydrogenase complex from *P. aerophilum*. Proteins were separated in a 4-12% Bis-Tris acrylamide gel and electroblotted onto PVDF membrane and then stained with Coomassie blue R-250. Each lane contains 15 μ g of protein.

4.6). The remaining major band after SDS-PAGE analysis of NR1/FDH1, an 18 kDa protein, was identified from genome analysis as a hypothetical protein within *P. aerophilum* with a calculated molecular weight of 14.4 kDa (PAE0909).

The additional SDS-PAGE bands around the β subunit present in the lane NR1-FDH1 (Fig. 4.6) represent degradation products of the β subunit of NR. The β subunit present in the lane loaded with NR1 also degraded into peptides during storage at 4°C, as indicated by SDS-PAGE, most likely due to endogenous proteases. Studies in *E. coli* (6, 20, 21), *B. halodenitrificans* (17) and in *Haloferax denitrificans* (13) also report the breakdown of the NR β subunit during storage, as shown by analysis using SDS-PAGE.

Metal content. The NR1-FDH1 complex contained 0.6 g-atoms Mo and 0.3 g-atoms W per mol of enzyme complex (based on M_r of 423,000 for NR/FDH complex). NR2/FDH2 contained 0.6 g-atoms W and 0.2 g-atoms Mo per mol of enzyme complex when analyzed by plasma emission spectroscopy. The Fe contents determined by colorimetric analysis were 40 g-atoms per mol of NR1/FDH1 complex, and 37 g-atoms per mol of NR2/FDH2 complex. ICP-MS analysis of selenium content in FDH was inconsistent, however, this metal is found in FDH from *E. coli*.

Sequence comparisons. Comparison of the operons and amino acid sequences of the FDH from *P. aerophilum* and FDH-N and FDH-O from *E. coli* (Fig. 4.1) reveals a moderately high similarity, from 31 to 50%, suggesting that *P. aerophilum* contains a respiratory FDH that is similar to those in *E. coli*. However, the genome sequence of *P. aerophilum* does not contain genes that encode a second FDH of this type, as is the case with *E. coli*. The identities and similarities between *P. aerophilum* FDH and both FDH-N and FDH-O are the same. The α and

β subunits of the *P. aerophilum* enzyme show relatively high sequence similarity with the homologous subunits of the FDHs in *E. coli*, and are thought to contain the same cofactors. The α subunit of *P. aerophilum* is slightly larger than the analogous subunits of *E. coli*, while the β subunit is slightly smaller (Fig. 4.1). Although the γ subunit of the *E. coli* enzymes has a low amino acid sequence similarity to the corresponding protein (PAE2660) of the *P. aerophilum* FDH (which is annotated as a hypothetical protein), it is assumed to contain the same heme cofactors. The γ subunits of these enzymes are thought to bind directly to the membrane, hence, the low similarity between the γ subunits of *P. aerophilum* and *E. coli* might reflect the differences between the ester-linked fatty acid membranes of bacteria and the ether-linked phospholipids and isoprenoids in archaeal membranes.

The crystal structure of *E. coli* FDH-N (15) showed that a single Mo atom is coordinated in a triangular prism pattern by two dithiolate groups from each of the two MGD cofactors, by a selenate group from Se-Cys¹⁹⁶ and by a hydroxide ion in the α subunit (FdnG). There is also [4Fe-4S] cluster present in the α subunit that is coordinated by four Cys residues. These residues are also conserved in the sequence of *P. aerophilum* FDH α and in FDH-O of *E. coli* (Fig. 4.8A). In addition to these residues in the α subunit, the Cys residues that bind four additional [4Fe-4S] clusters in *E. coli* FdnH (15) are also present in the β subunit of *P. aerophilum* FDH and in *E. coli* FdoH (Fig. 4.8B).

In *E. coli*, the γ subunit (FdnI) contains two *b*-type hemes named according to their location with respect to the membrane. The His ligands that coordinate both the periplasmic and

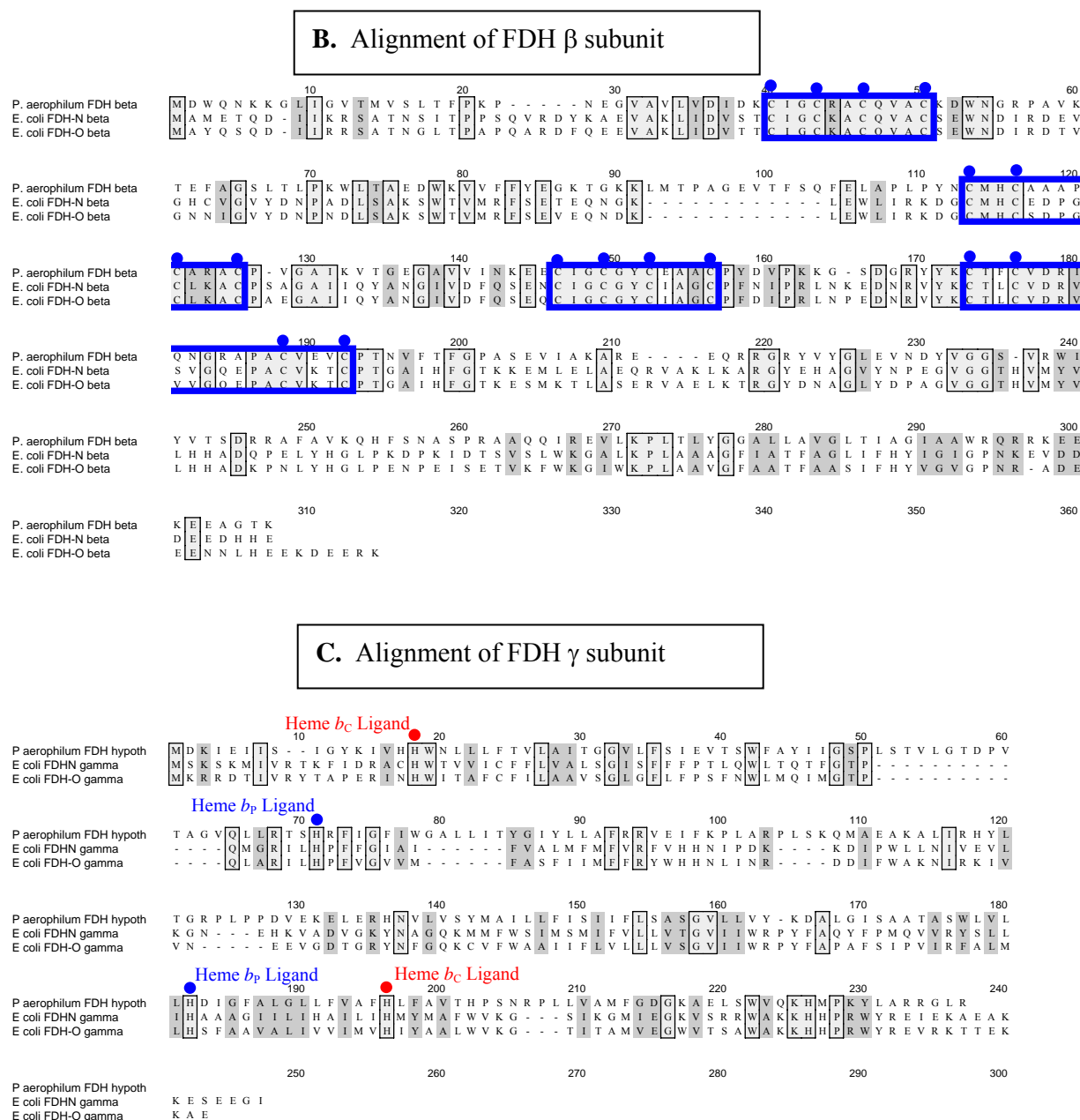


Fig. 4.8. Alignment of sequences of the α , β and γ subunits of the respiratory FDH from *Pyrobaculum aerophilum* and *Escherchia coli* FDH-N (*fdnGHI*) and FDH-O (*fdhoGHI*). Identical amino acids are boxed and shaded light gray. Similar amino acids are shaded dark gray. (A) FDH α subunit. Residues that bind the Fe-S clusters are boxed in blue, and blue dots denote ligands. Mo binding site is denoted by red box as identified in (15). (B) FDH β subunit. Fe-S cluster binding sites are boxed in blue and blue dots denote ligands. (C) FDH γ subunit. His residues of the heme located on the cytoplasmic side, heme b_C , are denoted by red dots, and His residues of the heme located on the periplasmic side, heme b_P , are denoted by blue dots, as identified in (15). Amino acid sequence alignments *P. aerophilum* and of *E. coli* were performed using MacVector (Accelrys Software Inc.) from sequences retrieved from the NCBI database.

the cytoplasmic hemes, heme b_p and heme b_c , respectively, have also recently been determined based on the crystal structure of FDH-N (15). These His ligands are also conserved in the sequence of the hypothetical protein (PAE2660) of *P. aerophilum* FDH and in FdoI from FDH-O (Fig. 4.8C).

DISCUSSION

The formate-nitrate respiratory chain is a well-studied system in *E. coli*. The current study of nitrate respiration in *P. aerophilum* has been modeled after the *E. coli* system, due to the high homology between the genes that encode for the primary enzymes in this pathway, nitrate reductase and formate dehydrogenase. The key differences in the formate-nitrate respiration chain between *E. coli* and *P. aerophilum* lie not in the organization or in the components of the system, but rather in the ability of *P. aerophilum* to incorporate either Mo or W into the active sites of formate dehydrogenase and nitrate reductase and produce active enzymes. These differences are rooted in the fact that there is an abundance of W in the natural high-temperature environment of the hyperthermophilic archaeon, *P. aerophilum*, as opposed to the high abundance of the analogous metal, Mo, in the mesophilic environment of the bacterium, *E. coli* (31). Often, when W is present rather than Mo, in organisms with naturally-occurring Mo-containing enzymes, or when Mo is present rather than W in organisms that naturally contain tungstoenzymes, the result is an inactive enzyme, especially in the case of NR (11, 23, 29). *P. aerophilum*, however, is dependent upon the presence of W when grown at or near its optimum growth temperature (100°C) (Chapter 2 and (2)). Furthermore, at these high temperatures, growth is inhibited when Mo is present in the growth medium in equal concentrations to W, or as the only oxyanion (Chapter 2). Moreover, it was shown that both W and Mo were taken up by *P.*

aerophilum during anaerobic growth on nitrate, and the NR and FDH were membrane-bound (Chapter 2).

As in *E. coli*, NR and FDH co-purify in *P. aerophilum*. In *P. aerophilum*, purification of these enzymes results in two forms of purified NR (NR1, a Mo-containing containing enzyme, and NR2, a W-containing enzyme) and two forms of a NR-FDH complex (NR1-FDH1, most likely a W-containing FDH, and NR2-FDH2, most likely a FDH containing both W and Mo). Each form was characterized with respect to the metal composition of the pterin cofactor, catalytic activity measured in a standard anaerobic cuvette assay, activity in an in-gel assay, and apparent molecular weight of the subunits. The purification of NR was the initial focus of this research. The necessity of freezing the 4% n-octyl β -glucoside solubilized membranes in liquid N₂, although beneficial as it increased the activity of NR, was detrimental to the activity of FDH (upon subsequent thawing) with the loss of almost 50% of the activity. Of the approximately 88% of FDH activity solubilized from the membrane fraction, the NR1/FDH1 complex comprised 70 % of the total FDH complex purified, constituting 96% of the total FDH activity. On the other hand, the NR2/FDH2 complex, which comprised 30% of the total purified protein, constituted only 4% of the total FDH activity, and exhibited a specific activity that was approximately 24 times less than that of the NR1/FDH1 complex. EPR spectra of [Fe-S] clusters and Mo (V) of *P. aerophilum* NR1 and NR1/FDH1 (Fig. 3.5) are consistent with a cofactor composition similar to that of NRA from *E. coli* (9, 22), which further indicates that the W content in the NR1-FDH1 complex is associated with the FDH. NR2 (0.7 mol W and 0 to 0.08 mol Mo per mol enzyme) (Chapter 3) was found to be a W-containing NR, thus the Mo content in the NR2-FDH2 complex (0.6 mol W and 0.2 mol Mo per mol of enzyme complex) seems to be associated with the FDH. However, in this complex it is quite possible that both the NR and

the FDH contain both W and Mo in their active sites. Further studies will be required to resolve this issue.

In addition to the effect on activity, it is possible that the freezing and thawing of the 4% n-octyl β -glucoside-solubilized membranes resulted in a loss of Mo or W associated with the FDH in the NR-FDH complexes. The content of W and Mo in the purified complexes, 0.6 g-atoms Mo and 0.3 g-atoms W per mol of NR1/FDH1 complex and 0.6 g-atoms W and 0.2 g-atoms Mo per mol of NR2/FDH2 complex, was lower than expected given that both NR and FDH are expected to contain either a W or a Mo ion. The Fe content (40 g-atoms per mol of NR1/FDH1 complex, and 37 g-atoms per mol of NR2/FDH2 complex), however, is consistent with the notion that the NR contains one [3Fe-4S] and four [4Fe-4S] (5, 14), and FDH contains five [4Fe-4S] clusters (15).

In *E. coli* there is a FDH produced during growth of the organism under aerobic conditions (FDH-O), and another that is functional during anaerobic growth (FDH-N). In *P. aerophilum*, however, there is only one FDH, although it appears to exist in two forms when solubilized *in vitro*. The deduced amino acid sequences of the subunits of *P. aerophilum* FDH are equally similar to those of the corresponding subunits of both FDH-O and FDH-N of *E. coli*. Residues identified as cofactor ligands in FDH-N and FDH-O of *E. coli* (4, 24) were conserved in the *P. aerophilum* enzyme, and therefore were predicted to contain the same cofactors. From an evolutionary perspective, it is clear that an operon duplication event occurred in *E. coli* that did not occur in *P. aerophilum*. This may reflect the physiological needs of the two organisms, as *E. coli* is metabolically very diverse and can thrive in aerobic and anaerobic environments and therefore requires a FDH that can function under either environmental condition. *P. aerophilum*, on the other hand, can only thrive in an environment with a low percentage of oxygen

(microaerophilic), or anaerobically, therefore one FDH which can function in a low oxygen (0.3 – 3.0% (w/v) oxygen) or anaerobic environment is sufficient. Thus the FDH in *P. aerophilum* may be in part reflective of the microaerophilic nature of the organism.

FDH from *P. aerophilum* is obviously distinct, however, from the corresponding mesophilic *E. coli* FDHs, in that it exhibits its highest activity at extreme temperatures (90 °C). Furthermore, FDH was not active at room temperature, and in fact was active only at or above 50 °C, unlike the NR activity in the NR/FDH complexes of *P. aerophilum*, which was active at room temperature (Chapter 3). The membrane-bound FDH activity in *P. aerophilum* could only be reliably measured using the BV-linked assay, which is the assay used to measure the soluble FDH in *E. coli*. Consequently, in *P. aerophilum* the relationship between the BV-linked and the PMS-linked membrane-bound activities could not be established. Hence, comparisons between FDH activity in *P. aerophilum* and FDH activity from other mesophilic and thermophilic enzymes could not be made.

Because FDH in *P. aerophilum* was purified as a complex with NR, despite numerous and various attempts to separate FDH from the complex, and identification of the protein bands corresponding to the predicted FDH subunits was unsuccessful, many characteristics of the FDH enzyme of *P. aerophilum* remain unknown. In addition to addressing these issues, development of a standard assay using PMS as an electron carrier which gives reliable results at high temperature, would be beneficial to further characterize not only FDH, but also the formate-nitrate respiratory system in *P. aerophilum*.

REFERENCES

1. **Afshar, S., E. Johnson, S. de Vries, and I. Schroder.** 2001. Properties of a thermostable nitrate reductase from the hyperthermophilic archaeon *Pyrobaculum aerophilum*. *J. Bacteriol.* **183**:5491-5.
2. **Afshar, S., C. Kim, H. G. Monbouquette, and I. Schroder.** 1998. Effect of tungstate on nitrate reduction by the hyperthermophilic archaeon *Pyrobaculum aerophilum*. *Appl. Environ. Microb.* **64**:3004-3008.
3. **Andreesen, J. R., and L. G. Ljungdahl.** 1973. Formate dehydrogenase of *Clostridium thermoaceticum*: incorporation of selenium-75, and the effects of selenite, molybdate, and tungstate on the enzyme. *J Bacteriol.* **116**:867-73.
4. **Berg, B. L., J. Li, J. Heider, and V. Stewart.** 1991. Nitrate-inducible formate dehydrogenase in *Escherichia coli* K-12. I. Nucleotide sequence of the *fdnGHI* operon and evidence that opal (UGA) encodes selenocysteine. *J Biol Chem.* **266**:22380-5.
5. **Bertero, M. G., R. A. Rothery, M. Palak, C. Hou, D. Lim, F. Blasco, J. H. Weiner, and N. C. Strynadka.** 2003. Insights into the respiratory electron transfer pathway from the structure of nitrate reductase A. *Nat Struct Biol* **10**:681-7.
6. **Clegg, R. A.** 1976. Purification and some properties of nitrate reductase (EC 1.7.99.4) from *Escherichia coli* K12. *Biochem J* **153**:533-41.
7. **Enoch, H. G., and R. L. Lester.** 1975. The purification and properties of formate dehydrogenase and nitrate reductase from *Escherichia coli*. *J Biol Chem* **250**:6693-705.
8. **Fitz-Gibbon, S. T., H. Ladner, U. J. Kim, K. O. Stetter, M. I. Simon, and J. H. Miller.** 2002. Genome sequence of the hyperthermophilic crenarchaeon *Pyrobaculum aerophilum*. *Proc. Natl. Acad. Sci. U S A* **99**:984-9.

9. **George, G. N., N. A. Turner, R. C. Bray, F. F. Morpeth, D. H. Boxer, and S. P. Cramer.** 1989. X-ray-absorption and electron-paramagnetic-resonance spectroscopic studies of the environment of molybdenum in high-pH and low-pH forms of *Escherichia coli* nitrate reductase. *Biochem J.* **259**:693-700.
10. **Giordano, G., L. Grillet, J. Pommier, C. Terriere, B. A. Haddock, and E. Azoulay.** 1980. Precursor forms of the subunits of nitrate reductase in chlA and chlB mutants of *Escherichia coli* K12. *Eur J Biochem* **105**:297-306.
11. **Giordano, G., B. A. Haddock, and D. H. Boxer.** 1980. Molybdenum-limited growth achieved either phenotypically or genotypically and its effect on the synthesis of formate dehydrogenase and nitrate reductase by *Escherichia coli* K12. *FEMS Microbiol Lett* **8**:229-235.
12. **Giordano, R., C. L. Medani, M. A. Mandrand-Berthelot, and D. H. Boxer.** 1983. Formate dehydrogenases from *E. coli*. *FEMS Microbiol Lett* **17**:171-177.
13. **Hochstein, L. I., and F. Lang.** 1991. Purification and properties of a dissimilatory nitrate reductase from *Haloferox denitrificans*. *Arch Biochem Biophys* **288**:380-5.
14. **Jormakka, M., D. Richardson, B. Byrne, and S. Iwata.** 2004. Architecture of NarGH reveals a structural classification of Mo-*bis*MGD enzymes. *Structure (Camb)* **12**:95-104.
15. **Jormakka, M., S. Tornroth, J. Abramson, B. Byrne, and S. Iwata.** 2002. Purification and crystallization of the respiratory complex formate dehydrogenase-N from *Escherichia coli*. *Acta Crystallogr D Biol Crystallogr* **58**:160-2.
16. **Jormakka, M., S. Tornroth, B. Byrne, and S. Iwata.** 2002. Molecular basis of proton motive force generation: structure of formate dehydrogenase-N. *Science* **295**:1863-8.

17. **Ketchum, P. A., G. Denariatz, J. LeGall, and W. J. Payne.** 1991. Menaquinol-nitrate oxidoreductase of *Bacillus halodenitrificans*. *J Bacteriol* **173**:2498-505.
18. **Knappe, J., and G. Sawers.** 1990. A radical-chemical route to acetyl-CoA: the anaerobically induced pyruvate formate-lyase system of *Escherichia coli*. *FEMS Microbiol Rev* **6**:383-98.
19. **Lovenberg, W., B. B. Buchanan, and J. C. Rabinowitz.** 1963. Studies on the chemical nature of Clostridial ferredoxin. *J. Biol. Chem.* **238**:3899-3913.
20. **Lund, K., and J. A. DeMoss.** 1976. Association-dissociation behavior and subunit structure of heat-released nitrate reductase from *Escherichia coli*. *J Biol Chem* **251**:2207-16.
21. **MacGregor, C. H., C. A. Schnaitman, and D. E. Normansell.** 1974. Purification and properties of nitrate reductase from *Escherichia coli* K12. *J Biol Chem* **249**:5321-7.
22. **Magalon, A., R. A. Rothery, G. Giordano, F. Blasco, and J. H. Weiner.** 1997. Characterization by electron paramagnetic resonance of the role of the *Escherichia coli* nitrate reductase (NarGHI) iron-sulfur clusters in electron transfer to nitrate and identification of a semiquinone radical intermediate. *J Bacteriol.* **179**:5037-5045.
23. **Mukund, S., and M. W. W. Adams.** 1996. Molybdenum and vanadium do not replace tungsten in the catalytically active forms of the three tungstoenzymes in the hyperthermophilic archaeon *Pyrococcus furiosus*. *J. Bacteriol.* **178**:163-7.
24. **Plunkett, G. I., V. Burland, D. L. Daniels, and F. R. Blattner.** 1993. Analysis of the *Escherichia coli* genome. III. DNA sequence of the region from 87.2 to 89.2 minutes. *Nucleic Acids Res.* **21**:3391-3398.

25. **Pommier, J., M. A. Mandrand, S. E. Holt, D. H. Boxer, and G. Giordano.** 1992. A second phenazine methosulphate-linked formate dehydrogenase isoenzyme in *Escherichia coli*. *Biochim Biophys Acta* **1107**:305-13.
26. **Raaijmakers, H., S. Teixeira, J. M. Dias, M. J. Almendra, C. D. Brondino, I. Moura, J. J. Moura, and M. J. Romao.** 2001. Tungsten-containing formate dehydrogenase from *Desulfovibrio gigas*: metal identification and preliminary structural data by multi-wavelength crystallography. *J Biol Inorg Chem.* **6**:398-404.
27. **Sawers, G.** 1994. The hydrogenases and formate dehydrogenases of *Escherichia coli*. *Antonie Van Leeuwenhoek* **66**:57-88.
28. **Sawers G, H. J., Zehelein E, Bock A.** 1991. Expression and operon structure of the sel genes of *Escherichia coli* and identification of a third selenium-containing formate dehydrogenase isoenzyme. *J Bacteriol.* **173**:4983-93.
29. **Scott RH, S. G., DeMoss JA.** 1979. In vitro incorporation of molybdate into demolybdoproteins in *Escherichia coli*. *J Bacteriol.* **137**:719-26.
30. **Shevchenko, A., M. Wilm, O. Vorm, and M. Mann.** 1996. Mass spectrometric sequencing of proteins silver-stained polyacrylamide gels. *Anal Chem.* **68**:850-858.
31. **Silva, J. R. R. F. d., and R. J. P. Williams.** 1991. The biological chemistry of the elements : the inorganic chemistry of life, vol. xxi. Oxford University Press Clarendon Press, Oxford [England] New York.
32. **Völkl, P., R. Huber, E. Drobner, R. Rachel, S. Burggraf, A. Trincone, and K. O. Stetter.** 1993. *Pyrobaculum aerophilum* sp. nov., a novel nitrate-reducing hyperthermophilic archaeum. *Appl. Environ. Microbiol.* **59**:2918-26.

33. **Yamamoto, I., T. Saiki, S. M. Liu, and L. G. Ljungdahl.** 1983. Purification and properties of NADP-dependent formate dehydrogenase from *Clostridium thermoaceticum*, a tungsten-selenium-iron protein. J. Biol. Chem. **258**:1826-1832.

CHAPTER 5

COMPARISON OF MOLYBDENUM- AND TUNGSTEN-CONTAINING ENZYMES, COFACTOR BIOSYNTHESIS, AND METAL TRANSPORT IN *ESCHERICHIA COLI*, *PYROBACULUM AEROPHILUM*, AND *PYROCOCCUS FURIOSUS*¹

¹ Feingold, L.E. and M.W.W. Adams. 2006. To be submitted to *Journal of Bacteriology*.

ABSTRACT

Further insight into potential molybdoenzymes and tungstoenzymes in *Pyrobaculum aerophilum*, and their biosynthesis, was accomplished by bioinformatics analyses with analogous enzymes in *Escherichia coli* and *Pyrococcus furiosus*. *E. coli* was used as the reference microorganism for Mo-containing enzymes, Mo-cofactor biosynthesis, and Mo transport, and one that is a mesophile and is not known to utilize tungsten. In contrast, *P. furiosus* was used as the reference organism for W-containing enzymes, and one that is a hyperthermophile and not known to utilize molybdenum. The goal was to determine how *P. aerophilum* fits into the overall scheme both in the use of these metals, and in the types of enzymes it contains, and in the proteins responsible for the assembly of structures necessary to incorporate both Mo and W into the primary enzymes. The results show that *P. aerophilum* resembles Mo-containing mesophilic organisms, and contains homologs of the Mo-containing nitrate respiratory enzymes of the type found in *E. coli* in metal transport and incorporation. However, *P. aerophilum* also contains homologs of the W-containing hyperthermophilic enzymes, such as those found in *P. furiosus*. *P. aerophilum* therefore appears to represent a novel hybrid organism in evolutionary terms in its ability to utilize the metals molybdenum and tungsten.

INTRODUCTION

A wide range of redox enzymes found in archaea, bacteria, plants and animals are dependent upon molybdenum (Mo) for activity. Mo and tungsten (W) are both group VI transition metals, and are members of the second and third transition series, respectively. Both have known biological function. While most organisms, including bacteria, archaea, and eukaryotes,

including humans, are dependent on Mo for growth, only certain members of anaerobic prokaryotes are known to require W (24, 25, 31). These requirements for the two metals stem from their presence in the active sites of metalloenzymes. Mo-containing enzymes play a critical role in the global nitrogen and sulfur cycles, and both molybdo- and tungstoenzymes have roles in the anaerobic portions of the global carbon cycle.

Pyrobaculum aerophilum is a hyperthermophilic archaeon, and is a true denitrifier in that it reduces nitrate to N_2 through respiratory dissimilatory nitrate reduction (72). Analogous to its bacterial counterparts, *P. aerophilum* is also a facultative anaerobe. In contrast, however, *P. aerophilum* is a microaerophile utilizing between 0.6 and 3.0 % oxygen. Most importantly, growth of *P. aerophilum* is optimal at temperatures near 100 °C and is dependent upon W but inhibited by Mo [Chapter 2 and (1)]. W, however, is a known antagonist to the growth of many mesophilic microorganisms, especially those that respire anaerobically with nitrate, which are dependent on Mo (17, 67). In prokaryotic denitrification, the source of electrons for nitrate reduction is often formate, which is oxidized by formate dehydrogenase (FDH). Like all respiratory systems, the formate-nitrate reductase respiratory pathway is membrane-associated, and electron transfer between the nitrate reductase (NR) and the FDH is coupled by quinones (9, 41). Hence, this multienzyme complex catalyzes the oxidation of formate to carbon dioxide coupled with the transfer of reducing equivalents to nitrate in an energy-conserving pathway. Traditionally, both NR and FDH are molybdoenzymes, and in *Escherichia coli*, growth is inhibited when the essential Mo is replaced with W, resulting in inactive demolybdo NRs and FDHs (17, 67). In *P. aerophilum*, however, it has been established in research described in this thesis (Chapters 3 and 4) that both NR and FDH are active with either Mo or W coordinated into their active sites.

In addition to NR and FDH, other enzymes with active sites that could contain either Mo or W in *P. aerophilum* are enzymes that have been well characterized as tungstoenzymes in the hyperthermophilic archaea *Pyrococcus furiosus*, *Pyrococcus* strain ES-4 (7, 43, 45, 46, 48, 62), *Thermococcus litoralis* and *Thermococcus* strain ES-1 (23, 44). These include the aldehyde-oxidizing enzymes, aldehyde ferredoxin oxidoreductase (AOR), formaldehyde ferredoxin oxidoreductase (FOR), glyceraldehydes-3-phosphate ferredoxin oxidoreductase (GAPOR), and possibly two putative oxidoreductases, WOR4 and WOR5. When *P. furiosus* was grown on a medium in the presence MoO_4^{2-} and without WO_4^{2-} , the growth yield and rate were unchanged compared to cells in W-supplemented medium. Although the specific activities of the W-containing oxidoreductases (AOR, FOR, GAPOR) of *P. furiosus* did decrease, the enzymes did not incorporate Mo into their active site (47). Unfortunately, the cellular concentrations of W and Mo were not measured, so it is not known if Mo was taken up into the cells. The low levels of activity were attributed to the residual W present in the enzymes that originated from the contaminating W present in the growth medium (47). Activity assays conducted on the cytosolic fraction of *P. aerophilum* cells confirm the presence of enzymes that oxidize the same aldehydes as those used to characterize AOR (crotonaldehyde), FOR (formaldehyde) and GAPOR (glyceraldehyde-3-phosphate) (see Chapter 2). While no metal analyses were conducted on the proteins AOR, FOR and GAPOR from *P. aerophilum* in the current research, AOR was recently purified by others and was shown to be a tungstoenzyme (21). It is assumed that FOR and GAPOR also exist in *P. aerophilum* and are also W-containing enzymes like those in *P. furiosus* due to the dependence of W in the growth medium of *P. aerophilum* (Chapter 2).

The catalytic sites of both Mo- and W-containing enzymes (with the exception of nitrogenase) contain one atom of the metal and one or two molecules of an organic moiety called

pyranopterin forming the molybdenum cofactor (Moco). The core of the pyranopterin structure is conserved in all organisms examined, and within this wide range of eukaryotes, bacteria and archaea, the biosynthesis of the pterin cofactor is accomplished via a ubiquitous and highly conserved pathway consisting of approximately fifteen gene products (40). In *E. coli*, the biosynthesis of active Moco involves the *moa*, *mob*, *moe*, *mod* and *mog* operons to synthesize the pterin, transport and incorporate the metal, attach a dinucleotide and transfer the cofactor to the appropriate apoenzyme. In prokaryotic enzymes, the pterin cofactor usually has a dinucleotide of cytosine, guanine, adenosine or inosine on the sidechain; while in eukaryotic molybdoenzymes the pterin cofactor has a terminal phosphate on the pterin sidechain. The majority of tungstoenzymes, which so far have only been characterized from prokaryotes, contain pterin cofactors without a dinucleotide, except for the formylmethanofuran dehydrogenase (FMDH II) from *Methanobacterium wolfei* (66) and the acetylene hydratase (AH) from *Pelobacter acetylenicus* (59).

As shown in this research, *P. aerophilum* is a microorganism whose nitrate respiration pathway closely resembles that of *E. coli*, though contrary to *E. coli*, the NR and FDH are also active with W coordinated into their active sites. The presence of active W-containing enzymes is reflective of the hyperthermophilic nature of this organism, a property that is shared by *P. furiosus*. In an effort to further elucidate how *P. aerophilum*, which utilizes both Mo and W, relates to organisms that function with only with molybdoenzymes (*E. coli*) and those that function only with tungstoenzymes (*P. furiosus*), the genes encoding the aforementioned Mo- and W-containing enzymes, and those encoding proteins involved in the pathways for Mo uptake and transport and molybdopterin biosynthesis in *E. coli* and *P. furiosus*, were compared with the analogous genes in *P. aerophilum*. *E. coli* was used as the representative and reference

microorganism for Mo-containing enzymes (encoded by *nar*, *fdn* and *fdo*) as well as for Mo uptake, transport and Moco biosynthesis (encoded by *moa*, *mob*, *moe*, *mod* and *mog* genes). *P. furiosus* was used as the organism representative of W-containing enzymes (encoded by *aor*, *for*, *gor* and genes and encoding WOR4 and WOR5).

MATERIALS AND METHODS

Sequence retrieval and gene identification and comparison. The sequences of *E. coli*, *P. aerophilum*, and *P. furiosus* genes were obtained from the TIGR website (<http://www.tigr.org/>). Sequences of the relevant genes from the reference organisms (*E. coli* for *nar*, *fdn*, *fdo*, *moa*, *mob*, *moe*, *mod* and *mog*, and *P. furiosus* for *aor*, *for*, *gor*, and for those encoding WOR4 and WOR5) were then used to conduct BLAST searches in the genomes of *P. aerophilum*, and either *P. furiosus* or *E. coli* which are deposited in the National Center for Biotechnology Information (NCBI) database (<http://www.ncbi.nlm.nih.gov/>). Phylogenetic trees analysis was compiled using MacVector (Accelrys Software Inc.).

RESULTS AND DISCUSSION

NR and FDH respiratory enzymes. The two primary enzymes in the formate-nitrate respiratory chain of *E. coli*, FDH-N and NR, exhibit extensive similarity in charge, size and composition (15, 33). In *E. coli*, there are two membrane-bound respiratory nitrate reductases. The primary NR is NRA which is encoded by *narGHJI*, and is well characterized in *E. coli* as well as other bacterial sources (9, 28, 32, 41, 51). In *E. coli*, the catalytic α subunit, (NarG, 140 kDa) contains a Mo ion, which is coordinated by *bis*-molybdopterin guanine dinucleotide (Mo-*bis*MGD), and a [4Fe-4S] cluster. The β subunit, (NarH, 60 kDa) contains one [3Fe-4S] and

three [4Fe-4S] clusters, which function in electron transfer. The membrane-bound γ subunit (NarI, 30 kDa) functions to bind the $\alpha\beta$ complex to the membrane and to transfer electrons to the complex via two heme *b* groups (5, 6, 32). An additional (fourth) subunit, δ (NarJ, 26 kDa), has not been associated with any purified NR, but is assumed to function in the stabilization or in the assembly of the $\alpha\beta$ complex prior to interaction with the γ subunit (6, 35). The second NR is NRZ which is encoded by *narZYWV* and is also well characterized (9, 28, 41). Both NRA and NRZ have the same subunit composition, with similar molecular masses, and contain the same cofactors. In cells lacking NRA, NRZ catalyzes the same reaction with the same physiological substrates as electron donors (28). When both enzymes are present, it has been proposed that NRZ assists *E. coli* in the transition from an aerobic to an anaerobic metabolism. Interestingly, NRZ is constitutively expressed, while NRA needs anaerobiosis and the presence of nitrate to be expressed (9, 28). New contradictory evidence, however, indicates the expression of NRZ is highly dependent on growth phase and is stress-induced (12).

Comparison of the sequences of the genes that encode for the two NRs in *E. coli*, *narGHJI* and *narZYWV*, to the *P. aerophilum* genomic sequence reveals that there is only one copy of the *nar* operon in this organism, and that it shares a high identity and similarity with both NRs in *E. coli* (Table 5.1). The α (PAE3611) and β (PAE3612) subunits not only share a high similarity to NarGH (b1224, b1225) and NarZY (b1468, b1467), but the amino acid residues involved in binding the molybdenum ion and the cysteine residues coordinating the iron-sulfur clusters are also conserved in all three nitrate reductases (Fig. 3.13, Chapter 3). In addition, even though the γ subunit (PAE3614) exhibits a lower similarity with NarI (b1227) and NarV (b1465),

Table 5.1. Comparison of the genes encoding the respiratory nitrate reductases from *Escherichia coli* to the homologous genes in *Pyrobaculum aerophilum* and *Pyrococcus furiosus*.

<i>E. coli</i>		<i>P. aerophilum</i>				<i>P. furiosus</i>			
Gene Symbol	Locus	Locus	identity/ similarity (%)	% of aa analyzed	Annotation	Locus	identity/ similarity (%)	% of aa analyzed	Annotation
<i>narG</i>	b1224	PAE3611	47 / 63	100	NR α , NarG	PF1242	22 / 35	23	dehydrogenase subunit α
<i>narZ</i>	b1468	PAE3611	46 / 63	100	NR α , NarG				
<i>narH</i>	b1225	PAE3612	54 / 71	89	NR β , NarH	PF1479	31 / 48	21	putative OR, Fe-S subunit
<i>narY</i>	b1467	PAE3612	53 / 68	91	NR β , NarH				
<i>narI</i>	b1227	PAE2614	28 / 45	87	NR γ , NarI	PF1055	31 / 51	23	Threonine synthase
<i>narV</i>	b1465	PAE2614	26 / 43	87	NR γ , NarI				
<i>narJ</i>	b1226	PAE3610	28 / 45	72	NR δ , NarJ	PF0733	18 / 45	36	putative ABC
<i>narW</i>	b1466	PAE3610	26 / 47	74	NR δ , NarJ				

the His ligands of both hemes found in this subunit are conserved. The lower similarity between the γ and δ subunits (PAE3610 and b1226, b1466) of the enzymes is reflective of their involvement in binding the proteins to the membranes highlighting the differences between the ester-linked fatty acid membranes of bacteria and the ether-linked phospholipids and isoprenoids in archaeal membranes. Overall, even though *P. aerophilum* is a hyperthermophilic archaeon, its respiratory NR is very remarkably similar to that of the mesophilic bacteria, *E. coli*.

P. furiosus does not respire nitrate, so it was not surprising that it contained no close homologs of NR, and only a small portion of the sequences identified contained any similarity at all (Table 5.1). The homolog identified in *P. furiosus* to NarG and NarZ is annotated as an α dehydrogenase subunit (PF1242), and to NarH and NarY is a putative oxidoreductase containing an iron-sulfur cluster (PF1479). As shown in Table 5.2, both of the subunits encoded by these genes are more similar to FDH subunits. The high similarity between NR and FDH, which are both members of the DMSO Reductase family of molybdoenzymes, accounts for this identification as possible homologs in BLAST searches for both of these enzymes (15, 33).

In *E. coli* there are three genetically-distinct FDH isozymes that have been identified (18, 64, 65). Two are membrane associated, FDH-N is produced by nitrate and anaerobic conditions; and FDH-O is synthesized when cells are grown in the presence of oxygen or nitrate. FDH-N forms a formate-nitrate respiratory chain with NRA, and FDH-O is thought to form a formate-nitrate respiratory chain with NRZ (55, 65). The third FDH is a soluble enzyme, FDH-H, that is produced during fermentation and is a component of the formate-hydrogenlyase pathway.

E. coli FDH-N is encoded by *fdnGHI* and the purified enzyme consists of three subunits in the ratio of $\alpha_4\beta_4\gamma_2$. It has a total molecular weight of 608 kDa ($\alpha=112$ kDa, $\beta=32$ kDa and $\gamma=25$ kDa) (15). The α subunit (b1474), which is the site of formate oxidation, contains a

molybdopterin cofactor, Se in the form of selenocysteine, and a [4Fe-4S] cluster. The β subunit (b1475) functions in electron transfer and contains four [4Fe-4S] clusters, while γ subunit (b1476) contains two heme *b* groups and is the site of menaquinone reduction (34). Much less is known biochemically about the FDH-O isozyme, which is encoded by *fdoGHI* (b3894, b3893, b3892). It was reported to be structurally very similar to FDH-N (64). The molecular weights of its subunits (α =112 kDa, β =33 kDa and γ =24 kDa) are also very similar to those of FDH-N (54). FDH-O is produced in aerobically-grown cells, and catalyzes the oxidation of formate where oxygen is the terminal electron acceptor of the respiratory chain. It is also synthesized during nitrate respiration by *E. coli* (65), and is thought to transfer electrons to the quinone pool (55, 65).

The formate hydrogenlyase (FHL) system is present in *E. coli* during fermentative growth under anaerobic conditions. The FHL pathway consists of FDH-H, a hydrogenase (HYD3) and two electron carriers (64). The synthesis of FDH-H, which oxidizes formate to carbon dioxide (64), is repressed by the presence of the exogenous electron acceptors oxygen and nitrate (13). FDH-H is encoded by *fdhF* (b4079), and is a 79 kDa enzyme that contains a Mo ion coordinated by two molybdopterin guanine dinucleotide (MGD) cofactors, as well as a [4Fe-4S] cluster, and a selenocysteine residue (3, 68, 75).

Comparison of the sequences of the genes that encode for the three FDHs in *E. coli*, *fdnGHI*, *fdoGHI*, and *fdhF* to the *P. aerophilum* genome sequence reveals that there is only one copy of the operon encoding FDH in this organism (Table 5.2). The highest similarity of the *P. aerophilum* α (PAE2662), β (PAE2661) and γ (PAE2660) subunits is to FDH-N, although there is also a high identity and similarity to FDH-O. The amino acid residues involved in binding the molybdenum ion and the selenocysteine, as well as the cysteine residues coordinating the iron-

Table 5.2. Comparison of the genes encoding the formate dehydrogenases from *Escherichia coli* to the homologous genes in *Pyrobaculum aerophilum* and *Pyrococcus furiosus*.

<i>E. coli</i>		<i>P. aerophilum</i>				<i>P. furiosus</i>			
Gene Symbol	Locus	Locus	identity/ similarity (%)	% of aa analyzed	Annotation	Locus	identity/ similarity (%)	% of aa analyzed	Annotation
<i>fdnG</i>	b1474	PAE2662	28 / 41	87	FDH α subunit	PF1521	28 / 42	50	FDH α chain
<i>fdoG</i>	b3894	PAE2662	26 / 39	71	FDH α subunit				
<i>fdnH</i>	b1475	PAE2661	39 / 50	70	FDH β subunit	PF1479	27 / 37	40	putative OR, Fe-S subunit
<i>fdoH</i>	b3893	PAE2661	34 / 46	84	FDH β subunit				
<i>fdnI</i>	b1476	PAE2660	15 / 13	100	Hypothetical	None			
<i>fdoI</i>	b3892	PAE2660	26 / 39	32	Hypothetical				
<i>fdhF</i>	b4079	PAE2662	27 / 45	53	FDH α subunit	PF1521	37 / 58	92	FDH α chain
						PF1242	24 / 43	81	dehydrogenase subunit α

sulfur clusters are conserved in the *P. aerophilum* FDH and in FDH-N and FDH-O (Fig. 4.8, Chapter 4). In addition, the His ligands of both hemes found in the γ subunit are conserved. As in the case with NR, the γ subunit exhibits a lower similarity with *fdnI* and *fdoI* due to its role as the integral membrane component of the enzyme. The identity and similarity of FDH α in *P. aerophilum* to FDH-H in *E. coli* is much lower than that of the α subunits of FDH-N and FDH-O. In contrast, the *P. furiosus* genome encodes a protein (PF1521) that is quite similar (58 %) to the FDH-H enzyme, and over a significant part (92 %) of the protein (Table 5.2). The identification of PF1521 as a homolog to FDH-N α and FDH-O α , although less than to FDH-H, has a similarity of 42 %, over 50 % of the protein, this is due in part to the cysteine residues that coordinate the [4Fe-4S] cluster in the α subunits. Similarly, PF1479, which is a 19 kDa protein is identified as a homolog to the β subunits of the respiratory FDHs due to the cysteine residues that coordinate the 4Fe-4S ferridoxin-type proteins.

Thus, the FDH in *P. aerophilum* is homologous to the membrane-bound respiratory FDHs in *E. coli*, and it also participates in the formate-nitrate respiration chain. The putative FDH (PF1521) in *P. furiosus* is predicted to function like FDH-H of *E. coli*, where it is a cytoplasmic fermentative enzyme, and further has no homolog of the membrane component (γ subunit) of the respiratory FDH enzymes. The prediction of similarity to FDH-H, rather than to the respiratory FDHs is expected as *P. furiosus* grows optimally with sugars and peptides as carbon and energy sources (16). Furthermore, like *P. aerophilum*, *P. furiosus* is dependent upon W for growth. Although the FDH from *P. furiosus* has not been purified or characterized, it is likely that it is a W-containing enzyme, and as such, is similar to the formate dehydrogenase from the mesophilic bacteria *Desulfovibrio gigas*. The *D. gigas* FDH is a tungsten-containing heterodimer of 110 and 24 kDa subunits. Furthermore, the large subunit (α) is homologous to *E.*

coli FDH-H and contains the W site and one [4Fe-4S] cluster (57). The structural homology of *D. gigas* with *E. coli* FDH-H shows that the residues essential for activity (SeCys158, His159, and Arg407 in *D. gigas*, and SeCys140, His141, and Arg333 in *E. coli* (10)) at the active site are conserved (57), and alignments conducted here show that these residues are also conserved in *P. furiosus*.

Overall, as illustrated in Fig. 5.1, the α and β subunits of NR and FDH from *P. aerophilum* are closely related to the analogous subunits in *E. coli*. Furthermore, the phylogentic tree shows the similarity between the α subunits of NR and FDH, and also the similarity of the β subunits of NR and FDH. The FDH from *P. furiosus* is homologous to the FDH-H from *E. coli*, and a putative iron-sulfur protein shows homology to the β subunits of NR and FDH. Furthermore, the γ and δ subunits of *E. coli* NR, and the γ subunit from *E. coli* FDH are not highly homologous with the corresponding subunits in *P. aerophilum* and *P. furiosus* (Fig. 5.1), yet there is similarity between them in *E. coli*.

Aldehyde oxidoreductase-type enzymes. *P. aerophilum* and *P. furiosus* are both hyperthermophilic archaea, and are both dependent on W for growth. All of the aldehyde-oxidizing enzymes from *P. furiosus*, AOR, FOR, GAPOR, WOR4 and WOR5, are tungstoenzymes with a single type of subunit of ~ 70 kDa and have high sequence similarity (greater than 50%) (7, 46, 48, 61, 62). The enzymes differ, however, in quaternary structure. AOR, WOR4, and WOR5 are dimeric, FOR is tetrameric, and GAPOR exists as a monomer. Each of these enzymes contains a mononuclear tungsten atom coordinated by a bispterin cofactor, and a single [4Fe-4S] center in each subunit (31, 36), however sequence comparisons in WOR4 (61) and WOR5 (7) show only three cysteinyl residues coordinating the iron-sulfur

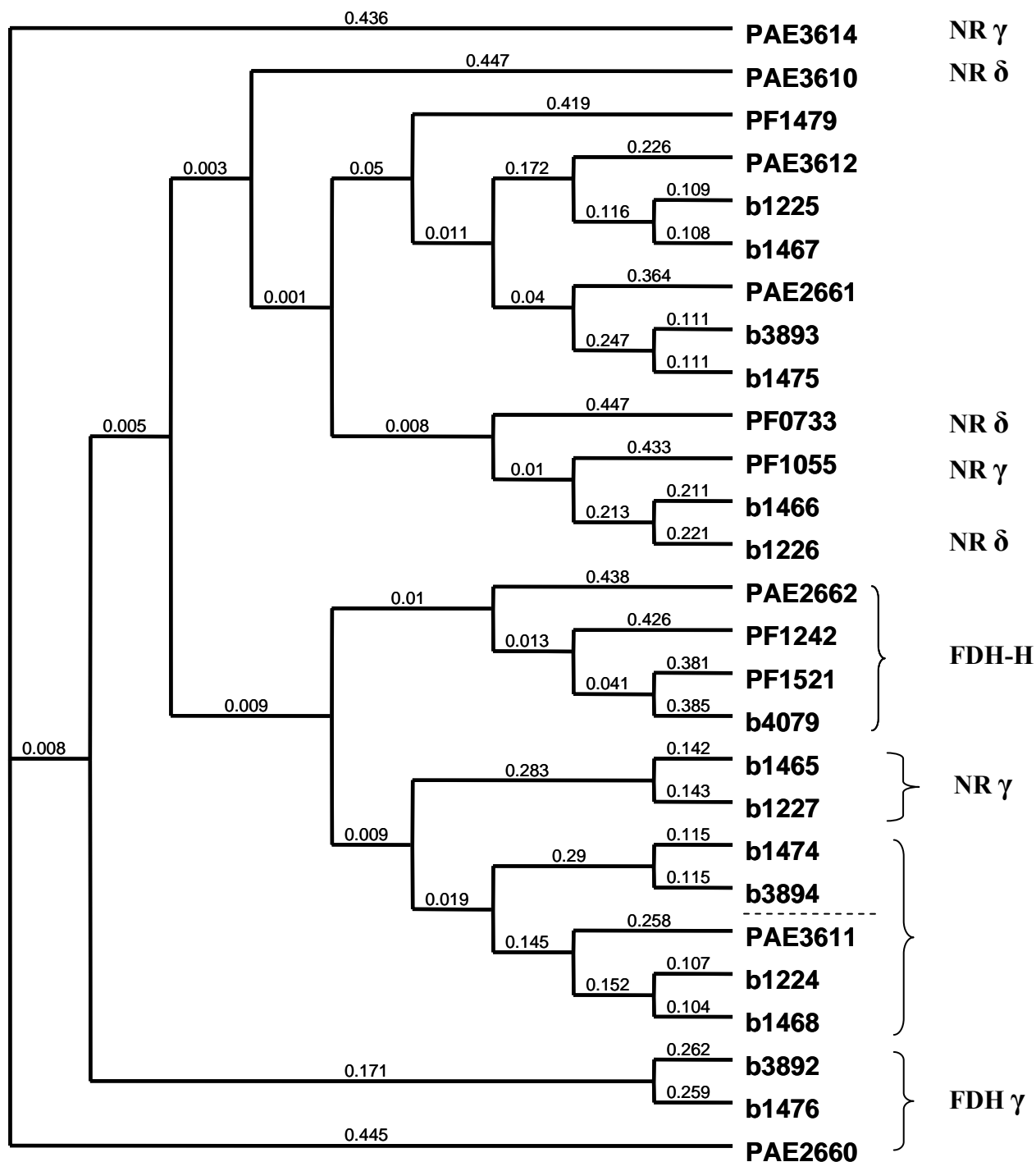


Fig. 5.1. Phylogenetic tree of nitrate reductase (NR) and formate dehydrogenase (FDH) subunits from *Escherichia coli* (loci designated b), *Pyrobaculum aerophilum* (loci designated PAE), and *Pyrococcus furiosus* (loci designated PF) as determined by genomic sequence analysis. The tree was constructed using MacVector (Accelrys Software Inc.) from sequences retrieved from the National Center for Biotechnology Information (NCBI) database (<http://www.ncbi.nlm.nih.gov/>). Bootstrap values are indicated at the branch points.

cluster, with a glycine residue replacing the fourth cysteine in WOR4, and an aspartate residue in WOR5. In both cases the implication is that of the presence of a [3Fe-4S] cluster, yet spectroscopic data indicates that of a [4Fe-4S] cluster (7, 61). Furthermore, in all of these tungstoenzymes (with the possible exception of WOR4), ferredoxin serves as the physiological electron acceptor (7, 31, 61).

AOR and FOR are thought to play a role in peptide fermentation, and have a broad substrate specificity, with AOR the most active on aldehydes derived from amino acids, and FOR the most active on aldehydes with one to three carbons (48, 62). On the other hand, the only known substrate for GAPOR is glyceraldehyde-3-phosphate, which it converts to 3-phosphoglycerate in an unusual Emden-Meyerhof glycolytic pathway (46). WOR4 may play a role in S° reduction, as the enzyme could not be purified from cells grown in the absence S° , however the specific function of this enzyme is unknown (61). WOR5 displays a broad substrate specificity like AOR and FOR, yet, it shows highest activity with hexanal, and based on activities and K_m values for the various aldehydes like crotonaldehyde used in AOR assays, and formaldehyde used in FOR assays, it is clearly distinguishable (7).

Activity assays conducted on the cytosolic fraction of *P. aerophilum* cells confirm the presence of enzymes with activities like AOR, FOR and GAPOR (Chapter 2). AOR was recently purified from *P. aerophilum* (21), and is the first AOR characterized from the crenarchaeota. AOR from *P. aerophilum* shares a similar size (68.3 kDa) and substrate specificity to the *P. furiosus* AOR. In addition, the AOR from *P. aerophilum* contains a [4Fe-4S] cluster and a W ion. The EPR properties of the enzyme are similar to those of *P. furiosus* AOR (21, 48). However, the specific activity of *P. aerophilum* AOR was approximately 5-fold lower than that in *P. furiosus*, which was measured with the same assay. An important

difference between the two enzymes is that in *P. aerophilum* a 7Fe ferredoxin (containing a [3Fe-4S] and [4Fe-4S]) is the redox partner for AOR, while the AOR in *P. furiosus* uses a 4Fe-ferredoxin as a redox partner (21, 48). Although both AORs are homodimers, the *P. aerophilum* AOR does not contain the mononuclear iron (or the EXXH sequence motif that coordinates the mononuclear iron) that is located at the subunit interface in *P. furiosus* AOR (PF0346). FOR (PF1203) and GAPOR (PF0464) from *P. furiosus* also do not have the EXXH motif, and WOR4 (PF1961) and WOR5 (PF1480) have this motif but at a different location, therefore, all may lack the subunit-bridging metal ion (GAPOR is a monomer). Furthermore, the consensus sequence of the pterin binding motifs in *P. furiosus* AOR is not highly conserved in *P. aerophilum* AOR (11, 21).

P. aerophilum contains four homologs of the AOR family. Although all four are annotated as AOR, there are specific homologs for AOR (PAE0622), FOR (PAE3427) and GAPOR (PAE1029) with 40 to 60% overall amino acid sequence similarity (Table 5.3). The fourth AOR homolog in *P. aerophilum*, PAE2052, has a sequence similarity of ~30% to WOR4 and WOR5 in *P. furiosus*. However, the homologs for AOR and FOR share a greater similarity than PAE2052 with these two enzymes (Fig. 5.2 and Table 5.3). Thus, it appears that there is a protein (PAE2052) in *P. aerophilum* belonging to the AOR family of tungstoenzymes that is different from those found in *P. furiosus*. The *E. coli* genome surprisingly contains one homolog to the AOR tungstoenzyme family, and is annotated as a predicted oxidoreductase. b1673 is approximately the same size (70 kDa) as the AOR family found in *P. furiosus*, and shares ~30% similarity with all of enzymes in the *P. furiosus* AOR family except for GAPOR (Table 5.3). Moreover, the motifs that coordinate the bispterin and the [4Fe-4S] cluster in *P. furiosus* AOR and FOR are conserved in the *E. coli* homolog.

Table 5.3. Comparison of the genes encoding the aldehyde-oxidizing enzymes in *Pyrococcus furiosus* to the homologous genes in *Pyrobaculum aerophilum* and *Escherichia coli*.

<i>P. furiosus</i>		<i>P. aerophilum</i>				<i>E. coli</i>			
Gene Symbol	Locus	Locus	identity/ similarity (%)	% of aa aligned	Annotation	Locus	identity/ similarity (%)	% of aa aligned	Annotation
<i>aor</i>	PF0346	PAE0622	45 / 60	95	AOR	b1673	28 / 42	95	predicted oxidoreductase
<i>for</i>	PF1203	PAE3427	57 / 70	96	AOR	b1673	27 / 43	96	predicted oxidoreductase
<i>gor</i>	PF0464	PAE1029	38 / 55	90	AOR	b1673	25 / 40	25	predicted oxidoreductase
<i>wor4</i>	PF1961	PAE3427	36 / 55	93	AOR	b1673	27 / 43	96	predicted oxidoreductase
		PAE0622	34 / 51	92	AOR				
		PAE2052	32 / 50	84	AOR				
<i>wor5</i>	PF1480	PAE3427	35 / 52	74	AOR	b1673	27 / 43	96	predicted oxidoreductase
		PAE0622	32 / 48	74	AOR				
		PAE2052	30 / 45	78	AOR				

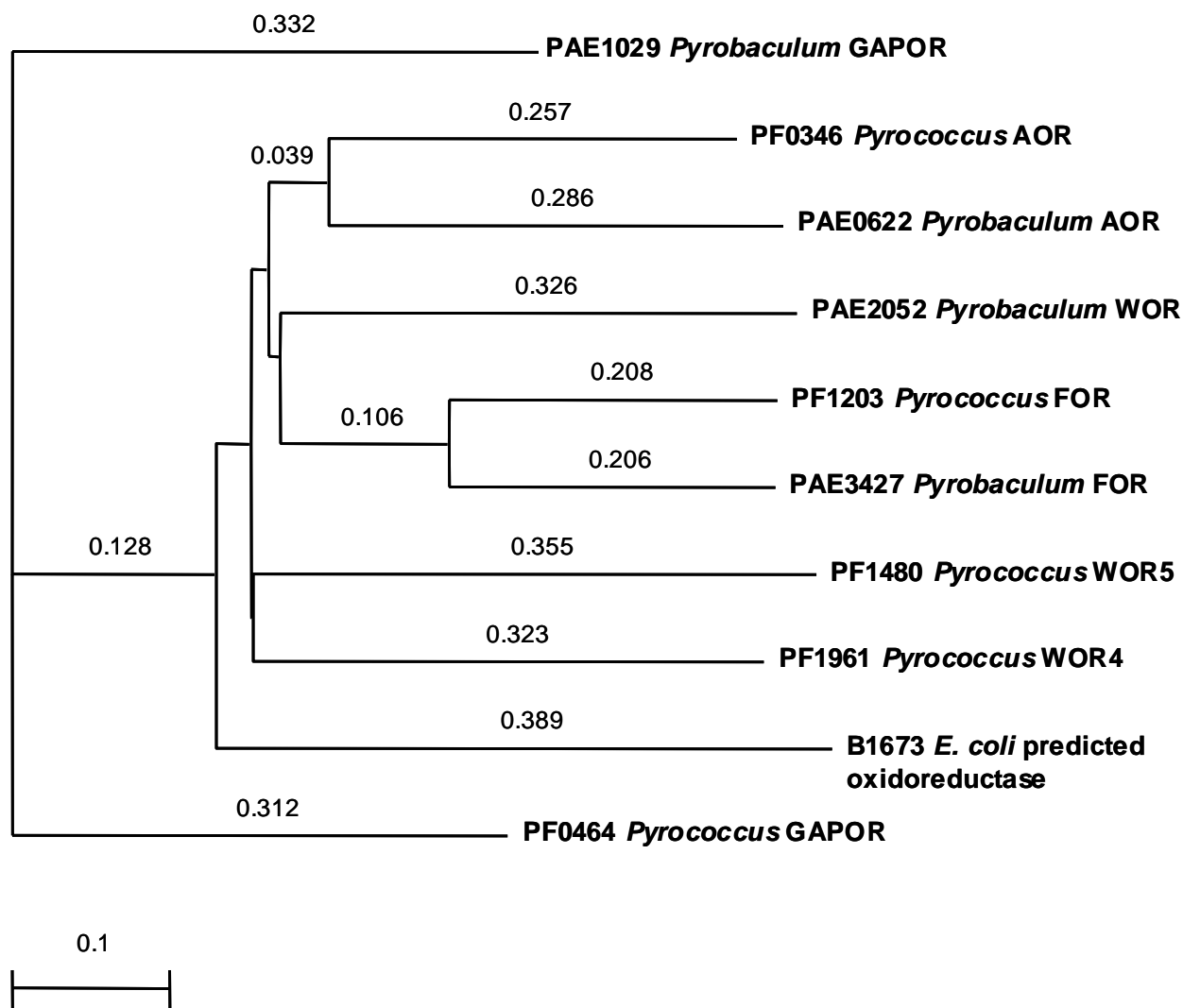


Fig. 5.2. Phylogenetic tree of the AOR family of tungstoenzymes from *Escherichia coli* (loci designated b), *Pyrobaculum aerophilum* (loci designated PAE), and *Pyrococcus furiosus* (loci designated PF) as determined by genomic sequence analysis. The tree was constructed using MacVector (Accelrys Software Inc.) from sequences retrieved from the National Center for Biotechnology Information (NCBI) database (<http://www.ncbi.nlm.nih.gov/>). Bootstrap values are indicated at the branch points. The bar indicates a branch length equivalent of 0.1 changes per amino acid.

Pterin cofactor biosynthesis, metal uptake and transport. Mo and W found in enzymes that catalyze two electron redox reactions, like those discussed here, are coordinated to an organic cofactor, molybdopterin (MPT), with the exception of nitrogenase. The Mo-cofactor, or Moco is the complex of Mo bound to MPT (58).

Most of the information on Moco biosynthesis is derived from initial studies using the chlorate resistant mutant strains (*chl*) in *E. coli* (70), which are now referred to as the *mo* mutants and Mo. gene products. Chlorate resistant mutants that are deficient in nitrate reductase activity survive in a chlorate medium. Chlorate is an analog for nitrate, and therefore serves as a substrate for nitrate reductase, however reduction to chlorite is lethal to the cell (70). A single mutation in the chlorate resistance strains affects a common component of all molybdoenzyme activity in the cell, which is the Mo-cofactor (70). Thus the pleiotropic loss of activities of molybdoenzymes in the chlorate resistance mutants of *E. coli* suggest that the mutant cells are defective in the biosynthesis of the Mo-cofactor, that is required by these enzymes (29).

The Moco biosynthetic pathway is highly conserved throughout all of the kingdoms, and in *E. coli* consists of five operons, *moa*, *mob*, *mod*, *moe* and *mog*, which include approximately fifteen genes that are specific to Moco biosynthesis. For all organisms studied so far, this conserved pathway can be divided into three steps. In the first step, a guanosine nucleotide is converted into the first stable intermediate in the biosynthetic pathway, precursor Z through the action of MoaA and MoaC (73). The second step, the conversion of precursor Z into MPT dithiolate, is accomplished by the addition of two sulfur atoms that is catalyzed by MPT synthase. MPT synthase, previously known as the converting factor, is heterotetrameric complex of Moad and Moae (52, 53). MoeB is also required in this step, as it functions to catalyze the transfer of sulfur to Moad shifting it from an inactive to an active enzyme (37, 52). *P.*

aerophilum and *P. furiosus* contain homologs to all of the enzymes involved in the first two steps of the Moco biosynthetic pathway, with similarities in their amino acid sequences from 30 to almost 50% (Table 5.4). It seems that both of these organisms share the same machinery in the initial steps of this highly conserved pathway. Besides those mentioned, *P. aerophilum* has additional homologs to MoaA and MoaC, it is difficult to speculate why the organism would need two sets of enzymes to form precursor Z, yet it is most likely that the similarity between the two sequences relates to a different use in a different synthetic pathway. However, it is possible that they are expressed under different conditions, or utilized in a highly specific way (Table 5.4). *P. furiosus* also has an additional homolog to MoaA and two homologs to MoeB. It is not known if *P. furiosus* requires all three of these subunits of the MPT synthase in order to transfer sulfur to MPT, but is highly possible that the homologs perform similar function in other biosynthetic pathways, such as the thiamine biosynthetic pathway.

In the third step of the pterin biosynthetic pathway in *E. coli*, Mo is inserted and coordinated into the MPT. MoeA and MogA are necessary for the incorporation of Mo (22, 49, 63). MoeA may be a thiolmolybdenum compound and donate the Mo ion during Moco production, and MogA serves as the molybdochelataase (22). ModA, B and C are required for the acquisition and transport of Mo into the cell (20). ModABC are all membrane proteins, so it is expected that the overall sequence similarity between the homologs from *P. aerophilum* and *P. furiosus* would be less than that of cytosolic proteins given the different nature of the membranes between bacteria and archaea. These homologs share an amino acid sequence similarity of ~30% to *E. coli* (Table 5.4). ModC is an ABC transporter, and most likely functions the same in

Table 5.4. Comparison of *Escherichia coli* molybdopterin biosynthetic genes, molybdenum uptake and molybdenum transport genes to homologs in *Pyrobaculum aerophilum* and *Pyrococcus furiosus*.

Pterin Biosynthesis									
<i>E. coli</i>		<i>P. aerophilum</i>				<i>P. furiosus</i>			
Gene Symbol	Locus	Locus	identity/ similarity (%)	% of aa aligned	Annotation	Locus	identity/ similarity (%)	% of aa aligned	Annotation
moaA	b0781	PAE0814	28 / 47	96	moaA metallo- Cofactor BP*	PF0090	31 / 51	84	moaA
		PAE0579	28 / 47	57		PF1454	25 / 46	52	Hypothetical
moaB	b0782	PAE0969	40 / 61	86	Mo-cofactor BP	PF0372	36 / 57	85	Mo-cofactor BP
moaC	b0783	PAE3581	33 / 46	75	Cons. Hypoth. Mo-cofactor BP	PF1854	46 / 65	83	Mo-cofactor BP
		PAE0799	28 / 44	75					
moaD	b0784	PAE2135	30 / 46	98	MPT converting factor subunit	PF0543	34 / 52	96	MPT converting factor subunit
						PF0345	28 / 42	99	MPT converting factor subunit
moaE	b0785	PAE0727	30 / 48	48	Mo-cofactor BP	PF0100	39 / 56	95	MPT converting factor subunit 2
moeB	b0826	PAE1056	34 / 51	98	MPT-BP moeB	PF0009	35 / 51	89	Mo-cofactor BP
						PF0003	26 / 45	72	moeB-like prot.
						PF1289	24 / 44	80	MPT-BP moeB

* BP is biosynthetic protein

Metal incorporation									
<i>E. coli</i>		<i>P. aerophilum</i>				<i>P. furiosus</i>			
Gene Symbol	Locus	Locus	identity/ similarity (%)	% of aa aligned	Annotation	Locus	identity/ similarity (%)	% of aa aligned	Annotation
mog	b0009	PAE0969	38 / 58	50	Mo-cofactor BP	PF0372	28 / 52	84	Mo-cofactor BP
moeA	b0827	PAE3465	35 / 53	87	Mo-cofactor BP	PF0542	33 / 51	88	Mo-cofactor BP
		PAE3466	31 / 45	95	Mo-cofactor BP	PF1783	30 / 48	96	Mo-cofactor BP
Molybdenum Transport									
modA	b0763	PAE3569	30 / 47	25	Hypothetical	PF1394	31 / 51	27	Phospho- glycerate DH
modB	b0764	PAE0062	27 / 38	63	Mo transport permease	PF1520	29 / 44	59	ABC transporter sulfate/ thiosulf. transport-like protein
						PF0081	36 / 53	41	
modC	b0765	PAE1222	31 / 48	80	ATP-BP, ABC transporter	PF0082	30 / 50	94	membrane protein/ ABC transporter
GMP Attachment									
mobA	b3857	PAE3453	33 / 51	72	MGD BP-A	PF0618	27 / 49	93	MGD BP
mobB	b3856	PAE1934	28 / 45	72	Hypothetical	PF0300	26 / 51	51	Hypothetical
		PAE1759	28 / 44	73	MGD BP-B	PF1134	21 / 39	81	Hypothetical

P. aerophilum and *P. furiosus* as it does in *E. coli*. ModA is periplasmic binding protein, and ModB is a membrane channel transport protein. While the homologous proteins from the three organisms probably perform the same function, small differences between the hyperthermophilic homologs and the mesophilic proteins would not be surprising given the preference for WO_4^{2-} over MoO_4^{2-} in hyperthermophiles. In *E. coli*, Moco is synthesized constitutively, and is synthesized in the absence of Mo, and when the FDH-NR respiration pathway is not induced (2). Furthermore, *E. coli* cells grown on Mo-deficient media synthesized a cofactor lacking Mo (an empty cofactor), and cells grown with WO_4^{2-} added to this media led to the accumulation of W-containing cofactor. Both the empty cofactor and the W-containing cofactor form an intact but inactive NR. NR activity could be restored by the addition of molybdate (2). Furthermore, the mechanism by which WO_4^{2-} and MoO_4^{2-} were taken up and incorporated by *P. aerophilum* cells in the current study (Chapter 2) appears not to discriminate between the two oxyanions. Perhaps, as in *E. coli*, the molybdate transporter of *P. aerophilum* binds MoO_4^{2-} and WO_4^{2-} with similar affinities (26) and uptake is dependent on the concentration of the oxyanion in the medium. Based on the measured intracellular concentrations, there does appear to be a greater demand for W in *P. aerophilum* cells, however. When both oxyanions were present in the medium or when only WO_4^{2-} was present, the intracellular concentration of W was much higher than that of Mo. Only when MoO_4^{2-} was the sole oxyanion added to the medium were concentrations of Mo and W approximately the same. In *E. coli*, cells can accumulate up to thirty times more Mo than is present in the medium. Furthermore, cells grown in the absence of MoO_4^{2-} can accumulate levels of WO_4^{2-} up to six times greater than the normal physiological concentration of MoO_4^{2-} (69). This is possible because *modABC* is repressed by the *modE* gene product. *modE* is activated by MoO_4^{2-} , and is six times less sensitive to WO_4^{2-} (19). *C. thermoaceticum* was also

found to concentrate W intracellularly (74). In *P. furiosus*, however, it is not known if the molybdate transporter binds MoO_4^{2-} and WO_4^{2-} with similar affinities. It is known that Mo was not incorporated into the active-sites of AOR, FOR or GAPOR (47). It is possible that *P. furiosus* contains a transporter that is specific for tungstate uptake, as is found in *Eubacterium acidaminophilum* (39). This cytoplasmic binding protein, TupA, shows specificity for tungstate. *E. acidaminophilum*, a mesophilic bacteria, does not require W for growth. Two enzymes in this organism, however, FDH-H and aldehyde dehydrogenase, are dependent upon W for activity (39). TupA has a sequence similarity of 48% to a solute-binding protein in *C. thermoaceticum*, which also has a W-containing soluble FDH. In *P. furiosus*, two homologs (PF1017 and PF1454), which are annotated as hypothetical proteins, share 30 and 40% sequence similarity with TupA, although only 10% of the total amino acids were analyzed for similarity. PAE0200, annotated as a putative binding protein, is a TupA homolog with 39% sequence similarity. MoeA and MogA, responsible for incorporation of Mo into the MPT, have homologs in *P. aerophilum* and *P. furiosus* with ~ 30% sequence similarity (Table 5.4). Interestingly, the Mog homologs, PAE0969 and PF0372, are the same as those for MoaB. MoaB is similar in structure to MogA (4). MogA, a molybdochelatease, is required for active NR, but not for FDH-H in *E. coli* (22). This is interesting in considering possible roles for MoaB or MogA in *P. aerophilum* and *P. furiosus*, since both of these organisms contain only one functional homolog of these two enzymes, and that *P. aerophilum* respire with NR, and *P. furiosus* contains a FDH-H, which is likely a W-containing enzyme. It seems that the differences in the transport and biosynthetic proteins are conserved enough for similar structure and function between the three organisms, yet also different enough to be organism and environmentally specific.

The biosynthesis of the molybdenum cofactor can be considered complete once the metal is incorporated into the pterin (40). In prokaryotes, however, there is a fourth step, which is the maturation of Moco by further modifications which are necessary before the cofactor is inserted into the apoenzyme and the cofactor is able to promote catalysis. For example, in bacteria a nucleotide is often attached, which is the case for NR and FDH and other members of the DMSO reductase family of enzymes. In these cases, a guanine is attached and forms the MGD cofactor (29, 42). Interestingly, the nucleotide can only be added to the MPT after the Mo is inserted (49). In addition to this modified MPT, MGD, most of the molybdoenzymes require a *bis*-MGD cofactor where the Mo atom is coordinated by four dithiolenes of two MGD molecules (5, 10, 32, 33). The requirement of the bispterin is also found in tungstoenzymes such as AOR from *P. furiosus* (11), but there is no nucleotide attached to AOR or FOR (30). In *E. coli*, the attachment of guanine is the most common, but other modifications in bacterial molybdoenzymes include the attachment of cytosine as in the case with carbon-monoxide dehydrogenases (CODH), which forms a mono-MCD cofactor (14). CODH is a member of the molybdenum hydroxylase family, which also includes xanthine oxidase, and these enzymes have only one cofactor attached to the Mo. A review of the Mo and W families of enzymes can be found in Chapter 1.

The *mob* operon in *E. coli* contains two genes, *mobA* and *mobB*, and these gene products are responsible for the attachment of the nucleotide. MobA catalyzes the conversion of MPT and GTP to MGD (27, 50). The role of MobB is not as well established, but it is known that although MobB is not essential for MGD synthesis or activation, its presence results in increased yields of active NR in *E. coli* (50). MobA and B homologs in *P. aerophilum* have ~30% amino acid sequence similarity to *E. coli* (Table 5.4), and the NR from *P. aerophilum* is expected to contain a *bis*-MGD cofactor (Fig. 3.14, Chapter 3). On the other hand, the tungstoenzymes from

P. furiosus do not contain the nucleotide form of MPT (30), yet homologs to MobA and b have ~25% amino acid sequence similarity to *E. coli* (Table 5.4).

After synthesis and maturation, the cofactor needs to be inserted into the proper apoenzymes. In *E. coli* several studies have indicated that Moco (MGD) is transferred or stored by carrier proteins rather than being directly transferred from the Moco biosynthetic machinery (2, 71). The production and storage of the Moco biosynthetic and delivery machinery enables *E. coli* to easily respond to high demands of mature Moco (71), and the association of a carrier protein helps to stabilize the labile cofactor (2).

In the final stages of the Moco biosynthetic pathway, i.e., the incorporation of Moco into the apomolybdoenzyme, there is a high amount of protein-protein interaction that occurs between the *mo* gene products, which is critical as it creates a functional cooperation between the Moco machinery and the apomolybdoenzyme (2, 8, 38, 49, 60, 71). For example, MogA and MoeA form a complex, which can only occur in the presence of MPT, in forming active Moco through the chelation of molybdenum by MPT (38, 49). Furthermore, it is thought that this MogA-MoeA complex delivers Mo-MPT to MobA forming a transient pairwise complex between MoeA and MobA in order for nucleotide attachment, and also for MGD transfer to the apomolybdoenzymes (38). MobB also interacts with several of the Mo. proteins and may also function to facilitate insertion of Moco through pairwise complexes (38). Other protein-protein interactions which facilitate Moco incorporation involve carrier proteins and Moco, and enzyme-specific chaperones. First noted in *E. coli* NarGHI, the NarJ chaperone is required in order for the *mo* gene products to interact with Nar G (49, 60, 71) as it functions to hold cofactor-deficient NarGH in a cofactor-binding conformation (8). Other chaperones have also been identified, such

as TorD in the maturation of trimethylamine-*N*-oxide reductase (56). A final example is the aforementioned carrier protein that associates with Moco in a stabilizing manner (2).

It appears, therefore, that Moco biosynthesis occurs on protein complexes rather than by individual *mo* gene products. These complexes also appear to protect the transfer of the oxygen-sensitive intermediates from MPT to active Moco to the apomolybdoenzyme (38). Although the highly conserved Moco biosynthetic pathway has been extensively studied, there is much more to be uncovered, such as the cooperation between the Moco machinery, the chaperones, the apomolybdoenzymes and the complexes that they form in archaea, bacteria plants, and animals.

CONCLUSIONS

P. aerophilum shares many similarities with mesophilic bacteria such as *E. coli* as shown by its homologous FDH and NR, which form the formate-nitrate respiratory pathway. Furthermore, as both *P. aerophilum* and *P. furiosus* are hyperthermophilic archaea, there is extensive similarity in the oxidoreductase type enzymes that each organism contains, specifically, the AOR family of tungstoenzymes. The highly conserved Moco biosynthetic pathway which produces the cofactor necessary for activity in all of these enzymes is also present in *P. aerophilum* based on genomic comparisons. There are differences, however, which are most likely responsible for the ability of *P. aerophilum* to utilize Mo in the active sites of its enzymes, as in *E. coli*, and also to utilize W, as in *P. furiosus*. Thus, *P. aerophilum* seems to be a hybrid or transitional microorganism with respect to its phylogeny, physiology and biochemistry of Mo and W.

REFERENCES

1. **Afshar, S., C. Kim, H. G. Monbouquette, and I. Schroder.** 1998. Effect of tungstate on nitrate reduction by the hyperthermophilic archaeon *Pyrobaculum aerophilum*. *Appl. Environ. Microb.* **64**:3004-3008.
2. **Amy, N. K., and K. V. Rajagopalan.** 1979. Characterization of molybdenum cofactor from *Escherichia coli*. *J Bacteriol* **140**:114-24.
3. **Axley, M. J., D. A. Grahame, and T. C. Stadtman.** 1990. *Escherichia coli* formate-hydrogen lyase. Purification and properties of the selenium-dependent formate dehydrogenase component. *J Biol Chem* **265**:18213-8.
4. **Bader, G., M. Gomez-Ortiz, C. Haussmann, A. Bacher, R. Huber, and M. Fischer.** 2004. Structure of the molybdenum-cofactor biosynthesis protein MoaB of *Escherichia coli*. *Acta Crystallogr D Biol Crystallogr* **60**:1068-75.
5. **Bertero, M. G., R. A. Rothery, N. Boroumand, M. Palak, F. Blasco, N. Ginet, J. H. Weiner, and N. C. Strynadka.** 2005. Structural and biochemical characterization of a quinol binding site of *Escherichia coli* nitrate reductase A. *J Biol Chem* **280**:14836-43.
6. **Bertero, M. G., R. A. Rothery, M. Palak, C. Hou, D. Lim, F. Blasco, J. H. Weiner, and N. C. Strynadka.** 2003. Insights into the respiratory electron transfer pathway from the structure of nitrate reductase A. *Nat Struct Biol* **10**:681-7.
7. **Bevers, L. E., E. Bol, P. L. Hagedoorn, and W. R. Hagen.** 2005. WOR5, a novel tungsten-containing aldehyde oxidoreductase from *Pyrococcus furiosus* with a broad substrate specificity. *J Bacteriol* **187**:7056-61.

8. **Blasco, F., J. P. Dos Santos, A. Magalon, C. Frixon, B. Guigliarelli, C. L. Santini, and G. Giordano.** 1998. NarJ is a specific chaperone required for molybdenum cofactor assembly in nitrate reductase A of *Escherichia coli*. *Mol Microbiol* **28**:435-47.
9. **Bonnefoy, V., and J. A. Demoss.** 1994. Nitrate reductases in *Escherichia coli*. *Antonie Van Leeuwenhoek* **66**:47-56.
10. **Boyington, J., V. Gladyshev, S. Khangulov, T. Stadtman, and P. Sun.** 1997. Crystal structure of formate dehydrogenase H: catalysis involving Mo, molybdopterin, selenocysteine, and an Fe₄S₄ cluster. *Science* **275**:1305-8.
11. **Chan, M. K., S. Mukund, A. Kletzin, M. W. Adams, and D. C. Rees.** 1995. Structure of a hyperthermophilic tungstopterin enzyme, aldehyde ferredoxin oxidoreductase. *Science* **267**:1463-9.
12. **Chang, L., L. I. Wei, J. P. Audia, R. A. Morton, and H. E. Schellhorn.** 1999. Expression of the *Escherichia coli* NRZ nitrate reductase is highly growth phase dependent and is controlled by RpoS, the alternative vegetative sigma factor. *Mol Microbiol* **34**:756-66.
13. **Cox, J. C., E. S. Edwards, and J. A. DeMoss.** 1981. Resolution of distinct selenium-containing formate dehydrogenases from *Escherichia coli*. *J Bacteriol* **145**:1317-24.
14. **Dobbek, H., and R. Huber.** 2002. The molybdenum and tungsten cofactors: a crystallographic view. *Met Ions Biol Syst.* **39**:227-63.
15. **Enoch, H. G., and R. L. Lester.** 1975. The purification and properties of formate dehydrogenase and nitrate reductase from *Escherichia coli*. *J Biol Chem* **250**:6693-705.

16. **Fiala, G., and K. O. Stetter.** 1986. *Pyrococcus furiosus* sp-nov represents a novel genus of marine heterotrophic archaeobacteria growing optimally at 100-degrees C. Arch. Microbiol. **145**:56-61.
17. **Giordano, G., B. A. Haddock, and D. H. Boxer.** 1980. Molybdenum-limited growth achieved either phenotypically or genotypically and its effect on the synthesis of formate dehydrogenase and nitrate reductase by *Escherichia coli* K12. FEMS Microbiol Lett **8**:229-235.
18. **Giordano, R., C. L. Medani, M. A. Mandrand-Berthelot, and D. H. Boxer.** 1983. Formate dehydrogenases from *E. coli*. FEMS Microbiol Lett **17**:171-177.
19. **Grunden, A. M., W. T. Self, M. Villain, J. E. Blalock, and K. T. Shanmugam.** 1999. An analysis of the binding of repressor protein ModE to *modABCD* (molybdate transport) operator/promoter DNA of *Escherichia coli*. J Biol Chem **274**:24308-15.
20. **Grunden, A. M., and K. T. Shanmugam.** 1997. Molybdate transport and regulation in bacteria. Arch Microbiol **168**:345-54.
21. **Hagedoorn, P. L., T. Chen, I. Schroder, S. R. Piersma, S. de Vries, and W. R. Hagen.** 2005. Purification and characterization of the tungsten enzyme aldehyde:ferredoxin oxidoreductase from the hyperthermophilic denitrifier *Pyrobaculum aerophilum*. J Biol Inorg Chem **10**:259-69.
22. **Hasona, A., R. M. Ray, and K. T. Shanmugam.** 1998. Physiological and genetic analyses leading to identification of a biochemical role for the *moeA* (molybdate metabolism) gene product in *Escherichia coli*. J Bacteriol **180**:1466-72.
23. **Heider, J., K. Ma, and M. W. Adams.** 1995. Purification, characterization, and metabolic function of tungsten-containing aldehyde ferredoxin oxidoreductase from the

- hyperthermophilic and proteolytic archaeon *Thermococcus* strain ES-1. J. Bacteriol. **177**:4757-64.
24. **Hille, R.** 2002. Molybdenum and tungsten in biology. Trends Biochem. Sci. **27**:360-367.
 25. **Hille, R.** 2000. Molybdenum enzymes. Subcell Biochem **35**:445-85.
 26. **Imperial, J., M. Hadi, and N. K. Amy.** 1998. Molybdate binding by ModA, the periplasmic component of the *Escherichia coli* mod molybdate transport system. Biochim Biophys Acta. **1370**:337-46.
 27. **Iobbi-Nivol, C., T. Palmer, P. W. Whitty, E. McNairn, and D. H. Boxer.** 1995. The mob locus of *Escherichia coli* K12 required for molybdenum cofactor biosynthesis is expressed at very low levels. Microbiology **141** (Pt 7):1663-71.
 28. **Iobbi-Nivol, C., C. L. Santini, F. Blasco, and G. Giordano.** 1990. Purification and further characterization of the second nitrate reductase of *Escherichia coli* K12. Eur J Biochem **188**:679-87.
 29. **Johnson, J. L., L. W. Indermaur, and K. V. Rajagopalan.** 1991. Molybdenum cofactor biosynthesis in *Escherichia coli*. Requirement of the chlB gene product for the formation of molybdopterin guanine dinucleotide. J Biol Chem **266**:12140-5.
 30. **Johnson, J. L., K. V. Rajagopalan, S. Mukund, and M. W. Adams.** 1993. Identification of molybdopterin as the organic component of the tungsten cofactor in four enzymes from hyperthermophilic Archaea. J. Biol. Chem. **268**:4848-52.
 31. **Johnson, M. K., D. C. Rees, and M. W. W. Adams.** 1996. Tungstoenzymes. Chem. Rev. **96**:2817-2839.
 32. **Jormakka, M., D. Richardson, B. Byrne, and S. Iwata.** 2004. Architecture of NarGH reveals a structural classification of Mo-*bis*MGD enzymes. Structure (Camb) **12**:95-104.

33. **Jormakka, M., S. Tornroth, J. Abramson, B. Byrne, and S. Iwata.** 2002. Purification and crystallization of the respiratory complex formate dehydrogenase-N from *Escherichia coli*. *Acta Crystallogr D Biol Crystallogr* **58**:160-2.
34. **Jormakka, M., S. Tornroth, B. Byrne, and S. Iwata.** 2002. Molecular basis of proton motive force generation: structure of formate dehydrogenase-N. *Science* **295**:1863-8.
35. **Ketchum, P. A., G. Denariatz, J. LeGall, and W. J. Payne.** 1991. Menaquinol-nitrate oxidoreductase of *Bacillus halodenitrificans*. *J Bacteriol* **173**:2498-505.
36. **Kletzin, A., and M. W. Adams.** 1996. Tungsten in biological systems. *FEMS Microbiol. Rev.* **18**:5-63.
37. **Lake, M. W., M. M. Wuebbens, K. V. Rajagopalan, and H. Schindelin.** 2001. Mechanism of ubiquitin activation revealed by the structure of a bacterial MoeB-MoaD complex. *Nature* **414**:325-9.
38. **Magalon, A., C. Frixon, J. Pommier, G. Giordano, and F. Blasco.** 2002. In vivo interactions between gene products involved in the final stages of molybdenum cofactor biosynthesis in *Escherichia coli*. *J Biol Chem* **277**:48199-204.
39. **Makdessi, K., J. R. Andreesen, and A. Pich.** 2001. Tungstate uptake by a highly specific ABC transporter in *Eubacterium acidaminophilum*. *J. Biol. Chem.* **276**:24557-24564.
40. **Mendel, R. R., and R. Hansch.** 2002. Molybdoenzymes and molybdenum cofactor in plants. *J Exp Bot.* **53**:1689-98.
41. **Moreno-Vivian, C., P. Cabello, M. Martinez-Luque, R. Blasco, and F. Castillo.** 1999. Prokaryotic nitrate reduction: molecular properties and functional distinction among bacterial nitrate reductases. *J Bacteriol* **181**:6573-84.

42. **Moura, J. J., C. D. Brondino, J. Trincao, and M. J. Romao.** 2004. Mo and W bis-MGD enzymes: nitrate reductases and formate dehydrogenases. *J Biol Inorg Chem* **9**:791-9.
43. **Mukund, S.** 1995. Ph. D. Dissertation. University of Georgia, Athens, GA.
44. **Mukund, S., and M. W. W. Adams.** 1993. Characterization of a novel tungsten-containing formaldehyde ferredoxin oxidoreductase from the hyperthermophilic archaeon, *Thermococcus litoralis*. A role for tungsten in peptide catabolism. *J. Biol. Chem.* **268**:13592-600.
45. **Mukund, S., and M. W. W. Adams.** 1990. Characterization of a tungsten-iron-sulfur protein exhibiting novel spectroscopic and redox properties from the hyperthermophilic archaeobacterium *Pyrococcus furiosus*. *J. Biol. Chem.* **265**:11508-16.
46. **Mukund, S., and M. W. W. Adams.** 1995. Glyceraldehyde-3-phosphate ferredoxin oxidoreductase, a novel tungsten-containing enzyme with a potential glycolytic role in the hyperthermophilic archaeon *Pyrococcus furiosus*. *J. Biol. Chem.* **270**:8389-92.
47. **Mukund, S., and M. W. W. Adams.** 1996. Molybdenum and vanadium do not replace tungsten in the catalytically active forms of the three tungstoenzymes in the hyperthermophilic archaeon *Pyrococcus furiosus*. *J. Bacteriol.* **178**:163-7.
48. **Mukund, S., and M. W. W. Adams.** 1991. The novel tungsten-iron-sulfur protein of the hyperthermophilic archaeobacterium, *Pyrococcus furiosus*, is an aldehyde ferredoxin oxidoreductase. Evidence for its participation in a unique glycolytic pathway. *J. Biol. Chem.* **266**:14208-16.

49. **Nichols, J., and K. V. Rajagopalan.** 2002. *Escherichia coli* MoeA and MogA. Function in metal incorporation step of molybdenum cofactor biosynthesis. *J Biol Chem* **277**:24995-5000.
50. **Palmer, T., A. Vasishta, P. W. Whitty, and D. H. Boxer.** 1994. Isolation of protein FA, a product of the mob locus required for molybdenum cofactor biosynthesis in *Escherichia coli*. *Eur J Biochem* **222**:687-92.
51. **Philippot, L., and O. Hojberg.** 1999. Dissimilatory nitrate reductases in bacteria. *Biochim Biophys Acta* **1446**:1-23.
52. **Pitterle, D. M., J. L. Johnson, and K. V. Rajagopalan.** 1993. In vitro synthesis of molybdopterin from precursor Z using purified converting factor. Role of protein-bound sulfur in formation of the dithiolene. *J Biol Chem* **268**:13506-9.
53. **Pitterle, D. M., and K. V. Rajagopalan.** 1993. The biosynthesis of molybdopterin in *Escherichia coli*. Purification and characterization of the converting factor. *J Biol Chem* **268**:13499-505.
54. **Plunkett, G. I., V. Burland, D. L. Daniels, and F. R. Blattner.** 1993. Analysis of the *Escherichia coli* genome. III. DNA sequence of the region from 87.2 to 89.2 minutes. *Nucleic Acids Res.* **21**:3391-3398.
55. **Pommier, J., M. A. Mandrand, S. E. Holt, D. H. Boxer, and G. Giordano.** 1992. A second phenazine methosulphate-linked formate dehydrogenase isoenzyme in *Escherichia coli*. *Biochim Biophys Acta* **1107**:305-13.
56. **Pommier, J., V. Mejean, G. Giordano, and C. Iobbi-Nivol.** 1998. TorD, a cytoplasmic chaperone that interacts with the unfolded trimethylamine N-oxide reductase enzyme (TorA) in *Escherichia coli*. *J Biol Chem* **273**:16615-20.

57. **Raaijmakers, H., S. Teixeira, J. M. Dias, M. J. Almendra, C. D. Brondino, I. Moura, J. J. Moura, and M. J. Romao.** 2001. Tungsten-containing formate dehydrogenase from *Desulfovibrio gigas*: metal identification and preliminary structural data by multi-wavelength crystallography. *J Biol Inorg Chem.* **6**:398-404.
58. **Rajagopalan, K. V., and J. L. Johnson.** 1992. The pterin molybdenum cofactors. *J Biol Chem* **267**:10199-202.
59. **Rosner, B. M., and B. Schink.** 1995. Purification and characterization of acetylene hydratase of *Pelobacter acetylenicus*, a tungsten iron-sulfur protein. *J Bacteriol.* **177**:5767-72.
60. **Rothery, R. A., A. Magalon, G. Giordano, B. Guigliarelli, F. Blasco, and J. H. Weiner.** 1998. The molybdenum cofactor of *Escherichia coli* nitrate reductase A (NarGHI). Effect of a mobAB mutation and interactions with [Fe-S] clusters. *J Biol Chem* **273**:7462-9.
61. **Roy, R., and M. W. W. Adams.** 2002. Characterization of a fourth tungsten-containing enzyme from the hyperthermophilic archaeon *Pyrococcus furiosus*. *J. Bacteriol.* **184**:6952-6956.
62. **Roy, R., S. Mukund, G. J. Schut, D. M. Dunn, R. Weiss, and M. W. Adams.** 1999. Purification and molecular characterization of the tungsten-containing formaldehyde ferredoxin oxidoreductase from the hyperthermophilic archaeon *Pyrococcus furiosus*: the third of a putative five-member tungstoenzyme family. *J. Bacteriol.* **181**:1171-80.
63. **Sandu, C., and R. Brandsch.** 2002. Evidence for MoeA-dependent formation of the molybdenum cofactor from molybdate and molybdopterin in *Escherichia coli*. *Arch Microbiol* **178**:465-70.

64. **Sawers, G.** 1994. The hydrogenases and formate dehydrogenases of *Escherichia coli*. *Antonie Van Leeuwenhoek* **66**:57-88.
65. **Sawers G, H. J., Zehelein E, Bock A.** 1991. Expression and operon structure of the sel genes of *Escherichia coli* and identification of a third selenium-containing formate dehydrogenase isoenzyme. *J Bacteriol.* **173**:4983-93.
66. **Schmitz, R. A., S. P. Albracht, and R. K. Thauer.** 1992. A molybdenum and a tungsten isoenzyme of formylmethanofuran dehydrogenase in the thermophilic archaeon *Methanobacterium wolfei*. *Eur J Biochem* **209**:1013-8.
67. **Scott RH, S. G., DeMoss JA.** 1979. In vitro incorporation of molybdate into demolybdoproteins in *Escherichia coli*. *J Bacteriol.* **137**:719-26.
68. **Stadtman, T. C., J. N. Davis, W. M. Ching, F. Zinoni, and A. Bock.** 1991. Amino acid sequence analysis of *Escherichia coli* formate dehydrogenase (FDHH) confirms that TGA in the gene encodes selenocysteine in the gene product. *Biofactors* **3**:21-7.
69. **Stewart, L. J., S. Bailey, B. Bennett, J. M. Charnock, C. D. Garner, and A. S. McAlpine.** 2000. Dimethylsulfoxide reductase: an enzyme capable of catalysis with either molybdenum or tungsten at the active site. *J Mol Biol* **299**:593-600.
70. **Stewart, V.** 1988. Nitrate respiration in relation to facultative metabolism in enterobacteria. *Microbiol Rev* **52**:190-232.
71. **Vergnes, A., K. Gouffi-Belhabich, F. Blasco, G. Giordano, and A. Magalon.** 2004. Involvement of the molybdenum cofactor biosynthetic machinery in the maturation of the *Escherichia coli* nitrate reductase A. *J Biol Chem* **279**:41398-403.

72. **Völkl, P., R. Huber, E. Drobner, R. Rachel, S. Burggraf, A. Trincone, and K. O. Stetter.** 1993. *Pyrobaculum aerophilum* sp. nov., a novel nitrate-reducing hyperthermophilic archaeum. Appl. Environ. Microbiol. **59**:2918-26.
73. **Wuebbens, M. M., and K. V. Rajagopalan.** 1995. Investigation of the early steps of molybdopterin biosynthesis in *Escherichia coli* through the use of *in vivo* labeling studies. J Biol Chem **270**:1082-7.
74. **Yamamoto, I., T. Saiki, S. M. Liu, and L. G. Ljungdahl.** 1983. Purification and properties of NADP-dependent formate dehydrogenase from *Clostridium thermoaceticum*, a tungsten-selenium-iron protein. J. Biol. Chem. **258**:1826-1832.
75. **Zinoni, F., A. Birkmann, T. C. Stadtman, and A. Bock.** 1986. Nucleotide sequence and expression of the selenocysteine-containing polypeptide of formate dehydrogenase (formate-hydrogen-lyase-linked) from *Escherichia coli*. Proc Natl Acad Sci U S A **83**:4650-4.

CHAPTER 6

SUMMARY AND CONCLUSIONS

The goal of this project was to evaluate the role of tungsten (W) and molybdenum (Mo) in the nitrate reduction pathway of *Pyrobaculum aerophilum*. The isolation of *Pyrobaculum aerophilum* approximately a decade ago, led to the discovery of the first nitrate reducer and the first facultative anaerobe in the phylum *Thermoproteales* (31). Other than that it is a true denitrifier and a microaerophile, relatively little was known about its respiratory pathway. This is a very important issue because other members of this genus, and hyperthermophiles in general, grow by either sulfur reduction, sulfur respiration or fermentation.

The fundamental issue addressed by this research is how and why do organisms choose to use Mo or W at the catalytic sites of key enzymes. The model organism is *Pyrobaculum aerophilum*, and the model system is nitrate reduction. Nitrate reductase (NR) catalyzes a high potential reaction ($E_o' + 420$ mV), and in organisms such as *Escherichia coli* the physiological electron donor is formate via formate dehydrogenase (FDH) ($E_o' -430$ mV) in the formate-nitrate respiratory chain (9, 11, 12, 18-20, 27, 28). Both of these enzymes are molybdoenzymes in *E. coli*. However, FDH has also been purified as a naturally-occurring tungstoenzyme from various thermophilic bacteria (3, 4, 32), but NR had not been previously purified from a thermophilic organism, let alone one growing at 100 °C. So, does *P. aerophilum* produce a W-containing NR

or a W-containing FDH? This might be expected (in terms of thermal stability), but perhaps not in the case of NR, in terms of how the redox chemistry will be carried out.

In order to address these fundamental questions a defined medium was established for reproducible growth and high yields of *P. aerophilum* (Chapter 2). *P. aerophilum* was grown at 98 °C, representing its optimum high temperature environment, and at 78 °C, representing its low temperature threshold of growth. Variable concentrations and combinations of molybdate and tungstate were added to the growth medium of *P. aerophilum* to evaluate uptake of the oxyanions under the two temperature extremes. It was shown that growth of *P. aerophilum* at 98 °C in the presence of nitrate requires tungstate (WO_4^{2-}) and is inhibited by the presence of molybdate (MoO_4^{2-}) in higher or equimolar concentrations. However, both WO_4^{2-} and MoO_4^{2-} support growth at the low (78 °C) temperature. Notwithstanding the difference in effect of the presence of the oxyanions under the two growth temperatures, elemental analyses showed that both oxyanions were taken up by the organism under both of these growth conditions.

Both enzymes were found to be membrane-bound in *P. aerophilum*. The specific activity of NR and of FDH on WO_4^{2-} -grown cells were each approximately the same in the two cell types grown at the different temperatures, while the activity in cells grown only on MoO_4^{2-} at 78 °C was slightly lower than in the cells grown only on WO_4^{2-} . Anaerobic growth of the organism was highly dependent upon pH, with slight changes greatly affecting cell yield and doubling time. Furthermore, the addition of formate during growth greatly enhanced the specific activity of both NR and FDH, and also increased growth rate and cell yield. The results presented in Chapter 2 are the first to show a temperature-dependent difference in W and Mo requirements.

Considering the differences in the redox potentials of the reactions catalyzed by FDH and NR, it is surprising that both enzymes are active when cells are grown in the presence solely of

either WO_4^{2-} or MoO_4^{2-} . It was therefore of great interest to determine which metal was incorporated into which enzyme under the various growth conditions, and to what extent the different forms of the enzymes (Mo- or W-containing), if they exist, are catalytically active.

The availability of the genomic sequences of *P. aerophilum* (13) and *E. coli* (7, 8) has allowed comparison between their respective nitrate reductases. The high identity and similarity between these NRs led to the prediction that *P. aerophilum* would contain one *E. coli*-like nitrate reductase. The genomic sequence of *P. aerophilum* confirms only one copy of the Nar operon, as opposed to the two, *narGHJI* and *narZYWV*, found in *E. coli*. This prediction was the initial basis for this research and raised two important questions. One, does the NR in *P. aerophilum* contain W rather than Mo? And two, does *P. aerophilum* also contain a non-conventional NR not recognized in the genome analysis? The purification and characterization of NR in *P. aerophilum* was undertaken as part of this study in order to determine the nature of the NR or NRs, in this organism and the composition of cofactors that they contain (Chapter 3).

NR and FDH co-purify in *P. aerophilum* during membrane solubilization and chromatography. The release of both of these enzymes was accomplished by sequential solubilization of the membranes. Membranes were initially solubilized with 0.5% n-octyl β -glucoside, which contained about 30% of the total NR activity, while extraction of the precipitated membranes with 4.0% n-octyl β -glucoside contained the majority (64%) of NR activity. As described in Chapter 4, the opposite was true for FDH, as the majority of the FDH activity (61%) was extracted by 0.5% n-octyl β -glucoside. Consequently, approximately 95% of total NR activity, and 84% of the total FDH activity was solubilized from the membrane fraction by the two detergent treatments. The membranes solubilized with 4.0% n-octyl β -glucoside had a specific activity of 74 U/mg for NR and 3.2 U/mg for FDH, and those solubilized in the initial

0.5% n-octyl β -glucoside treatment had a specific activity of 33 U/mg for NR and 6.2 U/mg for FDH.

The isolation, purification and characterization of the NR from *P. aerophilum* revealed two forms of the enzyme, NR (NR1 and NR2) and two forms of a NR-FDH complex (NR1-FDH1 and NR2-FDH2), which were isolated based primarily on metal composition of the pterin cofactor. The majority of the purified NR enzyme contained Mo, yet there was a substantial portion of active NR, which contained W.

Thus, the principal nitrate reductase, NR1 is a Mo-containing enzyme (0.8 g-atoms Mo and 0.02 g-atoms W per mol of enzyme) with a specific activity of 534 U/mg. Iron was present in NR1 at 20 ± 0.1 g-atoms per mol of enzyme, which is consistent with the notion that the NR contains one [3Fe-4S] and four [4Fe-4S] clusters. NR1 resembles other respiratory NRs found in mesophilic microorganisms not only in metal content, but also in subunit composition (9, 26). NR1 α had an approximate M_r value of 144 kDa. The β subunit was present as major polypeptide in monomer form as 53.5 kDa and as a dimer with M_r values of 123 kDa and 108 kDa. The γ subunit in NR1 appeared only as a faint band when analyzed by SDS-PAGE with an approximate M_r value of 33 kDa. Likewise, cytochrome *b* was established as an integral cofactor of *P. aerophilum* NR1 by visible spectroscopy, as in *E. coli* NR. These results for NR1 are similar to those found in a previous study of *P. aerophilum* (2), which was published while this work was in progress. In addition, EPR spectra of [Fe-S] clusters and Mo (V) of *P. aerophilum* NR1 also demonstrate a cofactor composition similar to that of NRA from *E. coli* (15, 24), which had not been shown previously. Residues identified in cofactor binding in *E. coli* (13, 40) were conserved in *P. aerophilum* and the overall high identity of sequences between the

subunits, including the regions that bind the MGD cofactor, further confirm the high similarity between *P. aerophilum* NR1 and *E. coli* NRA.

NR1 is distinct from these corresponding mesophilic enzymes in that it exhibits its highest activity at thermophilic and hyperthermophilic temperatures, notwithstanding its ability to reduce chlorate and maintain activity at mesophilic temperatures at the same level as that of mesophilic respiratory NRs. The purified NR enzymes and the NR/FDH enzyme complexes of *P. aerophilum* all exhibited maximal activity at 90 °C. Moreover, the specific activity of NR1 at its optimal temperature is from 7 to 28 times higher than specific activities of corresponding mesophilic enzymes from bacterial sources, such as *E. coli* and *B. licheniformis* (1, 22, 23, 30); and from 9 to over 20,000 times higher than NRs from the halophilic archaea *Haloferax denitrificans* (16) and *Haloarcula marismortui* (33), respectively. Furthermore, NR1 displays an apparent affinity for nitrate (40 µM) that is 5 - (16) to 95 - fold (14) higher than other reported mesophilic nitrate reductases. NR1 was most active at pH 7.0 (using HEPES buffer).

The primary distinction between the NRs in *P. aerophilum* and all reported NRs to date is however, the presence of NR2, which is a W-containing enzyme. While it is not surprising that NR is able to take up and incorporate W into the active site, it is surprising to find a level of activity (223 U/mg) that is comparable to that of the Mo-containing NR1 (534 U/mg), and to other Mo-only containing enzymes. NR2 represents 30% of the total purified NR, and constitutes 18% of the total NR activity.

Although Mo appears to be the preferable metal utilized in *P. aerophilum* NR, the incorporation of W into the NR active site does lead to a highly active enzyme. Partial purification of *P. aerophilum* cells grown in Mo-only media at 78 °C did not contain a second peak of NR activity, in other words, there was no NR2. Thus, it seems that if Mo is no longer

available, W is utilized in *P. aerophilum* NR. Furthermore, the genomic sequence of *P. aerophilum* confirms only one copy of NarGHJI (28) suggesting that NR1 and NR2 are the same enzyme with the exception of the metal incorporated into the active site.

NR2 contains 0.7 g-atoms W and 0.08 g-atoms Mo per mol enzyme and 16 ± 0.5 g-atoms Fe per mol enzyme. The predicted M_r values for the α and β subunits of NR2 were 140 kDa and 123 kDa, respectively. The 123 kDa polypeptide in NR2, confirmed by N-terminal amino acid sequence analysis as the β subunit, was present only in dimer form. Neither MS, nor MS/MS analysis of the 140 kDa polypeptide from NR2, however, yielded an irrefutable result, but based on activity and peak matches that were observed in MS, is presumed to be NR α subunit. It is possible that NR2 does not contain a cytochrome *b* in purified form.

An active W-containing NR is unprecedented, as this enzyme usually contains Mo. The possibility that the Mo-NR (NR1) functions in promoting catalysis in the same manner as the NR from *E. coli* is highly likely. The W-NR (NR2), however, could possibly function in this manner as well, which would mean that the redox potential of the W couples would be more positive as seen in the W-TMAOR from *E. coli* (20), but is not typical of tungstoenzymes. Another possibility is that there is a wide range in the different redox potentials of the electron carriers in the transport chain, as seen in the Ni-Fe hydrogenase from *D. gigas* (85).

Purified NR samples (NR1 and NR2) and the enzyme complexes (NR1-FDH1 and NR2-FDH2) each gave rise to a single protein band after nondenaturing PAGE. In agreement with the direct FDH assays, when the gels were stained with formate, the same protein bands from NR1-FDH1 and NR2-FDH2 exhibited FDH activity as well as NR activity, suggesting that both enzymes were within the same native complex. The purified NRs and the NR-FDH complexes exhibited nitrate reductase activity when stained with either nitrate or chlorate.

Comparison of the operons and amino acid sequences of the FDH from *P. aerophilum* and FDH-N and FDH-O from *E. coli* (Fig. 4.1) reveals a moderately high similarity, from 31 to 50%, suggesting that *P. aerophilum* contains a respiratory FDH that is similar to those in *E. coli*. However, the genome sequence of *P. aerophilum* does not contain genes that encode a second FDH of this type, as is the case with *E. coli*. The identities and similarities between *P. aerophilum* FDH and both FDH-N and FDH-O are the same. The α and β subunits of the *P. aerophilum* enzyme show relatively high sequence similarity with the homologous subunits of the FDHs in *E. coli*, and are thought to contain the same cofactors. Although the γ subunit of the *E. coli* enzymes has a low amino acid sequence similarity to the corresponding protein (PAE2660) of the *P. aerophilum* FDH (which is annotated as a hypothetical protein), it is assumed to contain the same heme cofactors. Further, the His ligands of the hemes are also conserved in the sequence of the hypothetical protein (PAE2660) of *P. aerophilum* FDH and in FdoI from FDH-O.

FDH was purified in complex with NR, and was also found in two forms, NR1/FDH1 and NR2/FDH2 (Chapter 4). The NR1/FDH1 complex contained 0.6 g-atoms Mo and 0.3 g-atoms W per mol of complex with a FDH specific activity of 33 U/mg, which was 24 times higher than the FDH specific activity in NR2/FDH2 (~ 3 U/mg). The NR2/FDH2 complex contained 0.6 g-atoms W and 0.2 g-atoms Mo per mol of complex. The Fe content (40 g-atoms per mol of NR1/FDH1 complex, and 37 g-atoms per mol of NR2/FDH2 complex), is consistent with the notion that the NR contains one [3Fe-4S] and four [4Fe-4S] (5, 14), and FDH contains five [4Fe-4S] clusters (15). The specific activity of NR in the NR1/FDH1 complex was 712 U/mg, and 373 U/mg in the NR2/FDH2 complex. Optimum FDH activity was obtained at pH 8.5 using CHES buffer. The NR/FDH complexes exhibited maximal FDH activity at 90 °C.

The two complexes, NR1-FDH1 and NR2-FDH2, also consisted of the three predicted major NR polypeptides. Attempts to identify the predicted polypeptides from FDH by N-terminal sequencing, internal sequencing or MS, however, were unsuccessful.

FDH from *P. aerophilum* is obviously distinct, however, from the corresponding mesophilic *E. coli* FDHs, in that it exhibits its highest activity at extreme temperatures (90 °C). Furthermore, FDH was not active at room temperature, and in fact was active only at or above 50 °C, unlike the NR activity in the NR/FDH complexes of *P. aerophilum*, which was active at room temperature (Chapter 3).

In *E. coli*, there is a FDH produced during growth of the organism under aerobic conditions (FDH-O), and another that is functional during anaerobic growth (FDH-N). In *P. aerophilum*, however, there is only one FDH, although it appears to exist in two forms when solubilized *in vitro*. The deduced amino acid sequences of the subunits of *P. aerophilum* FDH are equally similar to those of the corresponding subunits of both FDH-O and FDH-N of *E. coli*. Residues identified as cofactor ligands in FDH-N and FDH-O of *E. coli* (4, 24) were conserved in the *P. aerophilum* enzyme, and therefore were predicted to contain the same cofactors. From an evolutionary perspective, it is clear that an operon duplication event occurred in *E. coli* that did not occur in *P. aerophilum*. This may reflect the physiological needs of the two organisms, as *E. coli* is metabolically very diverse and can thrive in aerobic and anaerobic environments and therefore requires a FDH that can function under either environmental condition. *P. aerophilum*, on the other hand, can only thrive in an environment with a low percentage of oxygen (microaerophilic), or anaerobically, therefore one FDH which can function in a low oxygen (0.3 – 3.0% (w/v) oxygen) or anaerobic environment is sufficient. Thus, the FDH in *P. aerophilum* may be in part reflective of the microaerophilic nature of the organism.

In Chapter 5, genomic sequences of the molybdoenzymes, tungstoenzymes, the pterin biosynthetic pathway, and metal transport in *P. aerophilum*, *E. coli* and *P. furiosus* were compared, which provided insight into how *P. aerophilum* fits into what is currently known about how these two metals are utilized in the active sites of enzymes in anaerobic metabolism. *P. aerophilum* shares many similarities with mesophilic bacteria such as *E. coli* as shown by its homologous FDH and NR, which form the formate-nitrate respiratory pathway. Furthermore, as both *P. aerophilum* and *P. furiosus* are hyperthermophilic archaea, there is extensive similarity in the oxidoreductase type enzymes that each organism contains, specifically, the AOR family of tungstoenzymes. The highly conserved Moco biosynthetic pathway, which produces the cofactor necessary for activity in all of these enzymes, is also present in *P. aerophilum* based on genomic comparisons. There are differences, however, which are most likely responsible for the ability of *P. aerophilum* to utilize Mo in the active sites of its enzymes, as in *E. coli*, and also to utilize W, as in *P. furiosus*. Thus, *P. aerophilum* seems to be a hybrid or transitional microorganism with respect to its phylogeny, physiology and biochemistry of Mo and W.

Future research. In order to establish the catalytic mechanism of the NRs, future experiments focusing on the redox potentials of the Mo and W active sites, as well as the Fe-S clusters and hemes would need to be conducted, and structural analysis would of course help in resolving the speculation of the mechanism of the NRs in *P. aerophilum*.

Additional studies focusing on the FDH in *P. aerophilum* are needed. FDH was purified as a complex with NR, despite numerous and various attempts to separate FDH from the complex, and identification of the protein bands corresponding to the predicted FDH subunits were unsuccessful, thus many characteristics of the FDH enzyme of *P. aerophilum* remain

unknown. In addition to addressing these issues, development of a standard assay using PMS as an electron carrier, which gives reliable results at high temperature, would be beneficial in further characterization not only of the FDH, but also of the formate-nitrate respiratory system in *P. aerophilum*.

REFERENCES

1. **Adams, M. W. W., and L. E. Mortenson.** 1982. The Effect of Cyanide and Ferricyanide On the Activity of the Dissimilatory Nitrate Reductase of *Escherichia coli*. Journal of Biological Chemistry **257**:1791-1799.
2. **Afshar, S., E. Johnson, S. de Vries, and I. Schroder.** 2001. Properties of a thermostable nitrate reductase from the hyperthermophilic archaeon *Pyrobaculum aerophilum*. J. Bacteriol. **183**:5491-5.
3. **Almendra MJ, B. C., Gavel O, Pereira AS, Tavares P, Bursakov S, Duarte R, Caldeira J, Moura JJ, Moura I.** 1999. Purification and characterization of a tungsten-containing formate dehydrogenase from *Desulfovibrio gigas*. Biochemistry **38**:16366-72.
4. **Andreesen, J. R., and L. G. Ljungdahl.** 1973. Formate dehydrogenase of *Clostridium thermoaceticum*: incorporation of selenium-75, and the effects of selenite, molybdate, and tungstate on the enzyme. J Bacteriol. **116**:867-73.
5. **Antipov, A. N., N. N. Lyalikova, T. V. Khijniak, and P. L'Vov N.** 1998. Molybdenum-free nitrate reductases from vanadate-reducing bacteria. FEBS Lett **441**:257-60.
6. **Antipov AN, S. D., L'Vov NP, Kuenen JG.** 2003. New enzyme belonging to the family of molybdenum-free nitrate reductases. Biochem J. **369**:185-9.

7. **Blasco, F., C. Iobbi, G. Giordano, M. Chippaux, and V. Bonnefoy.** 1989. Nitrate reductase of *Escherichia coli*: completion of the nucleotide sequence of the nar operon and reassessment of the role of the alpha and beta subunits in iron binding and electron transfer. *Mol Gen Genet* **218**:249-56.
8. **Blasco, F., C. Iobbi, J. Ratouchniak, V. Bonnefoy, and M. Chippaux.** 1990. Nitrate reductases of *Escherichia coli*: sequence of the second nitrate reductase and comparison with that encoded by the narGHJI operon. *Mol Gen Genet* **222**:104-11.
9. **Bonnefoy, V., and J. A. Demoss.** 1994. Nitrate reductases in *Escherichia coli*. *Antonie Van Leeuwenhoek* **66**:47-56.
10. **Chaudhry, G. R., and C. H. MacGregor.** 1983. Cytochrome b from *Escherichia coli* nitrate reductase. Its properties and association with the enzyme complex. *J Biol Chem* **258**:5819-27.
11. **Chaudhry, G. R., and C. H. MacGregor.** 1983. *Escherichia coli* nitrate reductase subunit A: its role as the catalytic site and evidence for its modification. *J Bacteriol* **154**:387-94.
12. **Enoch, H. G., and R. L. Lester.** 1975. The purification and properties of formate dehydrogenase and nitrate reductase from *Escherichia coli*. *J Biol Chem* **250**:6693-705.
13. **Fitz-Gibbon, S. T., H. Ladner, U. J. Kim, K. O. Stetter, M. I. Simon, and J. H. Miller.** 2002. Genome sequence of the hyperthermophilic crenarchaeon *Pyrobaculum aerophilum*. *Proc. Natl. Acad. Sci. U S A* **99**:984-9.
14. **Frunzke, K., B. Heiss, O. Meyer, and W. G. Zumft.** 1993. Molybdopterin guanine dinucleotide is the organic moiety of the molybdenum cofactor in respiratory nitrate reductase from *Pseudomonas stutzeri*. *FEMS Microbiol Lett* **113**:241-245.

15. **George, G. N., N. A. Turner, R. C. Bray, F. F. Morpeth, D. H. Boxer, and S. P. Cramer.** 1989. X-ray-absorption and electron-paramagnetic-resonance spectroscopic studies of the environment of molybdenum in high-pH and low-pH forms of *Escherichia coli* nitrate reductase. *Biochem J.* **259**:693-700.
16. **Hochstein, L. I., and F. Lang.** 1991. Purification and properties of a dissimilatory nitrate reductase from *Haloferax denitrificans*. *Arch Biochem Biophys* **288**:380-5.
17. **Imperial, J., M. Hadi, and N. K. Amy.** 1998. Molybdate binding by ModA, the periplasmic component of the *Escherichia coli* mod molybdate transport system. *Biochim Biophys Acta.* **1370**:337-46.
18. **Iobbi-Nivol, C., C. L. Santini, F. Blasco, and G. Giordano.** 1990. Purification and further characterization of the second nitrate reductase of *Escherichia coli* K12. *Eur J Biochem* **188**:679-87.
19. **Jormakka, M., D. Richardson, B. Byrne, and S. Iwata.** 2004. Architecture of NarGH reveals a structural classification of Mo-*bis*MGD enzymes. *Structure (Camb)* **12**:95-104.
20. **Jormakka, M., S. Tornroth, B. Byrne, and S. Iwata.** 2002. Molecular basis of proton motive force generation: structure of formate dehydrogenase-N. *Science* **295**:1863-8.
21. **Ketchum, P. A., G. Denariatz, J. LeGall, and W. J. Payne.** 1991. Menaquinol-nitrate oxidoreductase of *Bacillus halodenitrificans*. *J Bacteriol* **173**:2498-505.
22. **Lund, K., and J. A. DeMoss.** 1976. Association-dissociation behavior and subunit structure of heat-released nitrate reductase from *Escherichia coli*. *J Biol Chem* **251**:2207-16.
23. **MacGregor, C. H., C. A. Schnaitman, and D. E. Normansell.** 1974. Purification and properties of nitrate reductase from *Escherichia coli* K12. *J Biol Chem* **249**:5321-7.

24. **Magalon, A., R. A. Rothery, G. Giordano, F. Blasco, and J. H. Weiner.** 1997. Characterization by electron paramagnetic resonance of the role of the *Escherichia coli* nitrate reductase (NarGHI) iron-sulfur clusters in electron transfer to nitrate and identification of a semiquinone radical intermediate. *J Bacteriol.* **179**:5037-5045.
25. **Magalon, A., R. A. Rothery, D. Lemesle-Meunier, C. Frixon, J. H. Weiner, and F. Blasco.** 1998. Inhibitor binding within the NarI subunit (cytochrome bnr) of *Escherichia coli* nitrate reductase A. *J Biol Chem.* **273**:10851-6.
26. **Moreno-Vivian, C., P. Cabello, M. Martinez-Luque, R. Blasco, and F. Castillo.** 1999. Prokaryotic nitrate reduction: molecular properties and functional distinction among bacterial nitrate reductases. *J Bacteriol* **181**:6573-84.
27. **Philippot, L., and O. Hojberg.** 1999. Dissimilatory nitrate reductases in bacteria. *Biochim Biophys Acta* **1446**:1-23.
28. **Sawers, G.** 1994. The hydrogenases and formate dehydrogenases of *Escherichia coli*. *Antonie Van Leeuwenhoek* **66**:57-88.
29. **Stewart, L. J., S. Bailey, B. Bennett, J. M. Charnock, C. D. Garner, and A. S. McAlpine.** 2000. Dimethylsulfoxide reductase: an enzyme capable of catalysis with either molybdenum or tungsten at the active site. *J Mol Biol* **299**:593-600.
30. **Van Riet, J., F. B. Wientjes, J. Van Doorn, and R. J. Planta.** 1979. Purification and Characterization of the Respiratory Nitrate Reductase of *Bacillus licheniformis*. *Biochim Biophys Acta* **572**:347-360.
31. **Völkl, P., R. Huber, E. Drobner, R. Rachel, S. Burggraf, A. Trincone, and K. O. Stetter.** 1993. *Pyrobaculum aerophilum* sp. nov., a novel nitrate-reducing hyperthermophilic archaeum. *Appl. Environ. Microbiol.* **59**:2918-26.

32. **Yamamoto, I., T. Saiki, S. M. Liu, and L. G. Ljungdahl.** 1983. Purification and properties of NADP-dependent formate dehydrogenase from *Clostridium thermoaceticum*, a tungsten-selenium-iron protein. J. Biol. Chem. **258**:1826-1832.
33. **Yoshimatsu, K., T. Sakurai, and T. Fujiwara.** 2000. Purification and characterization of dissimilatory nitrate reductase from a denitrifying halophilic archaeon, *Haloarcula marismortui*. FEBS Lett **470**:216-20.